SEISMIC IN-PLANE BEHAVIOR OF URM WALLS UPGRADED WITH COMPOSITES

THÈSE N^{O} 3111 (2004)

PRÉSENTÉE À LA FACULTÉ ENVIRONNEMENT NATUREL, ARCHITECTURAL ET CONSTRUIT

Institut de structures

SECTION DE GÉNIE CIVIL

ÉCOLE POLYTECHNIQUE FÉDÉRALE DE LAUSANNE

POUR L'OBTENTION DU GRADE DE DOCTEUR ÈS SCIENCES

PAR

Mohamed ELGAWADY

M.Eng in Civil Engineering-Structures, Cairo University, Egypte
et de nationalité égyptienne

acceptée sur proposition du jury:

Prof. I. Smith, M. Badoux, directeurs de thèse
Prof. D. Abrams, rapporteur
Prof. A. Dazio, rapporteur
Dr P. Lestuzzi, rapporteur
Prof. T. Triantafillou, rapporteur

Lausanne, EPFL
2004

To my mother and father

To my wife and children

ACKNOWLEDGEMENTS

I wish to express my appreciation to my co-advisors Professor Ian Smith and Professor Marc Badoux for their encouragement during writing of the thesis. Special thanks are also due to Dr. Pierino Lestuzzi my thesis supervisor for his direct help, interest, encouragement and insight during experimental and analytical work of this thesis.

The experimental work in this thesis was made possible through the financial and technical support of SIKA AG Company complemented with the financial support of the Swiss Commission for Technological Innovation (CTI). This support is very gratefully acknowledged.

Further, deep appreciation is extended to the following organizations and individuals:

- The Swiss Federal Institute of Technology in Zurich (ETHZ) for the use of the testing facility. Special thanks to Professor Peter Marti for his openness to EPFL-ETHZ collaboration.
- Morandi for donation of the half-scale brick units
- Mr. Markus Baumann (IBK-ETHZ), the head of the laboratory, for his invaluable support during the dynamic tests.
- Mr. Heinz Meier (SIKA) for his contribution of knowledge to the dynamic tests
- Mr. Victor Venetz (SIKA) for installing the composites on the masonry specimens and for demolishing the tested specimens
- Mr. Jorge Hegner, former graduate student (EPFL)
- Mr. Dhimitri Papa, trainee (IS-IMAC-EPFL)
- Mr. Christoph Gisler, Technician (IBK-ETHZ)
- Mr. Patrice Gallay, Technician (IS-IMAC-EPFL)

At last but not the least, I thank my mother and my father for everything they did, and are still doing for me. I am also thankful to my wife for her unwavering patience, understanding, and encouragement and to my sons for keeping me accompanied during the writing of the thesis.

Résumé

Les bâtiments existants en maçonnerie non armée (URM), dont beaucoup ont une importance historique et culturelle, constituent une fraction significative du parc immobilier mondial. Les récents séismes ont montré la vulnérabilité de ce type de bâtiments. Cette thèse étudie le comportement sismique, dans leur plan, de refends en maçonnerie non armée renforcés au moyen de matériaux composites (URM-FRP). Elle comprend des tests dynamiques et statiques-cycliques et le développement d'un modèle analytique.

Dans la partie expérimentale, dix refends en maçonnerie non armée à simple paroi ont été construits à l'échelle 1:2 en utilisant deux qualités de mortier et des briques en terre cuite alvéolées. Les refends ont d'abord été testés comme référence. Ensuite ils ont été renforcés sur une seule face au moyen de matériaux composites avant d'être testés à nouveau. Par conséquent, au total, onze refends ont été testés dynamiquement à l'aide du simulateur de séismes de l'ETHZ et neuf refends ont été testés de manière statique-cyclique dans le laboratoire de structures de l'EPFL.

Pour la partie analytique, un nouveau modèle en cisaillement et un modèle simple en flexion ont été développés. Pour l'analyse en cisaillement, la maçonnerie, l'époxy et les matériaux composites ont été idéalisés par des couches de matériaux élastiques, homogènes et isotropes. Les équations différentielles du système ainsi formé ont été établies à l'aide des principes de la théorie de l'élasticité plane. La solution s'exprime avec des doubles séries de Fourier. Elle peut être utilisée pour modéliser le comportement linéaire en cisaillement des refends URM-FRP. Une dégradation progressive de la rigidité a été introduite pour tenir compte des non-linéarités matérielles. Pour l'analyse en flexion, un modèle simple utilisant une approche élastique linéaire comprenant l'hypothèse habituelle de Navier-Bernoulli et un bloc rectangulaire équivalent de contraintes a été développé.

Les campagnes expérimentales montrent que la méthode de renforcement améliore la résistance latérale des refends d'un facteur compris entre 1.3 et 5.9, dépendant de l'effort normal appliqué, du taux de renforcement et du mode de rupture. Cependant, l'amélioration de la déformabilité latérale a été moins significative. Aucune réponse asymétrique due au renforcement sur une seule face n'a été observée durant les tests.

Plusieurs caractéristiques phénoménologiques ont été correctement déterminées par le modèle. Ces caractéristiques ont d'abord été mises en évidence dans la littérature en relation avec des tests sur des poutres en béton armé renforcées au moyen de matériaux composites. Elles concernent les relations entre les allongements du FRP et le taux de renforcement ainsi que l'interaction entre la résistance latérale et la contribution du FRP à la résistance latérale de l'ensemble. Les effets de la ductilité de l'époxy et de la contrainte de cisaillement admissible ainsi que de la ductilité de la maçonnerie et des contraintes admissibles ont été étudiés. Ces développements intéressent les ingénieurs structures mais également les producteurs de matériaux.

Concernant l'analyse en flexion, le modèle simple conduit à un dimensionnement non conservateur. La confrontation avec les données expérimentales montre que, jusqu'à une certaine limite, le rapport entre la résistance latérale mesurée et la résistance latérale en flexion estimée est proportionnel au taux mécanique de renforcement multiplié par le carré de l'élancement effectif. Un facteur de corrélation est proposé dans les limites de la campagne expérimentale.

ABSTRACT

Existing unreinforced masonry (URM) buildings, many of which have historical and cultural importance, constitute a significant portion of existing buildings around the world. Recent earthquakes have shown the vulnerability of such URM buildings. This thesis investigates the in-plane seismic behavior of URM walls retrofitted using composites. The thesis includes an extensive dynamic and static cyclic tests followed with development of an analytical model.

For the dynamic tests, five half-scale single wythe URM walls were built using either strong or weak mortar and half-scale hollow clay brick units. These five walls were dynamically tested as reference specimens. Then, these reference specimens were retrofitted on single side only using composites and retested. As consequence a total of eleven specimens were tested on the earthquake simulator at ETHZ.

For the static cyclic tests, five half-scale single wythe URM walls were built using weak mortar and half-scale hollow clay brick units. Of them, three specimens were tested as reference specimens. Then, two specimens of these three reference specimens were retrofitted using composites and tested again. The third reference specimen was retrofitted using post-tensioning and tested; then, the post-tension forces were released and the specimen was retrofitted using composites and retested. Finally, two virgin specimens were retrofitted directly after construction and tested. As consequence a total of nine specimens were tested in the Structural Laboratory at EPFL.

For analytical models, an innovative shear model is developed. In addition, a simple flexural model is developed. For shear analysis, masonry, epoxy, and composites in a URM wall retrofitted using composites (URM-FRP) were idealized as different layers with isotropic homogenous elastic materials. Then, using principles of theory of elasticity the governing differential equation of the system is formulated. A double Fourier sine series was used as the solution for the differential equations. The solution can be used to model the linear shear behavior of URM-FRP. To take into consideration material nonlinearity, step-by-step stiffness degradation has been implemented in a computer program. For flexural analysis, a simple model using linear elastic approach with the well-known assumptions of Navier-Bernoulli and Whitney's equivalent stress block is developed.

The experimental work shows that the retrofitting technique improved the lateral resistance of the URM walls by a factor ranged from 1.3 to 5.9 depending on the applied normal force, the reinforcement ratio, and mode of failure. However, improvement in lateral drift was less significant. Moreover, no uneven response was observed during tests due to single sided retrofitting.

Several phenomena and relationships have been correctly determined by the model. These phenomena and relationships are originally observed in the literature during tests on reinforced concrete beams that were retrofitted using composites. This includes the relationship between strains in FRP and reinforcement ratio as well as the interaction between masonry lateral resistance and FRP contribution to the lateral resistance of URM-FRP. In addition, effects of epoxy ductility and allowable shear stresses as well as masonry ductility and allowable shear stresses have been studied. Such development is of interest to the structural engineering community and material producers.

Regarding flexural analysis, the simple model leads to unconservative designs. Correlation analysis of the test data show that the ratio between the experimental lateral resistance to the estimated flexural lateral resistance is proportional to reinforcement mechanical ratio times the square of the effective moment/shear ratio up to a certain limit. Within the limits of experimental testing, a correlation factor is proposed.

TABLE OF CONTENTS

LIST OF ILLUSTRATIONS

LIST OF TABLES

1 INTRODUCTION

Existing unreinforced masonry (URM) buildings, many of which have historical and cultural importance, constitute a significant portion of buildings stock around the world. Most of these buildings were built with little or no considerations for seismic design requirements. Recent earthquakes have shown that many such buildings are seismically vulnerable; therefore, the demand for retrofitting strategies of these buildings has become increasingly stronger in the last few years, implying the evaluation of lateral resistance of existing URM buildings. Evaluation of the lateral resistance of URM buildings is after difficult because of uncertainties associated with estimating shear or flexural strength of individual walls [Ab 92]. Moreover, application of modern design codes means that most of the existing URM buildings need to be retrofitted. For example, under the URM Building Law of California, passed in 1986, building evaluations showed that approximately 96% of the URM buildings needed to be retrofitted, which would result in approximately $4 billion in retrofit expenditure [ED 02]. In Switzerland, recent research [La 02] carried out on a target area in Basel shows that from 45% to 80% of the existing URM buildings, based on construction details, will experience heavy damage or destruction during an earthquake of intensity VIII on MSK scale. Similar results have been obtained in a real earthquake event in Greece "Kalamata 1986" [KF 92a]. Therefore, improving existing and developing better methods of retrofitting existing seismically inadequate buildings is necessary. Numerous techniques are available to increase the strength and/or ductility of URM walls. There is reliability issues associated with some commonly used techniques. Modern composite materials offer promising retrofitting possibilities for masonry buildings. This thesis focus on in-plane behavior of unreinforced masonry walls retrofitted using fiber reinforced plastics (URM-FRP). Beyond the motivations, objectives and scope, and thesis outlines, this chapter includes introduction to seismic performance of URM with focus on in-plane behavior. In addition, the chapter discusses the improvement of the seismic performance of URM buildings.

1.1 Motivation for Research

The introduction of fiber reinforced plastics (FRP) into the field of masonry retrofitting has begun with the experimental work carried out at EMPA in Switzerland in 1994 [Sc 94]. Since that time, several researchers have carried out investigations on this topic. Although this technique is relatively new, several applications to existing URM structures have been reported (e.g. [SK 94 and Bo 01]). This is due to the well-known advantages of FRP over conventional retrofitting materials: inexpensive, negligible specific weight, corrosion immunity, and high tensile strength. Moreover, their flexibility and easy application allow a wide range of intervention scenarios for retrofitting in several damaging conditions. This research focus on the in-plane behavior of URM walls retrofitted using FRP. The importance of this research topic flows from the following considerations:

- In spite of the extensive research carried out in this area during the last decade, the literature review (see Chapter 2) shows that the research efforts concentrated on the out-of-plane behavior of URM-FRP. In addition, there is a lack of knowledge about in-plane behavior of URM-FRP. Moreover, the few studies on in-plane behavior of URM-FRP focused on flexural behavior. Studies on in-plane shear behavior of URM-FRP are rare. Worldwide, there was one dynamic test carried out on URM walls retrofitted using FRP [AH 99].
- Since numerous parameters affect the in-plane behavior of URM-FRP, the priority of the early experimental studies on this subject (e.g. [Sc 94, AH 99]) was to study the effectiveness of the technique rather than to quantify the effect of different parameters. Understanding of shear resistance mechanism based on this limited experimental data is not possible. Moreover, the behavior of URM walls in shear is by itself a complex challenge that has not been completely resolved, due to the lack of harmonized test methods and suitable input parameters for a reliable design model [Me 04].
- Existing models for shear resistance of URM-FRP are empirically developed and adapted from tests carried out on reinforced concrete RC elements.

1.2 Objectives and Scope of the Project

In order to bridge the existing lack of knowledge related to in-plane behavior of URM-FRP, this thesis contains a description of an extensive experimental and analytical research program. The primary objectives of this research are as follows:

- To understand the fundamental seismic in-plane behavior of URM-FRP. This includes the influence of key parameters such as effective moment/shear ratio, retrofitting configurations, reinforcement ratio, FRP structural shape, and material of the FRP on the seismic behavior. The critical aspects of the behavior for the seismic performance are the failure mode, the force deformation relationship and stiffness degradation.
- To develop an analytical model that describes the global shear behavior of URM-FRP. This includes examination of effects of different material parameters (FRP, epoxy, and masonry properties) on the shear resistance of URM-FRP; such examination of material parameters will help in any future material development. The model should be capable of examining aspects such as the phenomenon of using effective strain rather than the ultimate strain in the FRP; and to examine whether this effective strain is a constant value or variable. This point is discussed in detail in Chapter 5.
- Analytically examine whether or not there is interaction between masonry lateral resistance and FRP contribution to lateral resistance of URM-FRP. Such phenomenon has recently been reported for RC beams retrofitted using FRP. However, for RC no explanation or quantification exists.
- Investigate the ability of simplified models based on Bernoulli-Navier assumptions and Whitney's equivalent stress block to estimate the in-plane flexural resistance of URM-FRP.

To achieve these goals, a two phase experimental program has been carried out followed with development of analytical model for in-plane behavior of URM-FRP. The first phase of the experimental program includes dynamic in-plane tests carried out on URM walls retrofitted using FRP. The second phase of the experimental program includes static cyclic tests on URM walls retrofitted using FRP. The experimental tests have investigated the following parameter variations:

- Effective moment/shear ratio: slender (effective moment/shear ratio of 1.4), squat (effective moment/shear ratio of 0.7) and midget (effective moment/shear ratio of 0.5)
- Fiber type: aramid, glass, carbon, and hardwire
- Retrofitting configurations: diagonal shape (X) and full face
- Fiber structures: plates, fabrics, and grids
- Reinforcement ratio: ranged from (0.07% to 0.28%)
- Mortar compressive strength: weak (M2.5) and strong (M9).

For the dynamic tests, five half-scale single wythe URM walls were built using either strong or weak mortar and half-scale hollow clay brick units. These five walls were dynamically tested as reference specimens. Then, these reference specimens were retrofitted using FRP and retested. Consequently, a total of eleven specimens were tested on the earthquake simulator of ETHZ. Note that all of the retrofitted specimens were retrofitted on one face only. In many retrofitting intervention scenarios one face retrofitting is frequently preferred over two faces, either for convenience of construction (when added to the wall exterior surface) or to leave the exterior façade of the building unaltered.

For the static cyclic tests, five half-scale single wythe URM walls were built using weak mortar and half-scale hollow clay brick units. Of them, three specimens were tested as reference specimens. Then, two specimens of these three reference specimens were retrofitted using FRP and tested again. The third reference specimen was retrofitted using post-tensioning and tested; then, the post-tension forces were released and the specimen was retrofitted using FRP and retested. Finally, two virgin specimens were retrofitted directly after construction and tested. Consequently, a total of nine specimens were tested in the Structures Laboratory at EPFL. Note that the FRP was applied on the entire surface of a single face only.

Table 1.1: Summary of the specimens tested dynamically on ETHZ earthquake simulator

Specimen Name	Slenderness	Retrofitting Material[1] and Fiber Product	Retrofitting Configuration	Mortar Type	Test Type
L1-REFE	Slender	No retrofitting		Strong	Dynamic tests
L2-REFE	Slender	No retrofitting		Weak	
S1-REFE	Squat	No retrofitting		Strong	
S2-REFE	Squat	No retrofitting		Weak	
L1-LAMI-C-I	Slender	CFRP Plates	2 vertical plates	Strong	
L1-WRAP-G-F	Slender	GFRP Fabric	Full face	Strong	
L2-WRAP-G-F	Slender	GFRP Grid	Full face	Weak	
L1-WRAP-G-X	Slender	GFRP Fabric	X Pattern	Strong	
S1-WARP-G-F	Squat	GFRP Fabric	Full face	Strong	
S2-WRAP-A-F	Squat	AFRP Fabric	Full face	Weak	
S1-LAMI-C-X	Squat	Plates of CFRP	XX Pattern	Weak	

1. All specimens were retrofitted on one face only. The materials used for retrofitting were Glass (G), Carbon (C), and Aramid (A) FRP.

Table 1.2: Summary of the specimens tested static cyclic at EPFL

Specimen Name	Slenderness	Retrofitting Material[1] and Fiber Product	Retrofitting Configuration	Mortar Type	Test Type
S2-REFE-ST	Squat	No retrofitting		Weak	Static cyclic
M2-REFE1-ST	Midget	No retrofitting		Weak	
M2-REFE2-ST	Midget	No retrofitting		Weak	
M2-POST-ST					
S2-WRAP-G-F-ST	Squat	GFRP Fabric	Full face	Weak	
M2-WRAP-G-F-ST	Midget	GFRP Fabric	Full face	Weak	
M2-WRAP-A-F-ST	Midget	AFRP Fabric	Full face	Weak	
M2-2WRAP-G-F-ST	Midget	GFRP Fabric	Full face	Weak	
S2-WIRE-S-F-ST	Squat	Hardwire	Full face	Weak	

1. All specimens were retrofitted on one face only. The materials used for retrofitting were Glass (G), Carbon (C), Aramid (A) FRP, and Hardwire (S).

The following issues were not addressed by this research:

- During the experimental work, the anchorage of the Fiber Reinforced Plastic (FRP) was achieved by means of steel plates which were used at the end of the FRP to anchor the FRP to the footing and head beam. Although the anchorage of externally bonded reinforcement is a recognized crucial aspect, it was not the goal of this research to test the anchorage of the retrofitting system. The anchorage can be studied using simple tests (e.g. direct tension tests). However, using the model proposed in the thesis, it is possible to predict shear stresses at FRP ends and hence estimate the ultimate load for anchorage failure.
- Out-of-plane behavior of URM walls and URM-FRP are not studied. The out-of-plane behavior of URM walls and URM-FRP are extensively discussed experimentally and theoretically in the literature (e.g. [KE 03], [AE 01], [HD 01], [HM 01], [VE 00a], [VE 00b], and [ES 99]).
- In this research, the cost benefits analysis is excluded; cost benefits analysis maybe found elsewhere [Pe 04]. Based on this cost benefits analysis, a decision has been made to have a retrofitting. This research includes the structural aspect of such retrofitting.

1.3 Organization of the Thesis

The thesis is divided into 7 chapters. The chapters are as follows:

- Chapter 1 introduces a statement of the problem and the objectives of this research.

- Chapter 2 presents a view of the literature available on the behavior of masonry walls retrofitted using FRP.
- Chapter 3 details the first phase of the experimental program in this study, namely, dynamic tests; this includes specimen design, retrofitting materials and configurations, instrumentation, and the synthetic earthquakes.
- Chapter 4 details the second phase of the experimental program in this study, namely, static cyclic tests of URM walls retrofitted using FRP; this includes specimen design, retrofitting materials and configurations, instrumentation, and the applied loading history.
- Chapter 5 introduces a physical model to estimate in-plane shear resistance of URM-FRP. The chapter includes model assumptions, governing deferential equation for URM-FRP, material behavior, and the development of a computer program to estimate the lateral resistance of URM-FRP. In addition, the chapter presents parametric study, comparisons with existing empirical models as well as with experimental work.
- Chapter 6 discusses the flexural behavior of URM-FRP. This includes simple estimations of in-plane lateral resistance as well as comparisons with estimated performance levels according to FEMA 356.
- Chapter 7 provides conclusions and recommendations for future work in the area of URM-FRP.
- Appendix A presents a literature review for conventional retrofitting techniques for URM walls.

1.4 Performance of URM Buildings during Earthquakes

The potential vulnerability of old, unreinforced masonry buildings was observed a long time ago (Figure 1.1); however, there is evidence that URM buildings can survive major earthquakes (Figure 1.2). The conditions required for satisfactory performance are not fully understood, and the usual modern analytical tools are often unable to discriminate appropriately [Br 94a].

Although the structural typology of masonry buildings varies in different regions, their damage resulting from earthquakes can be classified in a uniform way. Figure 1.3 presents general summary of causes of masonry cracking, partial, and/or total collapse. Note that, there is interaction between these causes and normally final collapse is due to one or more of these causes. In addition, in some cases cracking or even collapse happened due to pounding of adjacent buildings. Figure 1.5 demonstrates typical deformations and damages to structural walls of a simple masonry building subjected to seismic loads. Moreover, Figures (1.11 to 1.13) summarize some major failure patterns of URM buildings that have been observed during past earthquakes.

1.4.1 Seismic performance of unreinforced masonry walls

Masonry is non-homogeneous and anisotropic composite structural material, consisting of masonry units, and mortar. Masonry behavior is complex; its behavior is not perfectly elastic even in the range of small deformations. The accurate prediction of the lateral load capacity of URM walls is difficult because of the complex block-mortar interaction behavior. The principle in-plane failure mechanisms of URM walls subjected to earthquake actions can be summarized as following (Figure 1.4):
Shear failure: Walls with low aspect ratios and high axial loads tend to develop a diagonal cracking failure. This unfavorable mode of failure occurs when the principal tensile stresses, developing in a wall under a combination of horizontal and vertical loads, exceeds masonry tensile resistance. Just before the attainment of maximum lateral load, diagonal cracks are developed in the wall either follow the path of the bed- and head-joints for relatively strong bricks and weak mortars or may go through the masonry units in case of relatively weak bricks and strong mortars, or both. The high the vertical load, the more likely that the cracks go through the brick. For high axial load with diagonal shear mode of failure, explosive failure may happen.
Sliding mode: in case of low vertical loads and /or low friction coefficient, which maybe due to poor quality mortar, horizontal cracks in the bed joints can form a sliding plane extending along the wall length. This causes the wall upper part to slide on the wall lower part.
Flexural (rocking) mode: in case of high bending moment/shear ratio or improved shear resistance failure happens with the crushing of the compressed zones at the wall edges. This causes the overturning of the wall.
Combinations of flexural and shear behavior may exist for elements that first crack in flexure, then redistribute shear stress across a smaller un-cracked portion, and subsequently crack in diagonal tension. Also for low axial force and aspect ratio combinations of rocking and sliding might happen.

1.5 Improve the Seismic Performance of Masonry Buildings

Earthquake-resistant design technology has progressed significantly in the last few decades. Thus, several retrofitting strategies have been developed (Figure 1.14). Retrofit strategies are defined [fi 03] broadly as basic approaches that are targeted to improve seismic performance, such as increasing strength and/or stiffness or reducing seismic demand. To accomplish the required retrofitting strategy, several conventional retrofitting measures do exist for URM buildings. These methods suffer several disadvantages; Appendix A discusses the details of conventional exiting methods such as shotcrete, ferrocement, post-tensioning, centre core …etc. The focus of this thesis is to develop retrofitting of URM using FRP. Such retrofitting increase mainly the strength of the retrofitted URM wall and if appropriately integrated in the whole building will increase the strength of the building. In all cases, the foundation system should be capable of transferring the increased ultimate loads from the retrofitted upper structure into the soil.

1.5.1 Criteria for a structural intervention

As mentioned, several retrofitting strategies and measures exist for URM buildings. Several criteria play an important role in the choice of measures and strategies; the following are examples of such criteria:

- Costs, both initial and future (including maintenance cost and possible future damage) versus the importance of the building
- Available workmanship (it is of fundamental importance that the measures should be feasible with respect to available workmanship and equipment)
- Availability of appropriate quality control
- Occupancy (impact of the use during and after the works)
- Aesthetics (invisible or intentionally identifiable as a new structural feature)
- Preservation of the architectural identity of historical buildings, reversibility of intervention
- Duration of intervention

Examination of these criteria shows that FRP is a promising technique for retrofitting. Retrofitting is a multidisciplinary problem. Before beginning a seismic retrofitting program at the local, regional, or national level, cooperation is required between parties such as building owners, governmental authorities, engineers, architects, and contractors. In order to facilitate seismic retrofit, it is necessary to:

- Develop methodologies to evaluate seismic capacity
- Develop techniques to strengthen existing buildings
- Train engineers
- Prepare subsidies for financial assistance low-interest loan, tax exemptions
- Increase public incentives for seismic rehabilitation.

Compton Junior High School, Long Beach Earthquake, 1933

Figure 1.1: Totally collapsed one story building made of brick walls and wood roof (Courtesy of EERC Library)

Coalinga Library, Coalinga Earthquake, 1983

Figure 1.2: No damage to one story building (Courtesy of EERC Library)

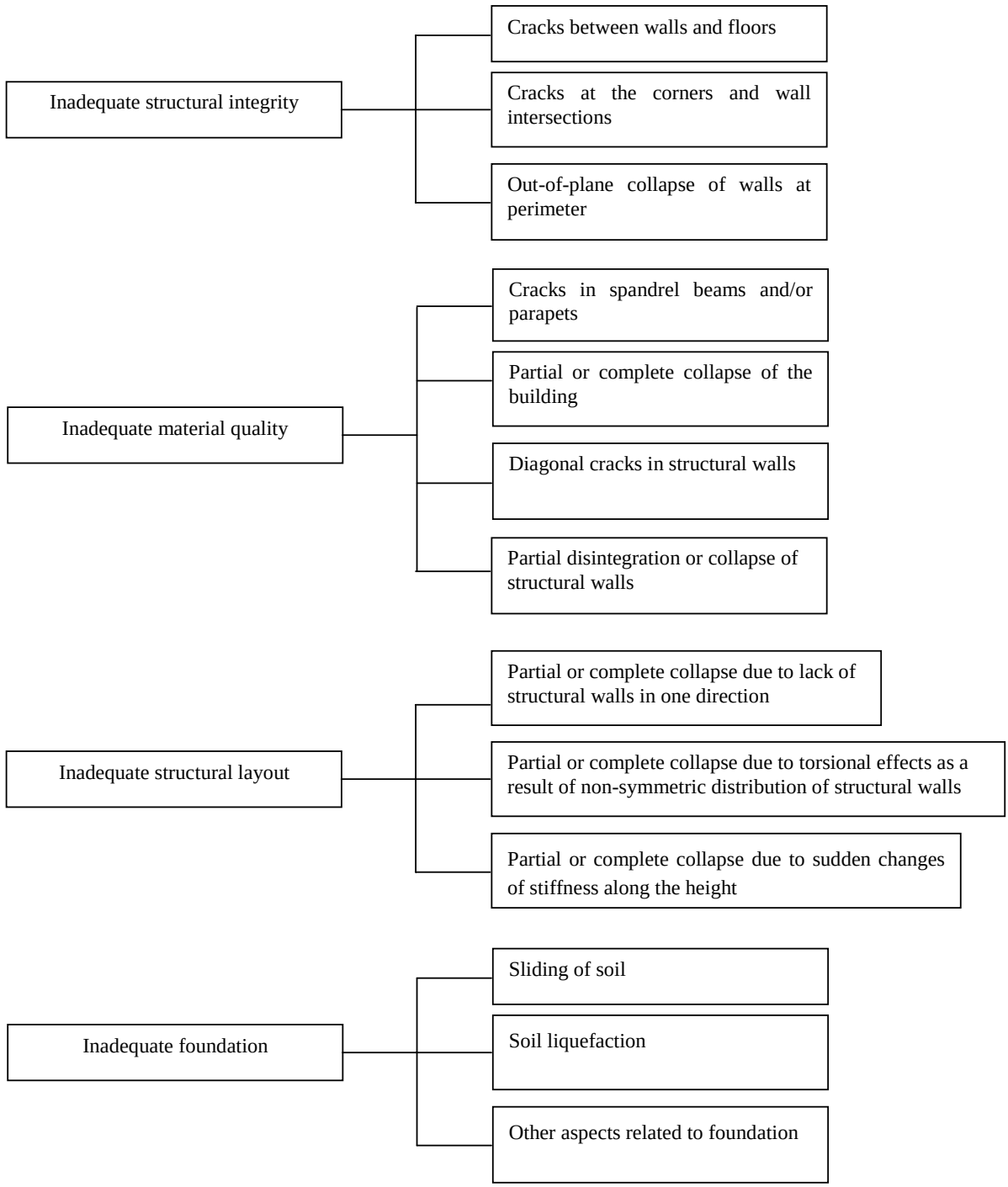

Figure 1.3: General summary of causes of unreinforced masonry cracking, partial, and total collapse

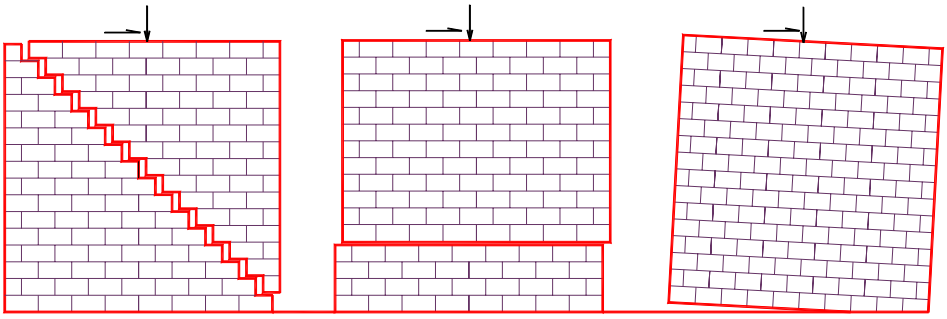

(a) (b) (c)

Figure 1.4: In-plane failure modes of a laterally loaded URM wall: a) shear failure, b) sliding failure, and c) rocking failure

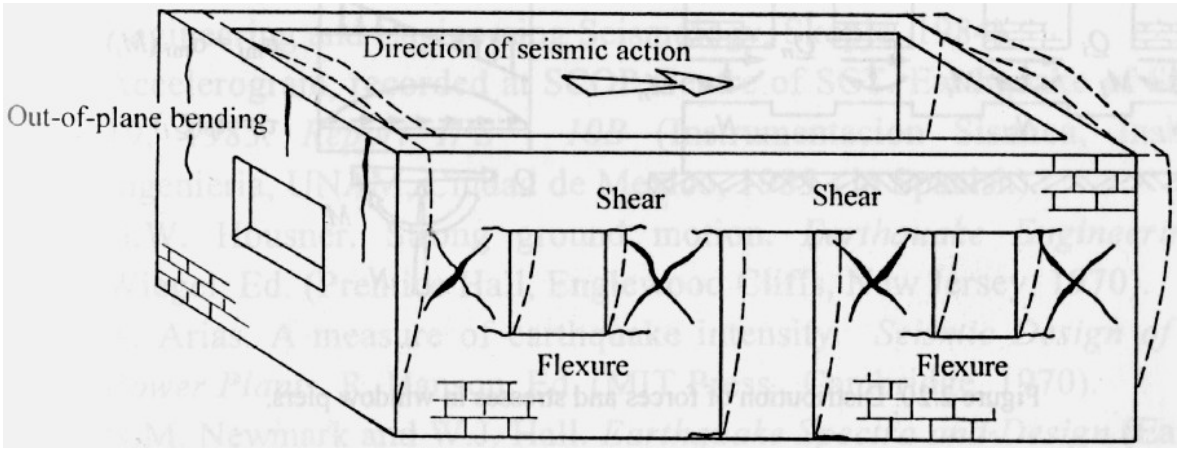

Figure 1.5: Typical deformation and damage to URM building (Courtesy of [To 99])

Figure 1.6: Cracks at the joints between walls and wooden floors (Courtesy of Tomazevic, personal communications)

Figure 1.7: Posočje, 1998: disintegration of a stone-masonry wall (Courtesy of Tomazevic, personal communications)

Figure 1.8: Montenegro, 1979: separation of walls at the corners (Courtesy of Tomazevic, personal communications)

North of Coalinga, Coalinga Earthquake, 1983 Downtown Coalinga, Coalinga Earthquake, 1983

Figure 1.9: Out-of-plane failure (Courtesy of EERC Library)

Watsonville, Loma Prieta Earthquake, 1989 Hollister Area, Loma Prieta Earthquake, 1989

Figure 1.10: Parapet failure (Courtesy of EERC Library)

Santa Monica, Northridge Earthquake, 1994

Watsonville, Loma Prieta Earthquake, 1989

Arvin, Kern County Earthquake, 1952

Long Beach Earthquake, 1933

Figure 1.11: In-plane shear failure (Courtesy of EERC Library)

Santa Cruz Area, Loma Prieta Earthquake, 1989

Figure 1.12: Combined out-of-plane/in-plane/pounding failure (Courtesy of EERC Library)

Hollister Area, Loma Prieta Earthquake, 1989

Figure 1.13: Hammering-induced cracking (Courtesy of EERC Library)

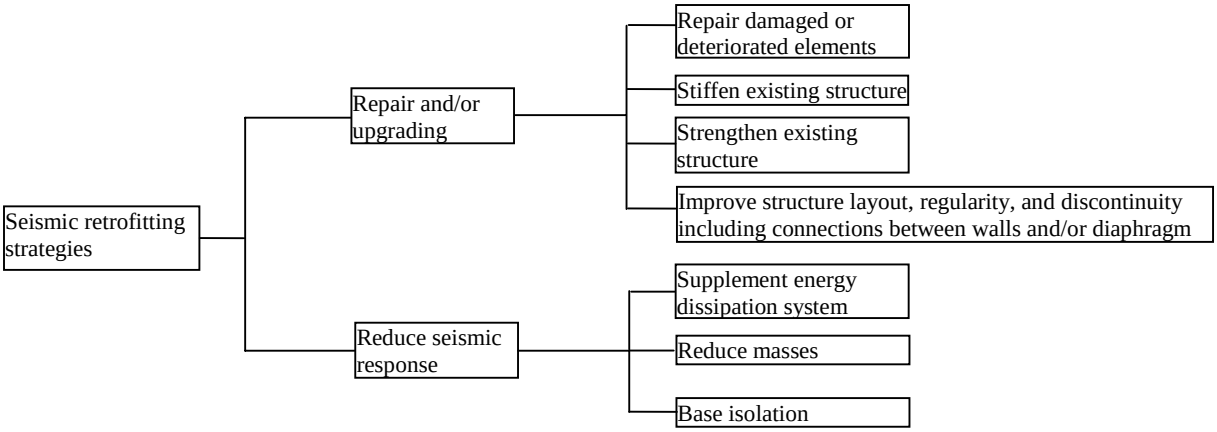

Figure 1.14: Seismic retrofitting strategies

2 LITERATURE REVIEW OF SEISMIC RETROFITTING OF MASONRY USING FRP

Numerous conventional techniques (e.g. shotcrete, grout injection, external reinforcement, center core, etcÖ) are available for retrofitting of seismically inadequate URM buildings. Appendix A summarized and discussed the advantages and disadvantages of these conventional techniques. The disadvantages of these techniques include: time consuming to apply, reduce available space, disturbance the occupancy, affect the aesthetics of the existing wall, etcÖ In addition, the added mass can also increase the earthquake induced inertia forces and may require strengthening of the foundations as well. Most of these problems may be overcome by using fiber reinforced plastic (FRP) instead of the conventional techniques. FRP includes different fiber types: glass FRP (GFRP), carbon FRP (CFRP), and aramid FRP (AFRP).

While extensive research was conducted and reported for retrofitting of reinforced concrete (r.c.) structures using FRP, much less has been reported for retrofitting of URM structures [LG 03, Tr 01]. As explained in Chapter 1, under seismic loading URM walls have two possible failure mechanisms: in-plane and out-of-plane. Therefore, researchers address either retrofitting to improve in-plane or out-of-plane behavior; this chapter attempts to cover both areas. Besides monotonic, static-cyclic and dynamic tests on URM-FRP, the chapter extends to cover tests carried out on reinforced masonry walls as well as triplet tests on masonry specimens retrofitted with FRP. Finally, the ultimate goal is to provide the spectrum of the experimental and theoretical research carried out on masonry walls retrofitted using FRP.

2.1 In-Plane Retrofitting of Unreinforced Masonry (URM) Walls

In the last decade, several static-cyclic and limited dynamic experimental tests have been carried out to investigate the in-plane behavior of URM-FRP. However, other experiments include small-scale diagonal tension test and triplet tests are more common [LG 03]. This chapter focuses on dynamic and static-cyclic experimental tests that carried out on URM-FRP. In general, these experiments show that URM-FRP have a force-drift relationship that is smoothly decreasing in stiffness and gaining resistance until there is a sudden loss of resistance (Figure 2.1). In addition, retrofitting of URM walls using composites increase the lateral resistance by a factor that ranged from 1.1 to 3 (Figure 2.1). However, the ultimate strength is not achievable unless other premature failure (e.g. anchorage) is controlled. URM-FRP exhibits the following modes of failure [ZX 03, HH 02, VG 02, AL 01, AH 99, RM 95, Sc 94]:

- Shear failure i.e. step cracks pass through either bed and head joint or masonry units
- Sliding i.e. complete separation at bed joints with a fracture of the fiber material
- Flexural failure
- Anchorage failure.

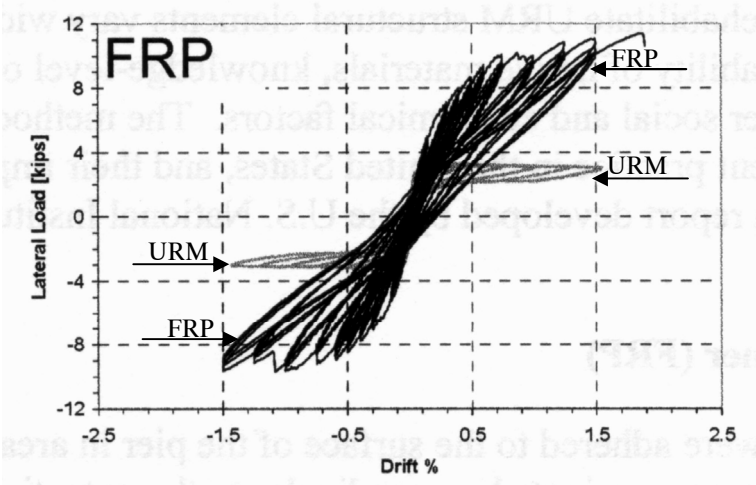

Figure 2.1: A superposition of the hysteresis curves of URM and URM-FRP specimens [AL 01]

2.1.1 Experimental Investigations on URM Walls

Static-cyclic tests

In the literature, the performed static-cyclic tests on URM-FRP covered wide range of aspect ratios (Table 2.1); specimens with aspect ratios ranged from 0.61 (squat) [Sc 94] to 2.0 (slender) [VG 02] have been tested. Normal stresses ranged from only the specimen own weight (i.e. no external normal force) [VG 02] to 1.2 MPa [ZX 03] have been applied on clay [MH 03, Sc 94, AL 01] or hollow concrete [ZX 03, HH 02, RM 95] brick masonry test specimens. GFRP [AL 01, HH 02, RM 95], CFRP [Sc 94, ZX 03], and/or polyester [Sc 94] were used for retrofitting of URM specimens. The FRPs were applied either on double sides [Sc 94, VG 02, ZX 03, AL 01, RM 95] or single side [Sc 94, HH 02] of precracked [ZX 03, AL 01] or uncracked [Sc 94, VG 02, ZX 03, HH 02, RM 95] specimens. FRPs increased the in-plane lateral resistance of URM by a factor that ranged from 1.1 to 2.6 (Table 2.2). The increment is influenced by the mode of failure (i.e. flexural or shear dominant), whether the retrofitting was applied on a single side or double side, and the specimen state before retrofitting (i.e. uncracked or precracked). However, other factors (e.g. reinforcement ratio and configuration) play a role in measured in-plane lateral resistance.

Schwegler [Sc 94] investigated the effectiveness of retrofitting on either one side or double sides. A comparison between two squats retrofitted specimens (single side BW1 and double side BW2 retrofitted specimens, Figure 2.2) shows that, in terms of stiffness and lateral resistance, up to the ultimate lateral resistance of the single side retrofitted specimen both specimens behaved in the same way (Figure 2.3). In addition, Reinhorn and Madan [RM 95] used different fabric reinforcement systems on the two sides of a test specimen (Figure 2.4). The difference in the reinforcement did not produce any discernible uneven (out-of-plane) displacement.

An important factor that influences the behavior of URM-FRP is the retrofitting configuration; Schwegler [Sc 94] used different retrofitting configurations (Figure 2.2). It was found that the best retrofitting configuration is the inclined plates (BW1, BW2, BW6) and the full surface coverage (BW7) (Figure 2.3). However, Zhao et al. [ZX 03] show that diagonal plates of CFRP significantly improved the lateral resistance of an uncracked specimen (Figure 2.5).

Other factor influence specimen behavior is whether the specimen is retrofitted after or before cracking. Zhao et al. [ZX 03] show that, for the same test parameters and using diagonal retrofitting configuration, while for uncracked specimen the retrofitting improved the ultimate lateral resistance by a factor of 1.5, for cracked specimen the retrofitting improved the ultimate lateral resistance by a factor of 1.1. In addition, the drift in the former case is approximately double the drift in the later case (Figure 2.5).

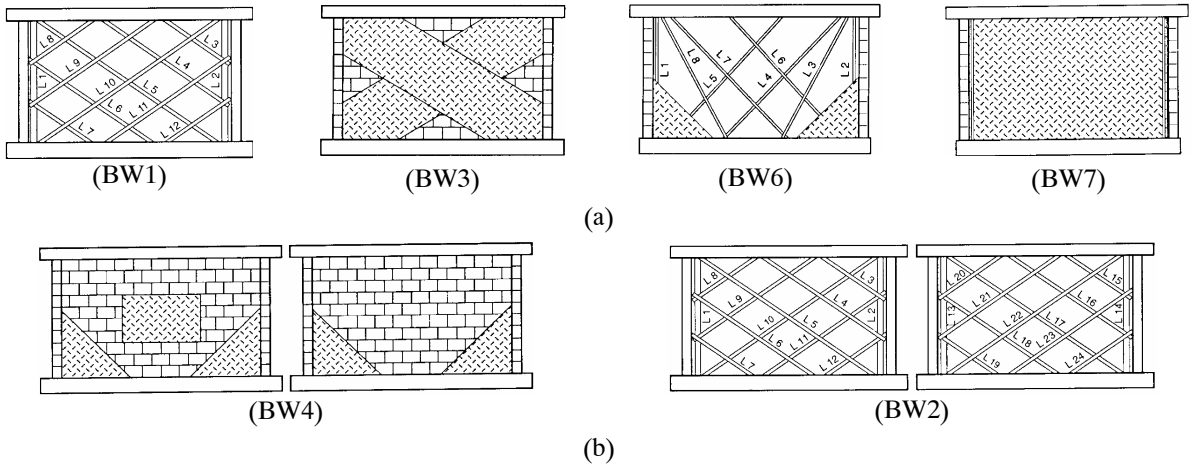

Figure 2.2: Different retrofitting schemes (a) one side, and (b) double side URM-FRP [Schwegler 1994]

Table 2.1: Literature review of the in-plane static cyclic tests carried out on URM-FRP

Reference	H/L	Retrofitting									Failure mode	Drift [%]	M.F.
		Configuration	Position	Mater-ial	FRP structure	Fiber orientation	NL	Dimensions [mm]	Strains				
									Warp	Weft			
Mosallam 2003	2.00	Full surface (horizontal)[a]	One S.	G	Fabric	unidirectional	1	1.3[b]	-	-	D.	0.6	1.19
Zhao 2003	0.71	-	-	-	-	-	-	-	-	-	D.C.	0.3	-
		Diagonal	Both S.	C	Plates	Woven	1	200 X 0.104[b]	0.34	0.05	D.C.	0.67	1.54
		Diagonal[c]		C					0.31	0.08	D.C.	0.36	1.11
Holberg 2003	1.38	Vertical	One S.	G	Plates	unidirectional	2	88.9X908	-	-	D.C.+ S	0.6[e]	1.8[f]
		Vertical[d] + diagonal					1				connection Failure	0.6[e]	2.4[f]
												0.6[e]	2.4[f]
												1.5[e]	2.4[f]
Abrams 2001	1.77	Vertical[g]	Both S.	G	Fabric	unidirectional	1	0.29[b]	-	-	D.C.	1.38	3
Reinhorn 1995	0.97	Full Surface[h]	Both S.	G	Fabric	Woven	1	-	-	-	D.+ T.	1.4	2.2
Schwegler 1993	0.61	Inclined	One S.	C	Plates	unidirectional	1	-	-	-	-	0.33	1.3
		Inclined	Both S.	C	Plates	unidirectional		-	-	-	-	1.18	1.72
		Diagonal	One S.	C	Fabric	Woven		-	-	-	-	0.2	1.13
		Corners[i]	Both S.	C	Fabric	Woven		-	-	-	-	0.6	1.07
		Inclined	One S.	C	Plates	unidirectional		-	-	-	-	1.01	1.43
		Full Surface	One S.	P	Fabric	Woven		-	-	-	-	0.57	1.33

H: specimen height L: specimen length NL: number of layers
M.F.: magnification factor i.e. increment in the lateral resistance due to the FRP
a: to reduce tendency of rocking, three layers of FRP were applied on the vertical direction b: layer thickness
c: cracked specimen d: two layers were used with vertical plates e: drift at max. lateral load
f: the test on the reference specimen was stopped just after rocking initiation g: the specimen was confined near its fixed end using FRP
h: different retrofitting configurations were used on both sides i: one face was retrofitted at its middle

Table 2.2: Increment in the in-plane lateral resistance of URM due to retrofitting using FRP

Parameters / Failure Mode	Specimen state before retrofitting		Position of retrofitting	
	Uncracked	Precracked	Single side	Double side
Flexural	-	-	2.3 [HH 02]	2.6* [FL 01, RM 95]
Shear	1.5** [ZX 03]	1.1** [ZX 03]	1.1-1.4 [Sc 94]	1.1 [Sc 94, ZX 03]-1.7 [Sc 94]

* In a single case [VG 02], the retrofitting improved the lateral resistance by a factor of 10. This value may be explained if we know that the reference specimen was tested under its weight only

** For the same test parameters and using diagonal retrofitting configuration,

The effect of FRP on the lateral drift of URM walls needs more experimental investigations and to be a primary goal of future research. During an experimental program and in order to quantify the effect of FRP on the drift of URM wall, the test on a reference (URM) specimen should be continued into the post-peak range (i.e. beyond ultimate load). In the literature, several research programs stopped the tests on reference specimens at or before their peak lateral force. They stopped the tests and retrofitted the cracked ìreferenceî specimen and test it again, since the primary goal of the research was to quantify the increment of the in-plane lateral resistance of URM due to FRP. However, the available experiments show that the FRP has insignificant effect on URM drift in case of flexural failure [AL 01]. In case of shear failure [Sc 94], the FRP improved the total drift by a factor of 3.0. As with the lateral resistance, the retrofitting configurations [Sc 94] and whether the specimen is retrofitted before or after cracking [ZX 03] influence the drift performance.

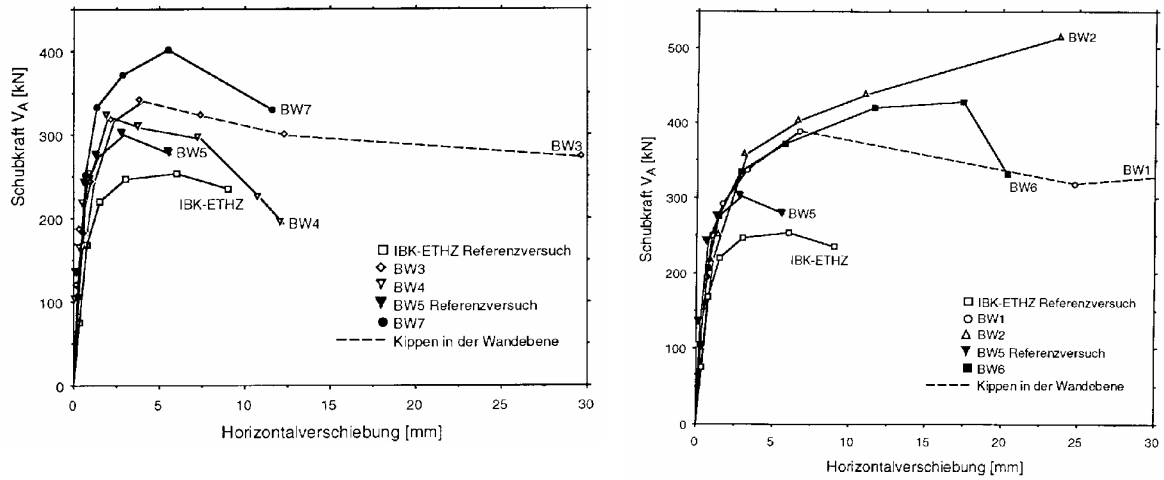

Figure 2.3: Backbone curves for URM specimens (IBK-ETHZ and BW5) as well as a single side (BW1, BW3, BW6, and BW7) and double sides (BW2 and BW4) URM-FRP [Sc 94]

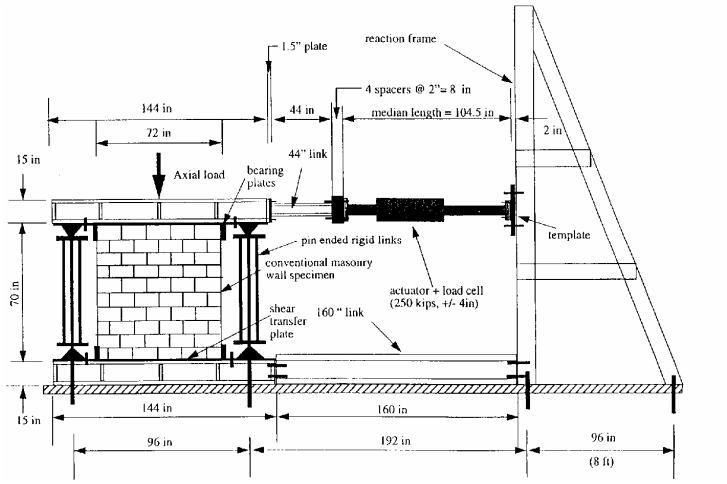

Figure 2.4: Test set-up with pin ended rigid links to restrained the overturning response of a specimen subsequent to flexural cracking at wall base [RM 95]

For seismic loading, the energy dissipated by the structural system through its components is an important issue. The same factors that influence the URM-FRP lateral resistance affects the energy dissipated by the URM-FRP. In addition, unlike the lateral resistance of URM-FRP, the FRP structural shape (i.e. grid, fabric, plates, etcÖ) influences the energy dissipation. In the available literature, the issue of energy dissipation is treated qualitatively and more research is required to investigate and quantify this important issue. Qualitatively, the URM-FRP has a limited capability to dissipate energy. In order to improve the drift and energy dissipation as well as to gain the advantages of composites, Holberg and Hamilton [HH 02] combined unidirectional GFRP with either external connection (conventional structural steel angle-plate, Figure 2.6a) or internal connection (i.e. reinforcing steel bars) that was designed to yield before the composite ruptured, resulting in a ductile failure mode. The connection was employed to transfer uplift from slender specimens to the concrete base (Figure 2.6b). However, in several cases the specimens failed due to out-of-plane eccentricity with a limited drift of 0.6%. In one case with internal connection, the system failed due to yielding of the steel bars this leads to a drift of 1.5% with high-energy dissipation (Figure 2.6c).

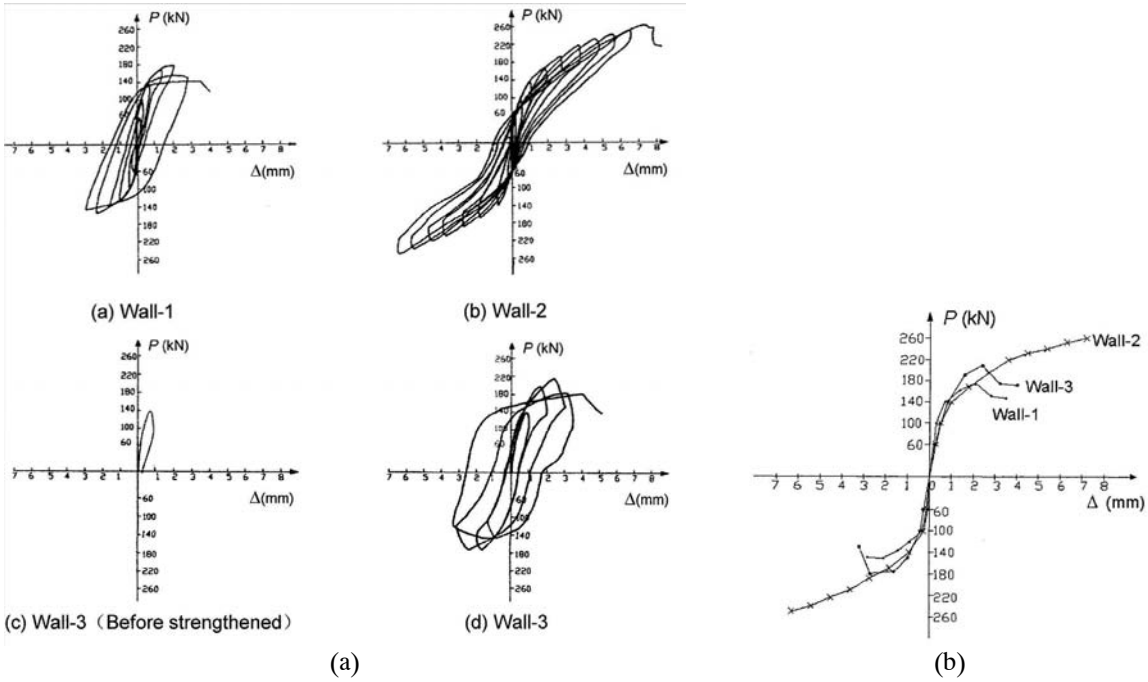

Figure 2.5: (a) Hysteresis and (b) backbone curves for URM wall (wall-1), uncracked URM-FRP (wall-2), and precracked URM-FRP (wall-3) [ZX 03]

Dynamic tests

To-date only a single dynamic experimental program was carried out on URM-FRP. Al-Chaar and Hassan [AH 99] tested a model specimen on tri-axial shaking table; the model specimen consisted of two unreinforced bearing walls with a reinforced concrete slab spanning them. One side of one wall was retrofitted with composites; the other wall was a typical as-built panel (Figure 2.7). The model was tested until the unretrofitted wall exhibited crack formation. Then the damage wall was reinforced with a layer of composites and the model was tested again. Another series of in-plane tests were also performed until failure was reached in the model. The test results show that the composite overlay enhances the seismic resistance of the retrofitted walls.

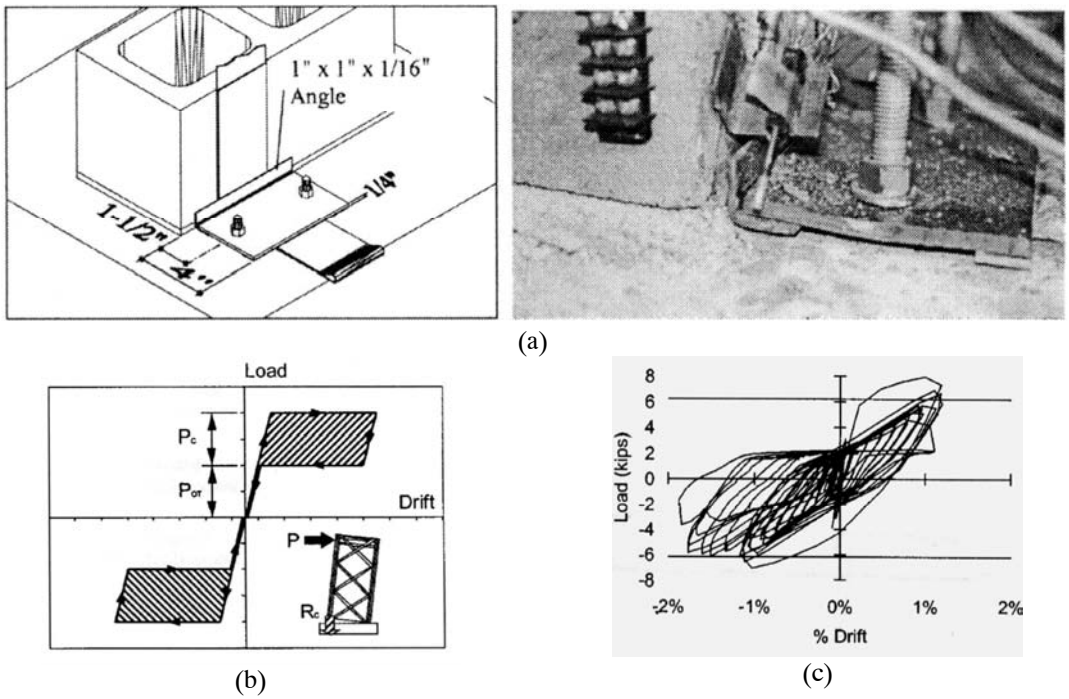

Figure 2.6: Ductile connection (a) external connection, (b) energy dissipation (the area between cracking load (P_{cr}) and connection yielding load (P_c) i.e. hatched area), and (c) hysteresis curves for a specimen with internal connection [HH 02]

Figure 2.7: A model specimen after testing on a tri-axial shaking table [AH 99]

2.1.2 Design models

Flexural design

A common method to calculate the flexural capacity of structural elements is the use of linear elastic approach. It is an easy method and intended to incorporate a realistic behavior of a URM-FRP by assuming that it behaves linearly up to failure. Similar to design of r.c. elements, design equations for URM-FRP are derived by replacing the flexural steel reinforcement with FRP flexural reinforcement [Tr 98]. The derivation based on several assumptions; of them:

- Full composite action between composite material and the brick surface is assumed
- Plane section remains plane before and after deformations.

The calculated lateral resistance of URM-FRP, using this approach, was approximately 1.8 [FL 01] of the measured (experimental) lateral resistance.

Shear design

The shear resistance of a URM-FRP can be calculated as the sum of URM shear resistance and shear resistance of FRP reinforcement [Tr 98]. The shear resistance of FRP reinforcement can be calculated as in equation 2.1 :

$$F_{FRP} = \rho_h \, E_{FRP} \, \varepsilon_{tu} \kappa \, t \, L \qquad (2.1)$$

where F_{FRP} is the contribution of FRP in the lateral resistance of URM specimen, ρ_h is the reinforcement ratio of FRP in horizontal direction, E_{FRP} is the modulus of elasticity of FRP, ε_{tu} is the ultimate strain of FRP, κ is an efficiency factor, t is the wall thickness, and L is the wall length. For a given URM-FRP, the only unknown in the above equation is the efficiency factor; several values are proposed for the efficiency factor. Triantafillou [Tr 98] derived an empirical polynomial function, for reinforced concrete beams, that relates the strain in the FRP at shear failure of the member to the axial rigidity of the composites $\rho_h E_{FRP}$. This polynomial was derived through curve fitting of 40 test data on r.c. beams published by various researchers. Triantafillou [Tr 98] proposed to use the same polynomial for masonry walls. Based on diagonal tension test on two specimens retrofitted using GFRP, Nanni and Tumialan [NT 03] proposed a value of κ equal to 0.3.

Similar to Triantafillou [Tr 98], Zhao et al. [ZX 03] calculated the shear resistance of URM-FRP as the sum of URM shear resistance ($P_{u,B}$ in Figure 2.8(a)) and shear resistance of FRP reinforcement ($P_{u,CFS}$ in Figure 2.8(a)). The shear resistance of FRP reinforcement had two components; the forces in the warp (T_{cf1} in Figure 2.8(b)) and in the weft (T_{cf2} in Figure 2.8(b)) directions. In order to calculate the ultimate stresses in the warp FRP and based on static-cyclic tests on two specimens, Zhao et al. [2003] proposed a value of κ equal to 0.2 for precracked and 0.3 for uncracked specimens. For ultimate stresses in the weft direction, it is proposed a κ equal to 0.03 for precracked and uncracked specimens. Using these strains and proposed model, the experimental results is approximately 113% of the calculated one.
In Eq. 2.1, AC125 [2001] proposed that ($\varepsilon_{tu} \kappa$) is equal to 0.004; however, ($E_{FRP} \, \varepsilon_{tu} \kappa$) should be less than 0.75 of the ultimate resistance of the FRP. Mosallam and Haroun [MH 03] used the recommendations of AC125 to calculate the shear capacity of URM-FRP. The comparison between the calculated values and the experimental results show that the AC125 overestimate the shear resistance by 40%.

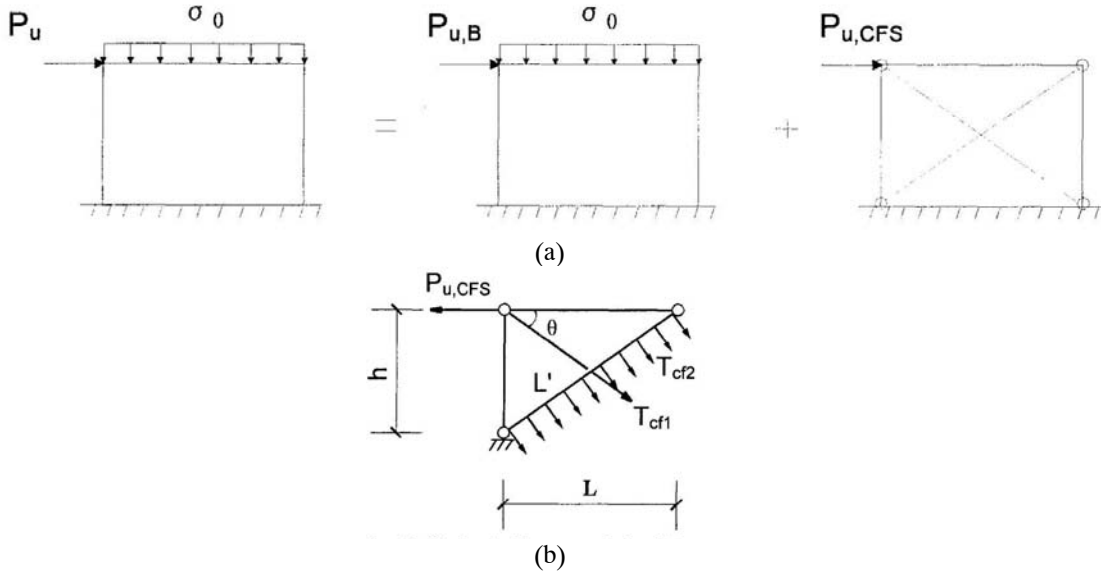

Figure 2.8: Proposed model for URM retrofitted using diagonal strips of FRP (a) calculation scheme, and (b) calculation model for the ultimate load ($P_{U,CFS}$)[ZX 03]

2.2 Out-of-Plane Retrofitting of URM

In the last fifteen years extensive efforts to investigate the out-of-plane behavior of URM-FRP have been done. Several researchers examining the possibility of applying FRP to brick masonry beams (e.g. [ES 91]). The tests show that beams had linear load deflection behavior until failure. However, this chapter focuses on

investigations carried out on walls rather than masonry beams. The experimental works carried out to investigate the out-of-plane behavior of URM-FRP limited to monotonic and static-cyclic loading (i.e. no dynamic tests). In general, these experiments show that retrofitting of URM walls using composites dramatically increase the flexural strength. However, the ultimate flexural strength is not achievable unless other premature failure (e.g. debonding or shear at supports) is controlled. Available literature indicates that URM-FRP exhibit the following modes of failure (Figure 2.9):

- Sliding shear i.e. complete separation at a mortar joint in the shear region with a fracture of the fiber material
- Flexural failure (either masonry compression failure or fiber rupture)
- Combination shear-flexural failure i.e. flexural cracks started at the region of maximum bending region then it continues at 45 degree as shear crack
- Delamination
- Combination of delamination and pullout of face shell
- Interface shear failure in case of multiple wall leaf.

[GT 03]

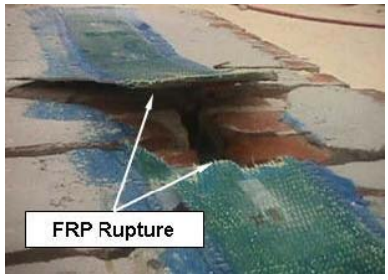

[GT 03]

[GT 03]

[GT 03]


[HD 01]

Figure 2.9: Different failure modes of URM-FRP tested in out-of-plane

2.2.1 Experimental investigations on URM

Monotonic tests

Simply supported URM-FRP specimens (Table 2.3) with slenderness ratios ranges from 4.7 [HM 03] to 23 [HD 01] were tested under three [HH 99] or four points bending loading [HM 03, HM 02] as well as uniform loading [HM 01, HD 01]. Different parameters have been tested: brick type (hollow concrete [HH 99, HD 01, HM 01, 02, 03] and clay [TM 02, Tu 01]), fiber type (GFRP [HM 01, 02, 03, HD 01] and AFRP [TM 02]), reinforcement ratio, number of layers (from 1 layer to 8 layers), and surface preparation (using wire brush and sand blasting [HM 01] as well as putty or not [NT 03]).

The results of these tests show that FRP increased the out-of-plane resistance of the retrofitted specimens by a factor of approximately 20. In other terms, the URM-FRP specimens resisted a lateral load that is comparable to a load resulting from the inertial forces of several times the gravity acceleration. In addition, the out-of-plane deflection was about 1/60 of the wall height, which is about 10 times the limit deflection required in recent Codes. Different modes of failure happened during the tests.

Table 2.3: Literature review of the out-of-plane monotonic tests carried out on URM-FRP

Reference	H/t	Retrofitting									Failure mode	Deflection	M.F.
		Configuration	Position	Mater-ial	FRP structure	Fiber orientation	NL	Dimensions	Strains				
									Warp	Weft			
Hamuosh 2003	4.7	Full Surface	One S.	GFRP	Fabric	Bidirectional	1	0.35 X 600	-	-	S. + F.	2.5[a]	-
							3				S.	2.4[a]	-
							5				S.	2.7[a]	-
							8				S.	3[a]	-
							2				S.	3.5	-
Tumialan 2002	12.3	Vertical	One S.	AFRP	Plates	Unidirectional	1	75 X 0.35			D.		
								125 X 0.35			D. or F.F.		
								175 X 0.35			D.		
								225 X 0.35			F.+S. or D.		
								300 X 0.35			F.+S. or S.		
				GFRP				75 X 0.28	1.5-2.3		D./F.F.		
								125 X 0.28	1.2-2.0		D./F.F.		
								175 X 0.28	-		D.		
								225 X 0.28			F.+S.		
								300 X 0.28			F.+S. or S.		
Hamuosh 2002	9	Full Surface	One S.	GFRP	Fabric	Bidirectional	2	0.4 thick	-	-	S.	2.9[b]	-
							1					3.2[b]	-
Hamuosh 2001	9	Vertical + Horizontal	One S.	GFRP	Fabric	Unidirectional	1	459 X612 X 1.3	0.3		S.	9.0[a]	20[a]
												7.0[a]	17[a]
		Full Surface				Bidirectional		0.4 thick				9.1[a]	19[a]
												7.8[a]	22[a]
Hamilton 2001	9	Vertical	One S.	GFRP	Plates	Unidirectional	1	69.9 X 0.32	-	-	D.	-	-
											F.F.+D.		
											F.F.		
											F.F.+D.		
	23						2	139.8 X 0.32			F.F.+D.	h/60	
							1	279.6 X 0.32	0.5		F.F.	h/55	

H: specimen height L: specimen length NL: number of layers
M.F.: magnification factor i.e. increment in the lateral resistance due to the FRP a: average of three specimens b: average of six specimens

For specimens with slenderness ratio of 4.7 [HM 03], shear at supports dominated the failure of the specimens. Other specimens with slenderness ratios up to 12 [HM 01, 02, HD 01, TM 02], shear failure [HM 01, 02], shear/flexural failure [TM 02], delamination [HD 01, TM 02], or fracture of composites happened [HD 01, TM 02]. For specimens with slenderness ratio more than 20 [HD 01], composite fracture dominated the failure of the specimens. However, other factors such as the reinforcement ratio and stiffness, brick type and compressive strength, and surface preparation play an important role in determining the mode of failure.

Another factor that influences the behavior of URM-FRP is the reinforcement ratio. Increasing the thickness of reinforcing fiber layers slightly increases the load caring capacity of the masonry wall system (Figure 2.10). However, beyond a certain upper limit of fiber area this increase levels off and reinforcing with more fiber area beyond this value does not appear to increase the wallís capacity significantly [HM 03]. Regarding the dowel action, Hamoush et al. [HM 02] found that no significant effect of the extension of the fiber to the support on the shear strength of the test specimens. However, using two layers of GFRP (double the reinforcement ratio) the structural integrity increased and the variation in the behavior of the retrofitted walls reduced, especially when the overlays are extended to the supports. For high values of glass fiber, high scatter in the experimental values of the initial stiffness appeared. This scatter suggested that the masonry begins to dominate the behavior of the wall system. In addition, Hamilton and Dolan [HD 01] show that for the same reinforcement ratio placing the strips directly on the masonry surface is better than using double-layered strips. Using several strips or plates provides redundancy in which each strip maintains its integrity until its strain capacity has been reached.

A less important factor that influences the behavior of URM-FRP is the surface preparation. Hamoush et al. [HM 01] have explored that using wire brush or sand blasting as surface preparation or even no surface preparation has insignificant influence on either stiffness or lateral resistance of concrete masonry walls. However, Nanni and Tumialan [NT 03] show that using putty as surface preparation for clay masonry walls improves both delamination and debonding load.

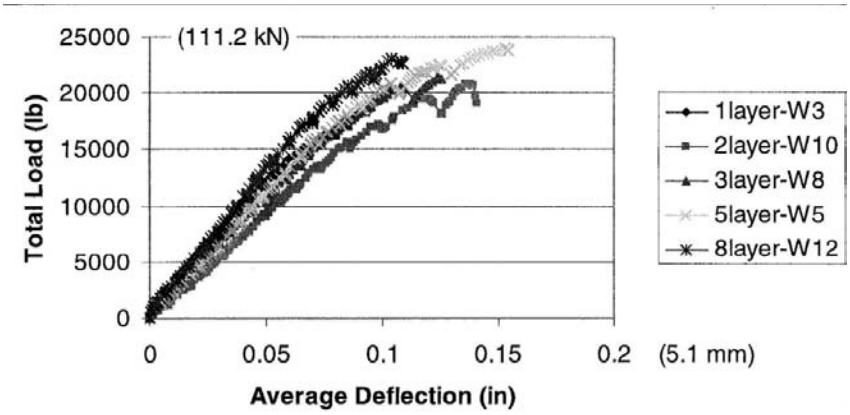

Figure 2.10: Comparison load vs. deflection for various numbers of layers [HM 03]

Static-cyclic tests

Velazquez [Ve 98] subjected seven half-scale URM walls retrofitted with FRP strips to out-of-plane cyclic loading. This study investigated various parameters: number of wythes (either single or double wythes) the wall height to thickness ratio (either 14 or 28) and the reinforcement ratio (ranges from 0.3 to 3 times the balance reinforcement ratio i.e. the reinforcement ratio at which the reinforcement steel reach its yield simultaneously with compression failure ,at the out most fiber, of concrete). Figure 2.11 gives a summary of the experimental results for different test specimens; it is worth to note that the S and D in the figure means single or double wythe and the numbers that follow the S/D are the percentage of the reinforcement amount with respect to the balance reinforcement. The experimental results show that the composites increased the out-of-plane resistance of the retrofitted specimens by a factor of 7.5. In other terms, the retrofitted specimens resisted a lateral load that is comparable to a load resulting from the inertial forces of 5 to 24 times the gravity acceleration. In addition, the out-of-plane deflections ranged from 1/25 to 1/75 of the wall height (Figure 2.11(a, b)). Specimens rotated at the top and bottom supports up to 7.5 degrees (Figure 2.11(c)). This gave an indication of how the composite strips transform a brittle wall into a flexible one. In most cases and after the specimens were subjected to a large number of loading cycles, peeling off of the composite strips controlled the specimens behavior. Specimens that failed due to excessive delamination, showed larger deflection and rotation capacity but less stiffness than

specimen that failed due to GFRP rupture. Regarding energy dissipation, failure due to excessive delamination proved to be a slowly progressing phenomenon, resulting in more dissipated energy when such failure took place. Moreover, to avoid very stiff behavior and for improved hysteretic response, the reinforcement ratio should be limited to two times that of the balanced condition.

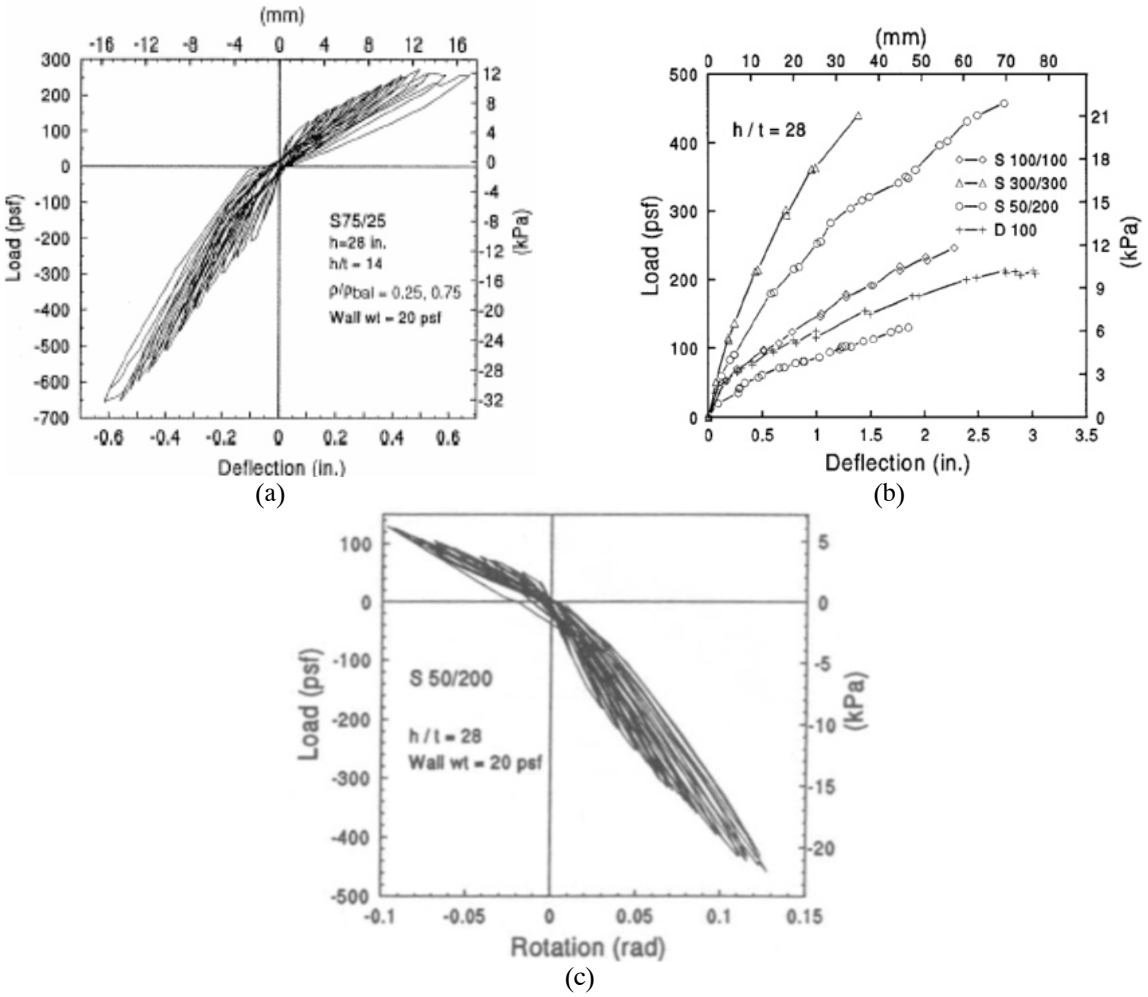

Figure 2.11: Static-cyclic test results (a) load vs. deflection at wall mid-height, (b)envelop for different test specimens, and (c) load vs. rotation at top support [Ve 98]

Dynamic tests

To date no dynamic tests have been carried out on URM-FRP.

2.2.2 Design models

Flexural design

Three approaches have been used to design URM-FRP for out-of-plane loading: yield line analysis, linear elastic approach, and classical laminate plate theory. Gilstrap and Dolan [GD 98] used the yield line analysis to predict the ultimate load capacity of two URM-FRPs. Although the cracks formed during the test were typical for yield line analysis, this procedure overestimated the ultimate load by a factor of 7. They attribute this unreliable prediction to the delamination process, which prevent composites from mobilized their ultimate strength.

Similar to in-plane flexural design, several researchers recommended using linear elastic approach to design URM-FRP for out-of-plane flexural. If other failure modes (e.g. debonding) are avoided, this approach fairly predicts the flexural capacity. For specimens that designed to fail in flexural, this analysis design approach

overestimated the resistance by a factor that ranged from 1.14 [HM 03] to 0.85 [HD 01]. However, to avoid other premature failure modes (e.g. debonding) Nanni and Tumialan [NT 03] suggested using κ (an efficiency factor) of 0.65 for clay masonry with putty and 0.45 for concrete masonry wall without surface preparation. The proposed κ factor was estimated based on comparisons between the calculated and experimental moment of resistance of several URM-FRP (Figure 2.12). Moreover, to avoid shear failure it was suggested to limit the adjusted reinforcement ratio (ω_f) to 0.6. The adjusted reinforcement ratio was introduced and defined as in Eq. 2.2

$$\omega_{FRP} = \frac{\rho_{FRP} E_{FRP}}{f'_m\left(\frac{h}{t}\right)} \tag{2.2}$$

where fí$_m$ is the masonry compressive strength and h/t is the wall slenderness ratio.

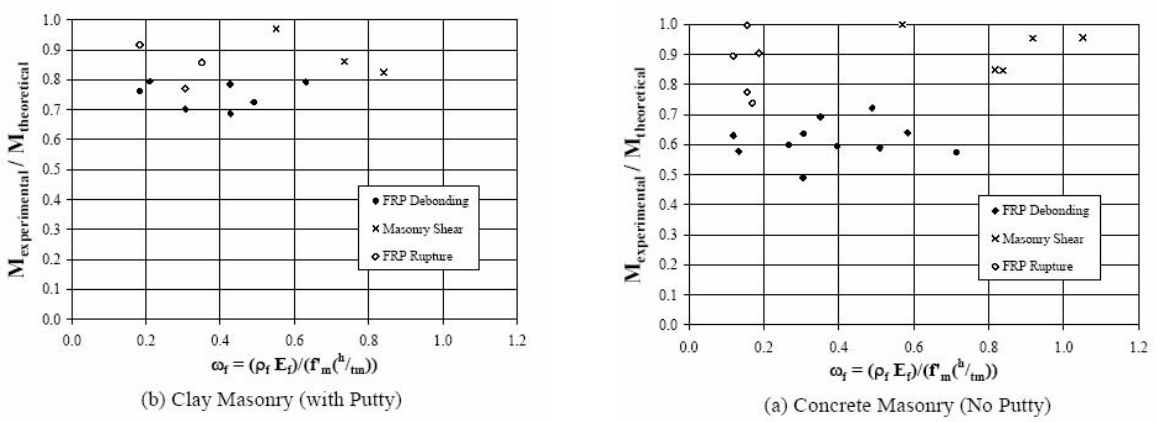

Figure 2.12: Influence of adjusted reinforcement ratio on the experimental/theoretical moment of resistance and modes of failure

Hamilton and Dolan [HD 01] recommended to design URM-FRP for the under reinforced condition. This accomplishes the following:

- It avoids having to predict the strength of an over reinforced cross section. This is made difficult by the sensitivity of the flexural strength to the masonry strength. Thus, it is necessary to have a good estimate of the in-place masonry strength. This requires in-place compression testing or removal of samples from the existing masonry compression tests
- It forces the failure to occur in the FRP composite.
- When designing the strengthening system, the engineer has much more confidence in the strength of the FRP composite as compared with the strength of the underlying masonry.

To determine the different limit states of URM-FRP, Velazquez [Ve 98] related these limits states to a certain values of longitudinal strains in composites. Based on their experimental work, longitudinal strains of 0.4%, 0.55%, and 1% are assumed to occur in composite strips when the first visible bed-joint crack, first fiber delamination, and fiber rupture take place, respectively. These strains values were proposed for glass fiber with approximately 2% ultimate strain. Similar to the limits by the UBC (Uniform Building Code) on the service load deflection of reinforced concrete masonry walls, it was recommended to use the same limit for URM-FRP (1/143 or 0.007 of the wall height). In addition, modifications of a constant in the UBC equations to calculate mid-height wall deflection are suggested for cracking and delamination loading level.

Velazquez et al. [VE 02] used classical laminate plate (CLP) theory to develop a model of the out-of-plane behavior of URM-WUC. Before cracking, the URM-FRP was simulated as three symmetrical layers: composite layer, masonry layer, and composite layer. By this way the bending extensional coupling stiffness matrix reduced to zero and a mathematical solution can be found. After cracking, masonry layer was divided into two layers: the first one represents the compressed zone (uncracked) and the second one represents the cracked zone (Figure 2.13). The compressed zone depth was calculated based on beam theory (Figure 2.13). Based on this model, Velazquez et al. captured the force deformation curves of seven URM-FRPs [Ve 98]. However, using CLP theory it is not possible to take into considerations delamination phenomena.

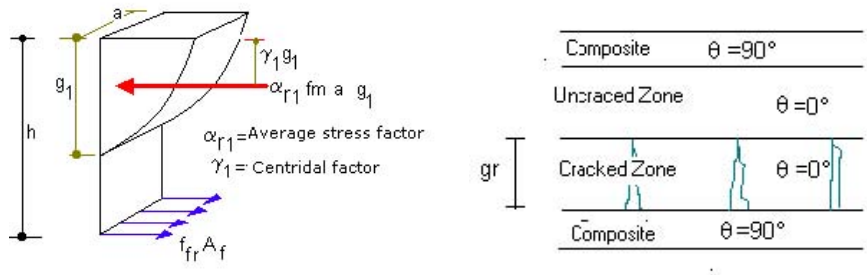

Figure 2.13: Cracked cross sectional and stress distribution [VE 02]

Shear design

In case of low slenderness ratio and/or high reinforcement ratio, shear failure may take place near supports. Hamoush et al. [HM 01, 02, 03], based on own experimental program, evaluated the shear strength of hollow concrete masonry walls assuming that the maximum shear stress occurred in the web of the blocks (i.e. not in the mortar joints) at failure. The shear stress was calculated using the maximum applied load and the standard elastic shear stress formula (VQ/I (B-b)) (where V is the shear force, Q is the first moment of the areas from the neutral axis of the solid portion of the block, I is the moment of inertia, B is the total width of the wall, and b is the total width of the cell) as directed by MSJC. The average calculated shear stress for test specimens was three times the allowable shear stress.

2.3 In-Plane Retrofitting of Reinforced Masonry Walls

Haroun et al. [HMA 03] subjected six full-scale masonry walls to cyclic loading. The specimens were full grouted and reinforced with five vertical reinforcement bars with reinforcement ratio of 0.54%. To simulate existing seismically inadequate masonry buildings no horizontal reinforcement were used in the specimens. This absence of horizontal reinforcement led to diagonal shear failure of the reference specimens (Figure 2.14). For the retrofitted specimens, Several parameters have been investigated: single or double sides retrofitting, whether the specimens were precracked or uncracked, fiber material type, and retrofitting configurations. The retrofitting increased the lateral resistance by a factor of 1.26 for double sides retrofitting and 1.16 for single side retrofitting. Unlike URM-FRP, whether the masonry specimen was retrofitted after or before cracking did not influences the test results. However, Haroun et al. [HMA 03] did not apply FRP directly on the cracked specimen: the cracked reinforced masonry specimen was first retrofitted using high strength epoxy resin, and then the FRP was applied. In addition, after applying the FRP, the pre-damaged toe was confined using U-shaped laminate. Regarding retrofitting on one or double side, both give approximately the same lateral resistance. However, the behavior of the specimens that retrofitted on double side was dominated by compression failure at the toes. The behavior of the specimens that retrofitted on single side was dominated by a combination of diagonal shear and toe compression failure.

Figure 2.14: Shear failure of reference reinforced masonry wall [HMA 03]

2.4 Out-of-Plane Retrofitting of Reinforced Masonry walls

2.4.1 Monotonic tests

Albert et al. [AE 01] subjected ten full-scale masonry walls to four points monotonic loading. The specimens were reinforced with no 9 gauge joint reinforcement every third course. To simulate existing seismically inadequate masonry walls no vertical reinforcement were used in the specimens. Several parameters have been investigated: fiber type (GFRP, CFRP), fiber structural shape (plats, sheet), retrofitting configuration, reinforcement ratio, normal stress level. Two modes of failure mainly happened during the experimental program: shear-flexural and flexural. These two modes are corresponding to modes of failure observed for URM-FRP. In addition, the test shows that, the load deflection curve the retrofitted specimens can be divided approximately into two distinct phases (Figure 2.15): gradual arc and straight line. The first phase of the curve mainly depends on the masonry properties and the applied normal force. The specimen that has the highest normal force has the highest initial stiffness. The second part of the curve represents the contribution of the FRP to the behavior of the specimens. However, the level of the normal force influences the slop of the second part of the curve due to the second order effect. It is worth to note that, for the same parameters, the loading type (either static-cyclic or monotonic) did not alter the characteristics of the curve. In addition, the slop of the second phase is found to be linearly proportional to the fiber adjusted stiffness. They define the fiber-adjusted stiffness as the fiber reinforcement ratio times the youngís modulus of the fiber. Finally, the characteristics of the load deflection curve were determined based on the strains measured in FRPs during the experiments. Although the model is based on strains measured during the test, the measured/predicted loads at cracking ranged from 0.6 to 1.6 and at ultimate load ranged from 0.5 to 1.3.

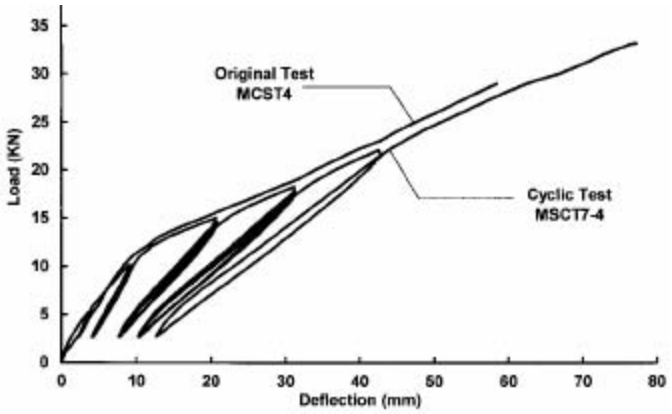

Figure 2.15: Load deflection response of monotonic and static-cyclic specimens [AE 01]

2.4.2 Static-cyclic tests

Kuzik et al. [KE 03] subjected eight full-scale reinforced masonry walls to four points static-cyclic loading. The specimens were reinforced vertically with different steel reinforcement ratios and horizontally with no 9 gauge joint reinforcement every third course. Several parameters have been investigated: FRP reinforcement ratio, flexural steel reinforcement ratio, normal stress level. Similar to monotonic tests [AE 01], the shear-failure mode dominated the failure of the specimens. The important parameter that influences the behavior of the specimens was the FRP reinforcement ratio. In addition, the steel reinforcement ratio mainly influences the ultimate resistance of the specimen. The normal force did not play an important role in the behavior of the specimens. It was proposed to use a model follows the rules of the Q-hysts model to predict the envelope of the behavior of the specimens. In order to determine the transition moment M_t (point c, Figure 2.16), Kuzik et al. multiplied the cracking moment M_r by an empirical factor based on FRP reinforcement ratio (Figure 2.17). In addition, a regression analysis was used to determine the ultimate strain of the FRP; this empirical ultimate strain was used with linear analysis to determine the ultimate moment Mu (point F, Figure 2.16)

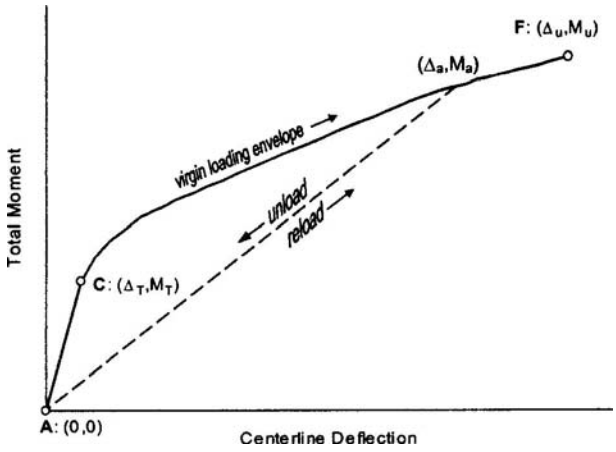

Figure 2.16: Proposed model for bending moment versus deflection response [KE 03]

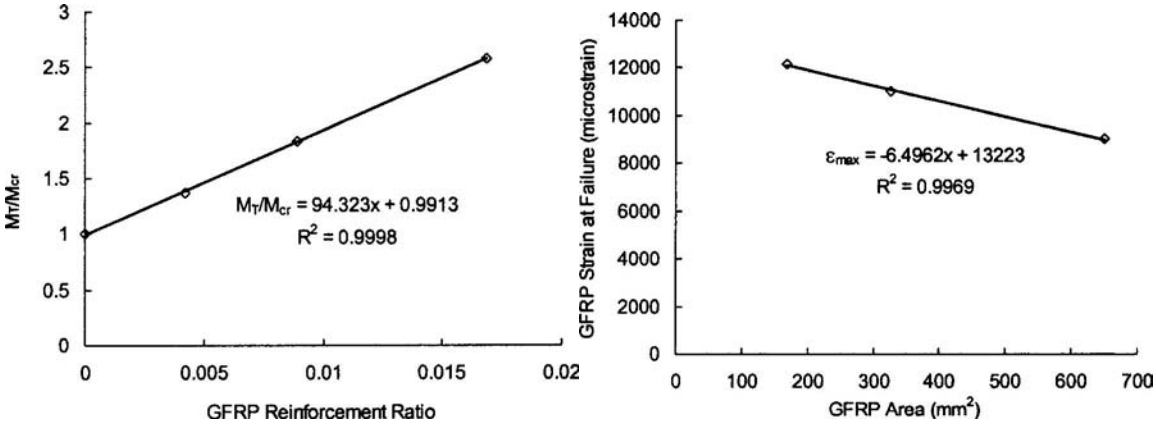

Figure 2.17: Regression analysis for transition moment and GFRP ultimate strain [KE 03]

2.5 Triplet Tests on Masonry Prisms Retrofitted Using FRP

To date, the triplet test is one of the simplest tests for assessing the shear strength of masonry walls. Several researchers started to use the same test to study the shear behavior of URM-FRP (Figure 2.18). Of them, Ehsani et al. [ESA 97] was the first to carry out triplet test on URM-FRP. Recently, in the US army corps of engineers they carried out tests on hundred triplet test specimens [BA 02]. These tests [ESA 97 and BA 02] examined several test parameters: different normal forces (ranged from zero to 100% of the masonry compressive strength), FRP was applied on one side or double side, FRP was applied either with 0°/90° or 45°/135° with the normal force. The specimens failed in three different modes of failure:

- Direct shear along one of the mortar joints and the FRP was sheared completely along the joint,
- Delamination,
- Combination of delamination and shear.

The mode of failure depends on the fabric length, strength, and fiber orientation [ESA 97]. The specimensí ultimate resistance influenced by the applied normal force; under zero normal force, applying FRP increased the ultimate resistance by a factor as much as 1.5 in case of single side and 2.2 in case of double sides. Moreover, the fiber orientation has a slight influence on the ultimate load. The fiber orientation has a significant influence on the specimen stiffness [ESA 97]. While fibers oriented at 45∫ showed almost linear stiffness until the ultimate load, fibers oriented at 90∫ showed gradual stiffness degradation until ultimate load (Figure 2.19). The secant stiffness at ultimate load for 45∫ is 3 times the 90∫. Finally, under small increment in the normal force, the increment in the ultimate resistance due to FRP diminishes (Figure 2.20). The FRP increased the ultimate resistance by a factor that ranged from 0.6 to 1.08 depends on the level of the normal force and whether FRP was applied on one or double side.

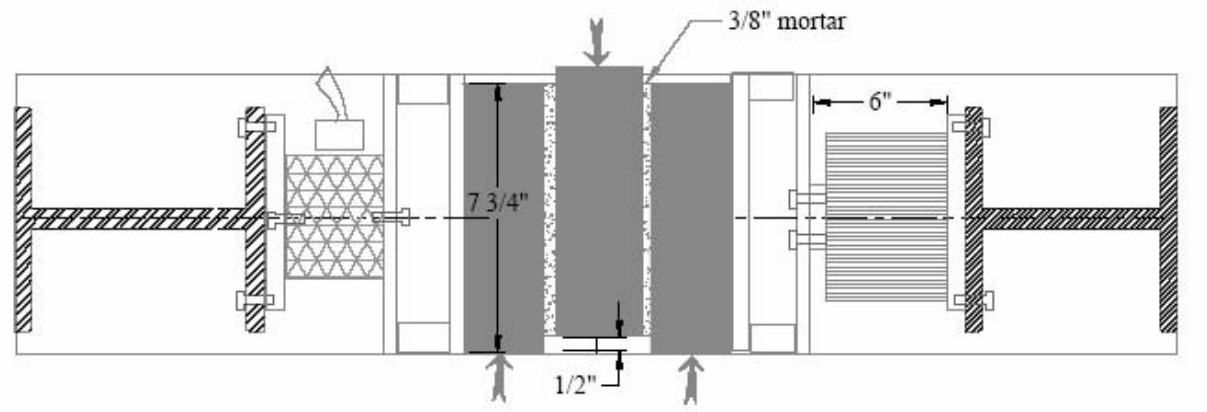

Figure 2.18: Test set-up for a triplet test [BA 02]

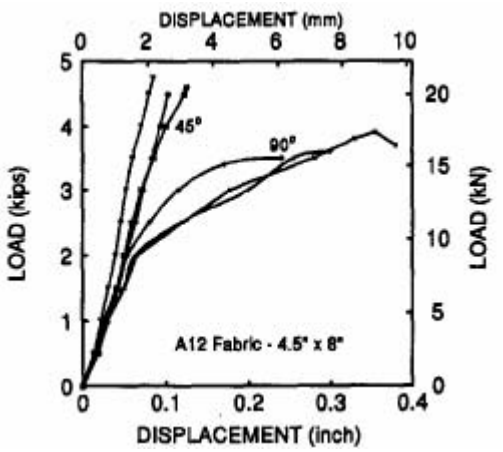

Figure 2.19: Load displacement curves for triplet specimens retrofitted using FRP with different fiber orientations 0/90∫ and 45/135∫ [ESA 97]

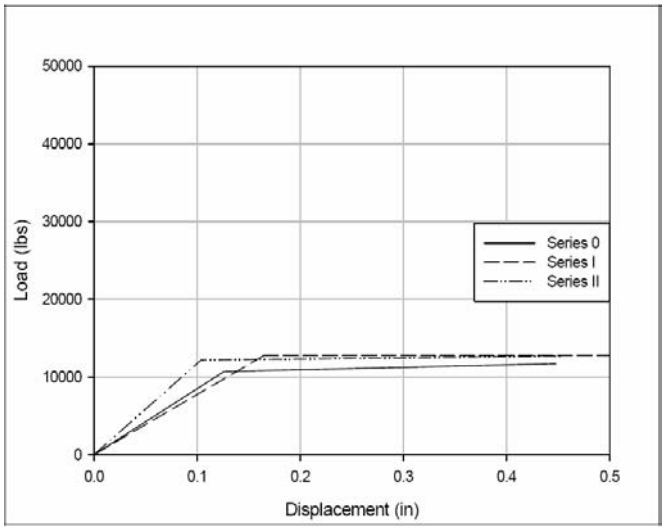

Figure 2.20: Idealized bilinear curve fit for unretrofitted (series 0) as well as retrofitted on one side (series I) and double sides (series II) test specimens on a triplet test under normalized normal force of 12.5% [BA 02]

2.6 Summary

This chapter summarizes important published work and major findings. In general, retrofitting of URM walls using composites is a very promising technique. The following over view is relevant:

- FRP improves the in-plane lateral resistance by a factor ranging from 1.1 to 3 and the out-of-plane resistance by a factor of more than 7.
- Triplet tests, under very low normal force, show that the FRP did not improve the ultimate resistance of masonry specimens.
- Investigation the behavior of URM-FRP needs more experimental research especially for in-plane retrofitting. Some important issues for earthquake resistance building should be carefully examined in future work (e.g. energy dissipation, lateral drift).
- To-date the existing models to calculate the shear capacity of URM-FRP is based on empirical maximum values for strain in FRP. These empirical values are proposed either based on limited number of specimens (2 specimens) or experiments on RC beams.
- A simple linear elastic approach seems appropriate for design of URM-FRP if other premature failure modes are avoided.
- For out-of-plane retrofitting and to avoid delamination, it is recommended to use a fraction (0.4-0.6) of the ultimate capacity of composites. However, this could be improved when a theoretical model to determine the beginning of delamination is developed.

2.7 Conclusions

- The literature review shows that there are limited experimental tests carried out to investigate the in-plane behavior of URM-FRP. In addition, there is only one dynamic experimental program carried out on URM-FRP [AH 99]. However, this experimental program was carried out in a qualitative way on limited number of specimens built with concrete masonry bricks.
- There is no analytical model that describes the shear behavior of URM-FRP.
- Simple flexural models based on Bernoulli-Navier assumptions and equivalent stress block to estimate the in-plane flexural resistance of URM-FRP need further investigations.

3 DYNAMIC TESTS ON URM WALLS RETROFITTED USING FRP

As presented in Chapter 2, the literature review shows that there are limited experimental tests carried out to investigate the in-plane behavior of URM-FRP. In addition, there is only one dynamic experimental program carried out on URM-FRP [AH 99]. However, this experimental program was carried out in a qualitative way on limited number of specimens built with concrete masonry bricks. So there is a lack of dynamic experimental work carried out on URM-FRP. During the experimental part of this thesis an extensive dynamic tests were carried out on URM-FRP. This dynamic work is the first work to address the in-plane behavior of hollow clay masonry walls retrofitted using FRP. Five half-scale walls were built, using half-scale brick clay units, and retrofitted on one face only. Two aspect ratios (1.4 and 0.7), two mortar types (M2.5, and M9), three fiber structures (plates, loose fabric, and grids), three fiber types (aramid, glass, and carbon) and two retrofitting configurations (diagonal ìXî and full surface shapes) were investigated. The test specimens were subjected to a series of synthetic earthquake motions with increasing intensities on a uni-axial earthquake simulator. This chapter presents summary of the dynamic tests. A complete description of the test procedure and results are available in [EL 02]

3.1 Experimental Program

3.1.1 Test specimens

During the experimental program a total of 11 specimens have been tested (Table 3.1). Test specimens were intended to represent structures built in the mid-20th century in Central Europe (Figure 3.1); due to the limitations of the test set-up (size and capacity) half-scale single wythe walls were constructed using half-scale hollow clay masonry units. The test specimens had 2 aspect ratios (Figure 3.2): slender walls ìLîfamily with effective moment/shear ratio of 1.4 and squat walls ìSîfamily with effective moment/shear ratio of 0.7; also, two mortar types were used: weak (type 2 or M2.5) and strong (type 1 or M9). Table 3.2 summarizes the construction material properties. In addition, different types of FRP (Table 3.3) and retrofitting configuration (Table 3.1, Figures 3.3 and 3.4) were used to retrofit the specimens. Test specimens were constructed on a pre-cast reinforced concrete footing. After allowing the specimen to cure (from 3-7 days), a pre-cast reinforced concrete head beam was fixed to the top of the specimen using strong mortar (Type 0 or M20, Table 3.2). Since anchorage problem is out of the scope of this research, anchorage failure of the FRP was prevented by clamping the FRP ends to specimenís footing and head beam using steel plates and screw bolts.

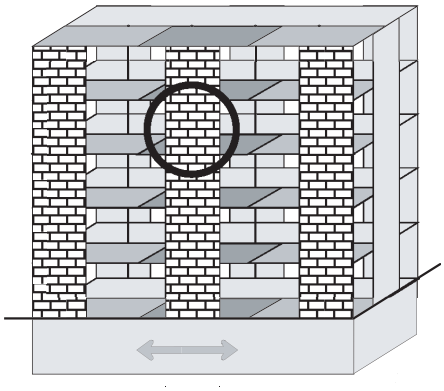

Figure 3.1: Reference building with external structural URM walls. The circle highlights the structural wall considered for the dynamic tests

3.1.2 Experimental tests

The test walls were tested twice; first, the URM specimens were tested, as reference specimens, till a predefined degree of damage; secondly, these reference specimens were retrofitted using FRP and retested. The specimens were retrofitted on one face only; since in many retrofitting intervention scenarios one face retrofitting is frequently preferred over two faces ones, either for convenience of construction (when added to the wall exterior surface) or to leave the exterior faÁade of the building unaltered. Table 3.1 gives a complete list of the tested specimens. Also, Figures 3.3 and 3.4 show summary of the tests that were carried out on the specimens. The following comments complete the table and figures:

- Each specimen is designated by a name reflects their characteristics, Table 3.1. explains the specimensí names. For instance, L1-WRAP-G-X means long specimen (L) with mortar type (1) retrofitted with fabric (WRAP) of glass (G) fiber in a diagonal shape (X) configuration.
- To study the shear resistance of slender URM specimens, there was one virgin URM specimen retrofitted with plates of CFRP (L1-LAMI-C-I). The goal of this specimen was to increase the flexural resistance of the specimen with minimum increase of its shear resistance in order to force a shear failure. As such, this specimen herein after is considered as a reference specimen.
- After testing of L1-LAMI-C-I and S1-LAMI-C-X the CFRP plates were taken off using hammer and chisel. These specimens were retrofitted, one more time, using glass fiber and retested again as L1-WRAP-G-X and S1-WRAP-G-F respectively.

Table 3.1: Tested specimens

Specimen	Slende-rness	Description	FRP Configuration
L1-REFE*	Slender	Reference specimen	--
L1-WRAP-G-F*	Slender	Specimen L1-REFE after retrofitting with fabrics of glass	Full surface
L1-LAMI-C-I*	Slender	Specimen has been retrofitted with vertical plates of carbon fiber	--
L1-WRAP-G-X*	Slender	Specimen L1-LAMI-C-I after taking off the carbon plates and re-retrofitting the specimen with fabrics of glass fiber	Diagonal (X)
L2-REFE	Slender	Reference specimen	--
L2-GRID-G-F	Slender	Specimen L2-REFE after retrofitting with grids of glass	Full surface
S1-REFE	Squat	Reference specimen	--
S1-LAMI-C-X	Squat	Specimen S1-REFE after retrofitting with plates of carbon	Diagonal (X)
S1-WRAP-G-F	Squat	Specimen S1-LAMI-C-X after taking off the carbon plates and retrofitting it with fabrics of glass	Full surface
S2-REFE	Squat	Reference specimen	--
S2-WRAP-A-F	Squat	Specimen S2-REFE after retrofitting with fabrics of aramid	Full surface

* the normal forces increased due to the absence of the railcar springs

Table 3.2: Summary of measured material properties

Test prEN	N	Average Stress [MPa]	S [MPa]	V [%]
Cohesion (c) (Triplet 1052-3)	3	0.16	0.01	7.64
Brick compressive stress (f_b) (772-1)	6	14.81*	0.57	4.99
Compressive strength of mortar type 0 (1015-11)	3	16.10	0.08	0.51
Compressive strength of mortar type 1 (1015-11)	4	8.98	0.40	4.41
Compressive strength of mortar type 2 (1015-11)	4	3.20	0.35	11.05
Compressive strength of masonry assemblage made with mortar type 2 (1052-1)	4	5.70	0.44	7.65
Compressive strength of masonry assemblage made with mortar type (1052-1)	3	7.17	0.29	4.00

N: Number of Specimens, S: Standard Deviation, V: Coefficient of Variation

*Normalized compressive strength of brick units

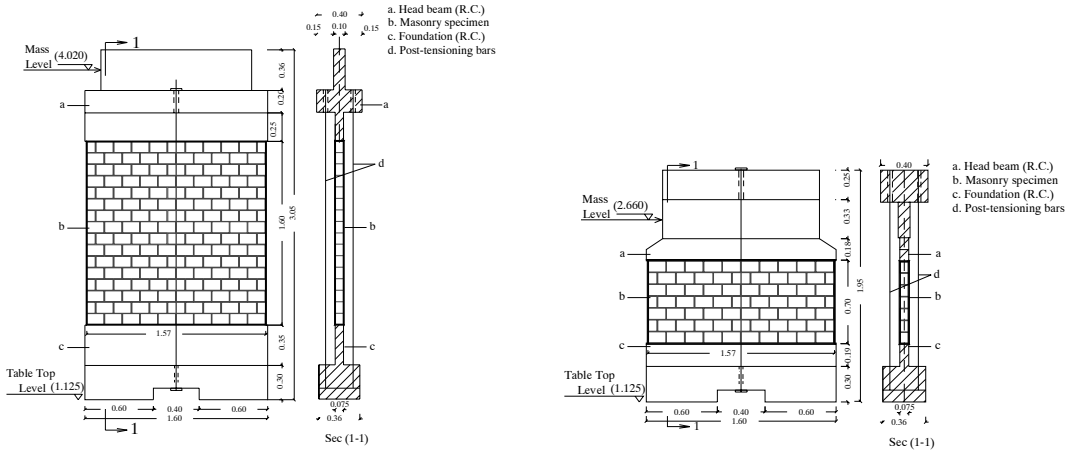

(a) (b)

Figure 3.2: Specimens dimensions in meter, (a) squat and (b) slender

3.1.3 Test set-up

The specimens were tested on the uni-axial earthquake simulator of the Swiss Federal Institute of Technology in Zurich (ETHZ). The test set up is illustrated in Figures 3.5 and 3.6; it includes the following features:

- A shaking table measuring 2 m by 1 m. It has a maximum displacement of ± 100 mm and is driven by a 100 kN servo-hydraulic actuator.
- The specimen is connected at its top to a movable 12-ton substitute mass placed on bearing wheels with a low coefficient of friction in the order of 0.5%. At its top, the specimen is guided with a low friction set-up to ensure that out-of-plane displacements are limited. More details about the test set-up are available in [EL 03].

Table 3.3: FRP used in the experimental program

Commercial name	F.O. [Degree]	FRP [Type]	$Warp_W$ [g/m^2]	$Weft_W$ [g/m^2]	f_t [MPa]	E [GPa]	ε [%]	E.U.	A.M.
SikaWrap-400A 0/90	0/90	Aramid	205	205	2880	100	2.8	Sikadur 330	Dry lay up
SikaWrap-300G 0/90	0/90	Glass	145	145	2400	70	3.0		
MeC Grid G4000	0/90	Glass	139	119	3450	72	4.0		
Sika CarboDur S512	0	Carbon	93	--	2800	165	1.7	Sikadur 30	Wet lay up
Sika CarboDur T	0	Carbon	26	--	2400	135	1.6		

Note: $Warp_w$, $Weft_w$: Weight of fiber in the warp and weft directions respectively; f_t: FRP tensile strength; E: Youngís modulus; ε: Ultimate strain; E.U.: Epoxy used to apply the FRP; A.M: application method of the FRP

3.1.4 Loading system

The head beam was connected to the 12 ton movable mass represents inertia mass (dark grey area in Figure 3.1) and the footing pad was clamped to the shaking table platform (Figure 3.6). For normal force, superimposed gravity load of approximately 30 kN was simulated using two external post-tensioning bars. This was in addition to 12 kN of self-weight from steel elements at wall top (due to the test set-up), reinforced concrete head beam, and masonry panel weight; this normal force corresponded to a compression stress of 0.35 MPa.

During testing of specimens L1-REFE, L1-WRAP-G-F, L1-LAMI-C-I, and L1-WRAP-G-X and due to increase of the wall height as a result to opening of flexural cracks the post-tensioning force increased many times; in the next specimens, railcar springs were used with the post-tensioning bars. As an example, Figure 3.7 shows the change in the post-tensioning force, for two slender specimens retrofitted using GFRP with the same reinforcement ratio, before and after the use of the springs.

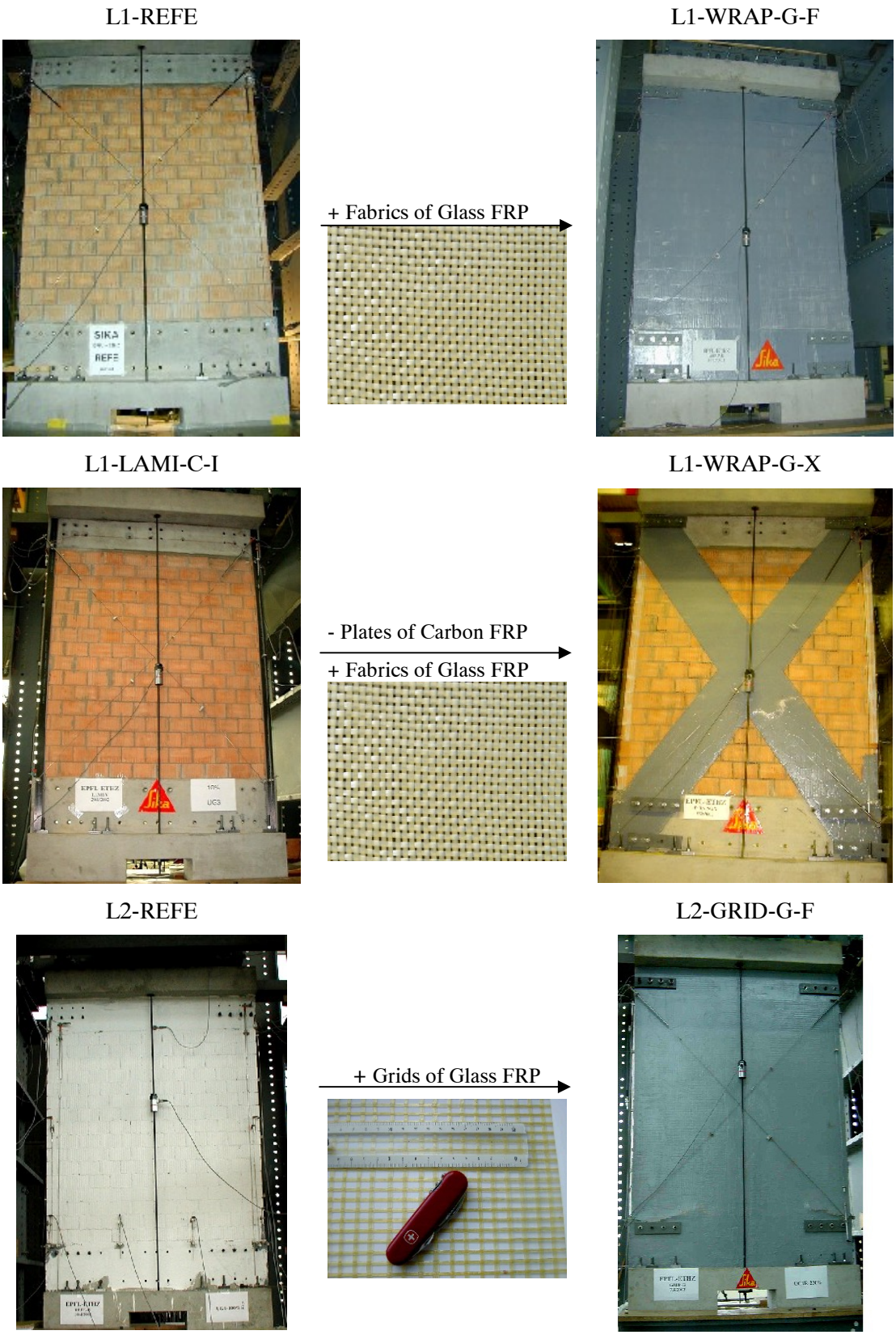

Figure 3.3: Overview of the tested slender specimens

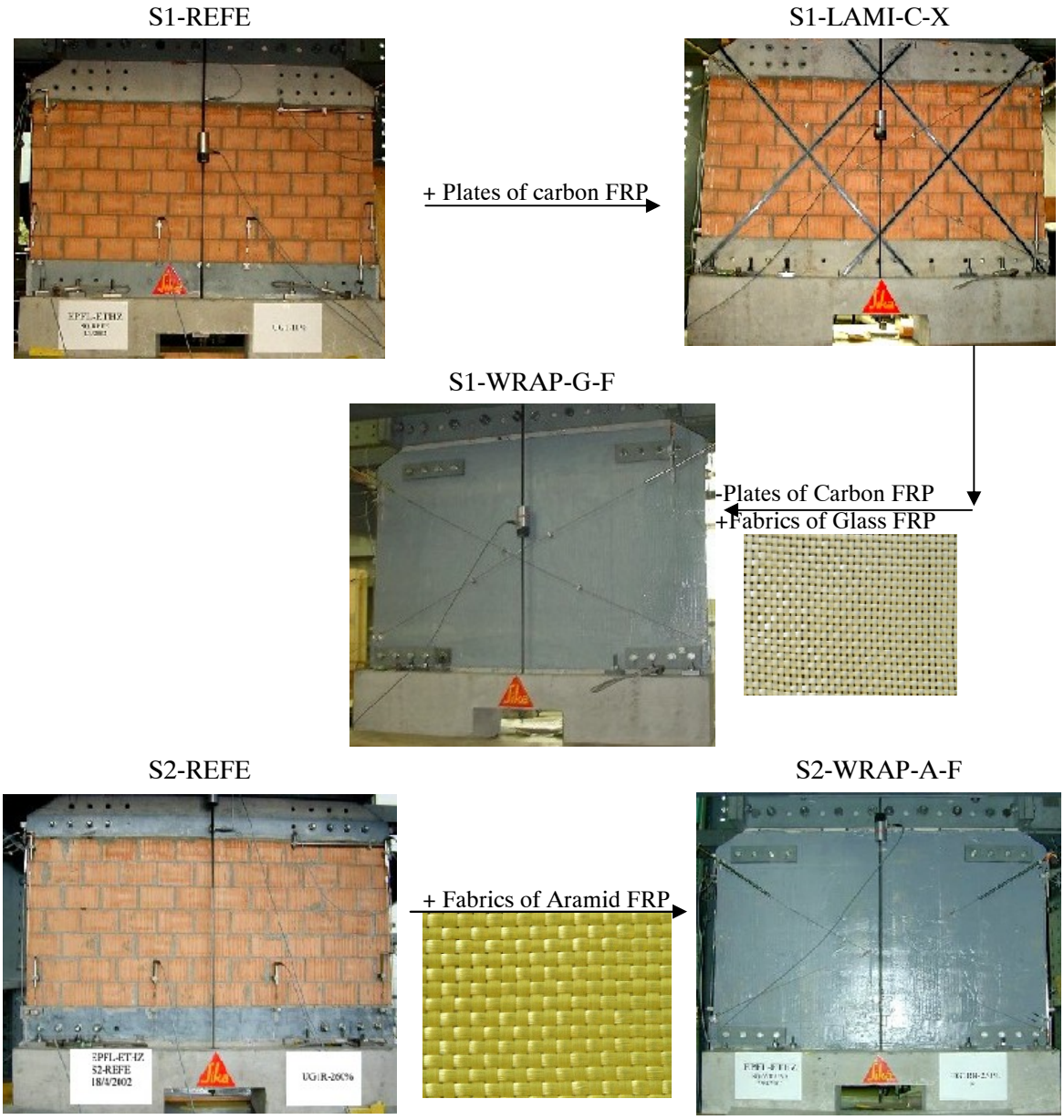

Figure 3.4: Overview of the tested squat specimens

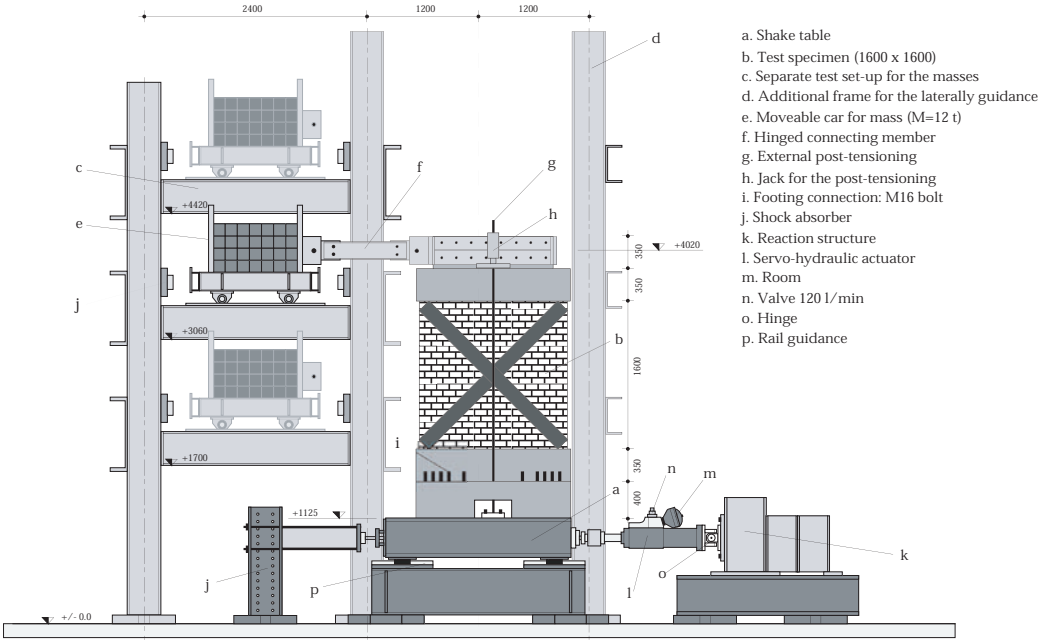

Figure 3.5: Test set-up

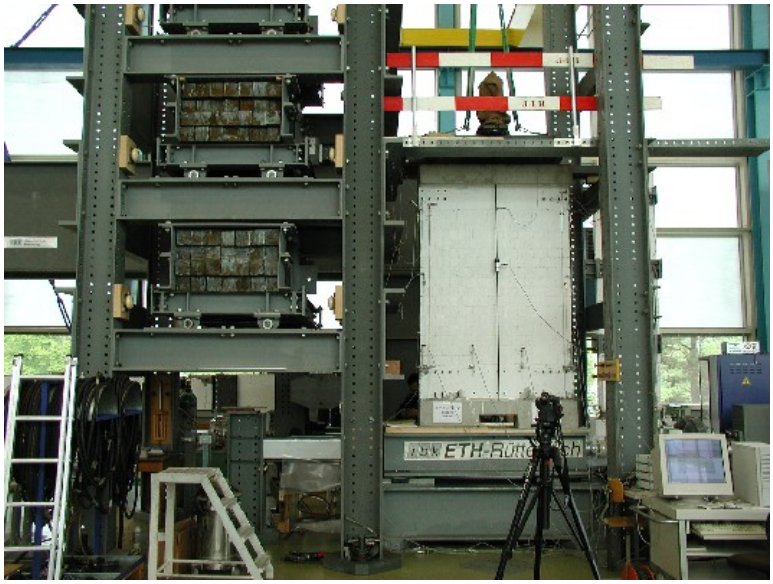

Figure 3.6: A slender specimen ready to test

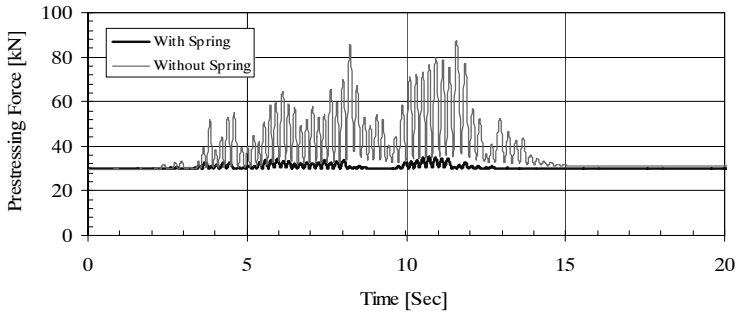

Figure 3.7: Sample of the variations in the post-tensioning forces with spring (L2-GRID-G-F) and without spring (L1-WRAP-G-F)

3.1.5 Dynamic excitations

The displacement inputs of the shaking table were based on synthetic acceleration time-histories compatible with Eurocode 8 [EC8 95] for rock soil type A and with a peak ground acceleration of 1.6 m/s^2, the earthquake last approximately 14 seconds. Three main types of synthetic earthquakes were used for the tests. The first (UG1, Figure 3.8) was for lower accelerations (up to about 120% of the reference spectrum) and used larger table displacements. For higher accelerations and because of the limitations on the table displacements, other synthetic earthquakes with smaller table displacements had to be used (UG1R and UG1RR). These supplementary earthquakes were derived from the first and exhibit the same acceleration response spectrum. The walls were subjected to dynamic excitations of nominal increasing intensity; the increment was usually 10% of acceleration. Table 3.4 summarizes the earthquake type and the corresponding number of test runs as well as the maximum nominal earthquake intensity for each test specimen.

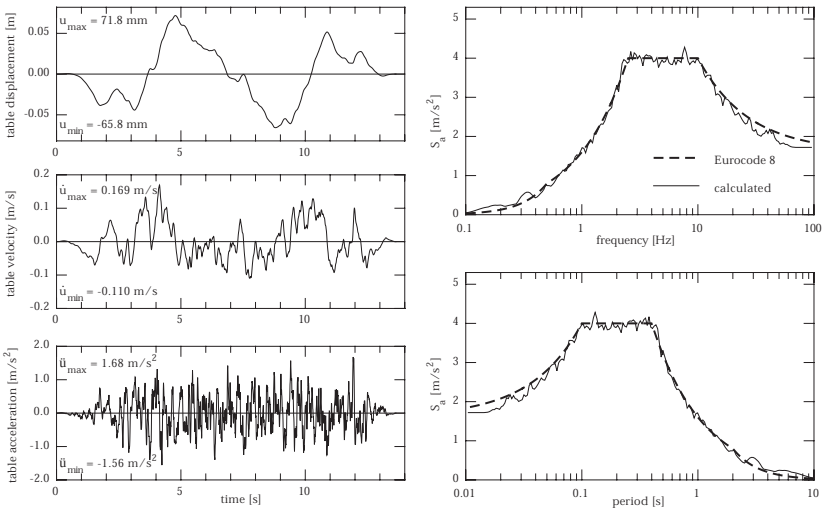

Figure 3.8: UG1, Eurocode 8 for rock soils Type A, spectrum-compatible synthetic earthquake

3.1.6 Instrumentation

The specimenís instrumentation included several accelerometers for vertical and horizontal acceleration. The displacements and deformation of the specimen were measured with linear variable displacement transducers (LVDTs). Additionally, the actual forces transmitted to the wall during the test forces and in the vertical pre-stressing bars were measured using load cells. In all cases the scanning frequency was 100 Hz.

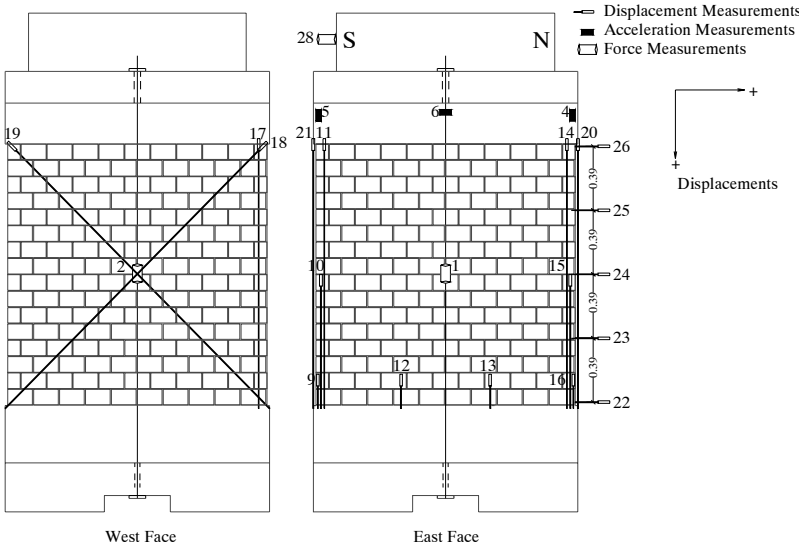

Figure 3.9: Overview of typical measurements for a slender specimen [m]

3.2 Experimental Results

The averages of the absolute maximum and minimum lateral forces and drifts as well as the mode of failure for each test specimen are presented in Table 3.4. In addition, the peaks measured forces, displacements, and drifts in the south (negative) and north (positive) directions are given in Tables 3.5 and 3.6, respectively. Different failure modes occurred during the tests, Figures 3.10 and 3.11 show the reference and retrofitted test specimens at the ends of tests, respectively. In addition, Figures 3.12 and 3.13 present typical failure details for test specimens (e.g. FRp rupture and masonry compression failure). In order to evaluate the enhancement in the retrofitted specimens, the lateral resistances of the retrofitted specimens are compared to those of the appropriate reference specimens (Figure 3.14). Nevertheless, it is difficult to fairly evaluate the enhancement in the ultimate drift due to the retrofitting, as the URM reference specimens did not reach their ultimate drift. Comparisons between the hysteresis curves of the retrofitted and the appropriate reference specimens are presented in Figures 3.15 to 3.18. However, when comparing specimens L1-LAMI-C-I and L1-WRAP-G-X with the reference specimen L1-REFE it should be keep in mind that L1-REFE has a strong increment in the post-tensioning force which influences the behavior of the reference specimen. So, the comparison is carried out between the test run where the retrofitted specimens had maximum lateral resistance and a test run of L1-REFE which had corresponding normal force. The envelopes of all the test runs are presented in Figure 3.20. By examining these curves, specimensí behavior during test runs can be summarized. The envelope is obtained by plotting the average of the absolute peak lateral force in the south and north directions from each test run against the average of the absolute peak wall drift in north and south directions. The peak lateral force values are normalized by 128.7 kN, the weight sum of the 12-ton mass, the head beam, half of the masonry panel, and the other test set-up steel elements at wall top.

Table 3.4: Main test results

Specimen Name	h [mm]	U.M.	U.C	E.T.	N.	E.I. [%]	P [kN]		F [kN]	Δ [mm]	F.M.
							Initial	Final			
L1-REFE	1600	--	--	UG1	11	100	30	90	31	11.8	R
L1-WRAP-G-F	1600	GFRP Fabric	Full face	UG1 UG1R	11 13	120 230	30	88	57	14.2	R
L2-REFE	1600	--	--	UG1	14	100	30	44	16	13.0	R
L2-WRAP-G-F	1600	GFRP Grid	Full face	UG1 UG1R	5 14	120 220	30	43	48	16.1	MF
L1-LAMI-C-I	1600	CFRP Plates	2 Vertical plates	UG3 UG1R	12 8	120 170	29	35	31	5.3	RS
L1-WRAP-G-X	1600	GFRP Fabric	X Pattern	UG1 UG1R	12 14	120 230	27	112	42	17.4	FS
S1-REFE	700	--	--	UG1 UG1R	11 14	120 230	30	45	29	2.3	RS
S1-WRAP-G-F	700	GFRP Fabric	Full face	UG1R UG1RR	8 26	250 470	29	33	74	2.1	NF
S2-REFE	700	--	--	UG1 UG1R	7 15	120 260	30	38	28	2.3	RS
S1-LAMI-C-X	700	CFRP Plates	XX Pattern	UG1R UG1RR	24 5	280 270	29	37	36	3.3	FD
S2-WRAP-A-F	700	AFRP Fabric	Full face	UG1R UG1RR UG1RRR	8 18 4	260 470 230	30	32	72	0.9	NF

Note: h: specimen nominal height, specimen nominal dimensions were 75 mm width, and 1600 mm length;
U.M.: retrofitting material and its structure; U.C.: retrofitting configuration;
E.T.: earthquake type; N: number of test runs;
E.I.: maximum nominal earthquake intensity; P: post-tensioning force;
F, Δ: the maximum of the average of the absolute peak lateral resistances and relative displacement measured in both directions, respectively;
F.M.: failure mode (R: Rocking, RS: Rocking and Shear, MF: Masonry compression failure and fiber rupture, FS: Fiber rupture due to shear failure, FD: fiber rupture due to debonding, and NF: no failure was reached)

3.2.1 Lateral resistance and mode of failure

For slender reference specimens (L1-REFE and L2-REFE), as expected, the specimensí behavior was dominated by a rocking mode that was initiated by flexural tension crack at bed joints in both sides of a specimen (i.e. north and south sides). These cracks extended through the wall length till it connected together. After the cracks connected, there was no continuity left between the upper part and the lower part of the wall (Figure 3.10(a) and (b)). Finally, the specimen displayed a characteristic rocking behavior and the post-tensioning force increased due to the increase of the wall height subsequent to the large opening of the rocking crack. In absence of the railcar springs, the increment was as high as three times the original post-tensioning force; using the railcar springs the increment reduced significantly. However, both specimens have the same lateral resistance (15 kN) under the same normal force. At the test end of L1-REFE, the lateral resistance was increased to 31 kN as the post-tensioning force reached 60 kN.

*Table 3.5: Summary of the peak measured forces and displacements in the **south direction***

	P_{max} [kN]	P_c [kN]	P_d [kN]	F_{min} [kN]	F_c [kN]	F_d [kN]	Δ_{min} [mm]	Δ_c [mm]	Δ_d [mm]	D_{min} [%]	D_c [%]	D_d [%]	F_c/F_{min}	F_d/F_{min}	Δ_c/Δ_{min}	Δ_d/Δ_{min}
Reference specimens																
L1-REFE	90	32	-	32	13	-	11.8	0.9	-	0.72	0.06	-	0.41	-	0.08	-
L2-REFE	44	30	-	16	10	-	13.0	0.9	-	0.80	0.06	-	0.63	-	0.07	-
L1-LAMI-C-I	45	31	-	32	15	-	5.2	1.0	-	0.32	0.06	-	0.47	-	0.19	-
S1-REFE	38	31	-	29	24	-	2.3	0.7	-	0.32	0.10	-	0.83	-	0.30	-
S2-REFE	35	29	-	29	24	-	2.4	0.4	-	0.33	0.06	-	0.83	-	0.17	-
Retrofitted specimens																
L1-WRAP-G-F	88	-	33	65	-	23	15.6	-	1.6	0.95	-	0.10	-	0.35	-	0.10
L2-GRID-G-F	43	31	31	48	26	31	12.4	1.8	2.4	0.76	0.11	0.15	0.54	0.65	0.15	0.19
L1-WRAP-G-X	112	29	74	39	14	39	17.8	0.9	10.5	1.09	0.06	0.64	0.36	1.00	0.05	0.59
S1-WRAP-G-F	33	-	29	76	-	44	2.2	-	0.7	0.31	-	0.10	-	0.58	-	0.32
S2-WRAP-A-F	32	-	-	75	-	-	0.9	-	-	0.13	-	-	-	-	-	-
S1-LAMI-C-X	35	30	32*	37	24	34*	3.4**	0.7	1.6*	0.47	0.09	0.22*	0.65	0.92	0.21	0.47

* Anchorage Failure, ** the ultimate displacement at the end of the last test run

P: post-tensioning force, F: lateral resistance, Δ: lateral relative displacement, and D: lateral drift

c: cracking, d: delamination

*Table 3.6: Summary of the peak measured forces and displacements in the **north direction***

	P_{max} [kN]	P_c [kN]	P_d [kN]	F_{max} [kN]	F_c [kN]	F_d [kN]	Δ_{max} [mm]	Δ_c [mm]	Δ_d [mm]	D_{max} [%]	D_c [%]	D_d [%]	F_c/F_{max}	F_d/F_{max}	Δ_c/Δ_{max}	Δ_d/Δ_{max}
Reference specimens																
L1-REFE	90	32	-	30	10	-	11.9	0.8	-	0.73	0.05	-	0.33	-	0.07	-
L2-REFE	44	30	-	16	11	-	13.1	0.9	-	0.80	0.06	-	0.69	-	0.07	-
L1-LAMI-C-I	45	31	-	31	16	-	5.3	1.1	-	0.32	0.07	-	0.52	-	0.21	-
S1-REFE	38	31	-	28	20	-	2.4	0.6	-	0.33	0.08	-	0.71	-	0.25	-
S2-REFE	35	29	-	28	20	-	2.3	0.4	-	0.32	0.06	-	0.71	-	0.17	-
Retrofitted specimens																
L1-WRAP-G-F	88	-	33	50	-	25	12.8	-	1.8	0.78	-	0.11	-	0.50	-	0.14
L2-GRID-G-F	43	31	31	47	30	34	19.7	1.9	2.3	1.20	0.12	0.14	0.64	0.72	0.10	0.12
L1-WRAP-G-X	112	29	74	45	11	32	17.0	1.0	10.3	1.04	0.06	0.63	0.24	0.71	0.06	0.60
S1-WRAP-G-F	33	-	29	73	-	36	2.0	-	0.7	0.28	-	0.10	-	0.49	-	0.35
S2-WRAP-A-F	32	-	-	69	-	-	0.8	-	-	0.11	-	-	-	-	-	-
S1-LAMI-C-X	35	30	32*	35	20	30*	3.2**	0.6	1.3*	0.45	0.08	0.18*	0.57	0.86	0.19	0.41

* Anchorage Failure, ** the ultimate displacement at the end of the last test run

P: post-tensioning force, F: lateral resistance, Δ: lateral relative displacement, and D: lateral drift

c: cracking, d: delamination

Specimen L1-LAMI-C-I was designed to investigate the shear behavior of slender URM walls by increasing the flexural resistance with minimal increase of the shear resistance (by the addition of two vertical CFRP plates). As expected, the presence of the vertical CFRP plates changed the failure mode of the wall from rocking to mixed modes of failure (shear and flexure, Figure 3.10(c)). The test can therefore be considered to give a good indication of the shear resistance of the wall; however, this wall also can be used to give an indication about the effectiveness of using vertical plates of CFRP to upgrade URM walls. the use of the vertical plates of CFRP increased the lateral resistance by a factor of 1.75 or that the shear resistance of this slender wall is at least 1.75 times its flexural resistance.

For squat reference specimens, both specimens had mixed modes of failure (Figures 3.10(d) and (e)). The presence of the weak mortar in S2-REFE induced the rocking mode to be the govern mode of failure. Both of them had approximately the same lateral resistance (28 kN).

Regarding the retrofitted specimens, all the retrofitting materials increased the lateral resistance by a factor ranged from 1.3 to 2.9 (Figure 3.14). For slender specimens, the full-face retrofitted specimens (L1-WRAP-G-F and L2-GRID-G-F) developed a rocking mode with masonry crushing at toe and fiber rupture at heal (Figure 3.13). Under a constant normal force of 57 kN, the strengthening enhanced the lateral resistance by a factor of 2.6 for fabric and 2.9 for grid. A superposition of the hysteresis loops of the corresponding reference slender specimen (L1-REFE and L2-REFE) and the retrofitted specimens (L1-WRAP-G-F and L2-GRID-G-F) at the test end are presented in Figure 3.15. For L1-WRAP-G-F and at the test end, the normal force tripled (due to increments of wall height as a result of opening of flexural cracks and due to the absence of the railcar springs); this increment in the normal force had insignificant effect on specimen lateral resistance. Nevertheless, the lateral resistance of the reference specimen (L1-REFE) approximately tripled when the normal force tripled. As a consequence, the enhancement in the lateral resistance, in case of high normal force, reduced to 1.9 times the original resistance. For squat specimens, the lateral resistances of the full-face retrofitted specimens (S1-WRAP-G-F and S2-WRAP-G-F) were higher than the capacity of the shaking table hydraulic jack. At the testsí end, there were no significant signs of failure; in addition, the retrofitting enhanced the lateral resistance of the specimens by a factor of 2.6.

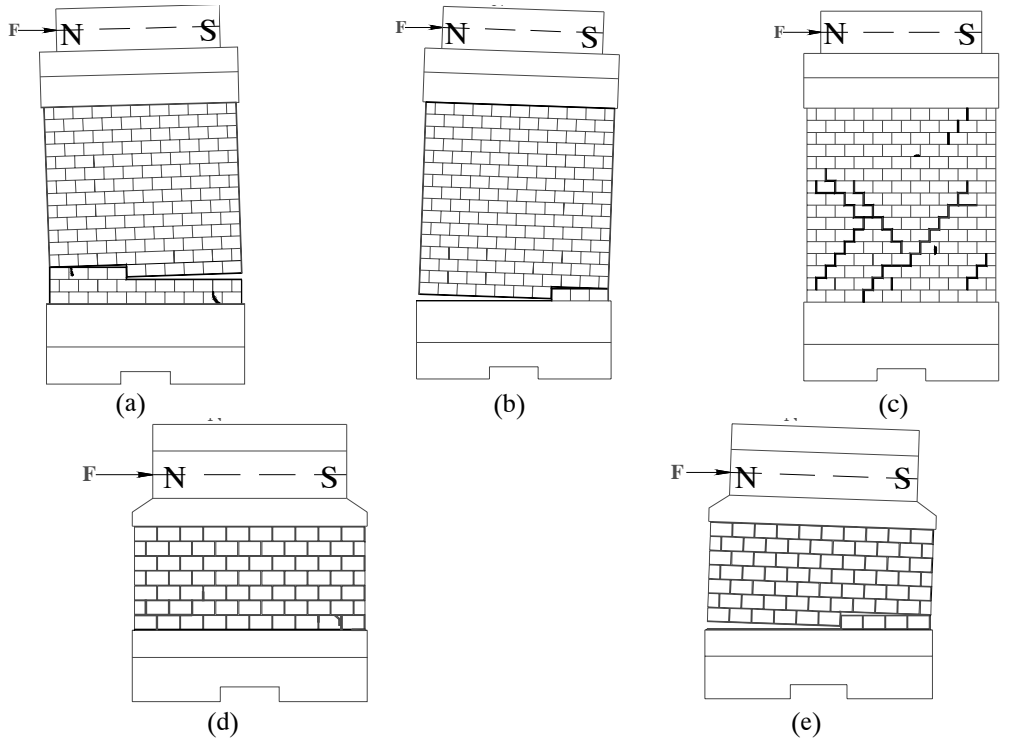

Figure 3.10: Failure modes of reference specimens (a) L2-REFE, (b) L1-REFE, (c) L1-LAMI-C-I, (d) S1-REFE, (e) S2-REFE

Specimens that retrofitted with diagonal shape (X) (L1-WRAP-G-X and S1-LAMI-C-X) were less successful. The behaviors of both specimens could be affected by the previous tests, which carried out on the specimens before strengthening: before strengthening, L1-WRAP-G-X was tested as L1-LAMI-C-I and S1-LAMI-C-X was tested as S1-REFE. These tests developed several step cracks in both specimens. So, the strengthening could be

considered as strengthening of URM wall that have been severely damage during a recent real earthquake event. For L1-WRAP-G-X and at failure, the FRP failed at the specimen mid-height due to shear and flexural cracks, which had developed first through mortar joints. For S1-LAMI-C-X and during the test, one plate failed due to anchorage failure at foundation level since no steel plates (which were used in the other specimens to prevent anchorage failure) were used in this specimen. Both strengthening configurations enhanced the lateral resistance by a factor of 1.5 for L1-WRAP-G-X and 1.3 for S1-LAMI-C-X.

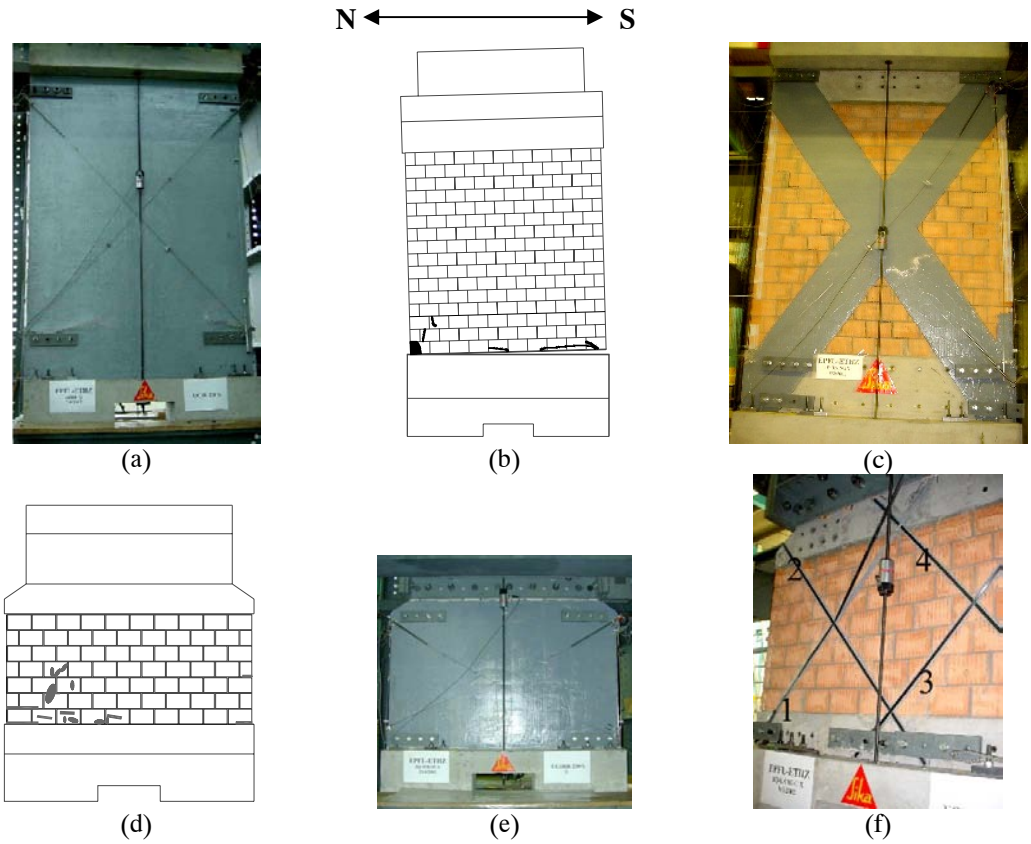

Figure 3.11: Failure modes of specimens (a) L2-GRID-G-F, (b) L1-WRAP-G-F, (c) L1-WRAP-G-X, (d) S1-WRAP-G-F, (e) S2-WRAP-A-F, and (f) S1-LAMI-C-X

Figure 3.12: Delamination and ì white linesî

(a) (b)

Figure 3.13: L2-GRID-G-F (a) grid rupture in the bottom heal, (b) masonry failure in the bottom toe

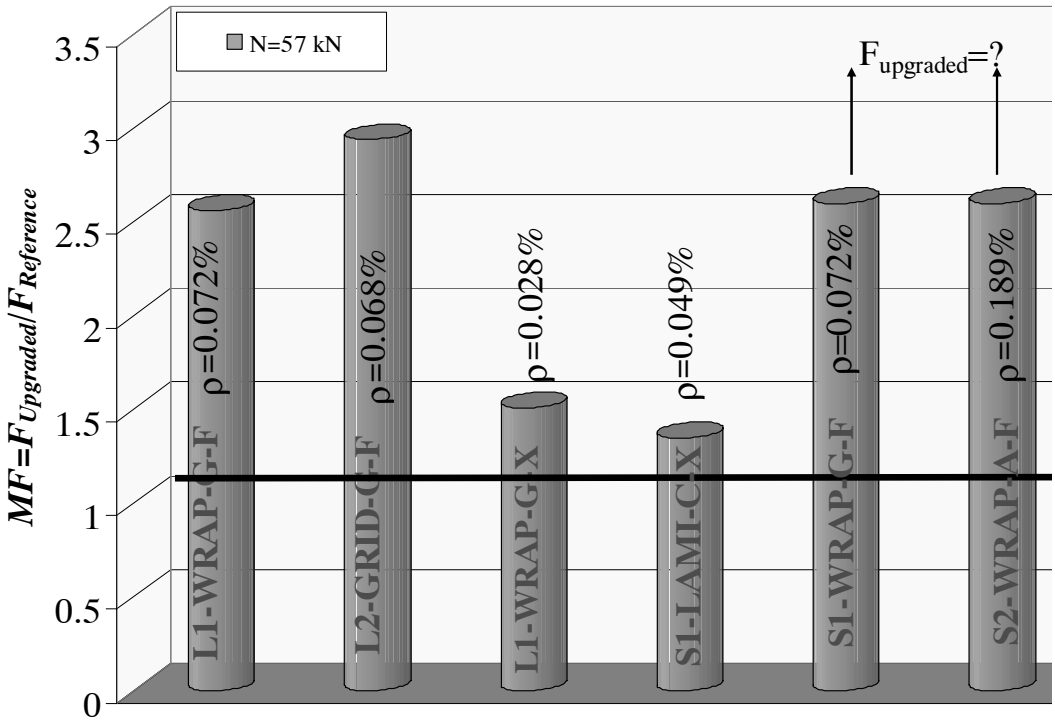

Figure 3.14: Improvements in the lateral resistance of the retrofitting specimens in comparison with the appropriate reference specimens under a normal force (N) of 57 kN

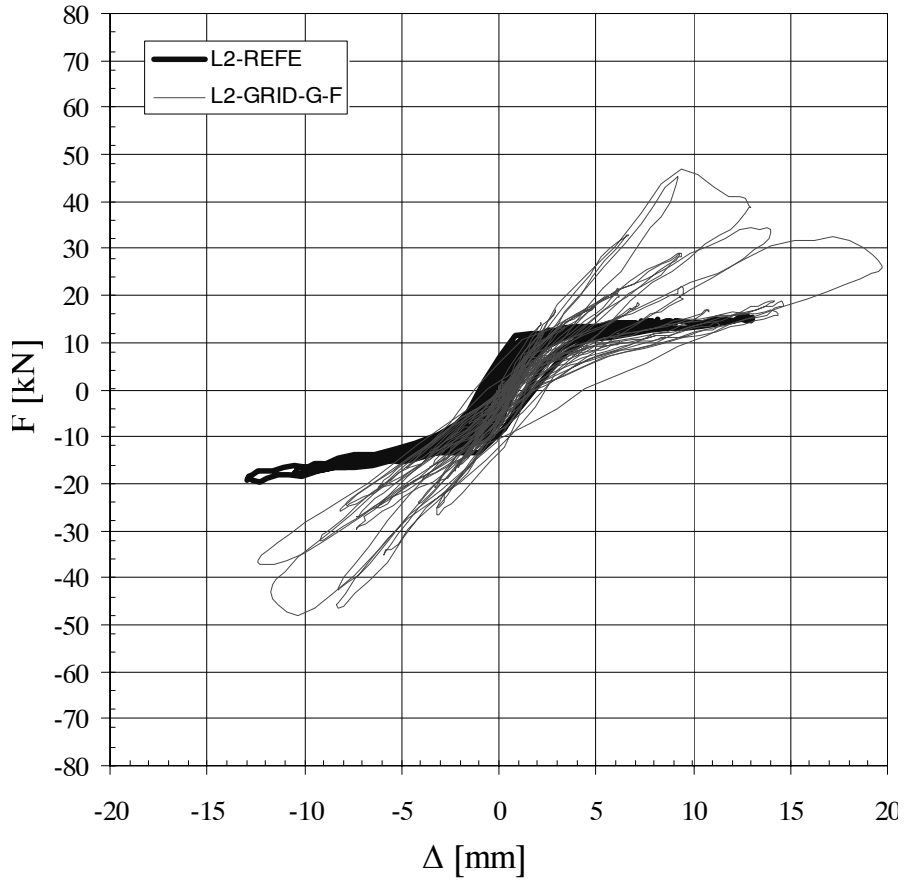

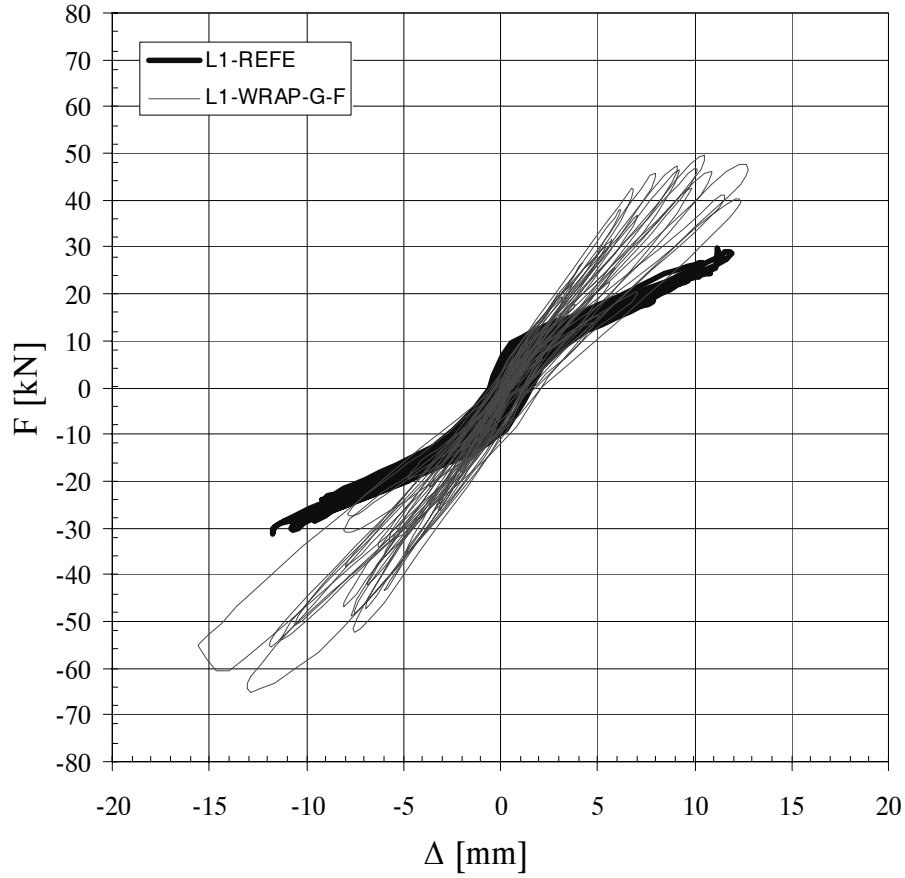

Figure 3.15: Superposition of the hysteresis loops of reference and fully covered retrofitted slender specimens

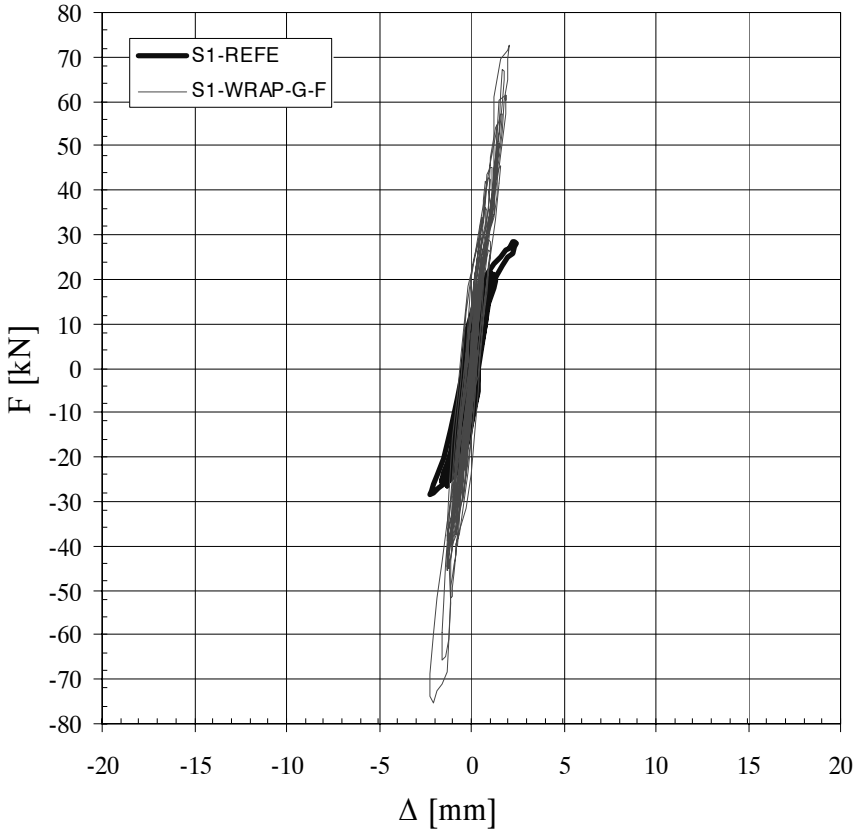

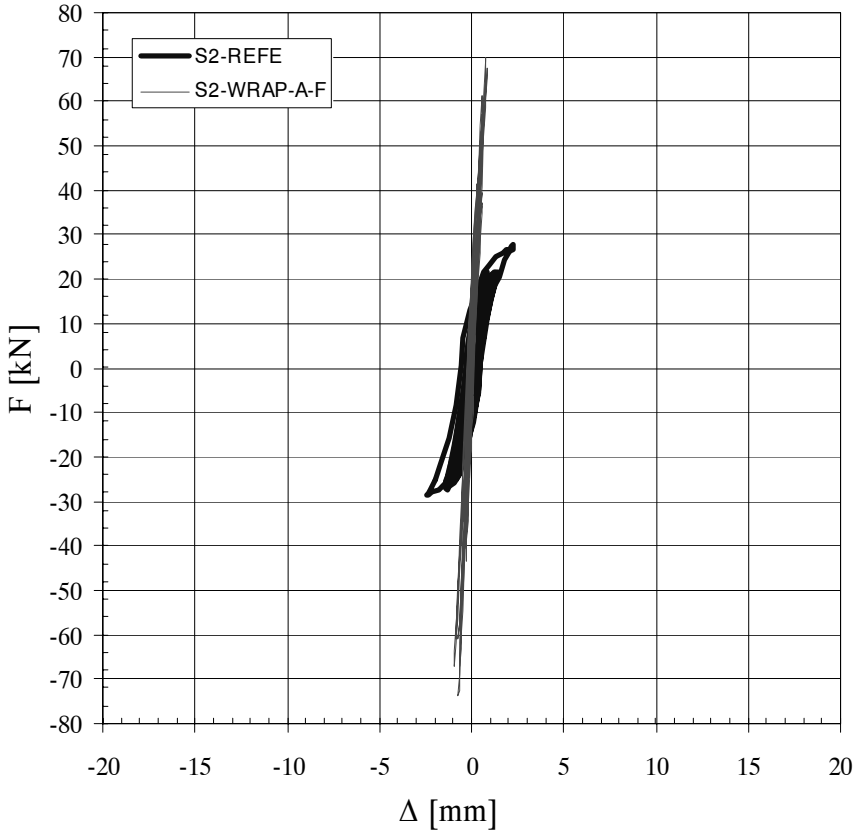

Figure 3.16: Superposition of the hysteresis loops of reference and fully covered retrofitted squat specimens

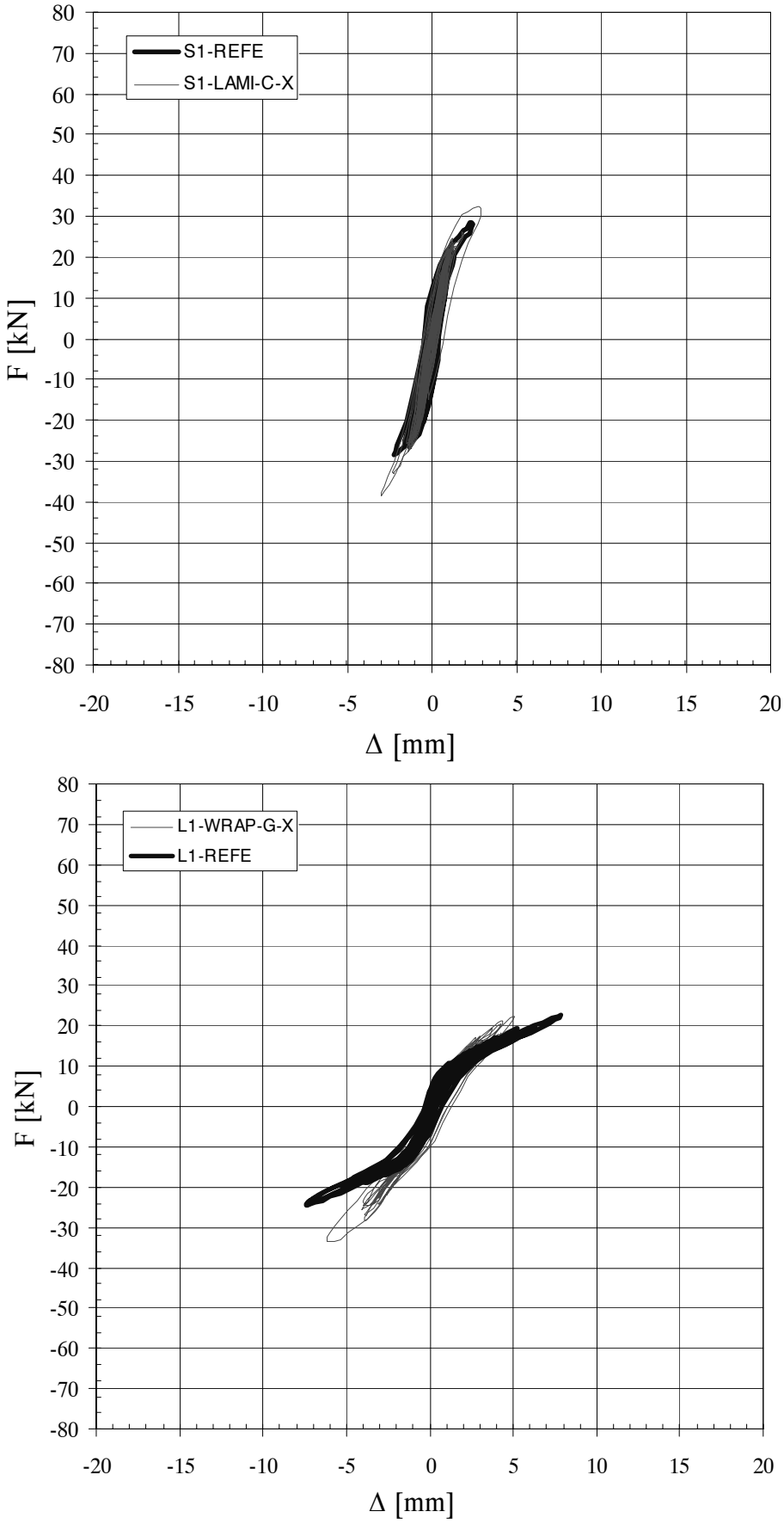

Figure 3.17: superposition of the hysteresis loops of reference and X (diagonal) shape retrofitted specimens

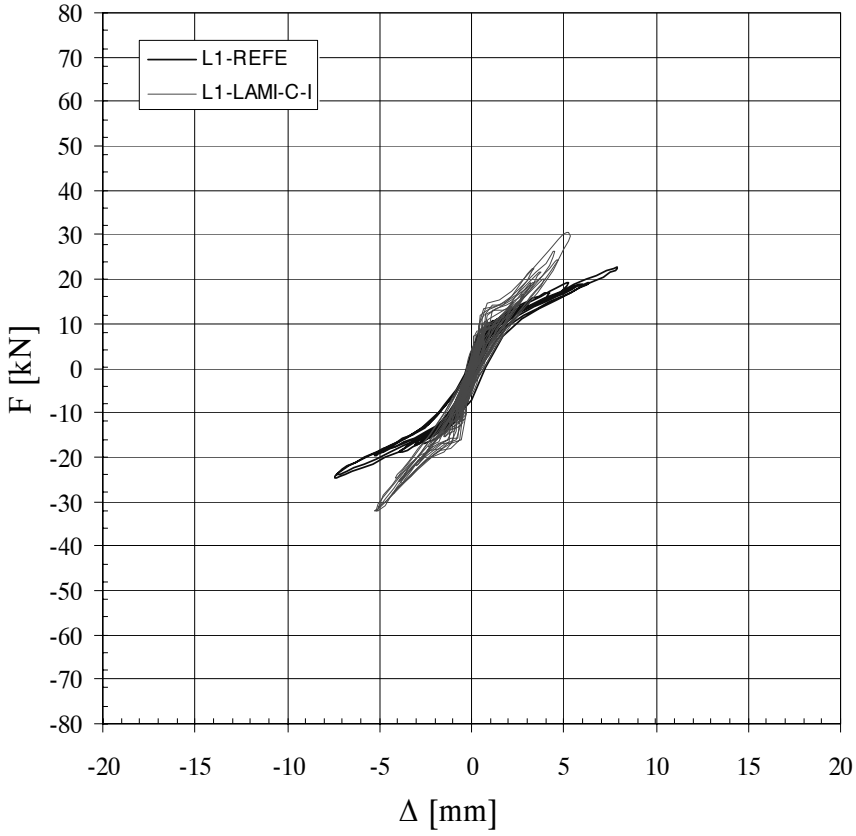

Figure 3.18: Superposition of the hysteresis loops of slender reference specimen and the specimen where two vertical plates were used

3.2.2 Lateral drift and stiffness

As shown in Figure 3.20, the ultimate lateral drifts of retrofitted slender specimens were dependent on the aspect ratio and mostly independent on the reinforcement ratio (ρ). For specimens L1-WRAP-G-F, L2-GRID-G-F, and L1-WRAP-G-X the ultimate drifts were approximately 1%. However, most of these displacements are attributed to the rocking mode. In order to have an indication of how much of the post-cracking horizontal displacements were due to rocking, the vertical LVD transducers through the specimen were examined. As an example, specimen L2-GRID-G-F was 1570 mm length time 1633 mm height. By multiplying the algebraic difference of the measured vertical displacement time-history by 1633/1570, an estimate of the horizontal displacement time-history caused by rocking was made. Figure 3.21 presents a sample of such estimation for the last test run. The comparison with the maximum measured lateral displacements shows that rocking is responsible for approximately 83% of the lateral displacements; therefore, the contribution of the shear deformation to the total lateral displacements is limited to 17%. These ratios are presented in Figure 3.19(b).

For squat (short) specimens (S1-WRAP-G-F, S2-WRAP-A-F, and S1-LAMI-C-X, Figure 3.20), it is difficult to prove that the ultimate lateral drifts of retrofitted specimens were dependent on the aspect ratio and mostly independent on the reinforcement ratio (ρ) since the specimens (S1-WRAP-G-F, S2-WRAP-A-F) did not reach its ultimate state due to the test set-up capacity. However, the measured maximum drift for the squat retrofitted specimens ranged from 0.1% to 0.5%.

Regarding the specimens stiffness, although the high degradation of the stiffness of the reference specimens at the testsí end; it should be notes that all the retrofitting materials success in recovering the initial stiffness of all the specimens. Another feature of the envelope of the slender specimens is that the secant stiffness at the tests ends are approximately 10% of the initial stiffness.

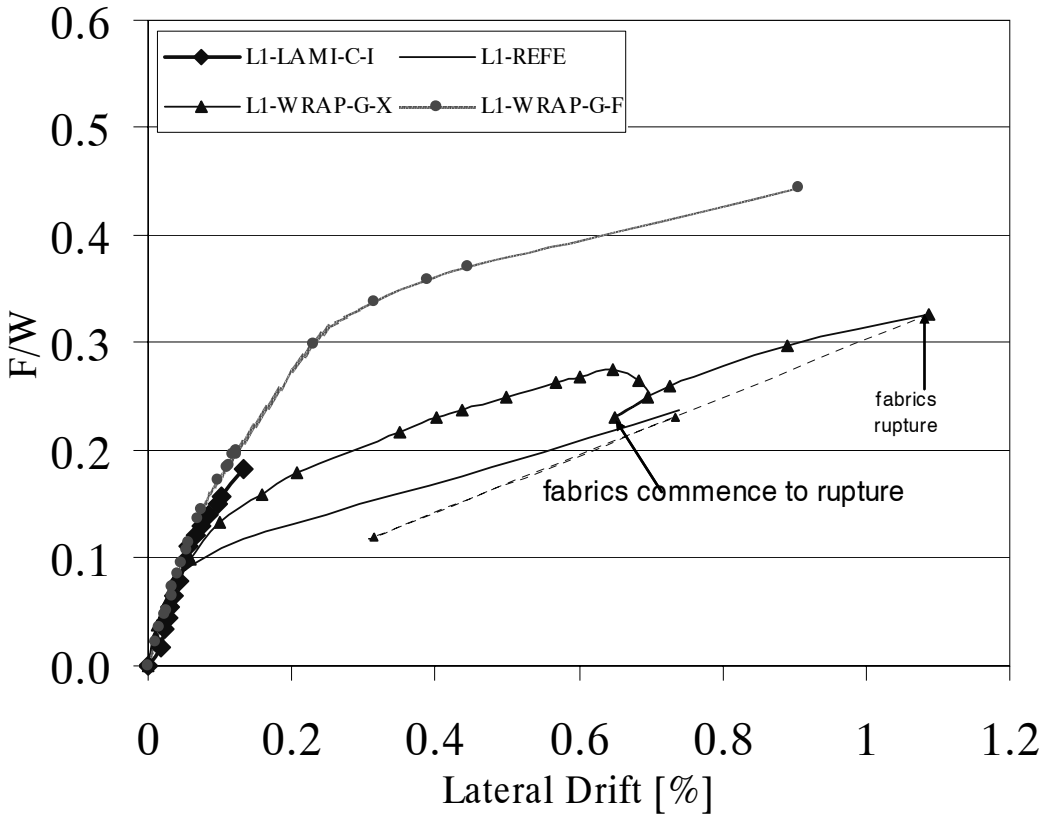

(a)

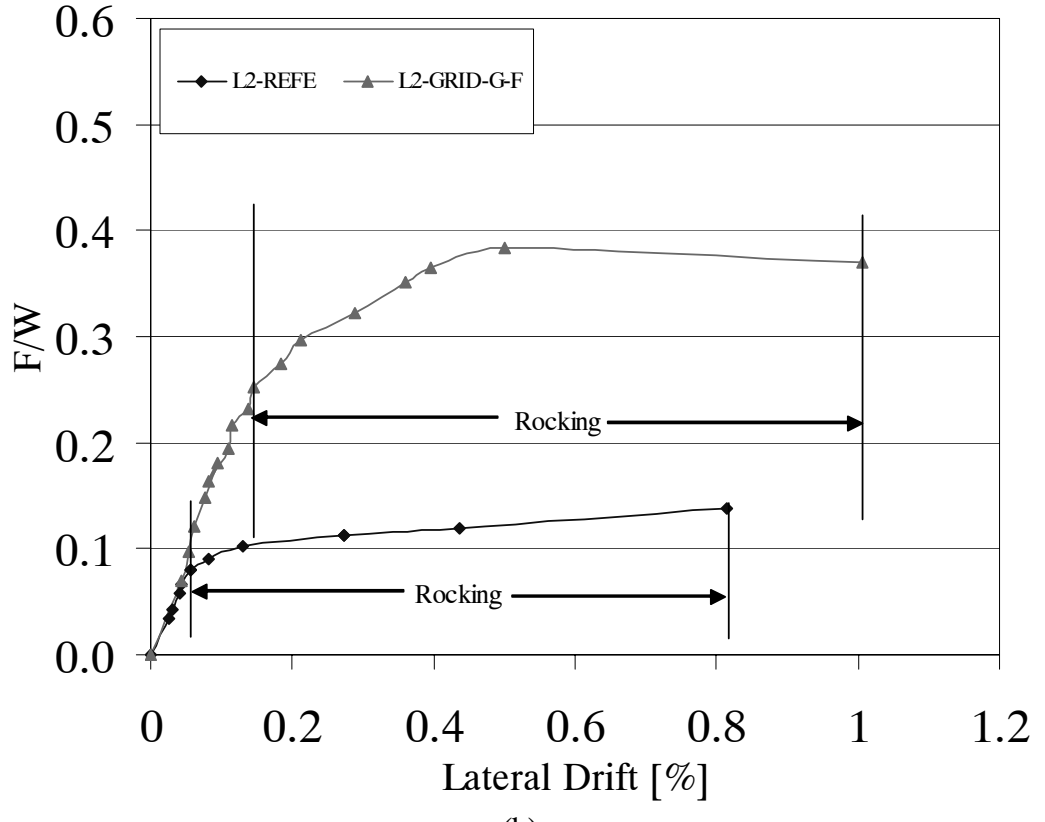

(b)

Figure 3.19: Normalized lateral force versus wall drift for slender specimens (a) L1-REFE, L1-WRAP-G-X, L1-WRAP-G-F, and L1-LAMI-C-I, (b) L2-REFE, and L2-GRID-G-F

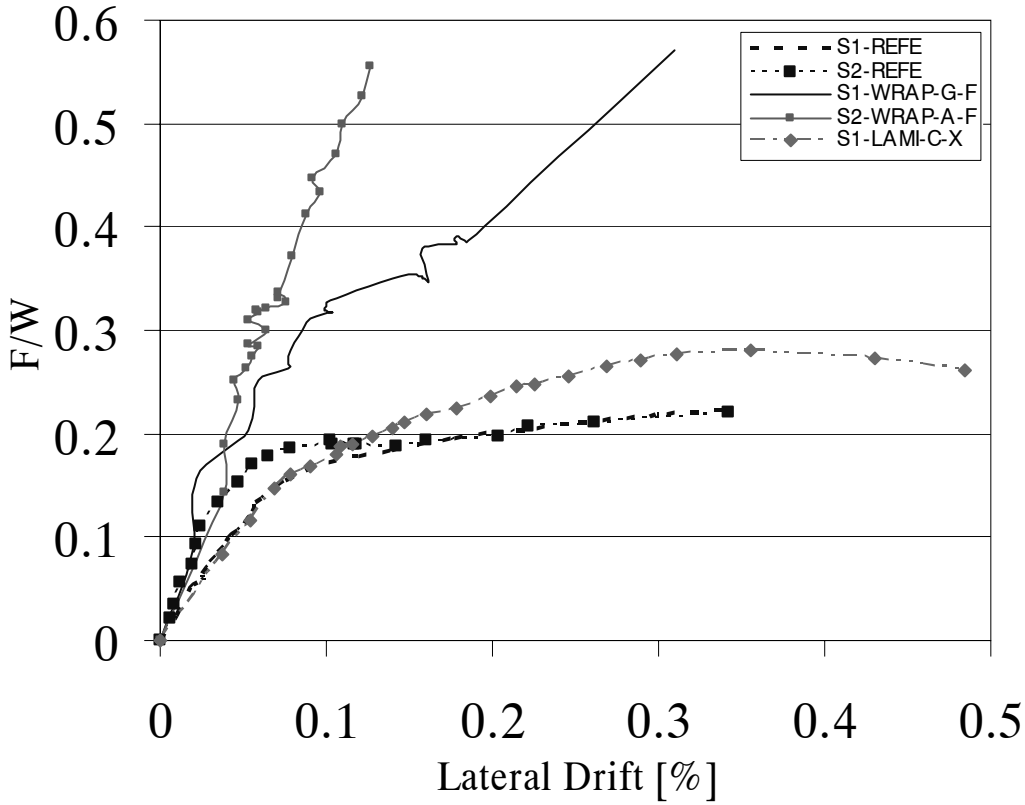

Figure 3.20: Normalized lateral force versus wall drift for squat specimens

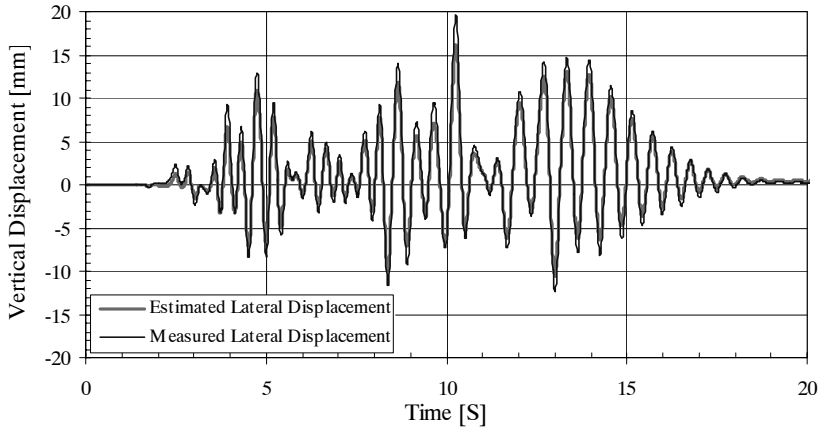

Figure 3.21: Measured lateral relative displacement and estimated lateral displacement due to rocking for specimen L2-GRID-G-F

3.2.3 Maximum strains at failure

Recently, several researchers proved that, during testing reinforced concrete beams, the FRP strain at failure is many times lower than its nominal ultimate strains. This phenomenon has been reported for reinforced concrete beams that have been tested in shear ([KG 98] and [Tr 98]) as well as in bending [BM 01]; moreover, this phenomenon was presented [KE 03] for URM walls that had been retrofitted using GFRP and tested for out-of-plane failure (see ß 2.4.2). All these researchers proposed an empirical efficiency factor for FRP; this efficiency factor is inversely proportional to FRP area and Youngís modulus. In order to investigate this phenomenon for the tested specimens, the maximum strains, calculated based on the measured deformations using the linear variable displacement (LVD) transducers, at the masonry and retrofitted faces of the failed test specimens are examined. The results show that just before failure, the maximum vertical strain for the GFRP fabrics was 1.2% (the nominal ultimate strain for fabric fiber is 3%), while for GFRP grids was 2.5% (the nominal ultimate strain for grid fiber is 4%). For the other retrofitting materials, no strains at failure were recorded since the FRP did not

fail in tension (either debonding and anchorage or no failure at all). It should be noted that these measured strains are measured over approximately 150 mm length of the FRP.

3.2.4 Specimens asymmetry

As mentioned earlier all the test specimens were retrofitted on single side only. As shown by other researchers [AH 99 and Sc 94] this system did not result in any asymmetry in deformations, which may result in more complicated failure mechanism. In order to evaluate this issue for the tested specimens, a comparison between the vertical strains, calculated based on measured displacements using LVD transducers, on the masonry face ìbare faceî and the retrofitted face was carried out. The comparison shows the following:

- For slender specimens, the retrofitted system succeeds in producing complete symmetric response in case of tension while there was a little asymmetry in case of compression. The strains indicate that the asymmetry increased by increasing the earthquake intensity, the rate of increase in the asymmetry during compression is many times larger than tension. The maximum asymmetry in tension was recorded during testing L2-GRID-G-F; the average vertical strain along the masonry face was approximately 118% of the average vertical strain along the FRP face. In compression, the maximum asymmetry was recorded during testing L1-WRAP-G-F; the average vertical strain along the masonry face was approximately 50% of the average strain along the FRP face.
- For squat specimens, the retrofitted system did not success in producing symmetric response. The maximum asymmetry in tension was recorded during testing S1-WRAP-G-F; the average vertical strain along the masonry face was approximately 290% of the average vertical strain along the FRP face. In compression, the maximum asymmetry was recorded during testing S2-WRAP-A-F; the average vertical strain along the masonry face was approximately 56% of the average strain along the FRP face.

3.2.5 Anchorage and delamination

As mentioned earlier, the study of the anchorage system was out of the scope of this research; hence, the anchorage failure was prevented by using steel plates at the FRP ends; the steel plates were used in all specimens except in the beginning of testing specimen S1-LAMI-C-X. In all specimens, except S1-LAMI-C-X, this technique prevented the anchorage failure.
Delamination is an important event, since it could be either a raison for stiffness degradation or early sign of failure. The stiffness degradation due to delamination was reported by others [ES 99] for out-of-plane failure of URM-WUC. In order to examine the effect of the strengthening material characteristics on delamination and hence on a specimen behavior, the lateral resistances from each test run were plotted versus the earthquake real intensity. As an example, Figure 3.22 compares the behavior of specimens L1-WRAP-G-F and L2-GRID-G-F both of them retrofitted using a single side full face glass fiber but with different characteristics. The figure shows that, the behavior of both specimens can be described through two phases: before and after delamination. The first phase (before delamination), by increasing the earthquake intensity (acceleration) the lateral resistance of both specimens increased linearly, approximately, in an identical way. In this phase no large variations in the post-tensioning forces, in both specimens, were recorded. The second phase started with delamination; after delamination both specimens behaved in a nonlinear way; there was nonlinear increase in the lateral resistance with increasing earthquake real intensity. This nonlinear behavior was combined with high increase in the post-tensioning force in case of L1-WRAP-G-F (note that no railcar springs were used). In case of L2-GRID-G-F, the post-tensioning force remained approximately constant till 232% of real earthquake intensity; after rupture of the grids, the real earthquake intensity decreased while the corresponding post-tensioning force increased many times. Moreover, examination of FRP strains at first delamination for all the tested specimens shows the following:

- The lateral resistance at first delamination (Fd) is proportional to the fiber ultimate strength and inverse proportional to the reinforcement ratio.
- Qualitatively Fd is influenced by three factors: the aspect ratio, the FRP product and material type, and the retrofitting configuration.
- The glass fiber fabrics delaminated at average tensile strains approximately ranged from 0.06% to 0.32%, depends on the reinforcement ratio.
- The glass fiber grids delaminated at average vertical tensile strains approximately 0.09%.
- The thermoplastic plates of CFRP ì Sika CarboDur Tî failed due to anchorage at average tensile strains of 0.4%; after reparation using fast epoxy, it delaminated at average tensile strain of 0.5%.

- For all specimens, that had delaminated, the average vertical compression strains along the masonry panel, at delamination, was approximately 0.04% independent on the reinforcement ratio or product.

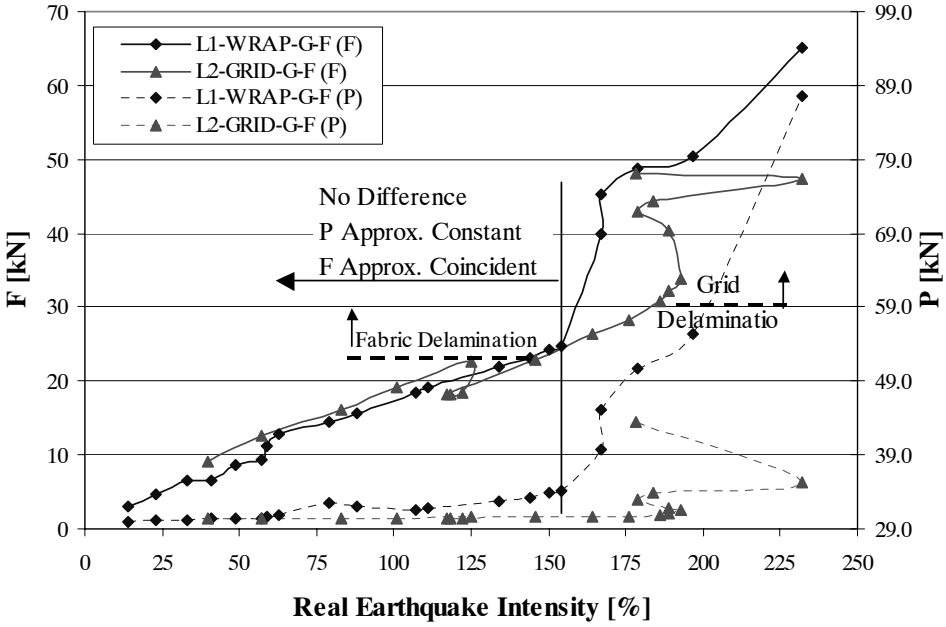

Figure 3.22: Comparison between measured lateral resistances (F) and post-tensioning forces (P) for long reinforced specimens L1-WRAP-G-F and L2-GRID-G-F

3.3 Summary

Five half-scale URM walls were built using half scale brick units. These five walls were dynamically tested as reference specimens. Then, these reference specimens were retrofitted using composites and retested. As a consequence, a total of eleven specimens were tested on the earthquake simulator of ETHZ. This research has investigated the following parameters:

- the aspect ratio: slender (aspect ratio of 1.4) and squat (aspect ratio of 0.7)
- the fiber type: aramid, glass, and carbon fiber
- the retrofitting configurations: diagonal shape (X) and wrapping
- the fiber structures: plates, fabrics, and grids
- the mortar compressive strength: weak (M2.5) and strong (M9).

The dynamic experimental testing of six URM-WUC specimens, led to the following findings:

- The retrofitting materials increased the specimensí lateral resistances by a factor of 1.3 to 2.9 compared to the reference (URM) specimens. Expectedly, the increase ratio is higher for lower normal force: the lateral resistance of the reference specimen increases, approximately in a linear fashion, by increasing the normal force; nevertheless, the increase in the normal force has little effect on the resistance of the retrofitted specimens.
- The enhancement in the ultimate drift for the slender retrofitted specimens was small, reaching up to 1.2. Furthermore, the ultimate drifts were independent on the reinforcement ratio and reinforcement type (grid or fabric); however, the ultimate drifts were dependent on the aspect ratio and the retrofitting configuration.
- Within the test conditions, retrofitting on single side appears to produce good behavior. No out-of-plane or uneven response of the specimens was observed. Small asymmetries in the transducers were recorded in the case of squat specimens. However, further investigations are required for squat specimens in the ultimate range.
- In some specimens there was debonding of the fibers/grids in the form of white spots. This debonding occurred at different lateral load levels, which ranged from 50% to 80% of the ultimate load resistance. The

lateral resistance at first delamination is strongly dependent on the reinforcement ratio and specimen aspect ratio as well as the fiber characteristics.

- The fabric prevented falling of debris from the wall after failure; thus, preventing possible injuries to occupants in the vicinity of the wall in the event of an earthquake in a real case.
- In general, the bi-directional surface type materials (fabrics and grids) applied on the entire surface of the wall (and correctly anchored) can help postpone the three classic failure modes of masonry walls: rocking (ìflexural failureî), step cracking and sliding (ìshear failuresî). In other terms, they are robust: even if the engineer is not sure of the expected failure mode before/after retrofit, the retrofit can help. Additionally, in some situations, they will postpone in-plane collapse by ìkeeping the bricks togetherî under large seismic deformations.
- Carbon plates or fabric strips used in a diagonal pattern (X or XX) was less successful. It was used in the retrofitting of two specimens; in both cases, ìprematureî failure developed (anchorage once and shear-flexure another). In both cases, the retrofit pattern and reinforcement ratio could have been improved to prevent the premature failure; however, the tests indicate that these retrofits are less robust and less redundant.

4 STATIC CYCLIC TESTS ON RETROFITTED URM

As explained in Chapter 3, the ultimate lateral resistance in the dynamic tests of the squat specimens was higher than the capacity of the shaking table hydraulic jack. Hence, it was decided to carry out a second phase of the tests. Static cyclic tests were carried out on nine specimens with two aspect ratios 0.67 and 0.50. Five half-scale walls were built, using half-scale brick clay units, and then retrofitted on the entire surface of one face only. Two fiber types (aramid and glass) as well as hard wire were used as retrofitting materials. The specimens, before and after retrofitting, are subjected to a series of force and displacement control test runs. This chapter presents summary of the experimental work and their main findings. A complete description of the test procedure and results are available in [EL 04]. In addition, the chapter includes comparison between the dynamic and static cyclic test results.

4.1 Experimental program

4.1.1 Test specimens

During the experimental static cyclic test program a total of nine specimens have been tested (Table 4.1). The test specimens were built to be similar to the squat specimens with weak mortar that have been tested during the dynamic tests. Half-scale single wythe walls were constructed using half-scale hollow clay masonry units. The test specimens had 2 moment/shear ratios (Figures 4.1 and 4.2): squat walls ìS familyî with effective moment/shear ratio of 0.67 and more squat ìmidgetî walls ìM familyî with effective moment/shear ratio of 0.50; also, one mortar type was used (type 2 i.e. M2.5, see ß 3.1.1). In addition, the specimens were retrofitted either using post-tension force or different types of retrofitting materials (Table 4.2). All the specimens were retrofitted on the entire surface of a single face only. The test specimens were constructed on the pre-cast reinforced concrete (RC) footing previously used for the dynamic tests. After allowing the specimen to cure (from 3-7 days), the pre-cast RC head beam of the dynamic tests was fixed to the top of the specimen using strong mortar (Type 0 i.e. M20, see ß 3.1.1). Since anchorage problem is out of the scope of this research, anchorage failure of the FRP was prevented by clamping the FRP ends to specimenís footing and head beam using steel plates and screw bolts (e.g. Figure 4.3).

Table 4.1: Tested specimens

Specimen	Slend-erness	Description	Retrofitting Configuration
S2-REFE-ST	Squat	Reference specimen	--
S2-WRAP-G-F-ST	Squat	Specimen S2-REFE-ST after retrofitting with fabrics of glass fiber	Full surface
M2-REFE1-ST	Midget	Reference specimen	--
M2-POST-ST	Midget	Specimen M2-REFE1-ST after retrofitting by doubling the post-tensioning force from 30 to 60 kN	--
M2-WRAP-G-F-ST	Midget	Specimen M2-POST-ST after taking off the added post-tensioning force (i.e. 30 kN) and retrofitting the specimen with fabrics of glass fiber	Full surface
M2-REFE2-ST	Midget	Reference specimen	--
M2-WRAP-A-F-ST	Midget	Specimen M2-REFE2-ST after retrofitting with fabrics of aramid fiber	Full surface
M2-2WARP-G-F-ST	Midget	Virgin specimen retrofitted directly after construction with 2 fabric layers of glass fiber	Full surface
S2-WIRE-S-F-ST	Squat	Virgin specimen retrofitted directly after construction with one layer of Hardwire	Full surface

4.1.2 Experimental tests

The test walls were tested twice; first, the URM specimens were tested, as reference specimens, till a predefined degree of damage; secondly, these reference specimens were retrofitted and tested again. However, two virgin specimens were retrofitted directly after construction and directly tested. One specimen was retrofitted using post-tension force while the others were retrofitted by applying either FRP or Hardwire on a single face. In many retrofitting intervention scenarios one face retrofitting is frequently preferred over two faces ones, either for convenience of construction (when added to the wall exterior surface) or to leave the exterior faÁade of the building unaltered. Table 4.1 gives a complete list of the tested specimens. Also, Figures 4.3 and 4.4 show summary of the tests that were carried out on the squat and midget specimens, respectively. The following comments complete the table and figures:

- Each specimen is designated by a name reflecting their characteristics, Table 4.1. explains the specimensí names. For instance, M2-WRAP-G-F-ST means midget specimen (M) with mortar type (2) retrofitted with fabric (WRAP) of glass (G) fiber in a full surface (F) configuration and tested in the static cyclic (ST) test.
- To study the effect of retrofitting using high normal force, a midget URM specimen (M2-REFE1-ST) was first tested till it cracked in both sides, and then retrofitted by doubling the post tensioning force (i.e. it was increased from 30 to 60 kN). The goal of this option was to compare the effect of higher normal force with the other retrofitting techniques.

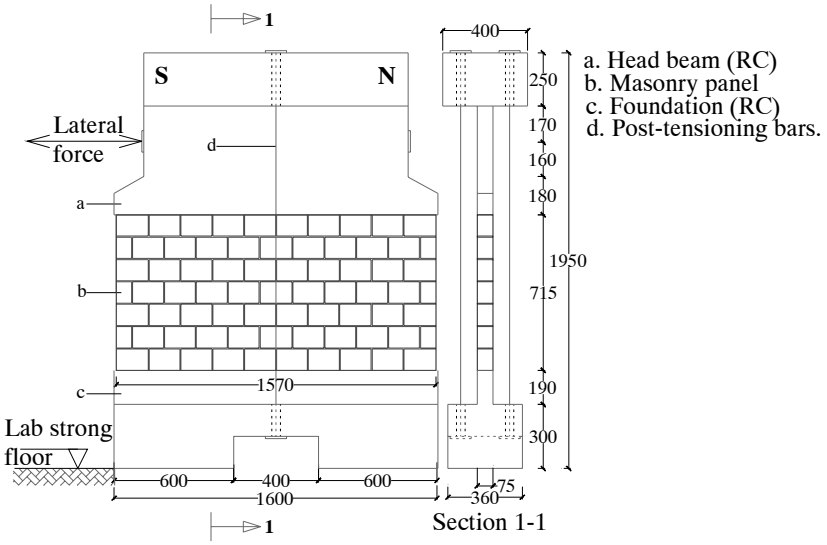

Figure 4.1: Typical dimensions of squat specimen [mm]

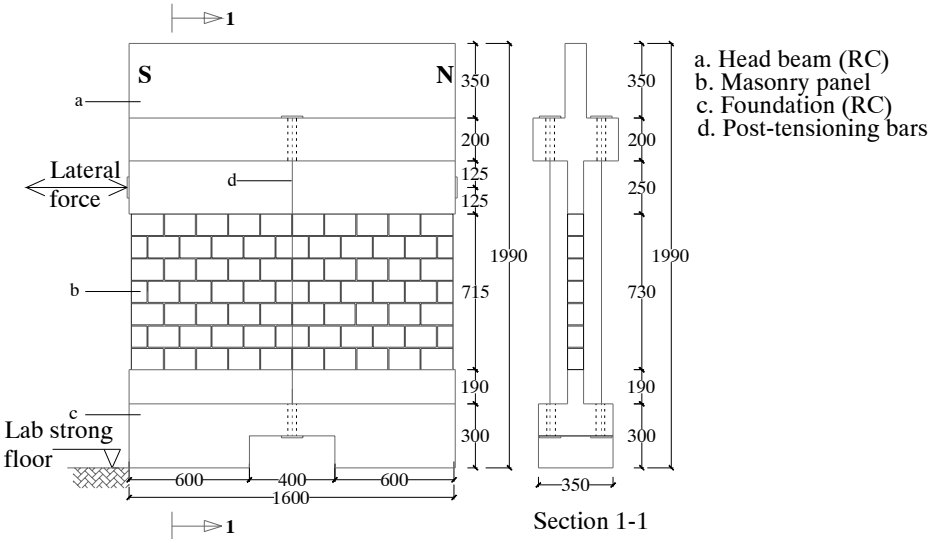

Figure 4.2: Typical dimensions of midget specimen [mm]

Table 4.2: Retrofitting materials used in the experimental program

Commercial name	F.O. [Degree]	FRP [Type]	$Warp_W$ [g/m^2]	$Weft_W$ [g/m^2]	f_t [MPa]	E [GPa]	ε [%]	E.U.	A.M.
SikaWrap-300A	0	Aramid	300	--	2880	100	2.8	Sikadur 330	Dry lay up
SikaWrap-300G 0/90	0/90	Glass	145	145	2400	70	3.0		
GYZ 12X-4-12	0	Hardwire	524*	--	3150	207	1.5		

Note: $Warp_w$, $Weft_w$: Weight of fiber in the warp and weft directions respectively; f_t: FRP tensile strength; E: Youngís modulus; ε: Ultimate strain; E.U.: Epoxy used to apply the FRP; A.M: application method of the FRP

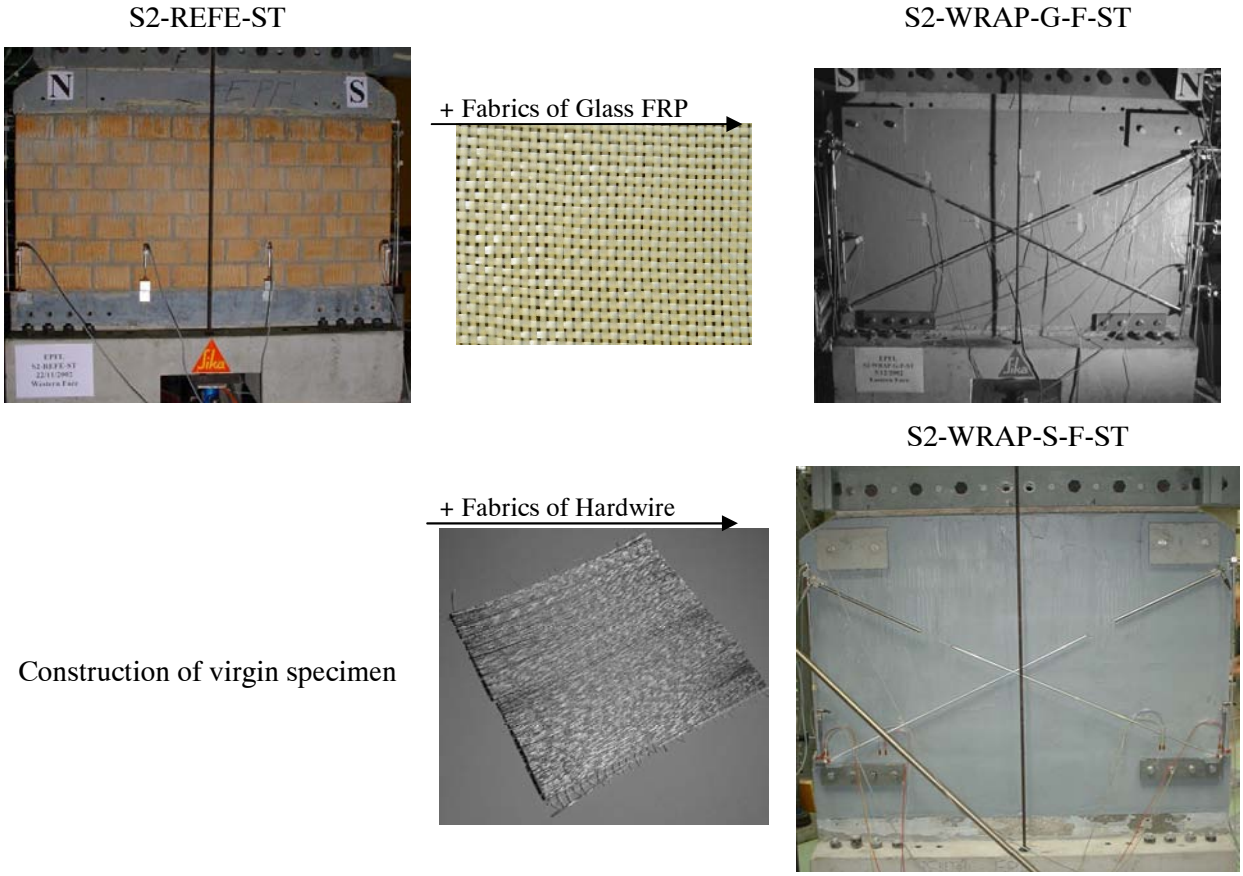

Figure 4.3: Overview of the tested squat specimens (S family)

4.1.3 Test Set-up

The test set up is illustrated in Figure 4.5. A test specimen was constructed on a precast RC footing, which was post-tensioned to the laboratory strong floor at the Swiss Federal Institute of Technology in Lausanne (EPFL) (Figure 4.6). After allowing the specimen to cure (from 3-7 days), the head beam was fixed to the top of the specimen using strong mortar (M20). Superimposed gravity load of approximately 30 kN was simulated using two external post-tensioning bars. This was in addition to 12 kN of self-weight from steel elements at wall top (due to the test set-up), reinforced concrete head beam, and masonry panel weight. This normal force corresponded to a stress of 0.35 MPa. Railcar springs were used with the post-tensioning bars to avoid increment in the post-tensioning force due to bars elongation. The post-tensioning bars elongate due to the increment in the specimen height because of flexural cracks opening. More details about the test set-up are available in [EL 04].

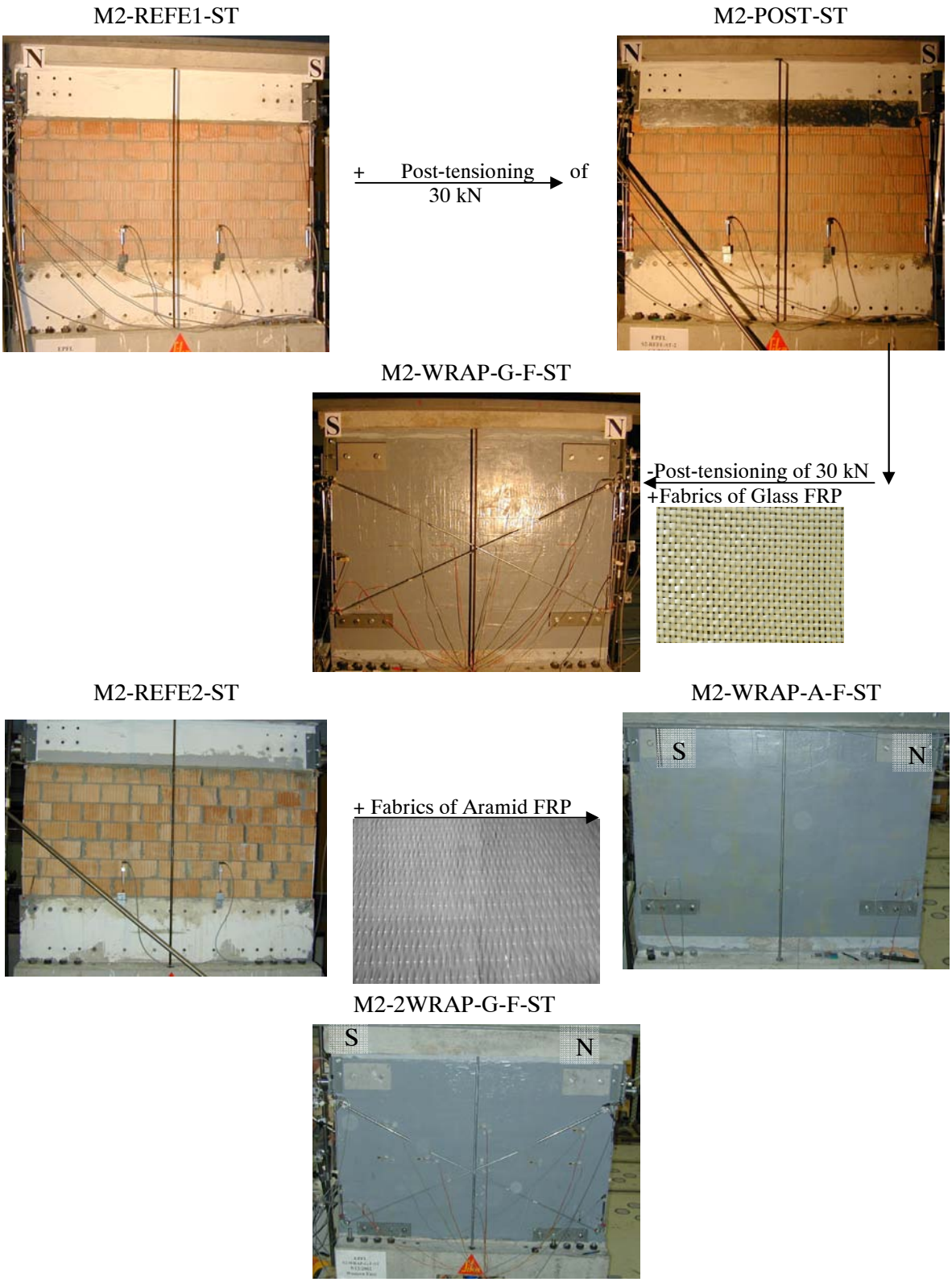

Figure 4.4: Overview of the tested midget specimens (M family)

4.1.4 Loading System

The horizontal load was applied to the RC head beam, which in turn distributes the force to the masonry wall. The load was applied manually using alternatively two hydraulic jacks and hand pumps. The specimens can be considered cantilever walls, i.e. fixed at the base and free at the top with an effective aspect ratio of 0.67 (height of the horizontal force above the base of the masonry wall of 1.06 m and width of 1.6 m) in case of S family and 0.50 (height of the horizontal force above the base of the masonry wall of 0.84 m and width of 1.6 m) in case of M family.

The specimens were subjected to a sequence of test runs (Figure 4.7): each test run is a half cycle. Before cracking (force control), the applied force was increased gradually with increment of approximately 5 kN. At each applied load level, the specimens were subjected to complete cycle (i.e. two consequent test runs). After cracking (displacement control), the first ram (test run in the cracked direction) was controlled by a predefined sequence of displacements, while in the other direction (i.e. next test run or half cycle) the test was controlled in accordance with the measured forces in the previous test run. In this way, equal forces were applied on both sides of a specimen. This is related well to what observed during the real time dynamic test [EL 03]. The predefined sequence of displacements was similar to that proposed in the ICBO (1997). At first cracking, the measured relative displacement at wall top was used to mark the ìfirst yield displacementî. Then, at each ductility level the specimens were subjected to three complete cycles. In specimen M2-WRAP-A-F-ST, the whole test was carried out in force control since the specimen behaved approximately linear elastic-plastic till the test end. In addition, one cycle was carried out at each loading level since no degradation in the stiffness was observed for the rest of the specimens due to repetitive three cycles. This specimen was loaded exactly in the same manner in both directions till approximately 80 kN. After 80 kN and due to test set-up problems, the test was continued in the south-north direction only. Reaching the ultimate lateral resistance of the specimen in south-north direction a monotonic loading was applied in the opposite direction till failure occurred at approximately 150 kN.

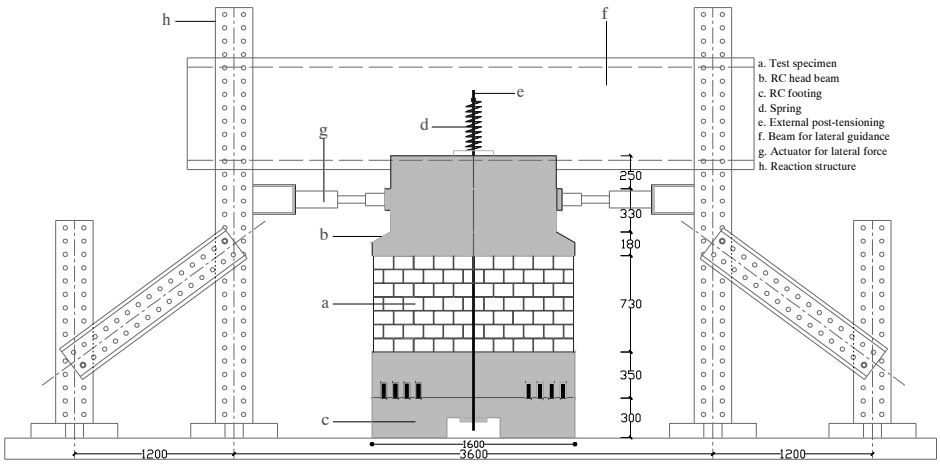

Figure 4.5: Test set-up [mm]

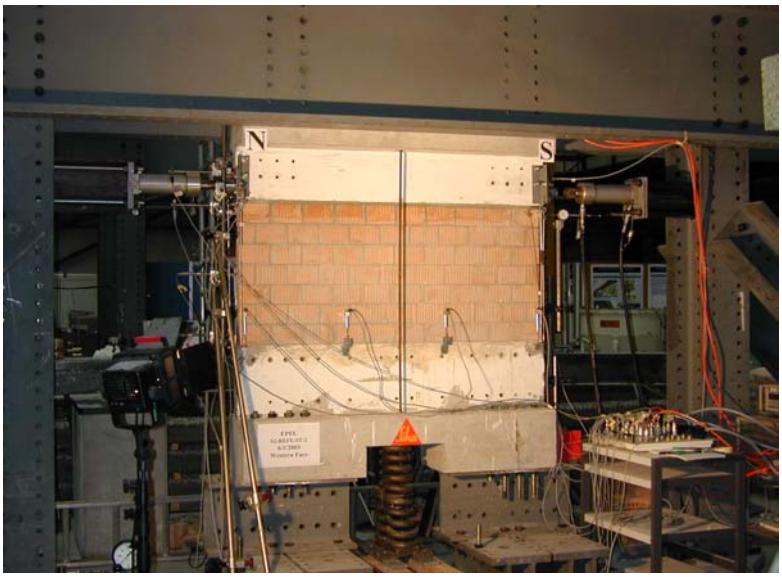

Figure 4.6: A midget specimen ready to test

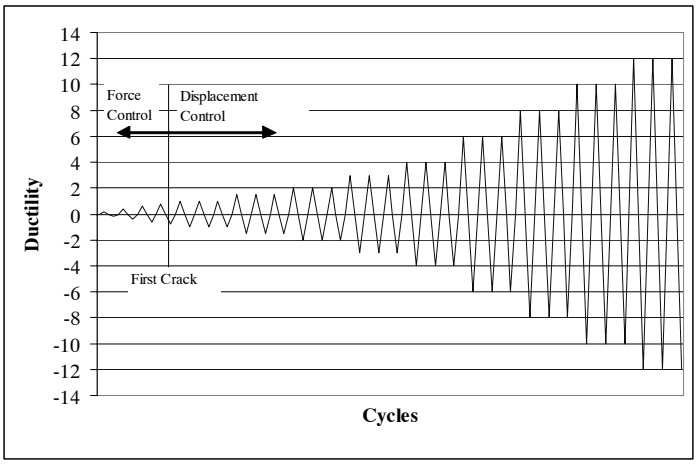

Figure 4.7: Loading sequence

4.1.5 Instrumentation

The specimens were instrumented with several devices as shown in Figure 4.8. Seventeen Linear Variable Displacement Transducers (LVDTs) measured vertical, horizontal, and diagonal displacements and deformations. For the specimens which retrofitted using either FRP or Hardwire the horizontal and/or the vertical strains in the FRP were measured using electrical strain gages (Figure 4.8 (b)). The forces in the post-tensioning bars as well as the lateral forces at the wall top were measured using four load cells.

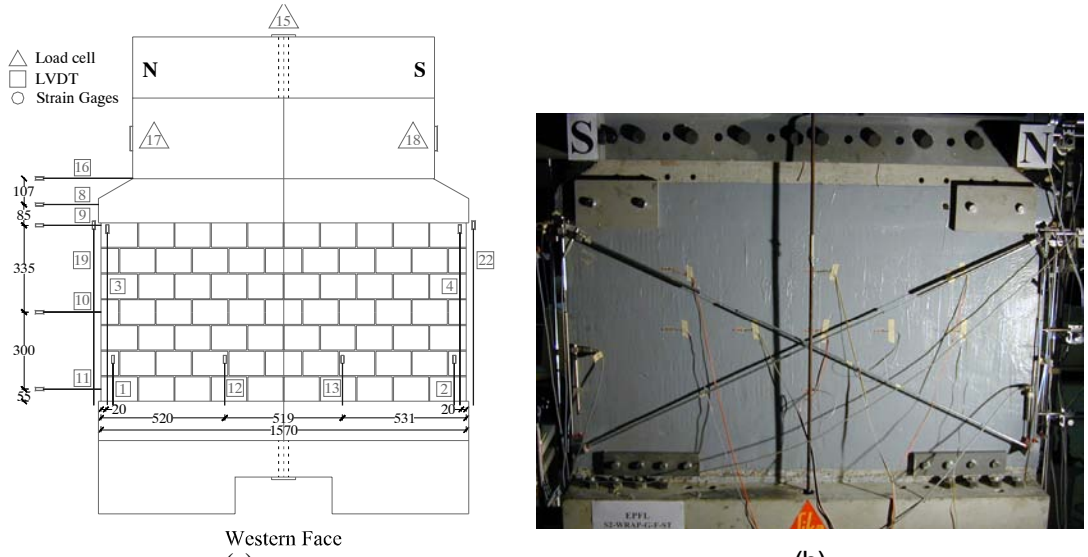

Figure 4.8: Overview of typical measurements for a squat specimen (S2-WRAP-G-F-ST) (a) western face and (b) eastern (retrofitted) face

4.2 Experimental results

The averages of the absolute maximum and minimum lateral forces and drifts as well as the mode of failure for each test specimen are presented in Table 4.3. In addition, the peaks measured forces, displacements, and drifts at the top of the masonry panels in the south-north and north-south directions are given in Tables 4.4 and 4.5, respectively. It should be noted that the lateral relative displacements in Tables 4.3 to 4.5 were the absolute maximum measured displacement; however, in 3 specimens the test was continued into the post peak till the lateral resistance dropped more than 40% of the ultimate lateral resistance. In theses cases the ultimate lateral displacement was determined when the lateral resistance dropped to 80% of its ultimate lateral resistance. Different failure modes occurred during the tests, Figures 4.9 and 4.10 show the reference and retrofitted test specimens at the ends of tests, respectively. In addition, Figures 4.11 and 4.12 present typical failure details for test specimens (e.g. FRP rupture and masonry compression failure). In order to evaluate the increment in the lateral resistance of the retrofitted specimens, the lateral resistances of the retrofitted specimens are compared to those of the appropriate reference specimens (Figure 4.13). Nevertheless, it is difficult to fairly evaluate the enhancement in the total drift due to the retrofitting, as the URM reference specimens did not reach their ultimate drift except for specimen S2-REFE-ST. Comparisons between the hysteresis curves of the retrofitted and the appropriate reference specimens are presented in Figures 4.14 to 4.16. The envelopes of all the test runs are presented in Figures 4.17 to 4.19. By examining these curves, specimensí behavior during test runs can be summarized. The envelope is obtained by plotting the absolute peak lateral force in the south and north directions from each test run versus the absolute peak wall drift in south and north directions, respectively. However, in two specimens (S2-WIRE-S-F-ST and M2-REFE2-ST) during loading in one direction the formed cracks and sliding did not recovered when loading in the opposite direction. This means that the envelope for these two specimens after certain test runs shifted into the negative direction (Figures 4.14 and 4.16). This shift was extracted before the determination of the envelope and therefore the level of the lateral resistance was marked by the horizontal line (Figures 4.17 and 4.19). In addition, for specimen M2-WRAP-G-F-ST, after FRP ruptured the masonry panel slid on its RC foundation; the specimen slid till a drift of 5% without any degradation in the coefficient of friction. However, Figure 4.18 shows the envelope till a drift of 2.5% only.

Table 4.3: Main Test Results

Specimen Name	h [mm]	U.M.	N.L.	E.T.	N.	P [kN]		F [kN]	Δ [mm]	F.M.
						Initial	Final			
S2-REFE-ST	1055	--	--	F.C. D.C.	6 69	30	35	36	7	R
S2-WRAP-G-F-ST		GFRP	1	F.C. D.C.	16 43	30	32	51	3	R

S2-WIRE-S-F-ST		HARD WIRE (vertical direction only	1	F.C. D.C.	12 30	30	34	84	11	R
M2-REFE1-ST	840	--	--	F.C. D.C.	10 12	30	31	28	1	DS*
M2-POST-ST		POST-TENS.	--	F.C. D.C.	4 34	60	63	66	5	R
M2-WRAP-G-F-ST		GFRP	1	F.C. D.C.	24 16	30	34	70	5	FS
M2-2WRAP-G-F-ST		GFRP	2	F.C. D.C.	26 26	29.6	34	95	6	R
M2-REFE2-ST		--	--	F.C. D.C.	8 4	31	32	27	8	DS*
M2-WRAP-A-F-ST		AFRP	1**	F.C.	44	28	31	160	11	R

h: specimen nominal height, specimen nominal dimensions were 75 mm width, and 1600 mm length;
*: diagonal shear due to test set-up problems; **: one vertical layer and one horizontal layer
U.M.: retrofitting method and material; N: number of test runs;
P: post-tensioning force; F, Δ: the maximum of the average of the absolute peak lateral resistances and relative displacement measured in both directions, respectively;
F.M.: failure mode (R: Rocking, RS: Rocking and Shear, and MF: Masonry compression failure and fiber rupture)

4.2.1 Lateral resistance and failure mode

For reference specimen S2-REFE-ST, the specimensí behavior was dominated by a rocking mode that was initiated by flexural tension crack at bed joints in both sides of a specimen (i.e. north and south sides). These cracks extended through the wall length till it connected together. After the cracks connected, there was no continuity left between the upper part and the lower part of the wall (Figure 4.9(c)). Finally, the specimen displayed a characteristic rocking behavior till one toe failed in compression. In addition, before the test end the specimen slid on its RC foundation with a coefficient of friction of 0.83. The sliding displacement was approximately 2 mm and the lateral resistance of the specimen was approximately 36 kN. For midget specimens (M2-REFE1-ST and M2-REFE2-ST), both tests was stopped before the specimens reached its ultimate lateral resistance since it was required to preserve the specimens without heavy damage prior to retrofitting. The test on the first specimen M2-REFE1-ST was stopped after flexural cracks formed at the toes in both directions. The test on the second specimen M2-REFE2-ST was stopped due to strong movement (rocking and sliding) of the head beam which led to stress concentration on limited length of the wall (i.e. the applied lateral force transferred though limited wall length in spite of the whole wall length) and formation of diagonal crack passing through head and bed joints. However, both specimens (M2-REFE1-ST and M2-REFE2-ST) had approximately the same lateral resistance (28 kN).

*Table 4.4: Summary of The Peak Measured Forces and Displacements in the **South-North Direction***

	P_{max} [kN]	P_c [kN]	P_d [kN]	F_{min} [kN]	F_c [kN]	F_d [kN]	Δ_{min} [mm]	Δ_c [mm]	Δ_d [mm]	D_{min} [%]	D_c [%]	D_d [%]	F_c/F_{min}	F_d/F_{min}	Δ_c/Δ_{min}	Δ_d/Δ_{min}
Reference specimens																
S2-REFE-ST	34.9	29.8	--	37.3	24.9	--	7.1*	0.4	--	1.02*	0.05	--	0.67	--	0.06	--
M2-REFE1-ST	30.2	30.1	--	30.7	30.0	--	0.5	0.4	--	0.07	0.06	--	0.98	--	0.80	--
M2-REFE2-ST**	31.1	30.2	--	28.2	20.2	--	15.5	0.5	--	2.25	0.07	--	0.72	--	0.03	--
Retrofitted specimens																
S2-WRAP-G-F-ST	33.2	29.9	--	54.9	20.2	--	3.6	0.4	--	0.52	0.05	--	0.36	--	0.11	--
S2-WIRE-S-S-ST	33.0	29.7	--	81.8	30.3	--	4.3	1.2	--	0.63	0.18	--	0.37	--	0.29	--
M2-POST-ST	61.7	60.0	--	65.0	35.0	--	2.9*	0.5	--	0.41*	0.08	--	0.54	--	0.20	--
M2-WRAP-G-F-ST	34.5	30.1	--	71.8	49.7	--	4.9	0.8	--	0.70	0.11	--	0.69	--	0.16	--
M2-2WRAP-G-F-ST	33.3	29.6	--	95.3	49.5	-	6.9	0.9	--	1.02	0.14	--	0.52	--	0.13	--
M2-WRAP-A-F-ST	29.4	27.6	--	170.1	35.9	--	17.2	0.8	--	2.49	0.11	--	0.21	--	0.05	--

* the test was stop before the 20% reduction in the lateral resistance, ** test set-up problems happened
P: post-tensioning force, F: lateral resistance, Δ: lateral relative displacement, and D: lateral drift
c: cracking, d: delamination

*Table 4.5: Summary of The Peak Measured Forces and Displacements in the **North-South Direction***

	P_{max} [kN]	P_c [kN]	P_d [kN]	F_{max} [kN]	F_c [kN]	F_d [kN]	Δ_{max} [mm]	Δ_c [mm]	Δ_d [mm]	D_{max} [%]	D_c [%]	D_d [%]	F_c/F_{max}	F_d/F_{max}	Δ_c/Δ_{max}	Δ_d/Δ_{max}
Reference specimens																
S2-REFE-ST	34.4	30.1	--	33.7	15.1	--	7.4	0.3	--	1.1	0.05	--	0.45	--	0.04	--
M2-REFE1-ST	30.5	30.3	--	26.0	20.4	--	0.7	0.4	--	0.10	0.05	--	0.78	--	0.50	--
M2-REFE2-ST**	32.4	30.9	--	26.7	26.7	--	0.5	0.5	--	0.08	0.08	--	1.00	--	1.00	--
Retrofitted specimens																
S2-WRAP-G-F-ST	31.1	30.1	--	46.7	30.1	--	1.8	0.5	--	0.26	0.10	--	0.64	--	0.38	--
S2-WIRE-S-S-ST	33.5	29.9	--	85.9	15.2	--	18.0	1.2	--	2.66	0.17	--	0.18	--	0.06	--
M2-POST-ST	64.7	60.4	--	66.2	35.1	--	7.7	1.0	--	1.11	0.14	--	0.53	--	0.13	--
M2-WRAP-G-F-ST	33.8	30.3	--	67.6	15.6	--	4.8	0.3	--	0.69	0.05	--	0.23	--	0.07	--
M2-2WRAP-G-F-ST	34.3	29.6	--	95.0	50.3	--	4.61	0.7	--	0.68	0.11	--	0.53	--	0.15	--
M2-WRAP-A-F-ST	32.1	27.7	--	150.6	30.0	--	4.8	0.6	--	0.70	0.08	--	0.20	--	0.11	--

* the test was stop before the 20% reduction in the lateral resistance, ** test set-up problems happened
P: post-tensioning force, F: lateral resistance, Δ: lateral relative displacement, and D: lateral drift
c: cracking, d: delamination

Regarding the retrofitted specimens, all the retrofitting techniques increased the lateral resistance by a factor that ranged from 1.7 to 5.9 (Figure 4.13). For squat specimens S2-WRAP-G-F-ST and S2-WIRE-S-ST, both specimens developed a rocking mode with masonry crushing at toe. In both specimens, before the specimens reached their ultimate resistances a vertical crack (Figure 4.11) passed through the masonry substrate behind the retrofitting material. This vertical crack followed by a FRP rupture or local buckling of Hardwire. The retrofitting increased the lateral resistance by a factor of 1.7 for S2-WRAP-G-F-ST and 2.33 for S2-WIRE-S-F-ST. It is worth to note that, although specimen S2-WIRE-S-F-ST was retrofitted using a unidirectional material oriented in the vertical direction no shear failure happened during testing the specimen. Limited shear cracking (cracking in the mortar joints and diagonal cracking in the epoxy at toes) appeared at lateral resistance of 63 kN. For S2-WRAP-G-F-ST, the limited increment in the lateral resistance is influenced by the heavy damage in the reference specimen prior to retrofitting. A superposition of the hysteresis loops of the corresponding reference squat specimen (S2-REFE-ST) and the retrofitted specimens (S2-WRAP-G-F-ST and S2-WIRE-S-F-ST) at the test end are presented in Figure 4.14.

For midget specimens, the specimen which was retrofitted using post-tensioning (M2-POST-ST) reached approximately the same lateral resistance as the one that retrofitted using one layer of GFRP (M2-WRAP-G-F-ST, Table 4.3). Both retrofitting techniques increased the lateral resistance by a factor of approximately 2.5. Doubling the number of layers of GFRP in specimen M2-2WRAP-G-F-ST increased the lateral resistance by a factor of 3.4 Finally, the lateral resistance of specimen M2-WRAP-A-F-ST where AFRP was used as retrofitting material was increased by a factor of approximately 5.9. All the midget retrofitted specimens failed in flexural with either masonry compression and/or FRP rupture. In specimen M2-WRAP-G-F-ST and after FRP rupture, the masonry panel slid over its RC foundation; this sliding

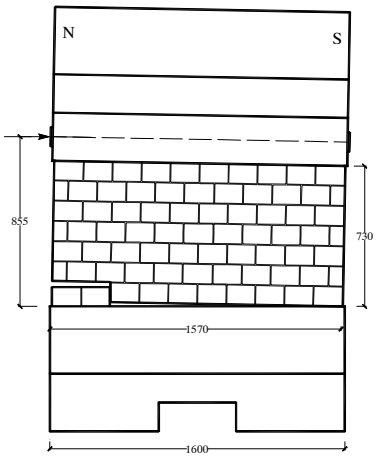

(a)

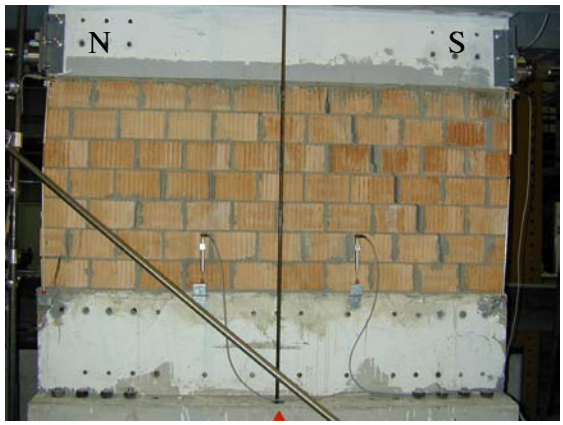

(b)

(c)

Figure 4.9: Failure modes of reference specimens (a) M2-REFE1-ST, (b) M2-REFE2-ST, (c) S2-REFE-ST

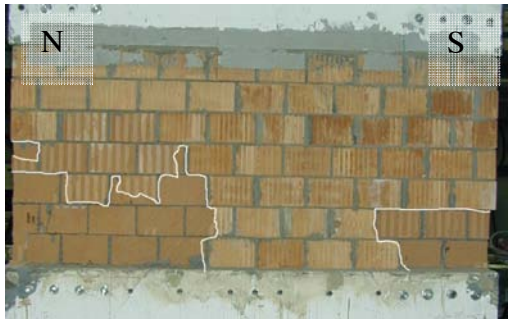

(a)

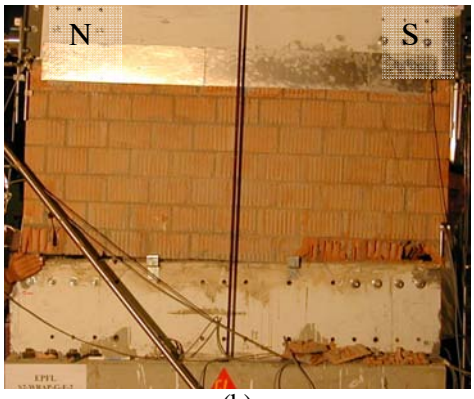

(b)

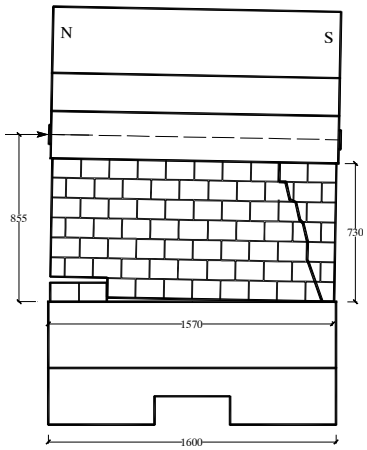

(c)

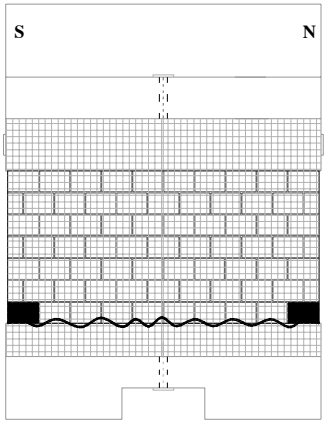

(d)

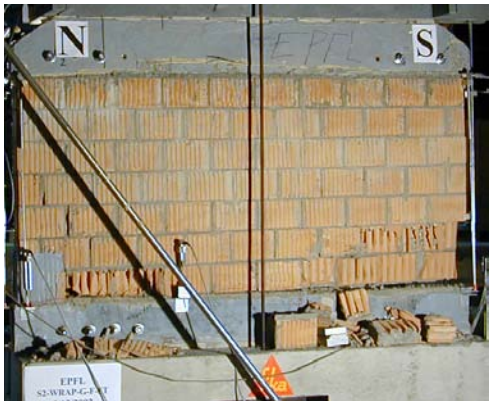

(e)

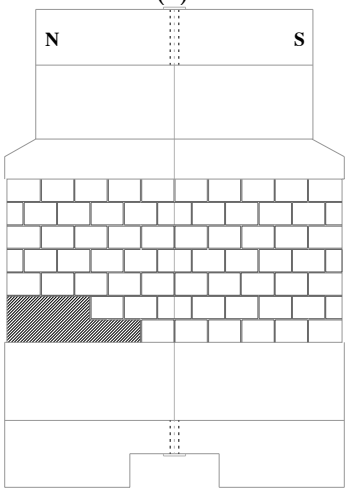

(f)

Figure 4.10: Failure modes of retrofitted specimens (a) M2-WRAP-A-F-ST, (b) M2-WRAP-G-F-ST, (c)M2-POST-ST, (d)M2-2WRAP-G-F-ST, (e) S2-WRAP-G-F-ST, and (f) S2-WIRE-S-F-ST

Figure 4.11: Development of vertical cracks between retrofitting material and masonry panel

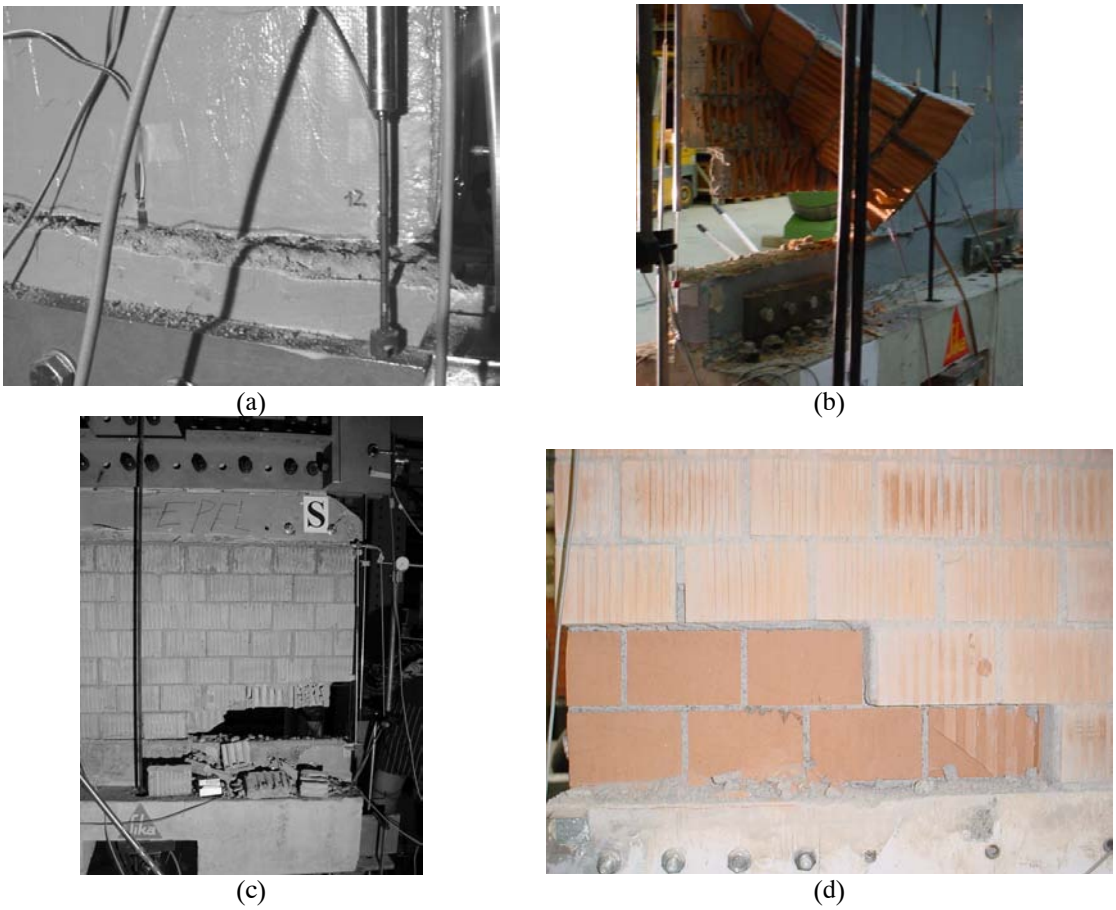

Figure 4.12: Rupture of FRP (a and b) and masonry failure (c and d)

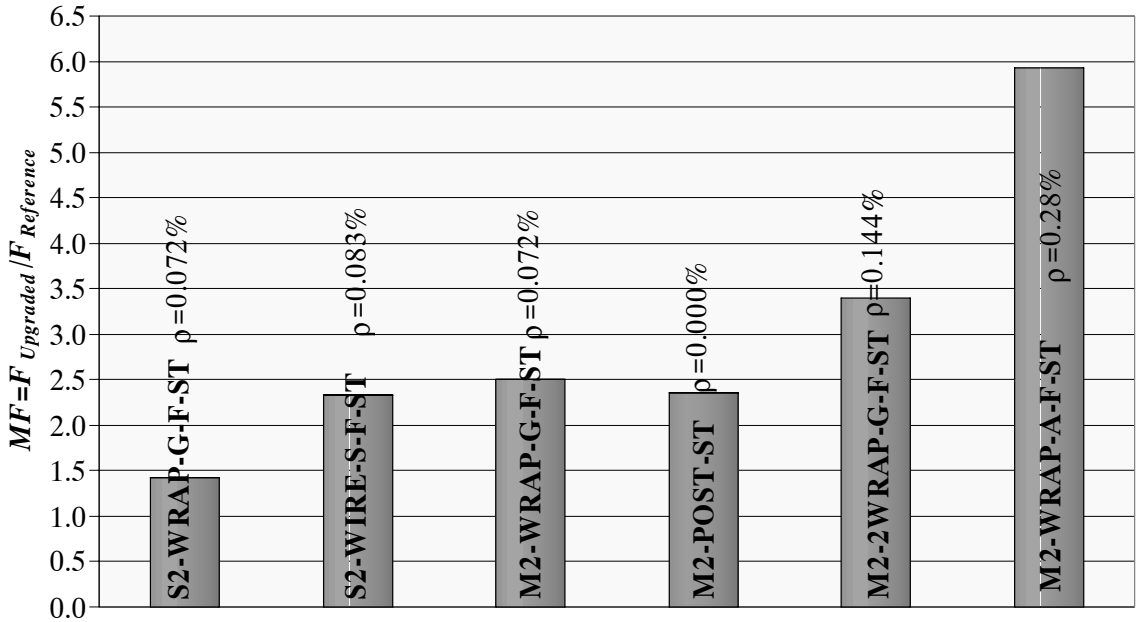

Figure 4.13: Improvements in the lateral resistance of the retrofitting specimens in comparison with the appropriate reference specimens

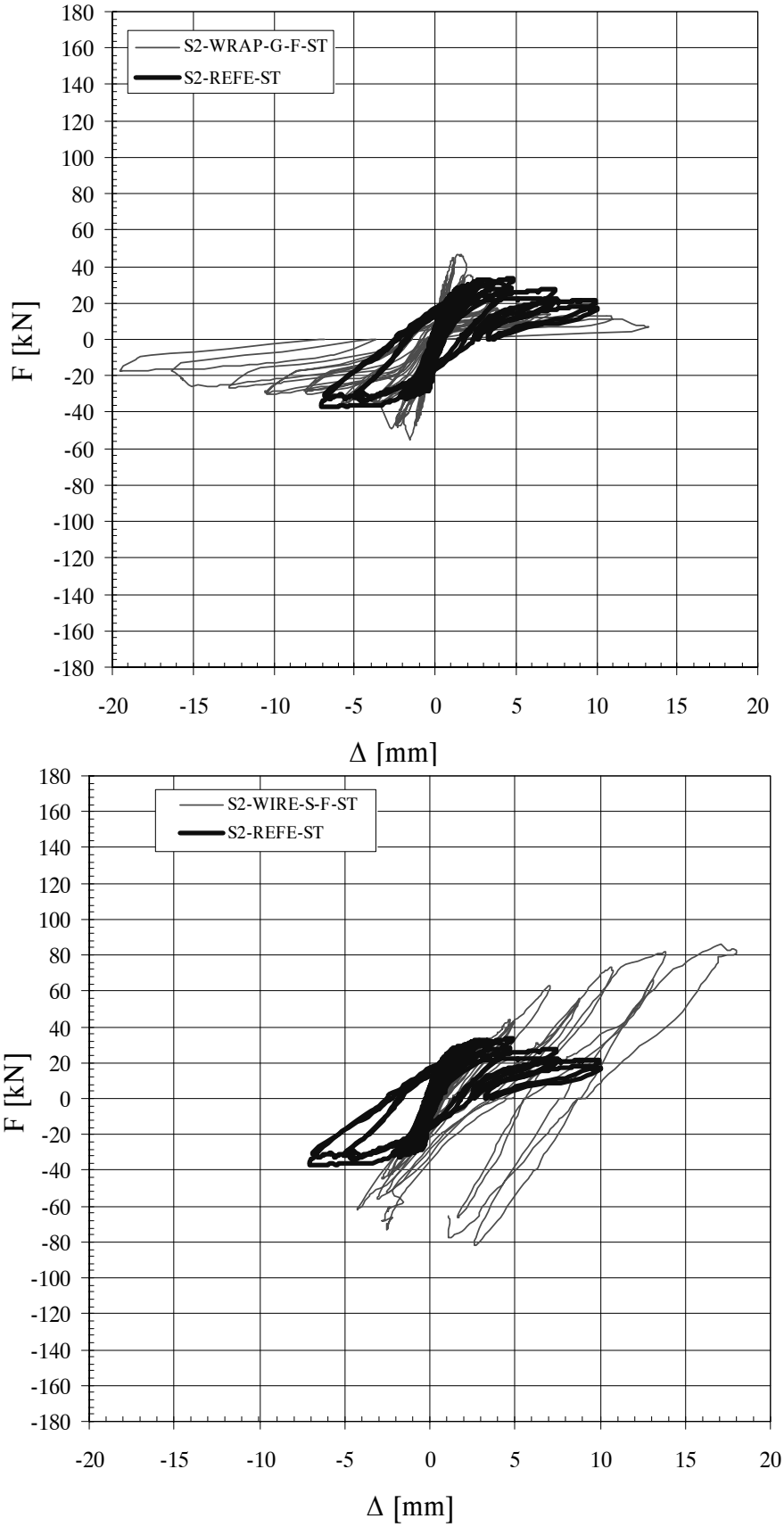

Figure 4.14: Superposition of the hysteresis loops of reference and retrofitted squat specimens

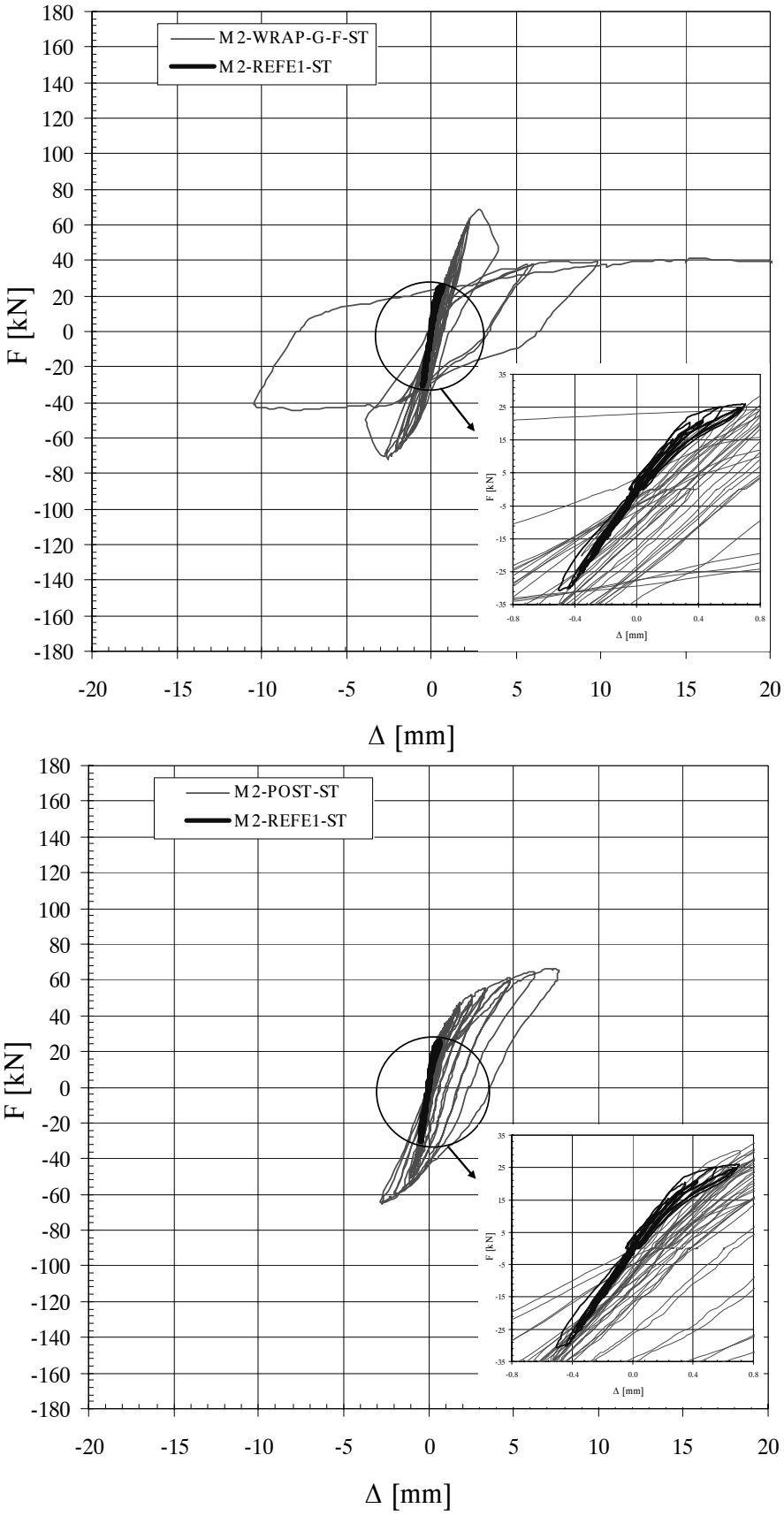

Figure 4.15: superposition of the hysteresis loops of reference and retrofitted midget specimens

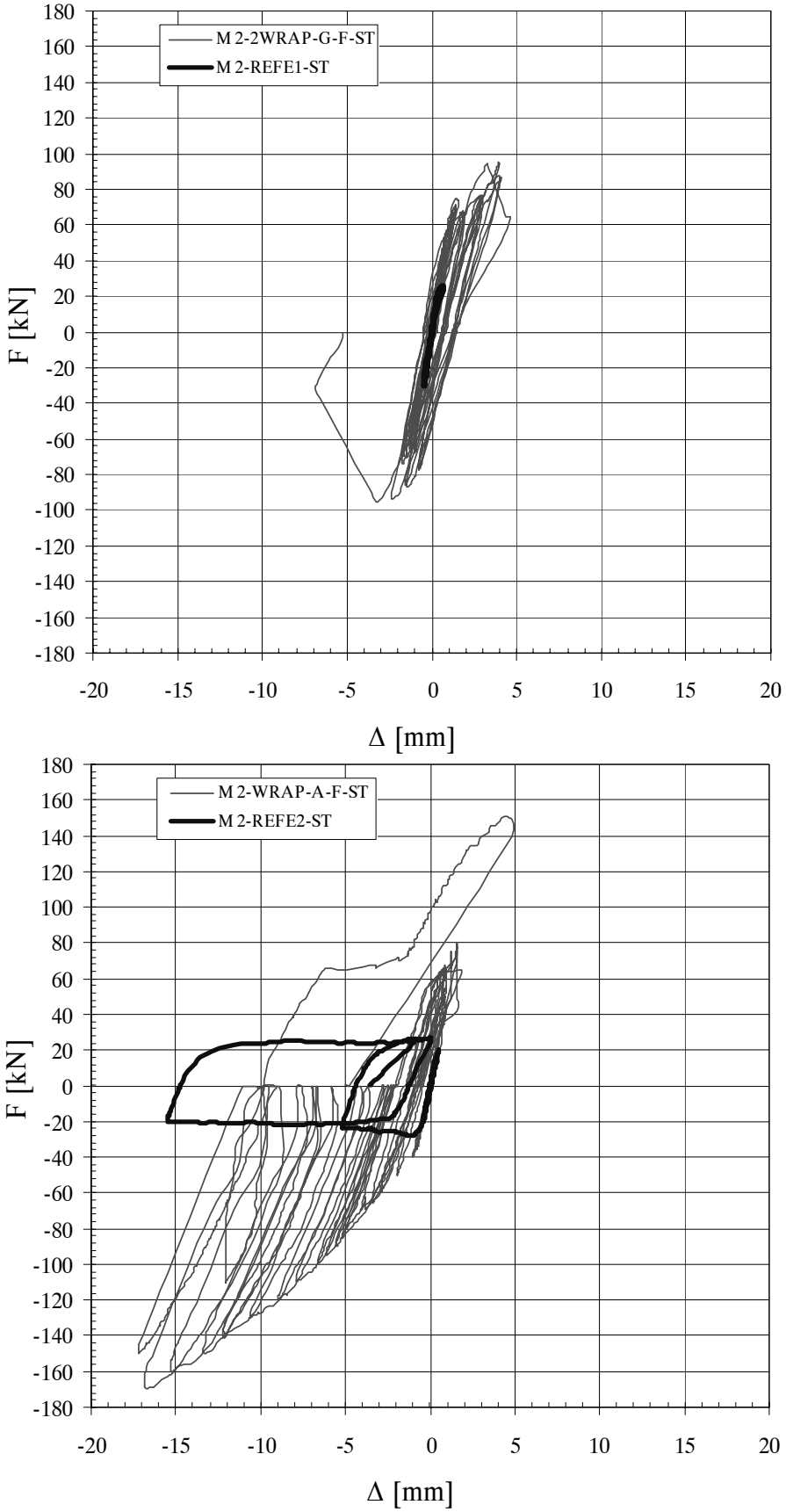

Figure 4.16: Superposition of the hysteresis loops of reference and retrofitted midget specimens

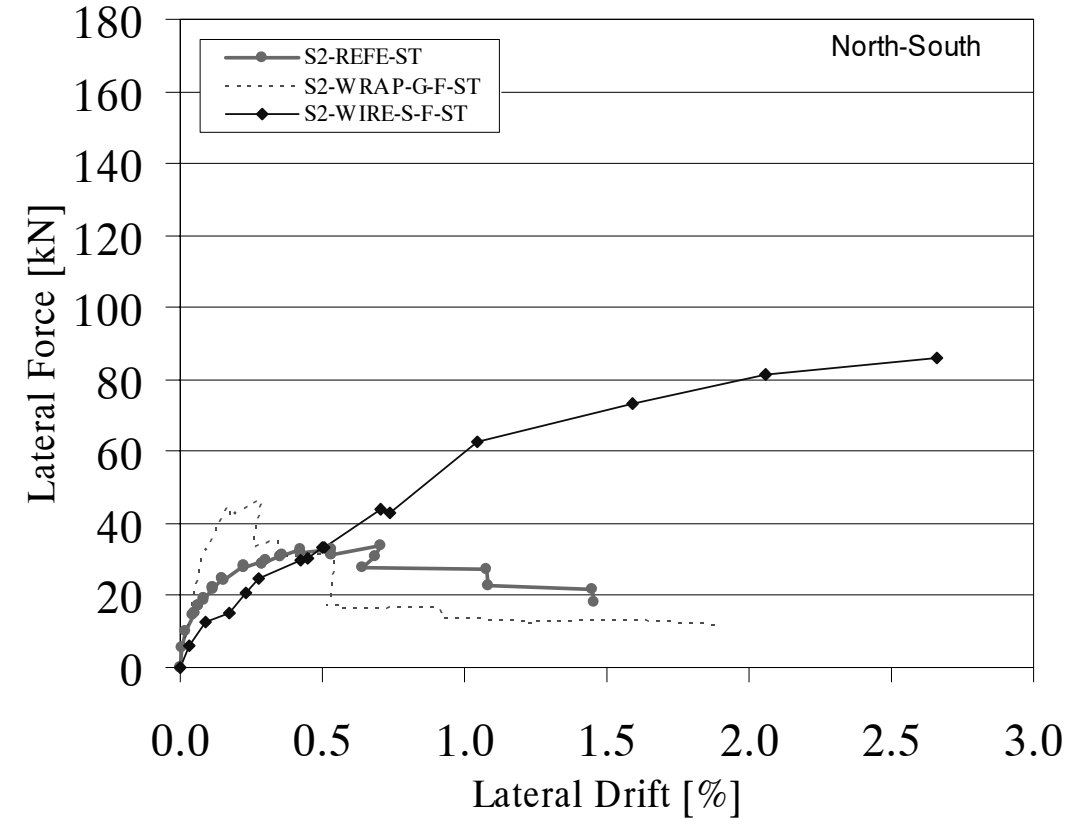

(a)

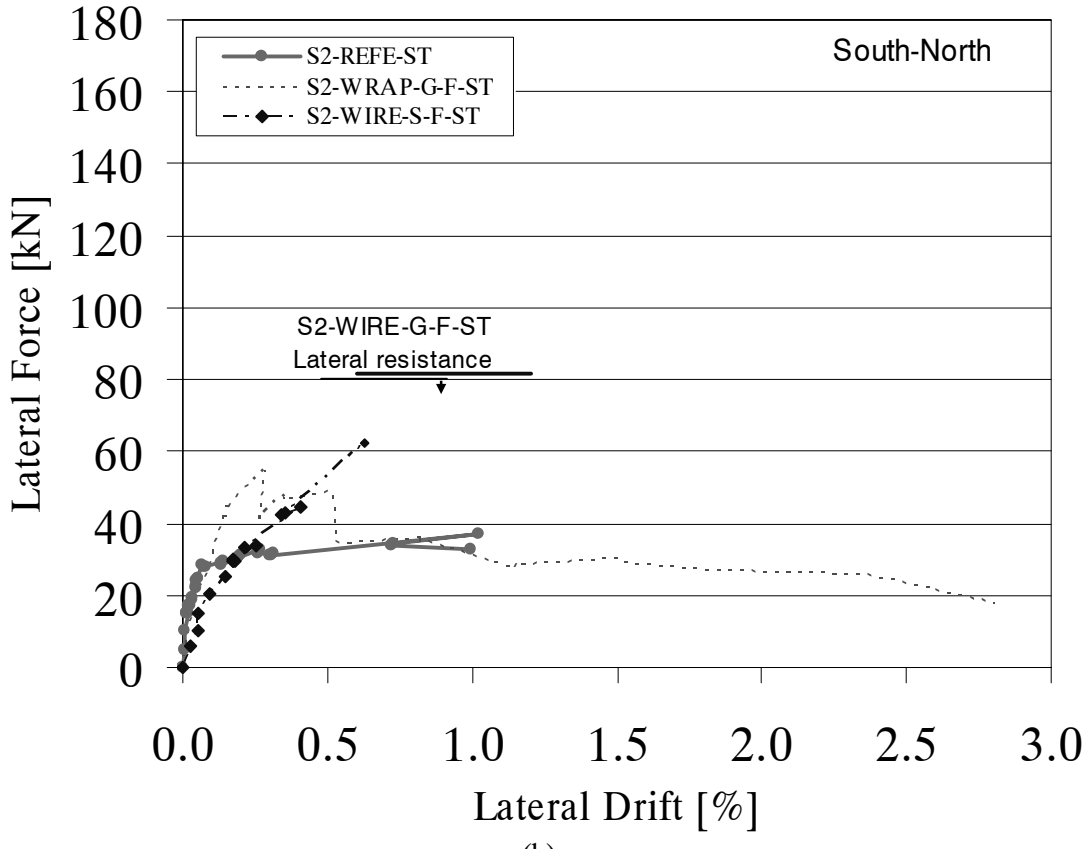

(b)

Figure 4.17: Lateral force versus wall drift for squat specimens (a) north-south (b) south-north directions

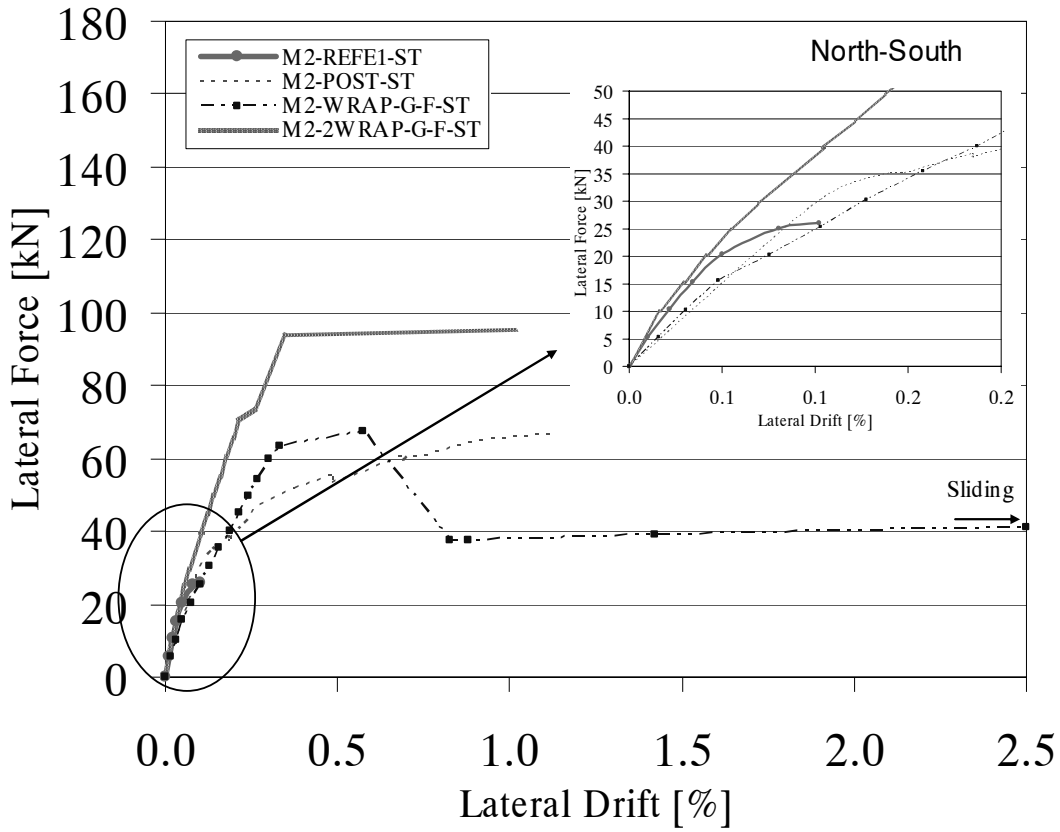

(a)

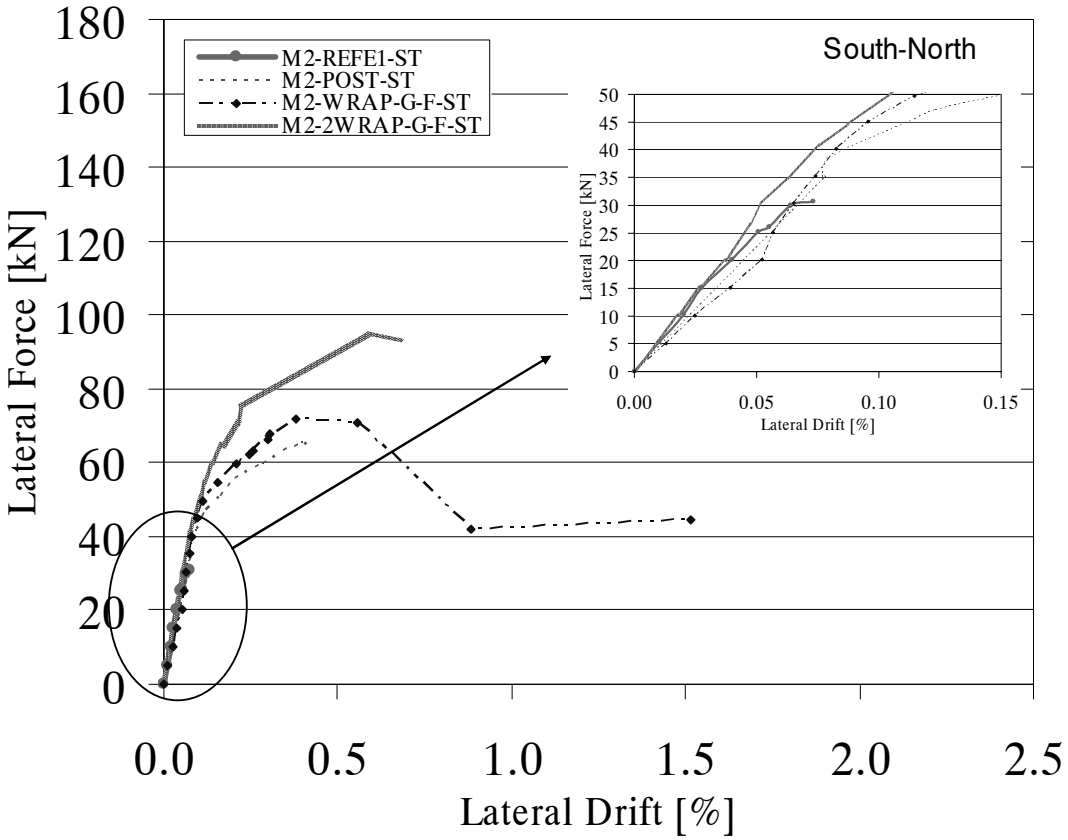

(b)

Figure 4.18: Lateral force versus wall drift for midget specimens (a) north-south (b) south-north directions

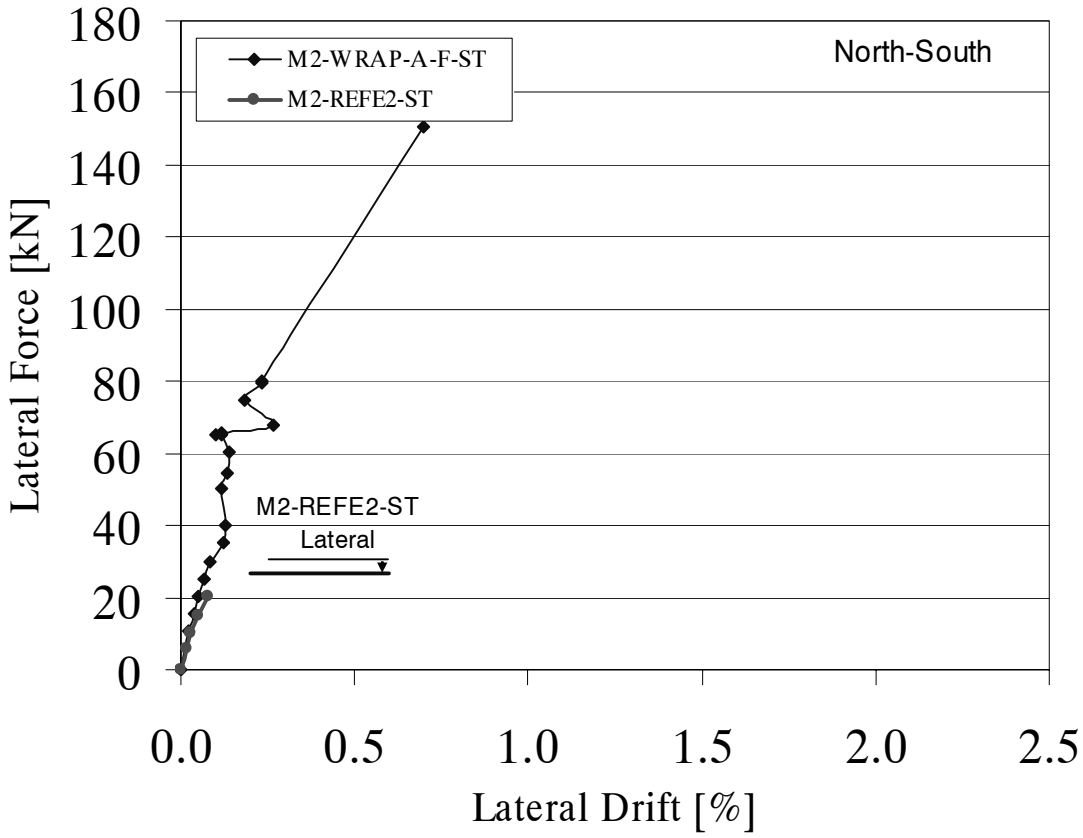

(a)

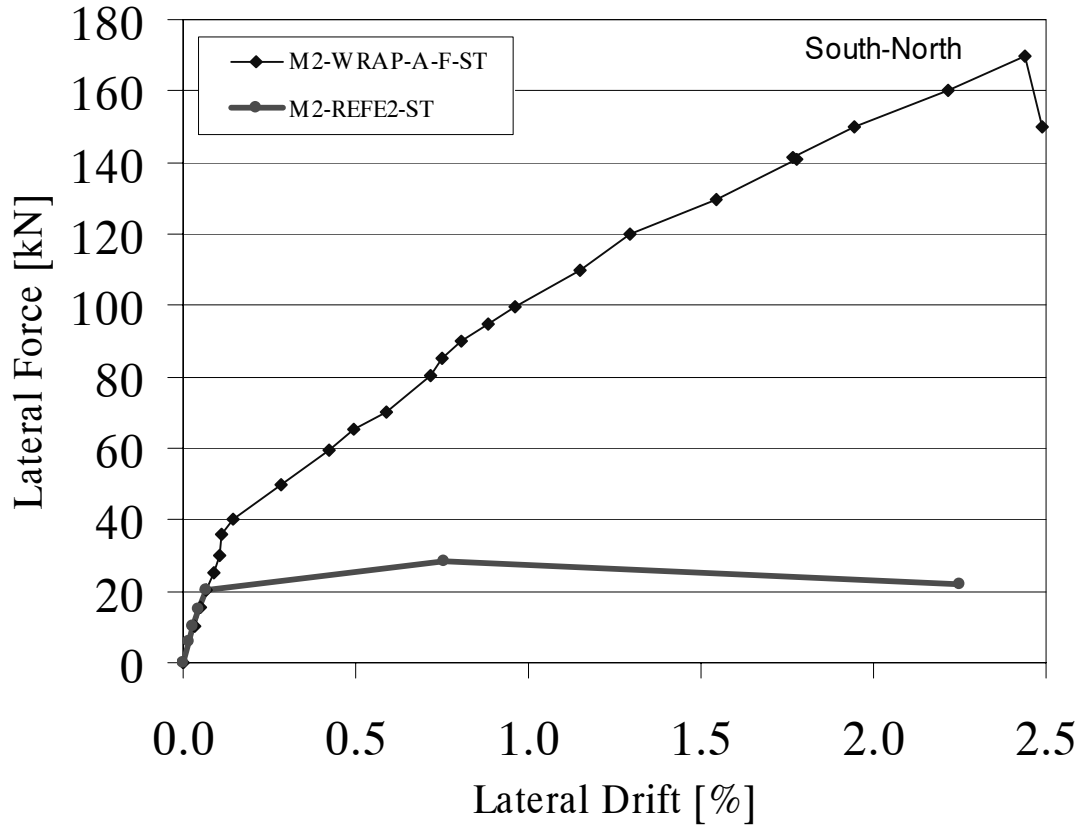

(b)

Figure 4.19: Lateral force versus wall drift for midget specimens (a) north-south (b) south-north directions

4.2.2 Lateral drift and stiffness

As shown in Figure 4.17 and Table 4.3, the retrofitting changed the ultimate lateral drift. The retrofitting material changed the lateral drift by a factor of 0.5 and 1.5 in case of specimen S2-WRAP-G-F-ST and S2-WIRE-S-F-ST, respectively. It should be noted that these factors are determined in the post peak region when the lateral resistance dropped by 20%. However, in case of S2-WRAP-G-F-ST (south-north direction), after GFRP rupture the specimen behaved in the same manner as the reference specimen (Figure 4.17 (b)). For midget specimens it is difficult to determine the effect of retrofitting on the lateral drift as the reference specimens did not tested till its ultimate drift. However, Table (4.3) shows that the specimens that are retrofitted using either post-tensioning, one layer of GFRP, or 2 layers of GFRP reached approximately the same lateral drift. This means that the reinforcement ratio did not influence the lateral drift, since specimen M2-2-WRAP-G-F has double the reinforcement ratio of specimen M2-WRAP-G-F-ST and both reached the same ultimate drift. Finally, specimen M2-WRAP-A-F-ST has a lateral drift approximately two times the other retrofitted specimens (M2-WRAP-G-F-ST and M2-POST-ST). However, it is believed that this increment in the lateral drift was due to the movement of the diagonal crack which formed during testing the reference specimen (M2-REFE-ST).

Regarding the specimens stiffness, although the high degradation of the stiffness of the reference specimens at the testsí end; it should be noted that all the retrofitting techniques success in recovering the initial stiffness of all the specimens. However, the initial stiffness of specimen S2-WIRE-S-F-ST was less than the initial stiffness of specimens (S2-REFE-ST and S2-WRAP-G-F-ST). This could be attributed to the expected variations in the masonry panel itself.

4.2.3 Maximum strains at failure

As discussed in Chapter 3, the FRP strains at failure of major interest; for the tested specimens, the maximum strains, either measured or calculated based on the measured deformations using the linear variable displacement (LVD) transducers, at the masonry and retrofitted faces of the failed test specimens are examined just before FRP failure. The results show the following:

- For vertical GFRP, the strains ranged from 0.5% in specimen S2-WRAP-G-F-ST to 1.6% in specimen M2-WRAP-G-F-ST. For specimen M2-2WRAP-G-F-ST where two layers of GFRP were used as retrofitting the vertical strain was 0.9%. As expected, for higher reinforcement ratio the strains are lower. In addition and since the FRP are subjected to cycles of compression and tension, the strains are dependent on the specimen state before retrofitting. For example, specimen S2-WRAP-G-F-ST was tested as reference specimen without FRP; during that test it was subjected to a sever damage. After retrofitting and due to invisible hair cracking which exist in the toe the FRP subjected to higher rate of tension/compression cycles. This may the low tensile strain measured within FRP in the specimen. However, the maximum strain measured in the GFRP (i.e. 1.6%) is corresponding well to the maximum strains measured in the dynamic tests (1.2%). It should be noted that the strains in FRP are too concentrated locally around the fractured section then drop rapidly; this is different of what is normally observed for reinforced steel bars. This makes it difficult to measure exactly the strains at ultimate failure of FRP. The measured value in the dynamic test was measured along approximately 150 mm; so it is an average rather than the ultimate value. For specimen M2-WRAP-G-F-ST, two values have been measured: 1.6% and 0.9% which measured using strain gages. However, the position of the crack with respect to measuring position is different. Figure 4.20 show the position of strain gages with respect to crack pass as well as schematic distribution of strains in FRP.
- For AFRP, the strains in the vertical FRP are approximately 0.9%. For the Hardwire the strains are 0.4-0.6%. what is interested is that the measured compression strains in the Hardwire approximately 50-83% of its tensile strains with maximum compressive strain of 0.6%; this is generally higher than compression strains in GFRP and AFRP. However, similar value of 0.60% is proposed by Japanese guidelines [YH 97] for grass fiber. For GFRP the compression strain ranged from 0 to 27% of the tensile strain with maximum value of 0.22%. For AFRP, the compression strain ranged from 10 to 50% of the tensile strain with maximum value of 0.35%. The Japanese guidelines [YH 97] proposed compression strain values of 0.2 to 0.3 for AFRP and 0.45% for GFRP. It is interested to note that, the measured compressive strains for AFRP and GFRP exceeded masonry linear behavior which is corresponding to approximately compressive strain of 0.2%. Figure 4.21 show typical lateral resistance strain in the vertical FRP for GFRP and Hardwire.

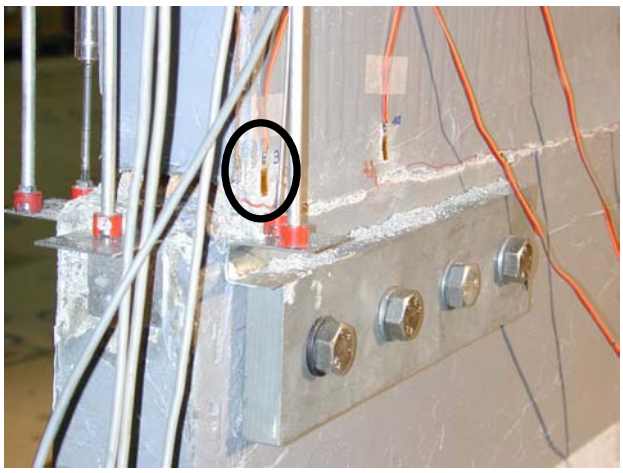

(a)

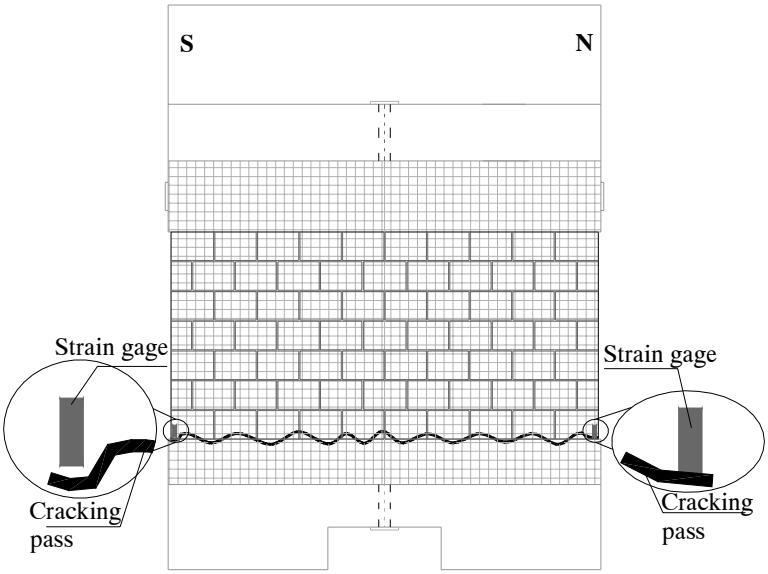

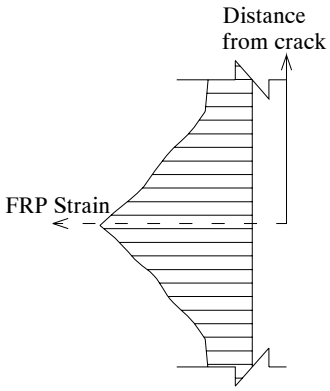

(b) (c)

Figure 4.20: FRP strains (a) position of strain gage, (b) position of two strain gages with respect to crack pass, and (c) schmatic strain distribution in FRP

4.2.4 Specimens asymmetry

As mentioned earlier all the test specimens were retrofitted on single side only. As shown by other researchers [AH 99 and Sc 94] this system did not result in any asymmetry in deformations, which may result in more complicated failure mechanism. In order to evaluate this issue for the tested specimens, a comparison between the vertical strains, calculated based on measured displacements using LVD transducers, on the masonry face ì bare faceî and the retrofitted face was carried out. The comparison shows the following:

- For squat specimen retrofitted using GFRP (S2-WRAP-G-F-ST), the retrofitting system succeed in producing complete symmetric response in case of tension while there was a little asymmetry in case of compression. The average vertical strain along the masonry face was approximately 93% of the average vertical strain along the FRP face; this ratio is close to the similar ratio measured during the dynamic test (it was approximately 118%). In compression, the average vertical strain along the masonry face was approximately 130% of the average strain along the FRP face in one direction (when loading in North-South direction). On the other direction, the average vertical strain along the masonry face was approximately 380% of the average strain along the FRP face. Regarding results of compression, these results are contrary to what is measured during the dynamic test. The possible explanation is that this specimen is tested till failure while in the dynamic test on the similar specimen (S1-WRAP-G-F) the test was stopped before

failure. Another factor is that this specimen is severely damaged during it was tested as reference specimen while the reference specimen of the similar dynamic specimen was not severely damaged.

- For squat specimen retrofitted using Hardwire (S2-WIRE-S-F-ST), contrary to FRP the retrofitting system did not success in producing symmetric strains during tension. The average vertical strain along the masonry face was approximately 211% of the average vertical strain along the Hardwire face. In compression, the average vertical strain along the masonry face was approximately 54% of the average strain along the Hardwire face.
- For midget specimens, the retrofitted system succeeded in producing symmetric response in case of tension. The average vertical strain along the masonry face was approximately 105% of the average vertical strain along the FRP face. In compression, since the deformations were too the LVDTs were very sensitive and there were instability in the measurements.

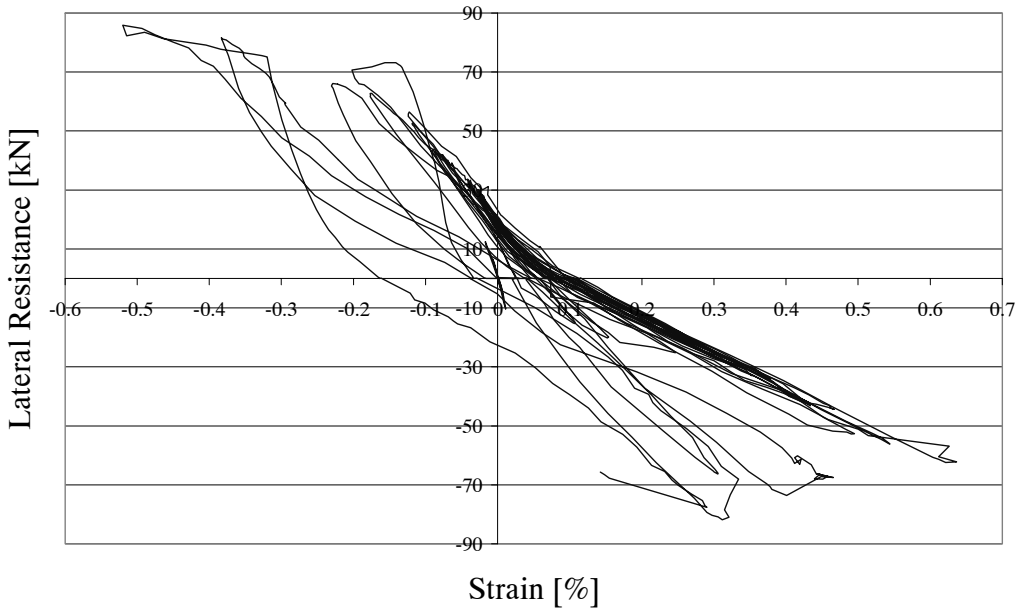

(a)

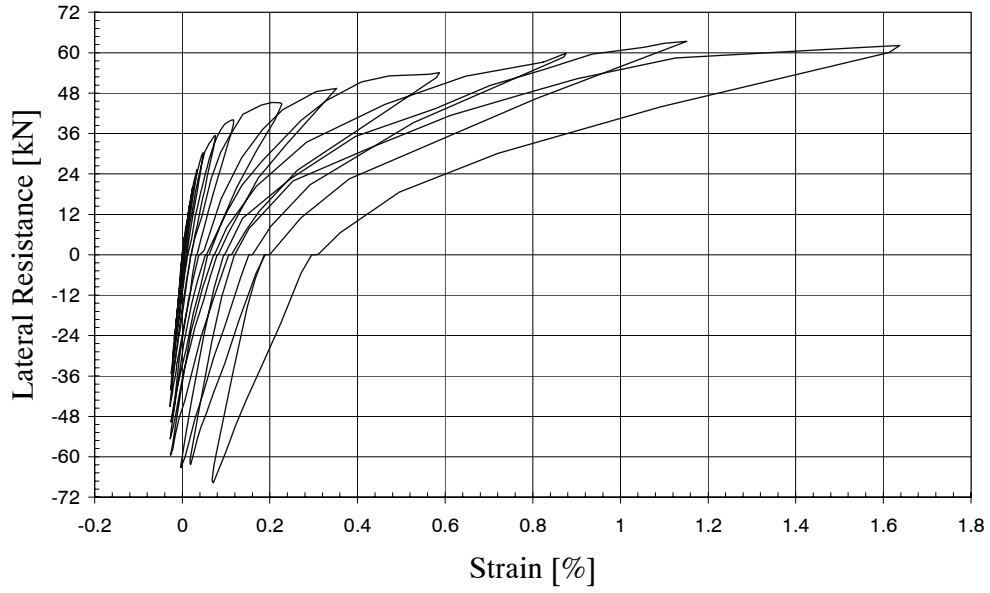

(b)

Figure 4.21: Typical lateral resistance vs. strains in the vertical (a) Hardwire (specimen S2-WIRE-S-F-ST) and (b) GFRP (specimen M2-WRAP-G-F-ST)

4.2.5 Comparison of dynamic and static cyclic test results

As explained in Chapter 3 a dynamic test was previously carried out on a squat reference specimen as well as a squat specimen retrofitted using GFRP. In addition, in this Chapter a static cyclic test on squat specimen before and after retrofitting using GFRP is presented. This section presents a comparison between specimens S2-REFE-ST and S2-REFE as well as S2-WRAP-G-F-ST and S1-WRAP-G-F. The specimens are identical in each aspect except that specimen S1-WRAP-G-F was constructed using mortar type 1 while specimen S2-WRAP-G-F-ST was constructed using mortar type 2 (keep in mind that mortar type 2 is stronger than type 1). Note that the dynamic test was stopped before the ultimate state of the specimens was reached. This happened due to different reasons. In case of the reference specimen, the test was interrupted in order to preserve the specimen for retrofitting and retest. In case of the retrofitted specimen, the test was interrupted because the maximum force capacity of the shaking table hydraulic jack was reached. This comparison shows the followings:

- For the reference and retrofitted specimens, the testing method has insignificant effect on the initial stiffness.
- Although the higher resistance of the mortar used in specimen S1-REFE, specimen S2-REFE-ST has a lateral resistance 1.2 times the lateral resistance of S1-REFE. This difference in lateral resistance is probably due to the test method.
- S1-WRAP-G-F has a lateral resistance 1.5 times the lateral resistance of S2-WRAP-G-F-ST. However, the comparison is difficult in this case because the state of the reference specimens were different before retrofitting. As the reference specimen was preserve in the dynamic test, it was heavily damaged in the static cyclic test. As a consequence it is believed that the high difference in the lateral resistance between the retrofitted specimens in the static cyclic and dynamic tests is due to state of the reference specimens before retrofitting as well as due to the test method.
- The ultimate drift reached in the static cyclic was much higher than the drift reached in the dynamic test. However, it is not possible to drawn a conclusion from that as the dynamic test was stopped before the ultimate drift of the specimens was reached.
- Until the end of the dynamic test, the behavior and mode of failure of the reference specimens was the same regardless of the testing method. However, at the end of the static cyclic sliding happened. This sliding was not possible to confirm for the dynamic test.

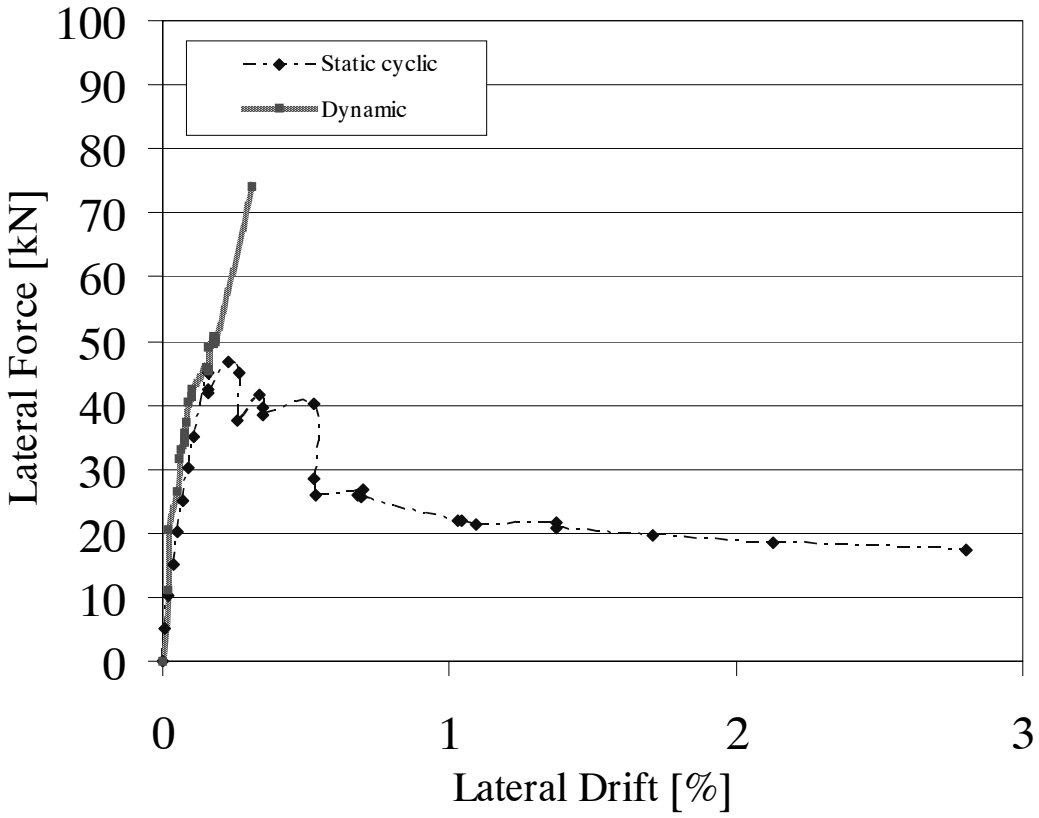

(a)

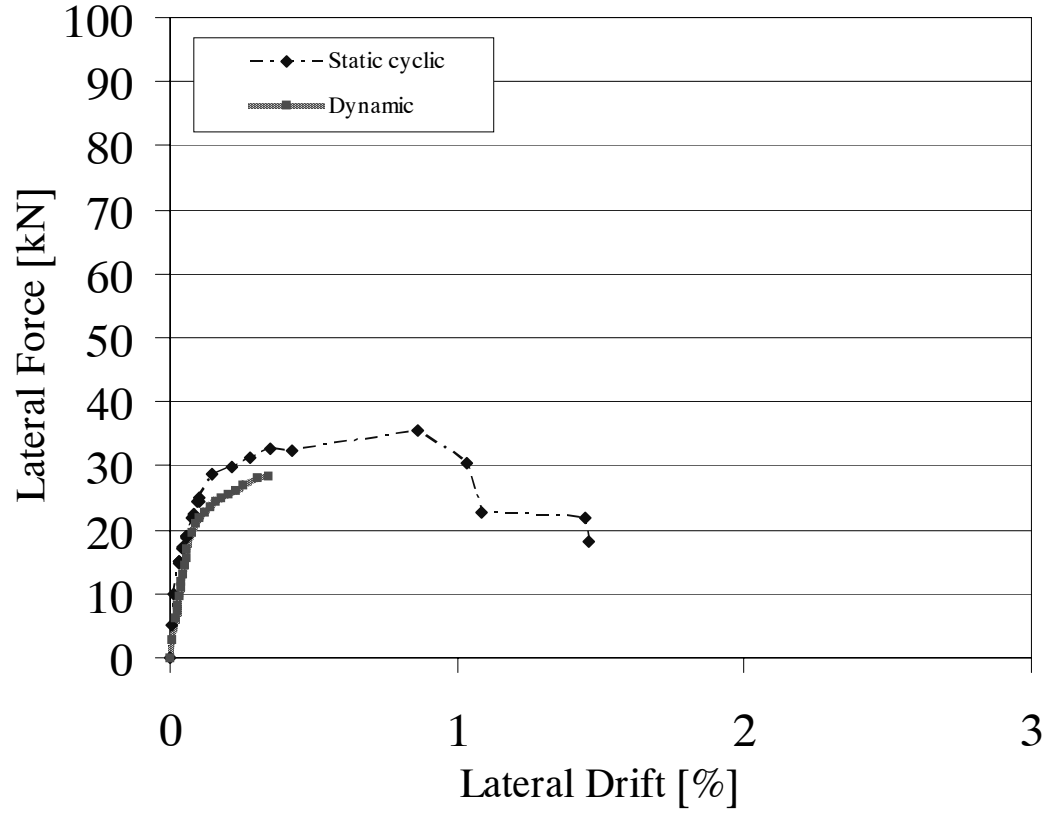

(b)

Figure 4.22: Average lateral force versus average wall drift for squat specimens (a) retrofitted specimens (S1-WRAP-G-F and S2-WRAP-G-F-ST) and (b) refernce specimens (S2-REFE and S2-

REFE-ST)

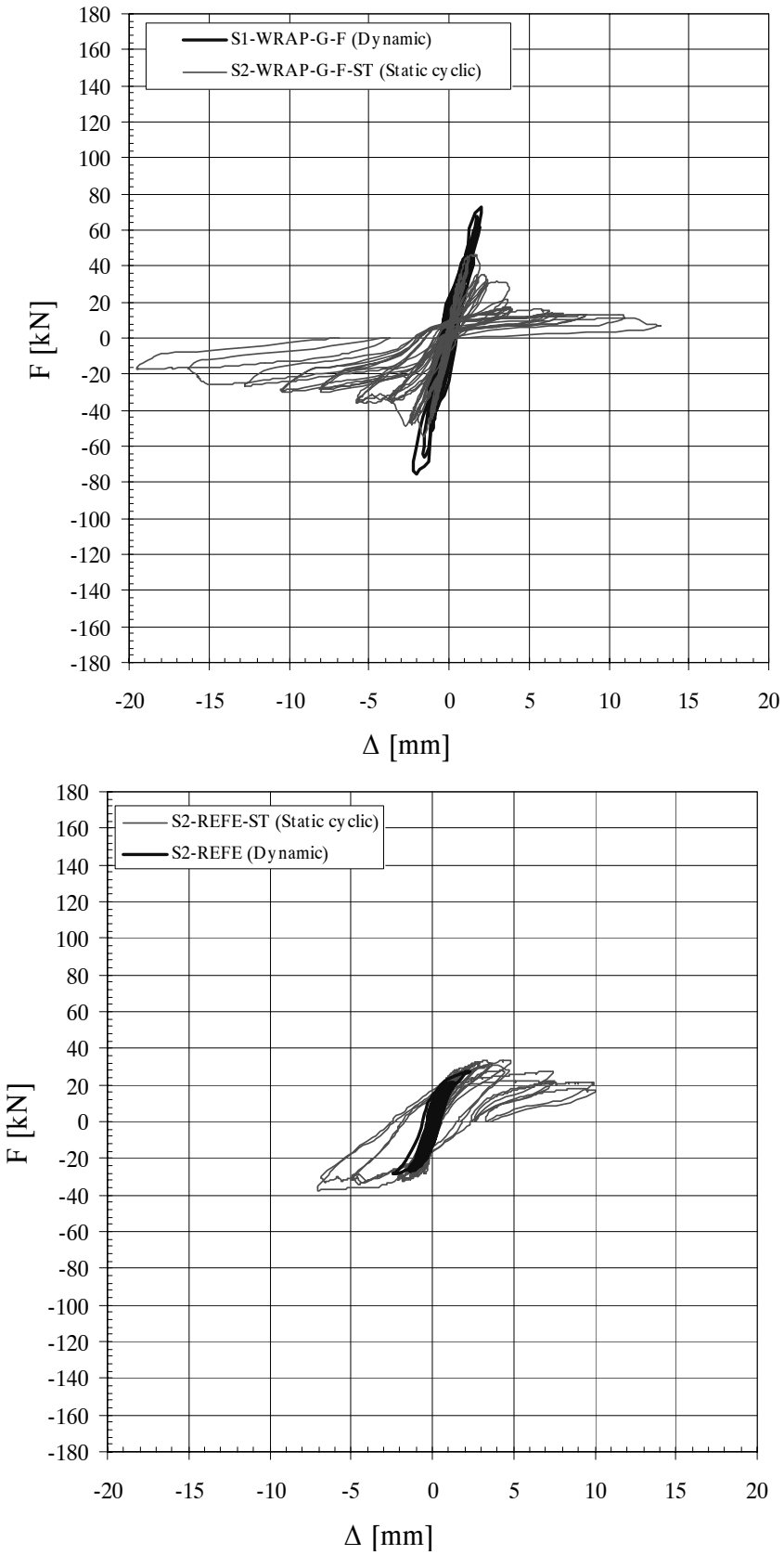

Figure 4.23: Superposition of the hysteresis loops of squat specimens tested in dynamic and static cyclic tsest (a) retrofitted specimens using GFRP, and (b) reference specimens

4.3 Summary

This chapter describes and summarizes static cyclic tests carried out on URM walls before and after retrofitting. Five half-scale URM walls were built using half scale brick units. Of them, three walls were tested as reference specimens. Then, these reference specimens were retrofitted and retested. The rest of the specimens i.e. two walls were retrofitted directly after construction. As a consequence, a total of nine specimens were tested before and after retrofitting. The retrofitting was carried out using either FRP, Hardwire, or post-tensioning. This test has investigated the following parameters:

- the aspect ratio: squat (aspect ratio of 0.67) and midget (aspect ratio of 0.50)
- the retrofitting technique: applying either post-tension force, FRP, and Hardwire
- the fiber type: aramid, and glass
- the reinforcement ratio: one layer, and two layers
- the retrofitting directions: in both directions i.e. horizontal and vertical, or vertical only

The static cyclic experimental testing of URM-FRP specimens, led to the following findings:

- The retrofitting materials increased the specimensí lateral resistances by a factor of 1.7 to 5.9 compared to the reference (URM) specimens.
- By defining the ultimate drift as the drift attained when the lateral resistance reduced by 20%; the GFRP reduce the ultimate drift of the retrofitted specimen by a factor of 0.5. Furthermore, the ultimate drifts were independent on the reinforcement ratio.
- Unlike dynamic tests, no debonding of the fibers in the form of white spots has been observed during the static cyclic tests.
- Using post-tensioning as retrofitting approximately doubled the lateral resistance of the reference specimen and approximately was equivalent to use a single layer of GFRP from lateral resistance and drift point of view.
- Doubling the reinforcement ratio did not produce double the lateral resistance; the lateral resistance in case of two layers of GFRP was approximately 1.4 times the lateral resistance in case of single layer of GFRP.
- Using Hardwire material increased the lateral resistance and drift, with respect to the reference specimen, by a factor of 2.3 and 1.5, respectively. In addition, despite the unidirectional Hardwire oriented in the vertical direction only, no shear failure was observed either in the masonry itself or in Hardwire.
- All the retrofitting procedure success in recovering the initial stiffness of the reference specimens.
- The initial stiffness for the reference and retrofitted specimens was approximately equal in the static cyclic and dynamic tests.
- The lateral resistance of the reference specimen in the static cyclic test is approximately 20% higher than the lateral resistance in the dynamic test.
- Within the test conditions, retrofitting on single side appears to produce good behavior. No out-of-plane or uneven response of the specimens was observed. Small asymmetries in the transducers were recorded in the case of squat specimens.
- The fabric prevented falling of debris from the wall after failure; thus, preventing possible injuries to occupants in the vicinity of the wall in the event of an earthquake in a real case.

5 ANALYTICAL MODEL FOR SHEAR BEHAVIOR OF MASONRY WALLS RETROFITTED USING FRP

As shown in the literature (Chapter 2) several theoretical and empirical models have been developed for out-of-plane analysis of unreinforced masonry walls retrofitted using FRP (URM-FRP). In contrast, there is a lack of analytical models for in-plane shear analysis of URM-FRP. The existing models for in-plane shear analysis of URM-FRP are empirical models developed originally for RC elements. However, the contribution of FRP to the shear strength of RC beams has not yet been correctly estimated [JCI 98]; the problem is still under investigation and the results obtained thus far are scarce and sometimes controversial [BC 04 and TA 00]. This is due in part to the complexity of shear problems as well as the lack of a rational behind the shear resistance mechanism of RC beams retrofitted using FRP [BC 04]. For RC beams retrofitted with FRP and after years of research as well as more than 100 tests, the parameters which influence the shear resistance are identified and qualitative relations between these parameters are established [BC 04]. Regarding in-plane shear behavior of URM-FRP, the problem is deeper since there is a lack of experimental and analytical work. This chapter presents an analytical model for in-plane shear behavior of URM-FRP. The introduction of this chapter includes discussion of three existing models for in-plane shear that were originally developed and calibrated with RC elements. The introduction is followed by derivation of governing differential equation for linear elastic model. Then, a computer program is developed to combine the solution of the differential equations with material nonlinearity. The material nonlinearity was represented by a step by step degradation in material properties; after each step the equations were resolved linearly. The proposed basic analytical model allows the fundamental investigation of in-plane shear behavior of URM-FRP. Finally, a parametric study and comparisons with existing models as well as the experimental work presented in Chapters 3 and 4 are carried out.

5.1 Existing Models for Shear Design of URM-FRP

Studies on shear retrofitting of URM using FRP are limited. Most testing was carried out either on out-of-plane or in-plane retrofitting of slender walls failing in flexural. In addition, since numerous parameters affect the behavior of URM-FRP, the priority of the early experimental studies on this subject (e.g. [Sc 96]) was to focus on the effectiveness of the technique rather than to quantify the effect of different parameters. Understanding of shear resistance mechanism based on these limited experimental data seems not possible. Moreover, the behavior of URM walls in shear is by itself a complex challenge that has not been completely resolved, due to the lack of a suitable harmonized test method and suitable input parameters for a suitable design model [Me 04]. In addition, several parameters influence shear behavior of URM; of them: aspect ratio of the wall, the applied normal force, cohesion, coefficient of friction, unit tensile strength. In case of URM-FRP, other failure modes are observed and new aspects related to the FRP are introduced which increase the complexity of shear problem. Examples of such new aspects include:

- Besides retrofitting configuration, the FRP technology offers a wide range of products with variations in type and fiber orientation, increasing thereby the number of parameters that influence the resistance mechanism involved
- FRP behaves linearly in tension up to failure, whereas conventional reinforced steel does not
- Adding externally bonded FRP to masonry surfaces makes adherence and bond mechanisms important.

Some relevant literature regarding shear retrofitting of RC beams show the following: the effectiveness of the retrofitting reinforcement, that is, the load carried by the FRP at the ultimate limit state, depends on its failure mechanism. As suggested by experimental evidence, failure of the FRP may occur either by debonding or by tensile fracture. This tensile fracture may occur at stresses lower than the tensile strength of the composite material (e.g. at debonded areas). In many cases, the actual failure mechanism is a combination of FRP debonding at certain areas and tensile fracture at others [Tr 98].

A detailed investigation on shear retrofitting of reinforced concrete beams shows that researchers have modeled FRP materials in an analogy with internal steel stirrups. They assume that the contribution of FRP to shear capacity emanates from the capacity of fibers to carry tensile stresses at specified (effective) strain, which is equal either to a constant value (e.g. the FRP ultimate tensile strain or reduced value) or to a variable value (e.g.

inversely proportional to the FRP axial rigidity). The next sections review the shear resistance of URM-FRP using the following three concepts:

- Variable value of FRP axial strain (an axial strain inversely proportional to the FRP axial rigidity); Triantafillou [Tr 98] has implemented this concept in a recent empirical design model.
- Combination of a constant and variable value of FRP axial strain (e.g. Triantafillou and Antonopoulos [TA 00] model); note that this model is proposed for RC beams retrofitted using FRP
- A constant value of FRP axial strain (e.g. AC 125 of ICBO [IC 01])

5.1.1 Triantafillou model [Tr 98]

The only available shear design model for URM-FRP which adapted the concept of variable axial strain in FRP has been developed by Triantafillou [Tr 98]. This empirical model is based on qualitative considerations and calibrated with tests on RC beams. The model assumptions are:

- Dowel action of vertical FRP is neglected in shear,
- Shear is resisted by masonry specimen and horizontal FRP only (equation 5.1),
- Horizontal FRP can be modeled in analogy to steel stirrups in reinforced concrete beams.

According to the model, the lateral resistance of URM wall retrofitted using FRP can be calculated as follows:

$$F = F_m + F_{FRP} \tag{5.1}$$

$$F_{FRP} = \rho_h \, E_{FRP} \, \varepsilon_{eff} \, t \, L \tag{5.2}$$

$$\rho_h = \frac{A_{FRP}}{Lt} \tag{5.3}$$

where

F_m = lateral resistance of URM specimen
F_{FRP} = contribution of FRP to the lateral resistance of URM specimen,
ρ_h = reinforcement ratio of FRP in horizontal direction,
E_{FRP} = modulus of elasticity of FRP,
ε_{eff} = effective FRP strain (this term refers to the maximum mobilized axial force in the FRP)
A_{FRP} = cross sectional area of FRP

The effective FRP strain ε_{eff} is the only unknown in equation 5.2 to determine the contribution of FRP in shear resistance of URM specimen. This ε_{eff} is significantly lower than the ultimate strain due to stress concentrations in the vicinity of a crack. To evaluate this term Triantafillou [Tr 98] derived a polynomial function, for reinforced concrete shallow beams, that relates the strain in the FRP at beam failure to the axial rigidity of FRP i.e. $\rho_h E_{FRP}$. This polynomial was derived through curve fitting on about 40 test data published by various researchers. The effective FRP strain (Figure 5.1) may be calculated as follows:

$$\varepsilon_{eff} = \begin{cases} 0.0119 - 0.0205(\rho_h E_{FRP}) + 0.0104\,(\rho_h E_{FRP})^2 & 0 \le \rho_h E_{FRP} \le 1GPa \\ 0.00245 - 0.00065(\rho_h E_{FRP}) & \rho_h E_{FRP} > 1GPa \end{cases} \tag{5.4}$$

The modeling approach has the following shortcomings:

1. Empirical model: it is not possible to use the model to study the effect of different parameters (e.g. epoxy properties) on the behavior of retrofitted walls.
2. Calibrated with tests on RC elements: there is a huge difference between concrete and existing masonry characteristics. Differences in strength, surface texture, and absorption capacity are expected to affect debonding, which was not introduced as a design variable. In addition, it is arguable that the behavior of URM is much complex than that of concrete [Zh 95]. Masonry is a two-phase material and its properties are therefore dependent upon the properties of its constituents, the brick and the mortar. The influence of mortar as a plane of weakness is a significant feature, which is not present in concrete.

3. Calibrated with shallow beams in which shear mechanism should be different than shear mechanism in structural walls. Note that, the AC125 [IC 01] proposed lateral resistance for RC beams, retrofitted using a certain amount of FRP, 40% higher than RC wall retrofitted using the same type and amount of FRP.
4. The relatively large scatter in Figure 5.1 indicates that other parameters not yet captured may influence the shear resistance
5. FRP fracture was assumed to occur simultaneously with shear failure, whereas in reality it may occasionally appear after the peak load (shear capacity) is reached.
6. One equation was used to describe both FRP fracture and debonding regardless of the type of FRP material
7. Both wrapped and unwrapped specimens were represented with the same line. As shown in Figure 5.1, stresses in wrapped specimens are generally higher than stresses in unwrapped specimens.
8. It is proposed to use Roberts's semi empirical equation [Ro 89] to estimate debonding failure load. It should be noted that, this equation is calibrated with beams where debonding (delamination) occurs near supports (i.e. maximum shear and minimum bending moment). In case of URM-FRP, supports are characterized with maximum moment and shear. Roberts's equation is no more valid in this case.
9. No experimental verification have been carried out on URM-FRP failing in shear

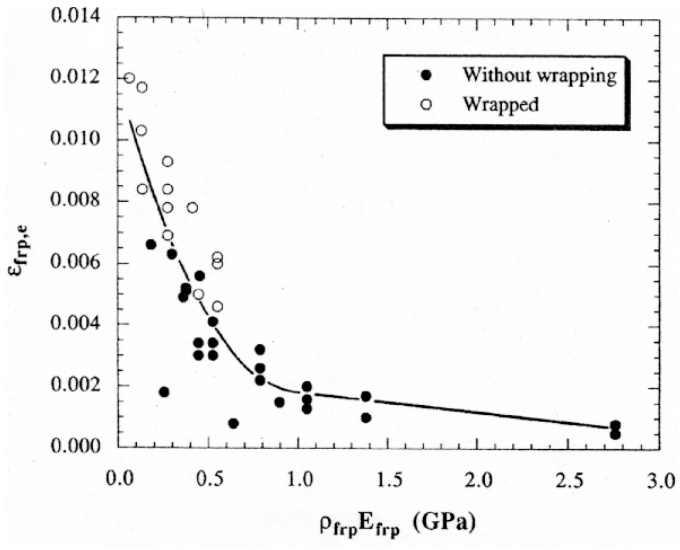

Figure 5.1: Effective strain in FRP($\varepsilon_{frp,e}$) in terms of FRP axial rigidity ($\rho_{frp} E_{frp}$)

5.1.2 Triantafillou and Antonopoulos model [TA 00]

Triantafillou and Antonopoulos [TA 00] have developed and simplified Triantafillou's model [Tr 98] and overcome several shortcomings of the original model. The new model is proposed for shear design of RC beams retrofitted using FRP. The model is calibrated with more experimental data and they separate the two modes of failure of FRP: FRP fracture and FRP debonding. In both cases, the ε_{eff} is estimated based on combinations of qualitative considerations and calibration with 75 test data. Based on this calibration, the following expression for effective FRP strain is proposed:

$$\frac{1}{\alpha}\varepsilon_{eff} = min\begin{cases} 0.00065\left(\dfrac{f_c^{\frac{2}{3}}}{\rho_h E_{FRP}}\right)^{0.56} & (\text{debonding}) \\ 0.17\left(\dfrac{f_c^{\frac{2}{3}}}{\rho_h E_{FRP}}\right)^{0.30}\varepsilon_{FRP}\ \text{for CFRP and}\ 0.048\left(\dfrac{f_c^{\frac{2}{3}}}{\rho_h E_{FRP}}\right)^{0.47}\varepsilon_{FRP}\ \text{for AFRP} & (\text{rupture}) \\ 0.005 & (\text{aggregate interlock}) \end{cases} \quad (5.5)$$

where

α = 1.25 is a reduction factor to transfer the mean value of ε_{eff} to a characteristic value

f_c = concrete characteristic compressive strength

The main advantage of this model is that it is separate between the two modes of failure (i.e. debonding and FRP rupture). However, besides shortcomings similar to the first four points in the original model, it is worth to note the following limitations and shortcomings:

1. In case of FRP debonding, the model is mainly calibrated using specimens retrofitted using CFRP and very limited specimens using GFRP and no specimens using AFRP. However, it was suggested to use the model with cautions for all types of FRPs
2. The model takes into considerations the concrete allowable shear stresses by limiting the strain in the FRP to a maximum value of 0.005. Note that, when the proposed value for the maximum strain is divided by a material safety factor (e.g. 1.3 [TA 00]), it yields a value approximately equal to 0.004, which has been proposed by other researchers (e.g. AC125) to insure concrete integrity and to prevent degradation in aggregate interlock action.

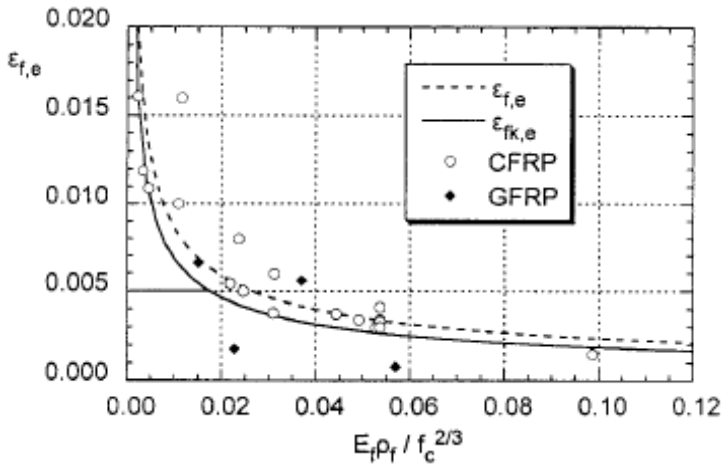

Figure 5.2: Effective strain in FRP ($\varepsilon_{f,e}$) in terms of $\rho_f E_f / f_c^{2/3}$ in case of shear failure combined with FRP debonding; $\varepsilon_{f,e}$ represents mean and $\varepsilon_{fk,e}$ represents characteristic [TA 00]

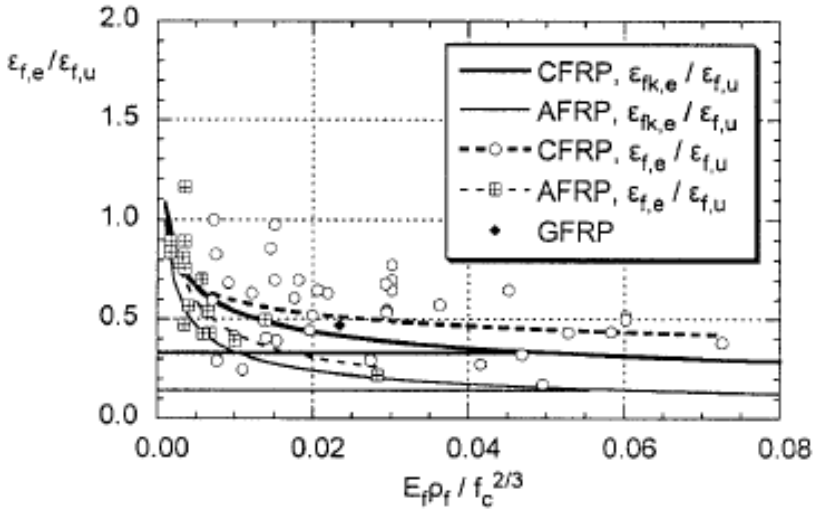

Figure 5.3: Normalized effective FRP strain ($\varepsilon_{f,e}/\varepsilon_{f,u}$) in terms of $\rho_f E_f/f_c^{2/3}$ in case of shear failure combined with FRP rupture [TA 00]

5.1.3 AC125 model

The AC125 of ICBO [IC 01] proposed that, for a wall (either masonry or RC) retrofitted on single side using FRP, the contribution of FRP in the lateral resistance can be calculated as follows:

$$F_{FRP} = 0.75\rho_h \, f_j \, t \, L \tag{5.6}$$

$$f_j = 0.004 \, E_{FRP} \leq 0.75 f_{FRP,u} \tag{5.7}$$

Where
$f_{FRP,u}$ = ultimate tensile strength of FRP.

It is worth noting that recent comparisons between equation 5.6 and experimental data of masonry walls retrofitted using FRP (see § 2.1.2) show that this recommendations overestimate the shear resistance by 40% [MH 03]. Besides the first two points in the shortcomings of Triantafillou's model [Tr 98], the modeling approach has the following shortcomings:

1. Used a constant strain in the FRP regardless of the FRP properties (e.g. reinforcement ratio). In addition, this constant strain (0.004) was estimated to prevent degradation in aggregate interlock action (in case of RC).
2. No experimental verification have been carried out on URM-FRP failing in shear

5.2 Analytical Model for Shear Behavior of URM-FRP

As shown in the literature (Chapter 2) and in section 5.1, the models used to calculate the shear resistance of URM-FRP have been adapted originally from RC and no analytical model has been developed for URM-FRP. In addition, these models add the contribution of FRP (F_{FRP}) to lateral resistance of URM wall (F_m) maintaining unchanged F_m. In this context, whether or not F_m is identical for URM and URM-FRP is not established. However, recent studies on RC beams retrofitted using FRP, revealed that the contributions of both internal shear steel reinforcement and FRP are in fact interacting parameters [CS 02]. So a new analytical model is required. In this section, an analytical model is developed for in-plane shear behavior of URM-FRP.

5.2.1 Objective

Through out the development of the analytical model five objectives were followed. Specifically, these objectives were:

- To have a simple analytical model capable to investigate the global shear behavior of URM-FRP

- Examine the phenomenon of using effective strain rather than the ultimate strain in the FRP; in addition, examine if this effective strain is a constant value or variable
- Examine whether or not F_m is identical for URM and URM-FRP as well as if F_m is not identical determine the interaction between F_m and F_{FRP}. Since synthesis of moor than 100 experiments on RC beams retrofitted using FRP show that there is an interaction between steel reinforcement ratio (longitudinal and transversal) and the increment in the lateral resistance due to FRP. Unfortunately, no quantified relation or explanation is given for this phenomenon.
- Examine and assess the effect of different material parameters (FRP, epoxy, and masonry properties) on the shear resistance of URM-FRP
- Determine the parameters which needs more experimental data and investigations

5.2.2 Derivation of governing equations

Consider the URM wall retrofitted on single side, using one layer of FRP on the entire surface, shown in Figure 5.4. The differential element in Figure 5.4 shows the in-plane shear stresses acting on the masonry (τ^{m}_{xy}) and FRP (τ^{f}_{xy}) as well as the two components of the epoxy shear stress ($\tau^{e}_{zx}, \tau^{e}_{zy}$). The model has the following assumptions:

- Isotropic elastic materials
- Homogeneous materials
- Forces are transferred from masonry wall to FRP through shear only (i.e. no flexure or normal force)
- Both masonry and FRP as well as epoxy have a constant thickness
- Epoxy carry out only surface stresses
- Uniform shear strain through the epoxy (adhesive) thickness
- Both masonry and FRP layer carry only in-plane shear stresses
- No dowel action
- The applied lateral forces are applied uniformly over the wall cross section
- The effect of asymmetry (due to applying FRP on single side) is neglected

The derivation of the differential equation governing the behavior of a shear loaded URM-FRP is presented in the following. Under any lateral force F, the applied in-plane shear/unit length (N_{xy}) is continuous at any point and must be equal the following:

$$N_{xy} = F/L \tag{5.8}$$

$$N_{xy} = \tau^{m}_{xy} t^{m} + \tau^{f}_{xy} t^{f} \tag{5.9}$$

where
F = applied lateral force
L = wall length
t^m = masonry thickness
t^f = FRP thickness

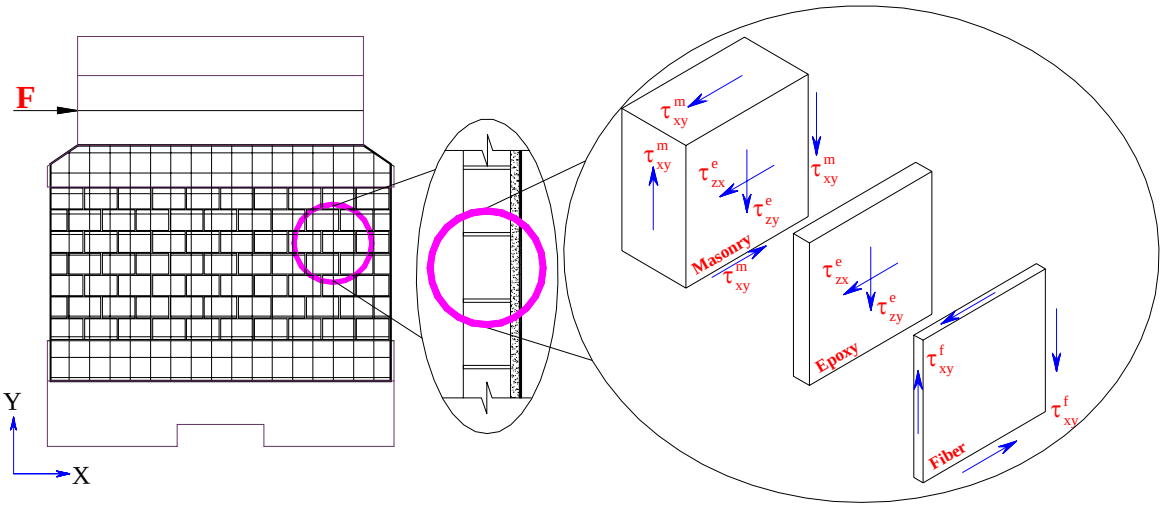

Figure 5.4: URM wall retrofitted using FRP (full surface, single side) and differential element of the same retrofitted wall showing masonry, epoxy, and fiber stresses

Taking into considerations the assumption of uniform shear strain through epoxy thickness, the epoxy shear strain through the thickness of the epoxy can be written as follows (Figure 5.5):

$$\gamma^{e}_{zx} = \frac{\tau^{e}_{zx}}{G^{e}} = \frac{1}{t^{e}}\left(u^{f} - u^{m}\right) \tag{5.10}$$

$$\gamma^{e}_{zy} = \frac{\tau^{e}_{zy}}{G^{e}} = \frac{1}{t^{e}}\left(v^{f} - v^{m}\right) \tag{5.11}$$

where
G^e = epoxy shear modulus
t^e = epoxy thickness
u^m = masonry element displacement in X direction
u^f = FRP element displacement in X direction
v^m = masonry element displacement in Y direction
v^f = FRP element displacement in Y direction

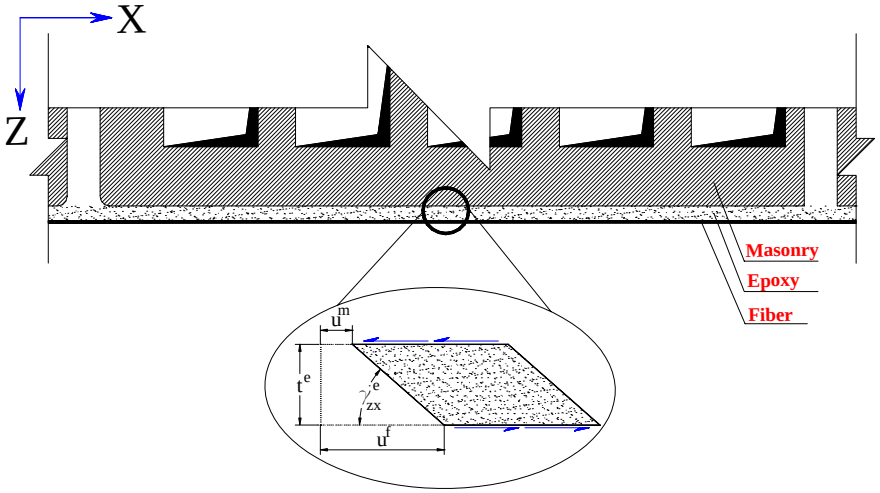

Figure 5.5: Consideration of the shear transmission through epoxy (equations 5.10 and 5.11)

Force equilibrium performed on a differential element of the masonry wall, shown in Figure 5.6, results in relationships between the epoxy stress components and the FRP layer. In X direction

$$\sum F_x = 0 \tag{5.12}$$

$$\tau_{yx}^{f} t^{f} dx - \left(\tau_{yx}^{f} + \frac{\partial \tau_{yx}^{f}}{\partial y} dy \right) t^{f} dx + \tau_{zx}^{e} dxdy = 0 \tag{5.13}$$

$$-\frac{\partial \tau_{yx}^{f}}{\partial y} t^{f} + \tau_{zx}^{e} = 0 \tag{5.14}$$

$$\frac{\partial \tau_{yx}^{f}}{\partial y} t^{f} = \tau_{zx}^{e} \tag{5.15}$$

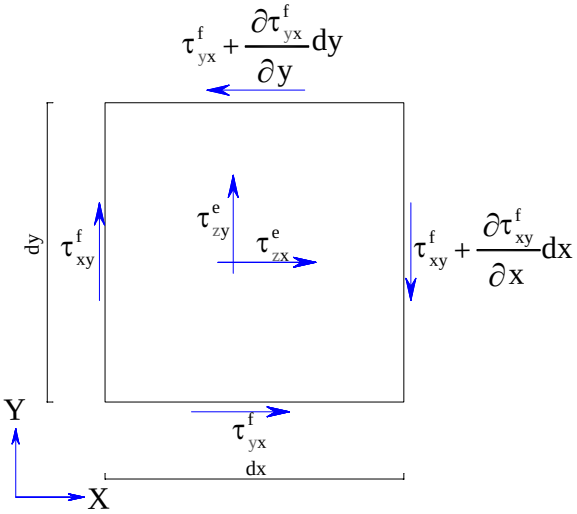

Figure 5.6: Shear stresses acting on an element of the FRP layer

in Y direction,

$$\sum F_y = 0 \tag{5.16}$$

$$\tau_{xy}^{f} t^{f} dy - \left(\tau_{xy}^{f} + \frac{\partial \tau_{xy}^{f}}{\partial x} dx \right) t^{f} dy + \tau_{zy}^{e} dxdy = 0 \tag{5.17}$$

$$\frac{\partial \tau_{xy}^{f}}{\partial x} t^{f} = \tau_{zy}^{e} \tag{5.18}$$

differentiate equations 5.15 and 5.18 with respect to y, x respectively and combine them considering $\tau_{xy} = \tau_{yx}$, then

$$\frac{\partial \tau_{zx}^{e}}{\partial y} + \frac{\partial \tau_{zy}^{e}}{\partial x} = \frac{\partial^2 \tau_{xy}^{f}}{\partial y^2} t^{f} + \frac{\partial^2 \tau_{xy}^{f}}{\partial x^2} t^{f} \tag{5.19}$$

$$\frac{\partial \tau_{zx}^{e}}{\partial y} + \frac{\partial \tau_{zy}^{e}}{\partial x} = t^{f} \nabla^2 \tau_{xy}^{f} \tag{5.20}$$

differentiate equations 5.10 and 5.11 with respect to y and x respectively

$$\frac{\partial \gamma_{zx}^{e}}{\partial y} = \frac{\partial \tau_{zx}^{e}}{\partial y} \frac{1}{G^{e}} = \frac{1}{t^{e}} \left(\frac{\partial u^{f}}{\partial y} - \frac{\partial u^{m}}{\partial y} \right) \tag{5.21}$$

$$\frac{\gamma_{zy}^{e}}{\partial x} = \frac{1}{G^{e}} \frac{\partial \tau_{zy}^{e}}{\partial x} = \frac{1}{t^{e}} \left(\frac{\partial v^{f}}{\partial x} - \frac{\partial v^{m}}{\partial x} \right) \tag{5.22}$$

combining equations 5.21 and 5.22

$$\frac{\partial \gamma^{e}_{zx}}{\partial y}+\frac{\partial \gamma^{e}_{zy}}{\partial x}=\left(\frac{\partial \tau^{e}_{zy}}{\partial x}+\frac{\partial \tau^{e}_{zx}}{\partial y}\right)\frac{1}{G^{e}}=\frac{1}{t^{e}}\left(\frac{\partial u^{f}}{\partial y}+\frac{\partial v^{f}}{\partial x}-\left(\frac{\partial u^{m}}{\partial y}+\frac{\partial v^{m}}{\partial x}\right)\right) \tag{5.23}$$

$$\left(\frac{\partial \tau^{e}_{zy}}{\partial x}+\frac{\partial \tau^{e}_{zx}}{\partial y}\right)\frac{1}{G^{e}}=\frac{1}{t^{e}}\left(\gamma^{f}_{xy}-\gamma^{m}_{xy}\right) \tag{5.24}$$

$$\frac{\partial \tau^{e}_{zy}}{\partial x}+\frac{\partial \tau^{e}_{zx}}{\partial y}=\frac{G^{e}}{t^{e}}\left(\gamma^{f}_{xy}-\gamma^{m}_{xy}\right) \tag{5.25}$$

since the left hand side in equations 5.20 and 5.25 is equal then,

$$\frac{G^{e}}{t^{e}}\left(\gamma^{f}_{xy}-\gamma^{m}_{xy}\right)=t^{f}\nabla^{2}\tau^{f}_{xy} \tag{5.26}$$

or

$$t^{f}\nabla^{2}\tau^{f}_{xy}-\frac{G^{e}}{t^{e}}\left(\gamma^{f}_{xy}-\gamma^{m}_{xy}\right)=0 \tag{5.27}$$

but

$$\gamma^{m}_{xy}=\frac{\tau^{m}_{xy}}{G^{m}}\ ,\ \gamma^{f}_{xy}=\frac{\tau^{f}_{xy}}{G^{f}} \tag{5.28}$$

substitute from equation 5.28 into equation 5.27 leads to:

$$t^{f}\nabla^{2}\tau^{f}_{xy}-\frac{G^{e}}{t^{e}}\frac{\tau^{f}_{xy}}{G^{f}}+\frac{G^{e}}{t^{e}}\frac{\tau^{m}_{xy}}{G^{m}}=0 \tag{5.29}$$

from equation 5.9, shear stress in the masonry can be written as following:

$$\tau^{m}_{xy}=\left(\frac{N_{xy}-\tau^{f}_{xy}t^{f}}{t^{m}}\right) \tag{5.30}$$

substitute into equation 5.29 and divided by t^{f}

$$\nabla^{2}\tau^{f}_{xy}-\frac{G^{e}}{t^{e}t^{f}}\frac{\tau^{f}_{xy}}{G^{f}}+\frac{-\tau^{f}_{xy}t^{f}}{t^{m}}\frac{G^{e}}{t^{e}t^{f}}\frac{1}{G^{m}}+\frac{N_{xy}}{t^{e}t^{m}t^{f}}\frac{G^{e}}{G^{m}}=0 \tag{5.31}$$

let $C_{o}=\frac{N_{xy}}{t^{e}t^{m}t^{f}}\frac{G^{e}}{G^{m}}$, $\lambda^{2}=\left(\frac{G^{e}}{t^{e}}\right)\left(\frac{1}{t^{f}G^{f}}+\frac{1}{t^{m}G^{f}}\right)$

$$\nabla^{2}\tau^{f}_{xy}-\lambda^{2}\tau^{f}_{xy}+C_{o}=0 \tag{5.32}$$

the following double Fourier sine series represent the solution of such differential [KK 01]:

$$\tau^{f}_{xy}=\sum_{m=1}^{\infty}\sum_{n=1}^{\infty}A_{mn}\,sin\frac{m\pi x}{L}\,sin\frac{n\pi y}{h} \tag{5.33}$$

where

$$A_{mn}=\frac{C_{mn}}{\left(\frac{m\pi}{L}\right)^{2}+\left(\frac{n\pi}{h}\right)^{2}+\lambda^{2}} \tag{5.34}$$

$$C_{mn} = \frac{4}{Lh}\int_0^a\int_0^b C_o \, sin\frac{m\pi x}{L} sin\frac{n\pi y}{h} dxdy \tag{5.35}$$

This solution satisfies both the governing differential equation and the assumed boundary conditions (i.e. $\tau^f_{xy} = 0$ at all the FRP boundaries)
substitute with equation 5.33 into equations 5.15 and 5.18, then

$$\tau^e_{zy} = \sum_{m=1}^{\infty}\sum_{n=1}^{\infty} A_{mn}\pi m\, t^f \, cos\frac{m\pi x}{L} sin\frac{n\pi y}{h} \tag{5.36}$$

$$\tau^e_{zx} = \sum_{m=1}^{\infty}\sum_{n=1}^{\infty} A_{mn}\pi n\, t^f \, sin\frac{m\pi x}{L} cos\frac{n\pi y}{h} \tag{5.37}$$

from equations 5.36, 5.37 the shear resultant in the epoxy layer can be calculated as follows:

$$\tau_{epoxy} = \sqrt{\left(\tau^e_{xz}\right)^2 + \left(\tau^e_{yz}\right)^2} \tag{5.38}$$

then, the contribution of the FRP to the shear force can be calculated as follows:

$$F_{FRP} = \tau^f L t^f \tag{5.39}$$

where
τ^f = the average shear stresses acting on the FRP layer
finally, the shear force and stresses resisted by the masonry can be calculated as follows:

$$F_m = F - F_{FRP} \tag{5.40}$$

$$\tau^m = \frac{F_m}{Lt} \tag{5.41}$$

F = applied lateral force
τ^m = the average shear stresses acting on the masonry layer

5.3 Material Models for URM, Epoxy, and FRP

To develop a reasonable analytical model for in-plane shear behavior of URM-FRP under seismic loading, a through knowledge of the constitutive relations of the material and failure mechanisms is necessary. However, one of the main objectives is to develop a simple model that is capable of examining the in-plane behavior of URM-FRP. In addition, the model should be easy enough to be integrated into a future design approach. These goals were kept in mind during model development.

5.3.1 Material model for masonry wall

Response of URM walls to lateral forces is nonlinear also at low level of load, due to the low tensile strength of bed and head-joints. As the damage due to cracking increases, masonry walls show both strength and stiffness degradation. A common approach followed for assessment purpose is to idealize the masonry behavior under lateral loading with a bilinear force deformation curve (Figure 5.7) [MC 97, To 99]. In the proposed analytical model similar bilinear curve was implemented for URM layer (Figure 5.9). The bilinear idealized curve characterized as follows:

- The initial stiffness K_i can be determined from the material properties and specimen geometry.

- The secant stiffness at failure K_s can be determined from an experimental program or based on accepted ultimate drift (since ultimate drift is more reliable parameter than ductility for URM walls, [MC 97]).
- The ultimate lateral force F can be determined based on an experimental or an analytical analysis.

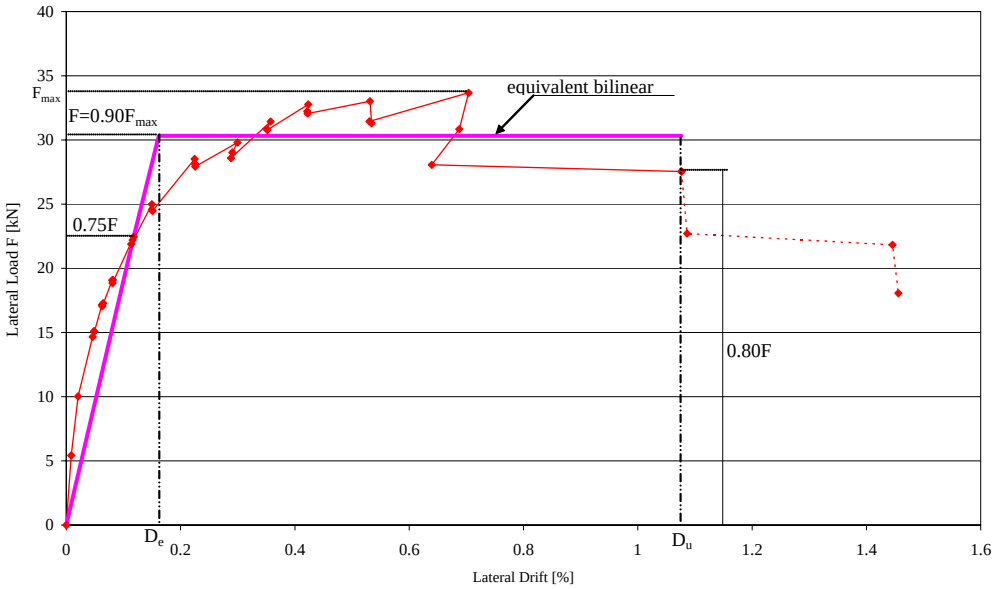

Figure 5.7: Behavior of masonry wall: idealized bilinear [MC 97] and force deformation curve for specimen S2-REFE-ST (see §4.1.1)

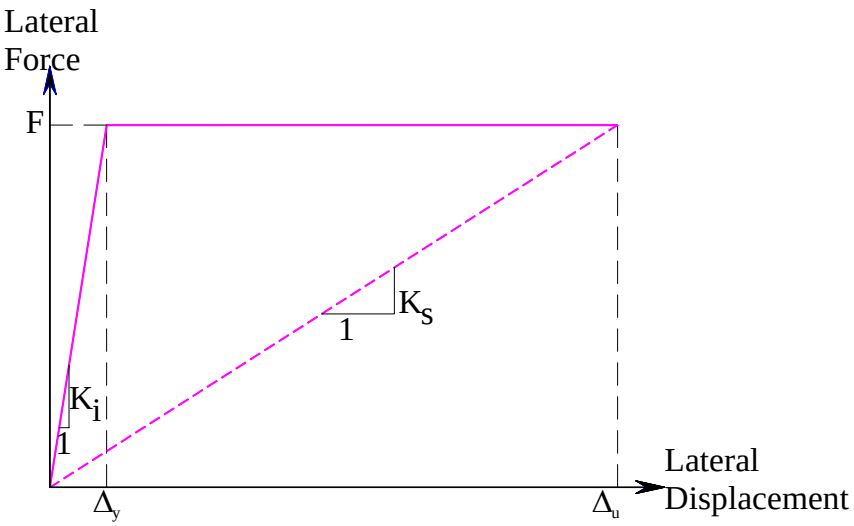

Figure 5.8: Behavior of masonry layer: idealized lateral force displacement relationship for masonry layer

5.3.2 Material model for epoxy

An important factor that influences the behavior of a structural element retrofitted using FRP is the shear behavior of the epoxy layer. The experimental investigations commonly adapted to characterize the local bond-slippage relationship between FRP and reinforced material (e.g. masonry, concrete…etc.), can be grouped into bonding tests and indirect tensile tests induced four-point flexural tests on beams; however, such tests are more common for RC and too limited for masonry. Campione et al. [CC 02] experimentally determined the characteristics of bond-slippage curves of CFRP stripes glued to small masonry specimens (150 X 100 X300 mm, Figure 5.9). The tests show that the behavior characterized by two phases:

- Elastic behavior in which a perfect bond exist between fiber and masonry
- Nonlinear behavior in which a progressive rupture at the interface occurs with loss of stiffness and increase in load and corresponding slippage.

The elastic part of the curves in which perfect bond exists is very small, less than 10% of the ultimate load. For the nonlinear part and based on characteristics of Figure 5.9, an idealized bilinear curve can represent the force slippage behavior (Figure 5.10). For retrofitting of RC beams using FRP, a literature review [NK 01] shows that besides idealized bilinear model other two models, cut off and tensile softening, have been used as relations between local force and slip (Figure 5.11). In the proposed analytical model and based on [CC 02] experimental data the elastic part of the curve is neglected; then, the nonlinear part is idealized as bilinear curve (Figure 5.10). This curve can be drawn as follows:

- The initial stiffness K_i can be determined from the material properties.
- The secant stiffness at failure K_s can be determined from an experimental program. However, experiments [CC 02] show that the scatter in K_s is very high; the average K_s measured during the experimental program of Campione et al. [CC 02] was approximately 0.14 of K_i.
- The ultimate force F can be determined based on maximum allowable shear stress; however, during an experimental work, the average "not the maximum" allowable shear stress can be measured (e.g. in [CC 02] the average shear stress at ultimate was 1.5 MPa).

Regarding the shear stress distribution of the epoxy over the retrofitted material (i.e. masonry), no data regarding such distribution are available in the literature. However, in order to characterize the behavior of RC beams retrofitted using CFRP, Al-Sulaimani et al. [AS 94] proposed curvilinear distribution of the shear stresses in the FRP-concrete interface. Based on their experimental results, a value of 3.5 MPa is estimated as maximum shear stresses. In addition, average shear stresses ranged from 0.8 to 1.2 MPa have been measured during the experimental work. Similar value of 1.3 MPa has been used by Uji [Uj 92] as an average shear stress for FRP-concrete bonding interface during debonding.

For RC beams retrofitted using plates of FRP or steel and loaded in bending, several analytical and experimental measurements show that at a very short length from the plate free end, of the order of the adhesive thickness, significance stress concentrations happened. In addition, significant normal stresses confined to a short length at the end of the plate appeared [Ro 89]. For masonry, the 2-D finite element study of Campione et al. [CC 02] shows similar trend (Figure 5.12) to the general trend of RC beams retrofitted using plates of FRP or steel. One drawback of the proposed analytical model is that the normal stresses (Figure 5.12 (b)) is not taken explicitly into account. But this may be at least partially justified in view of the following arguments:

- The effect of normal stresses may be taken into account to a certain extent through the choice of appropriate value of epoxy allowable shear stress at which the combination of shear and corresponding normal stresses lead to failure. However, more experimental work is required since the value of the maximum normal stress depends on relative stiffness of the epoxy and the retrofitted material (i.e. RC) [Ro 89]. In future, more complicated failure criterion can be developed.
- Introduction of normal stresses and deformations in the model leads to a too complicated 3-D model which may be a possible further development of the proposed model.

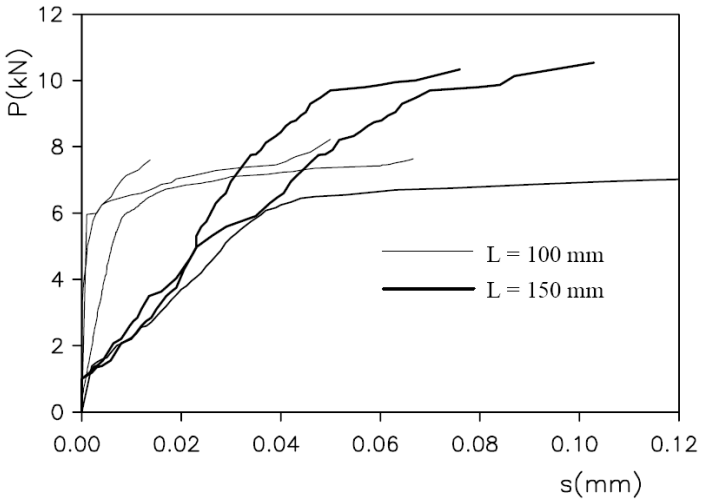

Figure 5.9: Epoxy behavior: force vs. slip curves in direct tension test of FRP glued to masonry (calcarenite ashlars) [CC 02]

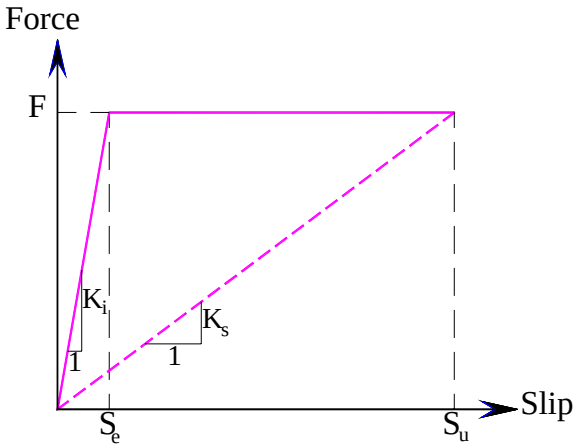

Figure 5.10: Epoxy behavior: idealized force slip curve for epoxy

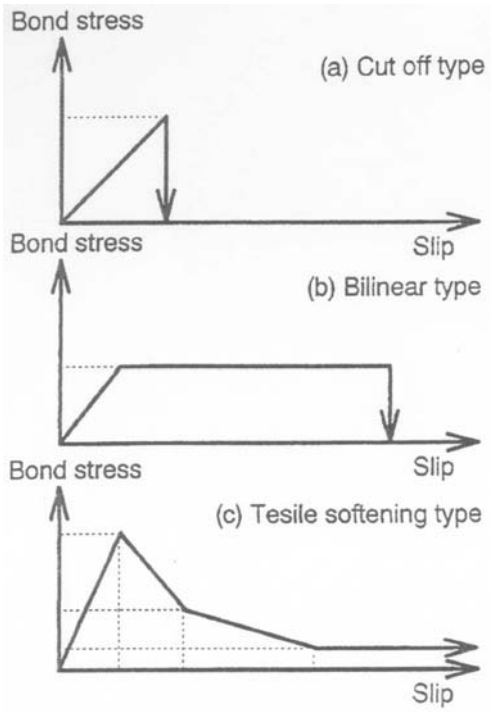

Figure 5.11: Epoxy models: typical bond stress-slip model for RC beams retrofitted using FRP [NK 01]

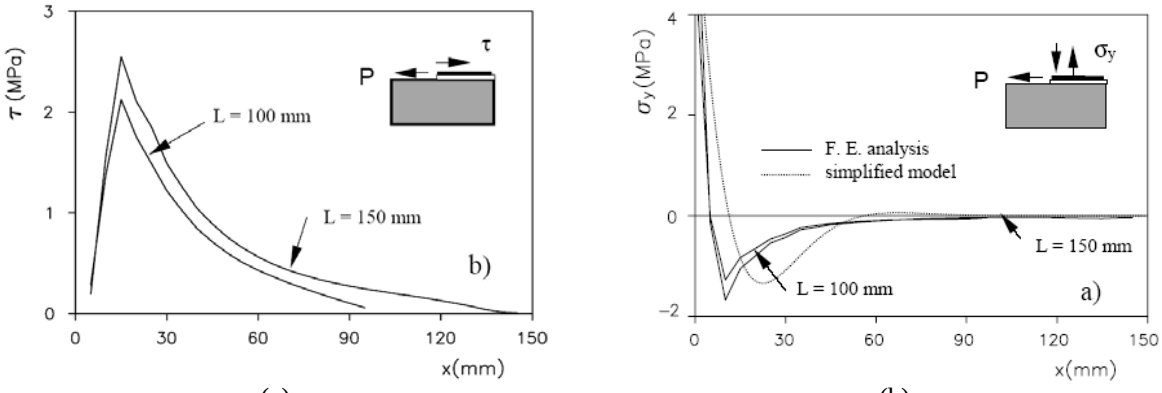

(a) (b)

Figure 5.12: Stresses at the interface between FRP and masonry: a) shear stresses, b) perpendicular stresses [CC 02]

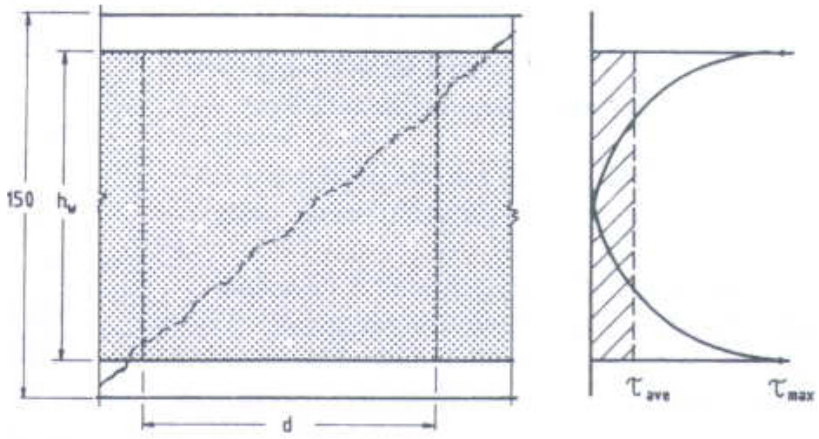

Figure 5.13: Shear stress distribution over the interface of RC beam retrofitted for shear using FRP [AS 94]

5.3.3 Material model for FRP

It is well established that FRP such as those used in the experimental program behave linearly up to failure. All the characteristics of the material are given by the FRP manufactures.

5.4 Nonlinear Shear Analysis of a URM-FRP

In structural analysis there are two types of nonlinearities, that need to be considered. One is "material nonlinearity" which is caused by the nonlinear stress-strain relation of progressive local failure, the other is "geometric nonlinearity" related to large displacements of the structure. Due to the nature of the problem, only material nonlinearity is considered in this research, as geometric nonlinearity is not applicable to URM-FRP under in-plane lateral loading where only small deflections occur.

The equations presented in § 5.2.2 can be used to model the linear shear behavior of URM wall retrofitted using FRP. To take into considerations the nonlinearity of the materials a step-by-step stiffness degradation of masonry as well as epoxy has been implemented in a program written in MATLAB [Ma 02]. Figure 5.14 shows the procedure and structure of the developed program for nonlinear analysis of shear behavior URM-FRP (NLSFRP). The force deformation behavior of a masonry wall as well as the epoxy layer have been idealized using bilinear curves (§ 5.3), the force deformation curve of FRP is idealized as linear elastic till failure. As shown in Figure 5.14, the program executed in following steps:

- The program calculate the shear stresses in the materials due to an initial lateral force F_i
- This force increase in each step by ΔF, this increment continues till one of the materials (masonry, epoxy, FRP) reaches its ultimate shear stresses.
- In case of FRP reached its ultimate resistance, NLSFRP stops and print the lateral resistance.
- In case of masonry or epoxy reached its ultimate resistance, a gradual degradation of the stiffness of the material, which reached its ultimate shear stress, starts. After any stiffness degradation, all the shear stresses are recalculated using the modified stiffness and the last applied lateral force. If the calculated shear stresses are smaller than or equal to allowable shear stress of all the materials (i.e. masonry, epoxy, FRP), then, F can be increased by ΔF. This step is repeated until a material (masonry, epoxy, or both) reaches its secant stiffness at ultimate drift (K_s, Figure 5.10). Then, NLSFRP stops.
- After NLSFRP stops, all the forces, stresses, and deformations as well as stiffness of the three layers (masonry, epoxy, FRP) are printed.

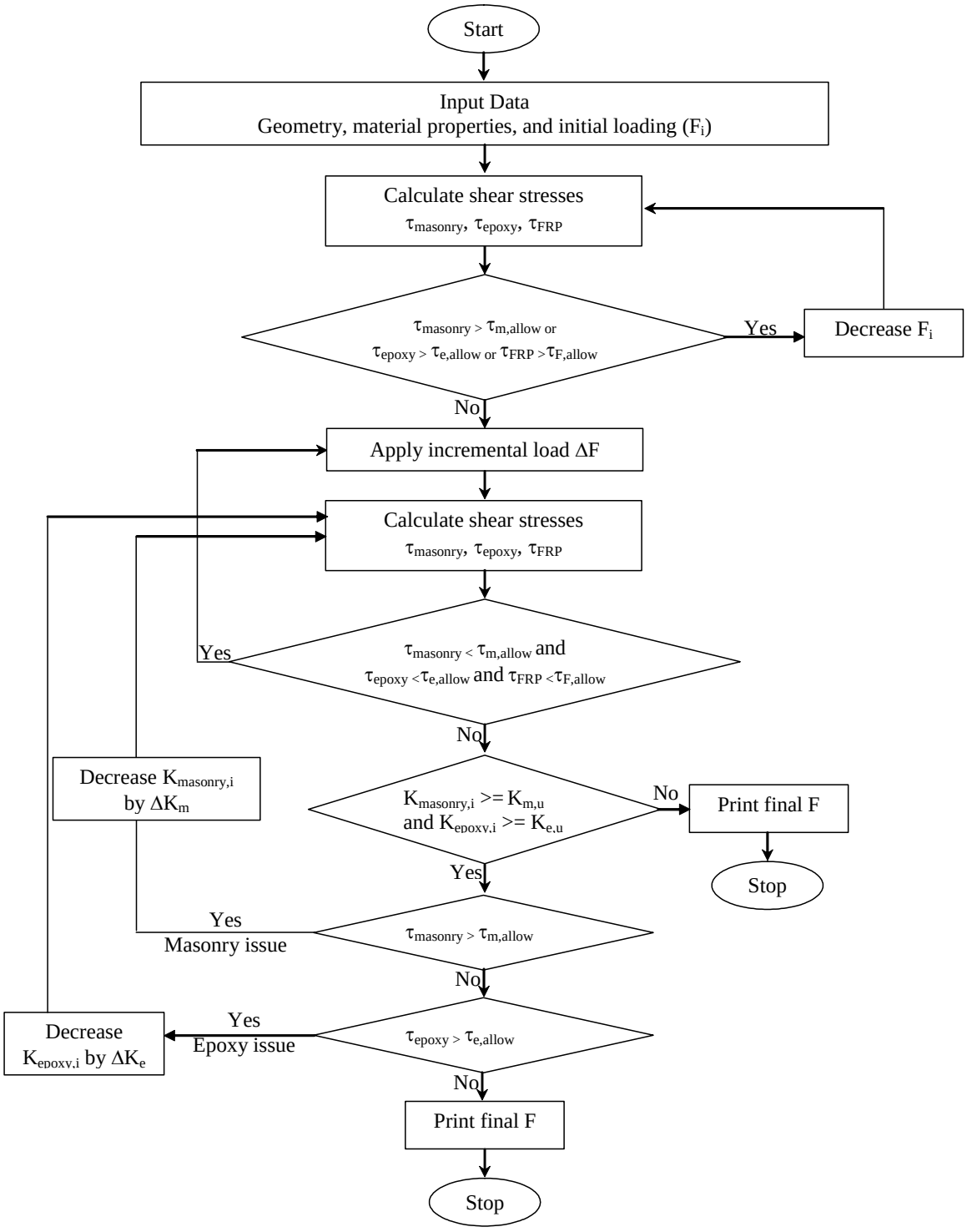

Figure 5.14: Flow chart for calculating the URM-FRP lateral resistance

5.5 Effect of Material Properties

In order to verify and investigate the sensitivity of the analytical model to different material and structural properties of URM, epoxy, and FRP, a comprehensive parametric study is carried out in this section. Some key parameters such as masonry allowable shear stress, epoxy allowable shear stress, masonry ductility, epoxy ductility, and epoxy shear modulus are examined. The main purpose of this study is to help fully understand the effect of the different parameters on the behavior of URM-FRP. It should be noticed that the parameters are selected to investigate the full range of analytical model characteristics and may not necessarily represent realistic characteristics of particular URM-FRP. Effects of the selected parameters on the URM-FRP are

presented through several figures; in these figures the horizontal axe represents the FRP axial rigidity i.e. ρE to be independent of FRP material type. However, in some cases a secondary horizontal axe is given on which the ρE is represented as equivalent number of layers of two different materials: light material GFRP of 145 g/m^2 with Young's modules of 70 GPa and heavy material AFRP of 205 g/m^2 with Young's modules of 100 GPa. In addition, in some figures comparisons with exiting models (§ 5.1) are illustrated. In these figures the following abbreviations have been used:

Trian [Tr 98] = Triantafillou model [Tr 98]
[TA 00] = Triantafillou and Antonopoulos model [TA 00]
AC 125 = AC125 of ICBO [IC 01] model
ElG_M-E = the proposed model, ELG abbreviation followed by two numbers: masonry property (e.g. allowable shear stress, ductility, etc.) and epoxy property (e.g. allowable shear stress, ductility, etc.).

The calculations were carried out on a stocky URM wall similar to S family which tested during the static cyclic tests (see Chapter 3) i.e. has length of 1565 mm and height of 1000 mm.

5.5.1 Effects of allowable shear stresses

This section includes the effect of allowable shear stresses of masonry and epoxy on FRP efficiency (ζ), contribution of FRP to lateral resistance of URM-FRP (F_{FRP}) as well as lateral resistance of URM-FRP (F). The FRP efficiency was defined as following: the ratio between the stresses in the FRP due to any amount of FRP axial rigidity (ρE) to the stresses in the FRP due to the lower value of ρE (i.e. 0.04 which corresponding to the minimum value of GFRP used in the experimental program). Note that, ζ is a relative value and in order to have the absolute value of the axial forces in FRP due to a certain amount of ρE the axial force in the FRP at ζ = 1 should be known first. This value could be known either using the proposed model or any other design equations. Three values of epoxy allowable shear stresses have been studied: 1.40 MPa (L type i.e. low allowable shear stress), 3.00 MPa (M type i.e. medium allowable shear stress), and 6.00 MPa (H type i.e. high allowable shear stress). The effects of applying these epoxy types to different URM walls with different allowable shear stresses have been studied. The URM wall has three different values for allowable shear stresses: 0.25 MPa (L type i.e. low allowable shear stress), 0.50 MPa (M type i.e. medium allowable shear stress), 1.50 MPa (H type i.e. high allowable shear stress). These different allowable masonry shear stresses can be related to different applied normal stresses or material properties.

Effect of allowable shear stresses on FRP efficiency

Figures 5.15 to 5.17 show the effect of changing epoxy allowable shear stress on FRP efficiency (ζ). In order to have an insight of ζ degradation rate, Figures 5.18 to 5.21 show ζ in terms of ρE; in the same figures masonry stiffness reduction factor (ID_m) and epoxy stiffness reduction factor (ID_e) at the end of NLSFRP are plotted. The figures are presented for four extreme cases (i.e. L and H masonry and epoxy types). Figures 5.15 to 5.21 show the following:

- For masonry of H type (Figure 5.15), the rate of degradation of ζ is very high for epoxy types M and L; in addition, for these epoxy types, the difference in ζ degradation rate is negligible. This is due to the fact that for epoxy type L (Figure 5.20) the limit on epoxy stiffness degradation dominates the URM-FRP behavior for all amounts of ρE. Similar explanation can be given for case of M epoxy type. In case of H epoxy type (Figure 5.19), the limit on masonry stiffness degradation dominates the URM-FRP shear behavior until approximately ρE equal to 0.14 GPa. For ρE less than or equal to 0.14 GPa, the rate of degradation of ζ is very slow. For ρE greater than 0.14 GPa, the limit on epoxy stiffness degradation dominates the URM-FRP shear behavior with a higher degradation rate of ζ.
- For masonry of type L (Figure 5.17), ζ rate degradation is very slow for epoxy type H where the limit on masonry stiffness dominates the URM-FRP shear behavior (Figure 5.18) up to approximately ρE equal to 1.12 GPa. For ρE less than or equal to 1.12 GPa, ζ degradation rate is very slow. For ρE greater than 1.12 GPa, epoxy stiffness dominates the URM-FRP shear behavior with a slow ζ degradation rate. Going from epoxy type H to type L, ζ degradation rate increases with the limit on masonry stiffness dominates the URM-FRP shear behavior (Figure 5.21) up to approximately ρE equal to 0.19 GPa. For ρE less than or equal to 0.19 GPa, the rate of degradation of ζ is very slow. For ρE greater than 0.19 GPa, epoxy stiffness dominates the URM-FRP shear behavior.
- In all cases epoxy dominates the behavior either from the beginning or just after a small amount of ρE except for the combination L masonry-H epoxy types. In the later case, masonry dominates the behavior

until high amount (1.12 GPa) of ρE. As a conclusion, when masonry dominates the shear behavior ζ degradation rate is slow and the inverse when epoxy dominates the behavior.

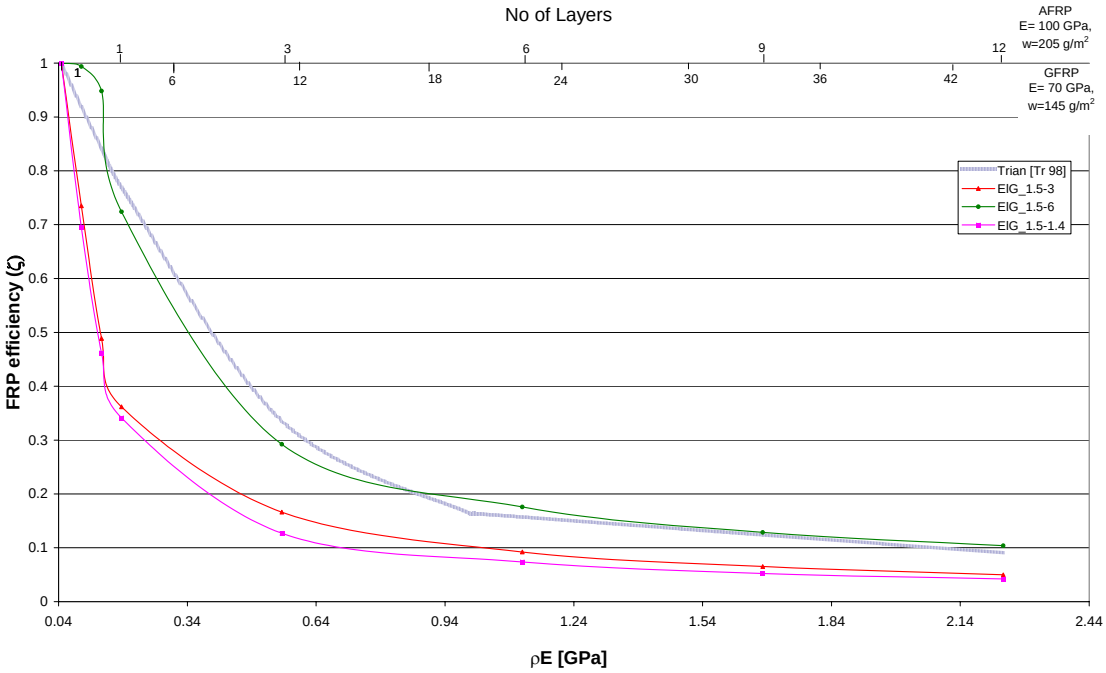

Figure 5.15: Effect of using type H masonry (1.50 MPa) with epoxy having different allowable shear stresses on FRP efficiency (ζ)

- For masonry type L (Figure 5.17), the degradation rate given by Triantafillou's model seems lower bound for all types of epoxy. For masonry type H (Figure 5.15), the degradation rate given by Triantafillou's model seems upper bound for all types of epoxy. Based on this note, one can say that the degradation rate given by Triantafillou [Tr 98] empirical equation (equation 5.4) is close to be an average of all the degradation rates given by different epoxy and masonry parameters. This is expected since Triantafillou developed his model based on curve fitting for different beams with different material parameters.
- For all masonry types (L, M, H), the epoxy type influences the rate of degradation of ζ: the higher the allowable shear stress of epoxy, the lower the rate of degradation of ζ.

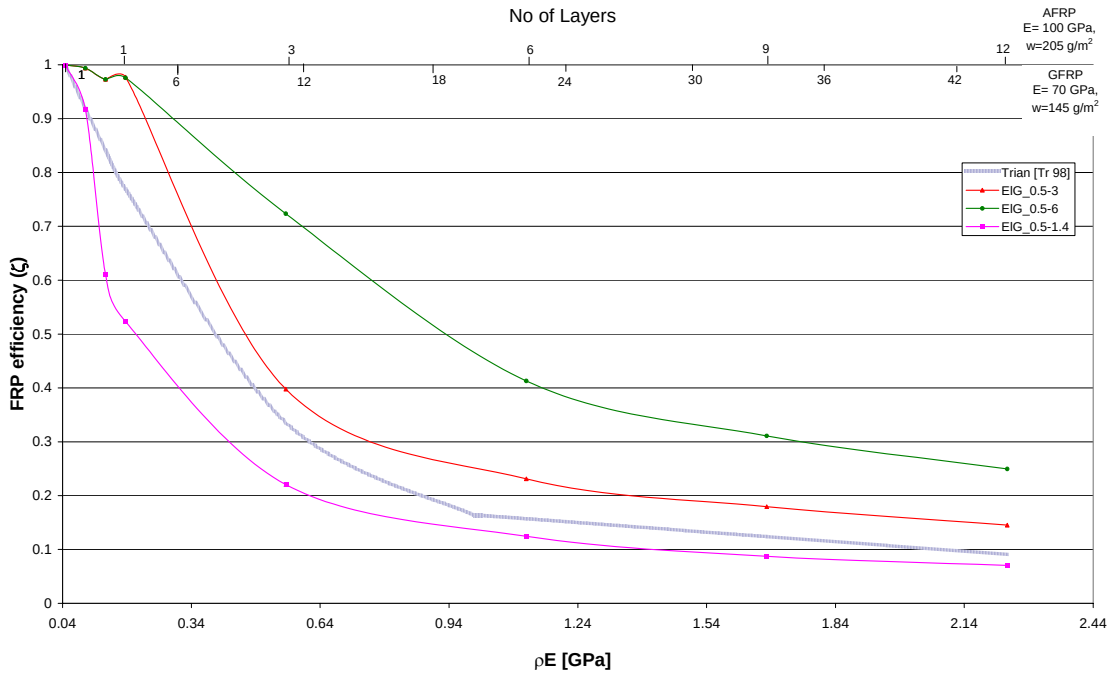

Figure 5.16: Effect of using M type masonry (0.50 MPa) with epoxy having different allowable shear stresses on FRP efficiency (ζ)

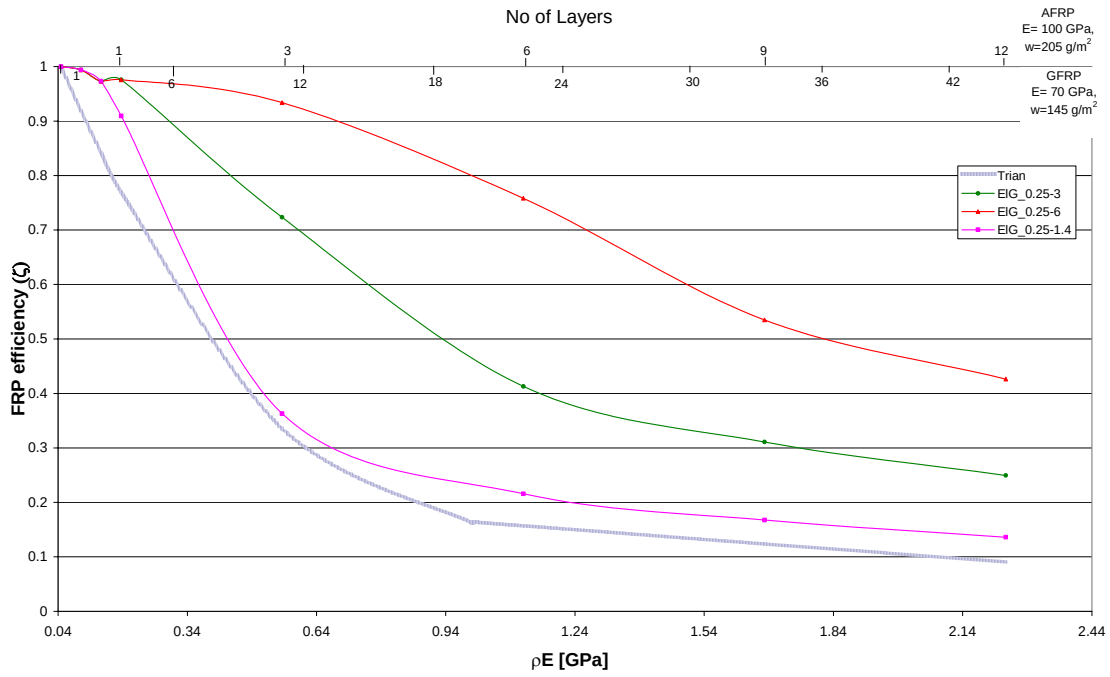

Figure 5.17: Effect of using L type masonry (0.25 MPa) with epoxy having different allowable shear stresses on FRP efficiency (ζ)

- It seems that there are three phases for ζ degradation rate. The first phase when ρE less than or equal to approximately 0.19 GPa, if epoxy dominates the behavior ζ degradation rate is very high. The second phase when ρE between 0.19 and 1.12 GPa, ζ degradation rate is slower than the previous phase. The third phase when ρE is greater than or equal to 1.12 GPa, ζ degradation rate is very slow and regardless of the material parameters (except L masonry- H epoxy) all the efficiency curves are parallel and approximately parallel to Triantafillou's curve. Note that, Triantafillou [Tr 98] used value of ρE =1 GPa as the limits between two phases of the degradation rate curve (equation 5.4).

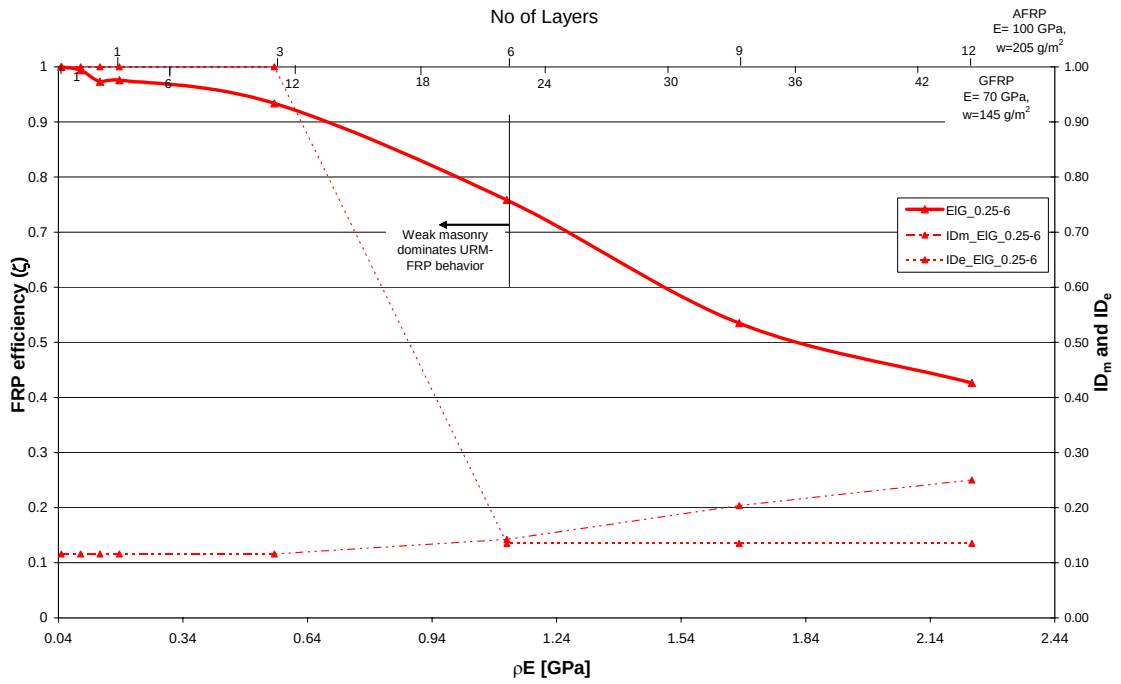

Figure 5.18: FRP efficiency as well as stiffness reduction factor (axis right) for H type epoxy (6 MPa) and L type masonry (0.25 MPa) at the end of NLSFRP

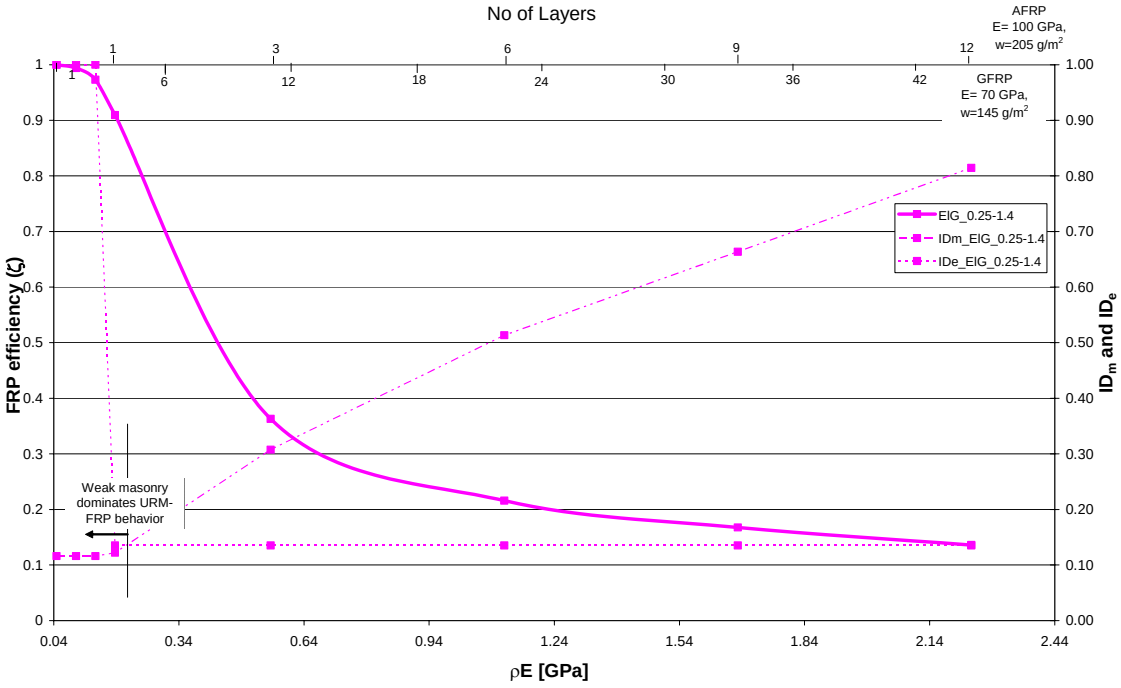

Figure 5.19: FRP efficiency as well as stiffness reduction factor (axis right) for H type epoxy (6 MPa) and H type masonry (1.5 MPa) at the end of NLSFRP

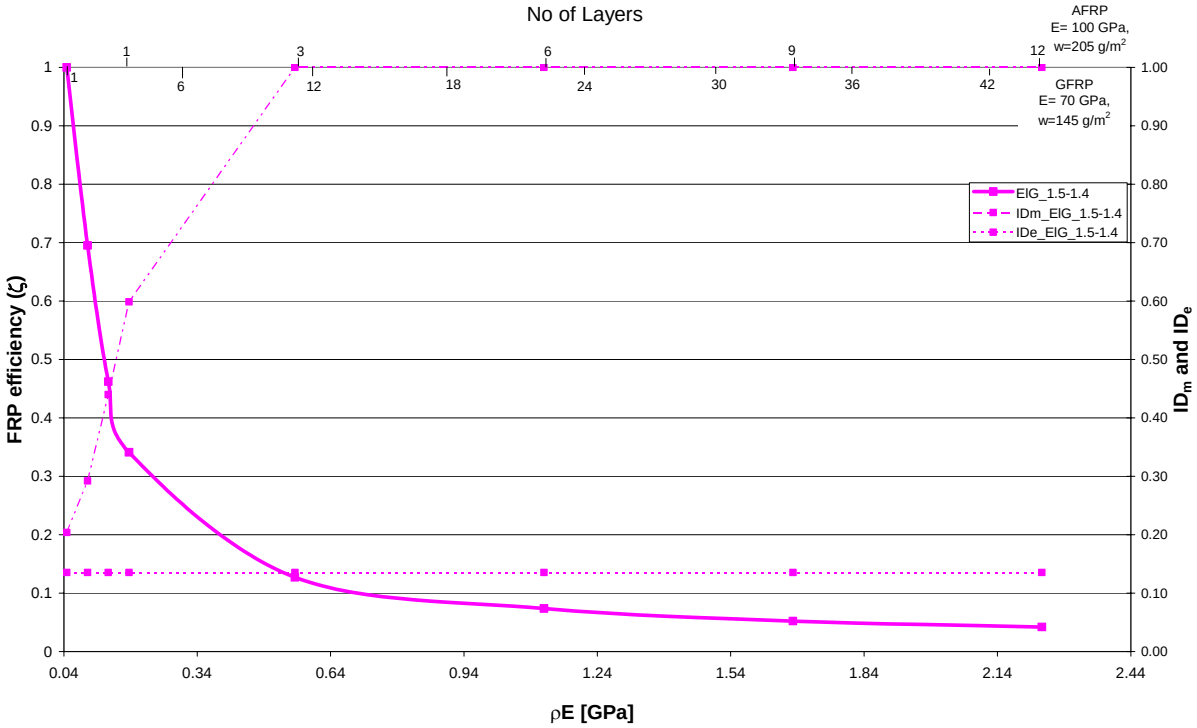

Figure 5.20: FRP efficiency as well as stiffness reduction factor (axis right) for L type epoxy (1.4 MPa) and H type masonry (1.5 MPa) at the end of NLSFRP

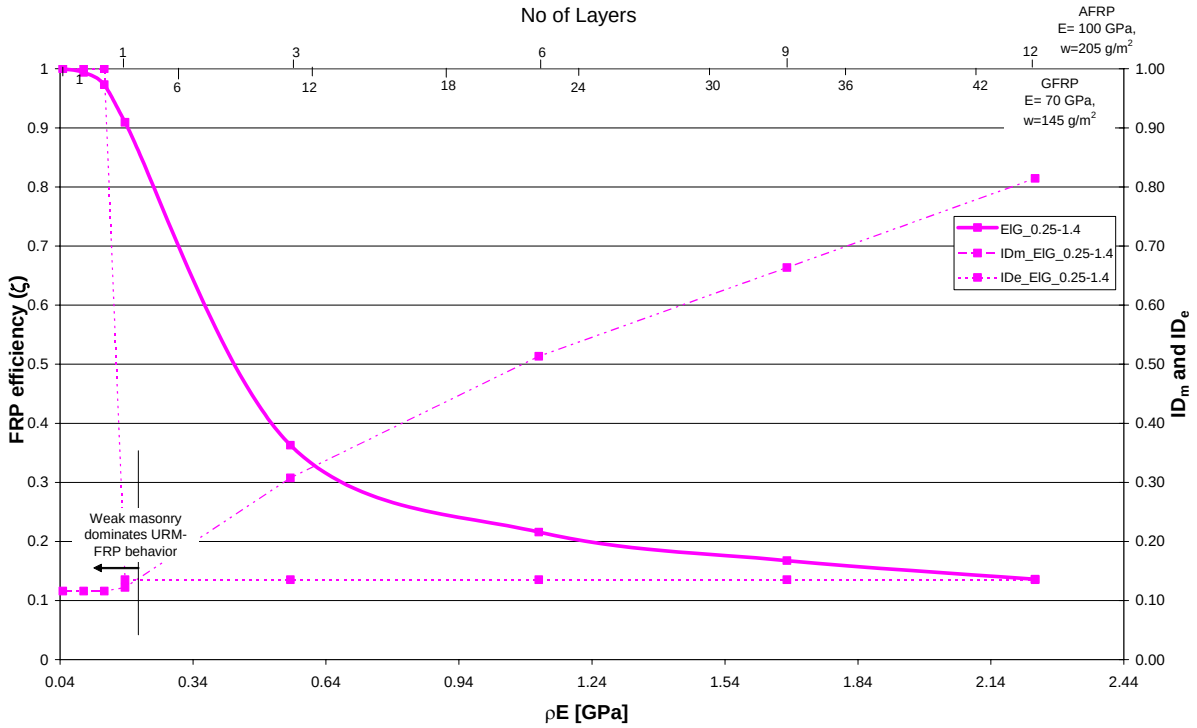

Figure 5.21: FRP efficiency as well as stiffness reduction factor (axis right) for L type epoxy (1.4 MPa) and L type masonry (0.25 MPa) at the end of NLSFRP

Effect of allowable shear stresses on contribution of FRP to the lateral resistance of URM-FRP

For L, M, and H types of masonry, Figures 5.22 to 5.24 show the effect of changing epoxy allowable shear stress on contribution of FRP to lateral resistance of URM-FRP, the figures show the following:

- All the curves trends to be a mix of Triantafillou [Tr 98] and Triantafillou and Antonopoulos [TA 00] models. However, the absolute values of F_{FRP} are close to Triantafillou and Antonopoulos [TA 00] model; which, seems to be an average of the different F_{FRP} estimated due to different material properties. The divergence between estimated F_{FRP} by the proposed model and Triantafillou and Antonopoulos [TA 00] model is influenced by material properties.
- For all cases with too limited exceptions in case of masonry type H and epoxy type H, Triantafillou's original model [Tr 98] estimated F_{FRP} higher than the proposed analytical model. The high difference between Triantafillou's model and the proposed model is expected since Triantafillou original model does not take into considerations the difference between two cases; wrapped retrofitting in which FRP rupture is the most probable mode of failure and unwrapped retrofitting in which debonding dominates the behavior. For all material properties examined here using the proposed model no FRP fracture happened. Note that, for RC retrofitted using FRP, analysis of all available experimental work in the literature [BC 04] show that approximately 96% of failure in case of on sides retrofitting is due to debonding (delamination). This ratio reduced to 50% and 0% in case of U shape and wrapping, respectively.
- The comparison between F_{FRP} estimated by AC125 [IC 01] and the proposed model seems difficult since the AC125 adapted a constant axial strain in the FRP. However, until ρE of 0.19 GPa, AC 125 estimated F_{FRP} too close to the average of F_{FRP} estimated using masonry type M and different epoxy types. For masonry type L, the difference is approximately 35%. For H masonry, the difference is too high except for L epoxy.
- By increasing epoxy allowable shear stress the FRP contribution to lateral resistance of URM-FRP increases. However, the increment in the F_{FRP} is approximately linear till a certain amount of ρE let's say $(\rho E)_{optimum}$. Increasing ρE beyond $(\rho E)_{optimum}$ has less significant effect on F_{FRP}. This $(\rho E)_{optimum}$ can be used as cost effective limits as suggested by other researchers (e.g. [BC 04] and [Tr 98]). However, $(\rho E)_{optimum}$ is not a constant value. It changes with changing material properties. For the same masonry type, by improving epoxy type, $(\rho E)_{optimum}$ increases with high increment in corresponding F_{FRP}. For the same epoxy type, by improving masonry type, $(\rho E)_{optimum}$ significantly decreases with limited effect on F_{FRP}.
- For the same epoxy type and ρE, the higher the masonry allowable shear stresses the higher F_{FRP}. However, the increment in F_{FRP} due to increasing masonry allowable shear stress depends on the epoxy type.

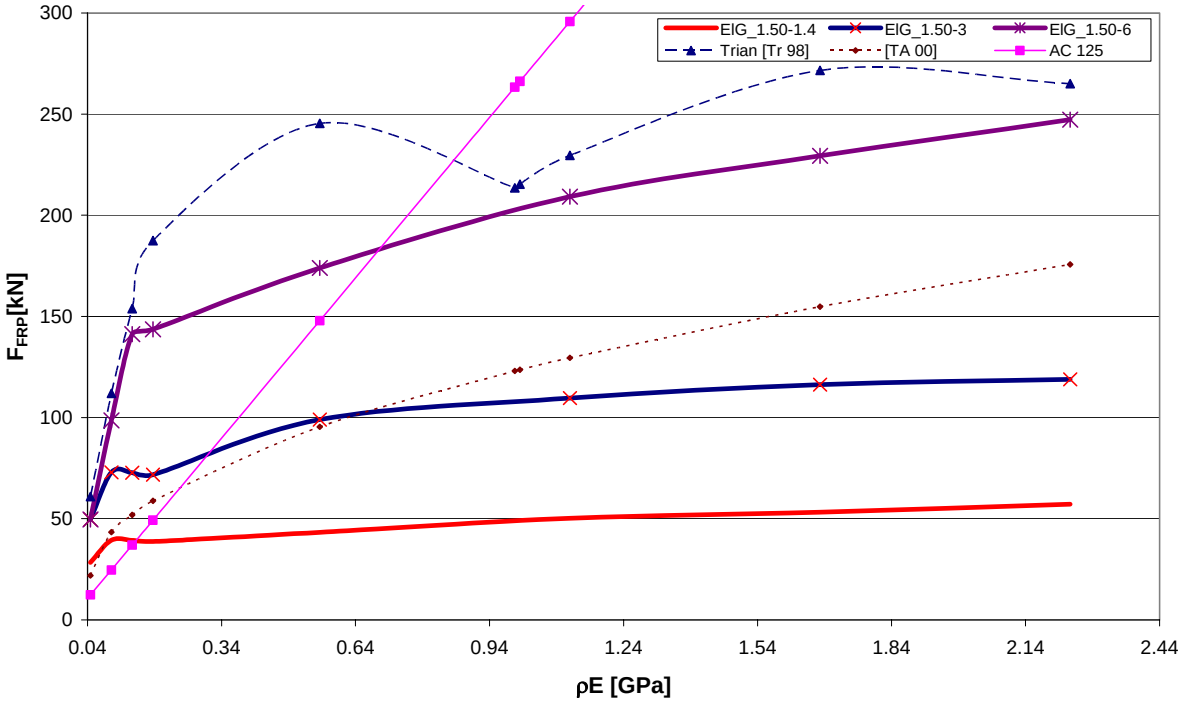

Figure 5.22: Effect of using H masonry (1.50 MPa) with epoxy having different allowable shear stresses on contribution of FRP to the lateral resistance

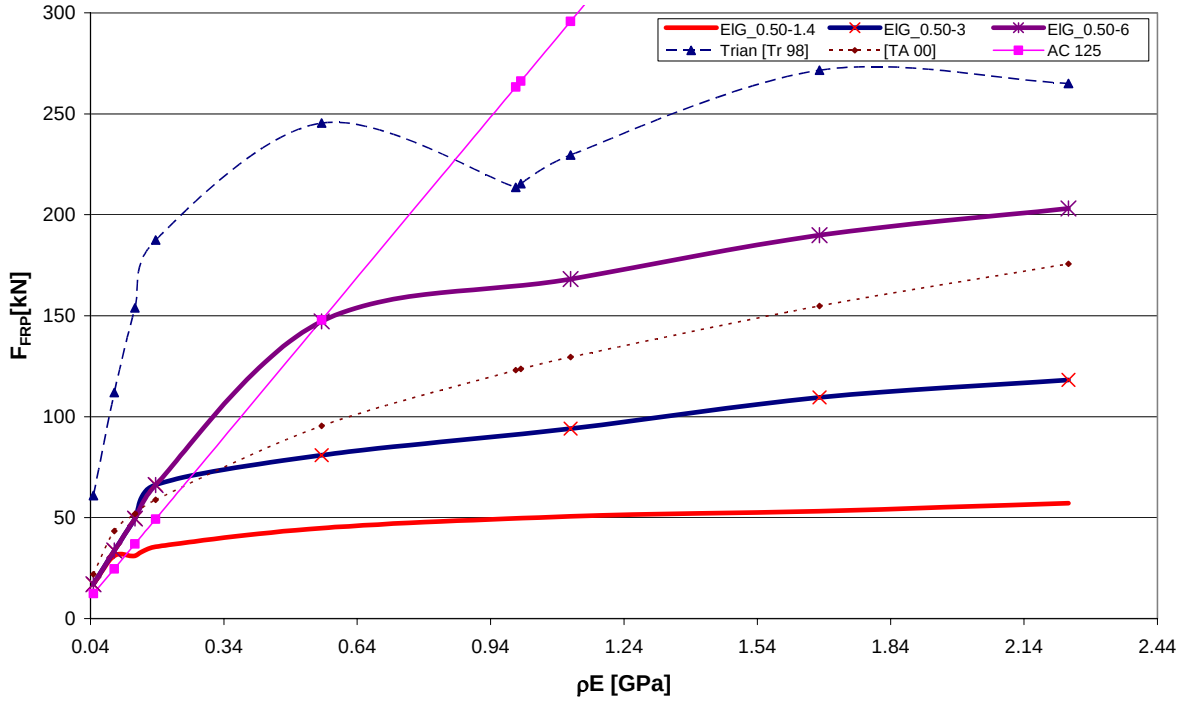

Figure 5.23: Effect of using M masonry (0.50 MPa) with epoxy having different allowable shear stresses on contribution of FRP to the lateral resistance

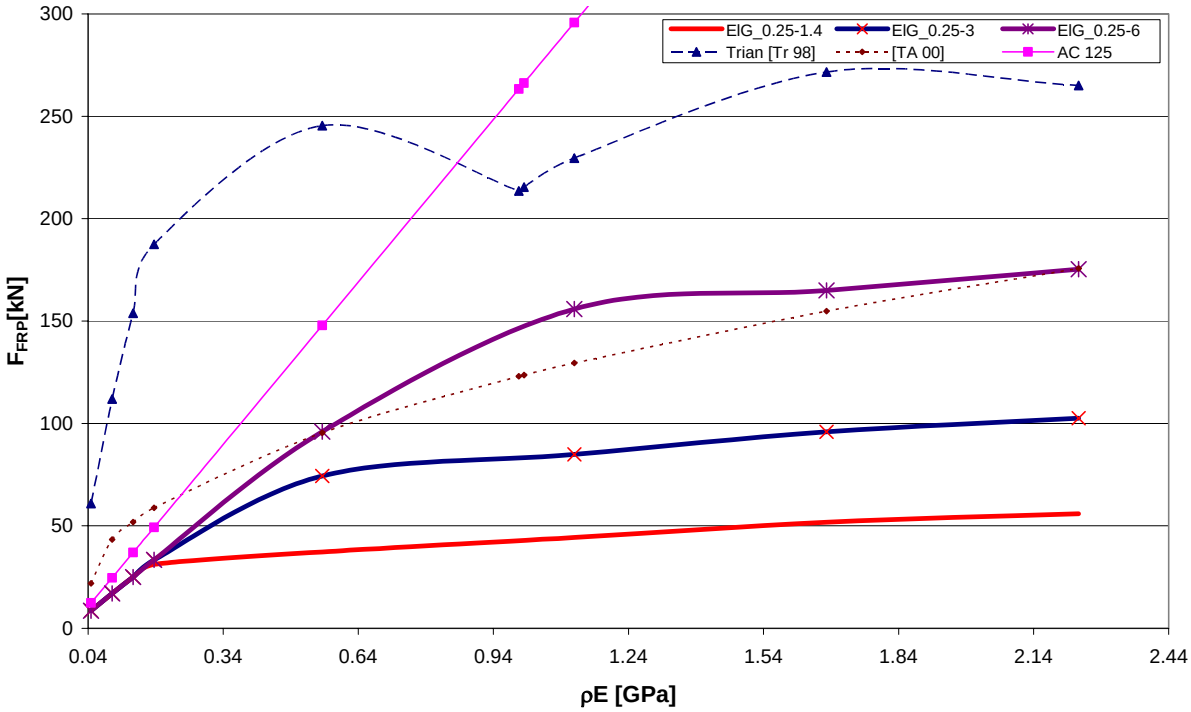

Figure 5.24: Effect of using L masonry (0.25 MPa) with epoxy having different allowable shear stresses on contribution of FRP to the lateral resistance

Effect of allowable shear stresses on lateral resistance of URM-FRP

For L, M, and H types of masonry, Figures 5.25 to 5.27 show the effect of changing epoxy allowable shear stress on lateral resistance of URM-FRP. In addition, Figure 5.28 shows for the different epoxy and masonry types the gain in the lateral resistance in terms of ρE. The gain is defined as follows:

$$\text{Gain} = \frac{F - F_m}{F_m}\% \tag{5.42}$$

The figures show the following:

- In general, by increasing epoxy allowable shear stress the lateral resistance of URM-FRP increases.
- For the same epoxy and masonry type, by increasing ρE, F increase until a certain upper limits $(\rho E)_{limit}$; beyond this limits any increment in ρE leads to reduction in F. The $(\rho E)_{limit}$ is influence by epoxy and masonry types: by increasing epoxy allowable shear stresses $(\rho E)_{limit}$ increases. Also, by reducing masonry allowable shear stresses $(\rho E)_{limit}$ increase. The $(\rho E)_{limit}$ is clear for masonry type H and epoxy types L and M in Figure 5.25; however, it is less clear in the other figures and in some cases it happened at ρE beyond the limit presented in the figures. This reduction in lateral resistance is due to the following: beyond $(\rho E)_{limit}$ URM-FRP reaches the limit on epoxy stiffness degradation too early before masonry reaches its allowable shear stress. However, after failure of FRP the lateral resistance of URM-FRP reduced to the lateral resistance corresponding to URM wall. In this context the amount of gain depends on the definition of failure: if failure defined at failure of FRP then it is possible to have negative gain; since at failure of FRP, masonry wall does not develop its ultimate lateral resistance. If failure defined at certain reduction in lateral resistance (e.g. 20-30% of the lateral resistance), then after rupture of FRP the URM wall alone will continue develop its lateral resistance until it reaches its ultimate lateral resistance.
- The previous remark lead to an important conclusion: using equation 5.1 (i.e. adding masonry lateral resistance to FRP contribution) is correct until a certain limit beyond this limit this equation is no more valid. To avoid such invalidity in the equation and in order to have cost effective use of FRP it is proposed to limit $(\rho E)_{limit}$ to a value of 0.19 GPa. For materials properties examined here, this value is smaller than $(\rho E)_{limit}$ and $(\rho E)_{optimum}$ which mean safe economic design. Note that, for RC retrofitted using FRP, analysis of existing experimental work [BC 04] show that there is interaction of beam shear resistance (in terms of reinforcement) and the contribution of FRP to shear resistance. However, for RC no explanation or quantification is given.
- In lights of Figure 5.28, the proposed limit on ρE is appropriate for all material properties except for H epoxy. In the later case a value of 0.54 GPa is more appropriate. For RC beams, Bousselham and Chaallal [BC 04] observed that beyond $\rho E/f_c^{0.67}$ of approximately 0.05 the gain tends to stabilized and they proposed to use such value as a criterion for cost effective design. If typical values of existing masonry compressive strength are considered (4-7 MPa) with this proposed limit, then the cost effective design criterion is corresponding to ρE of 0.13-0.17 GPa which corresponds well to the proposed value estimated by the analytical model.
- By increasing masonry allowable shear stress, the gain reduces. A similar phenomenon is observed for RC beams [BC 04]. In addition, By increasing epoxy allowable shear stress, the gain increases.

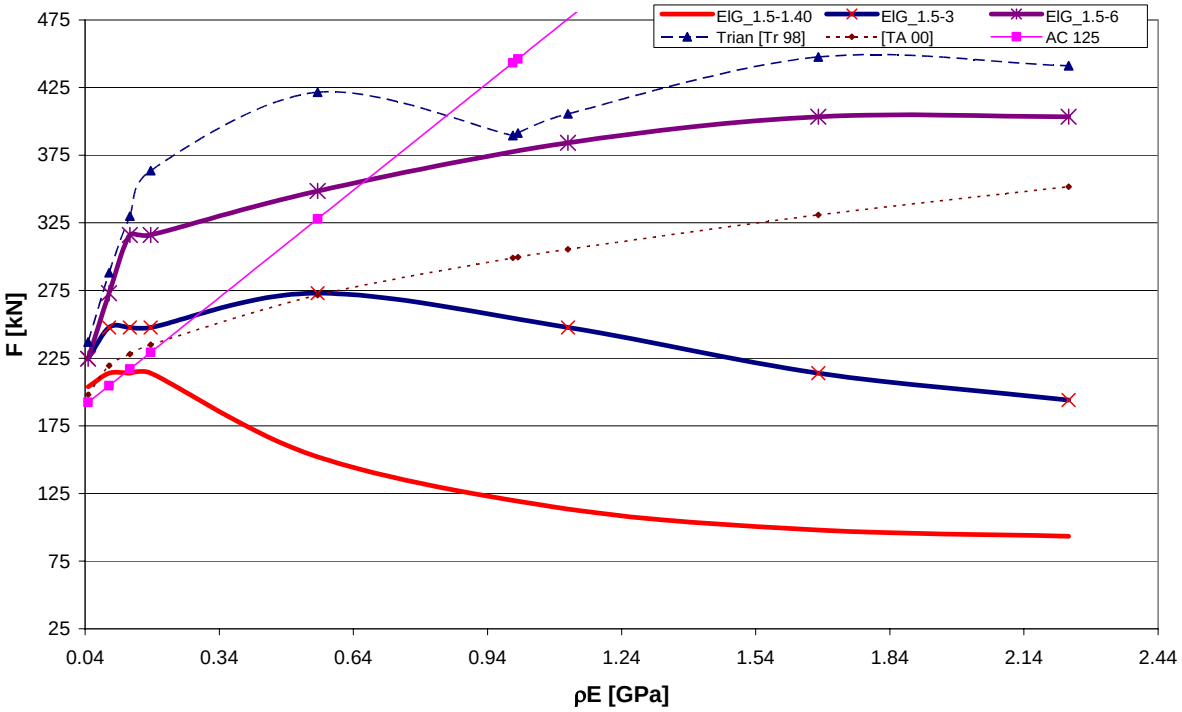

Figure 5.25: Effect of using H masonry (1.50 MPa) with epoxy having different allowable shear stresses on URM-FRP lateral resistance

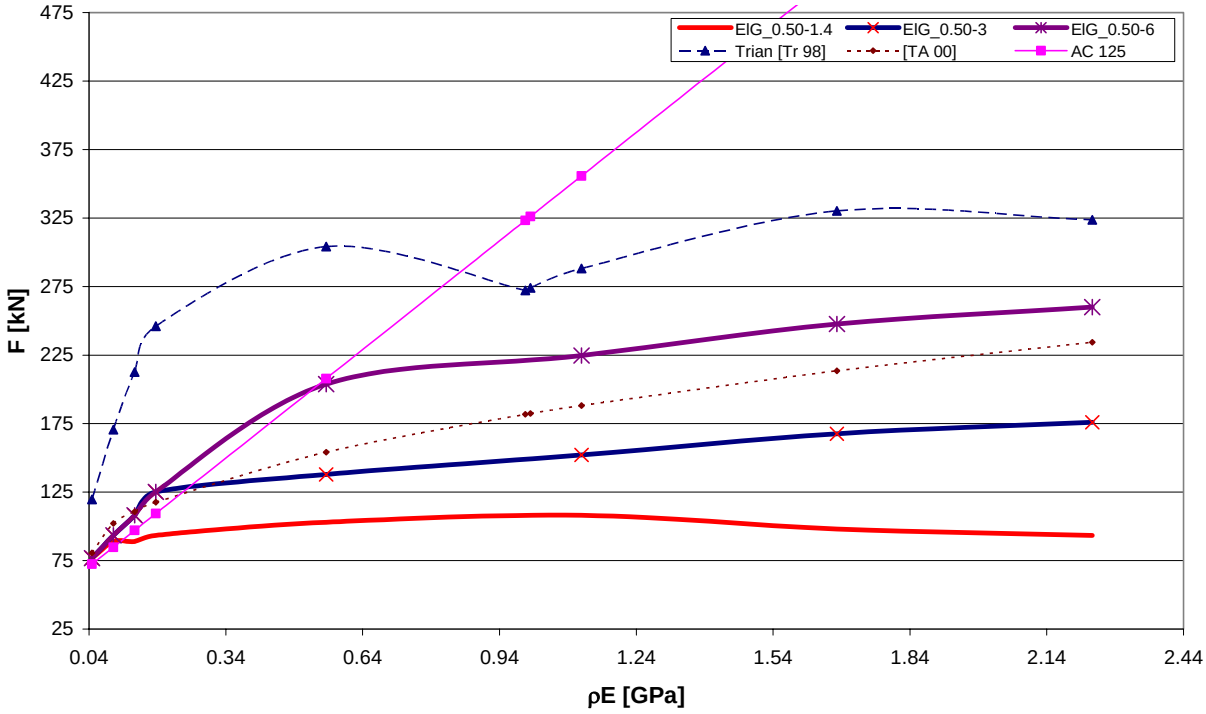

Figure 5.26: Effect of using H masonry (0.50 MPa) with epoxy having different allowable shear stresses on URM-FRP lateral resistance

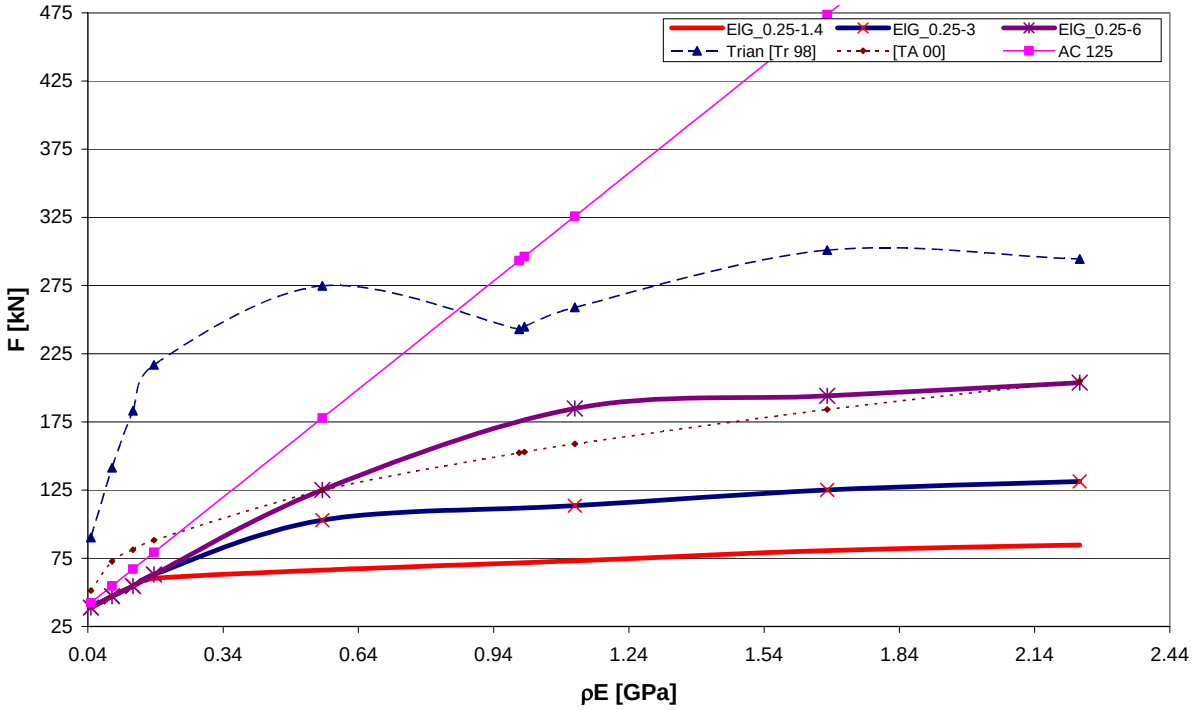

Figure 5.27: Effect of using L masonry (0.25 MPa) with epoxy having different allowable shear stresses on URM-FRP lateral resistance

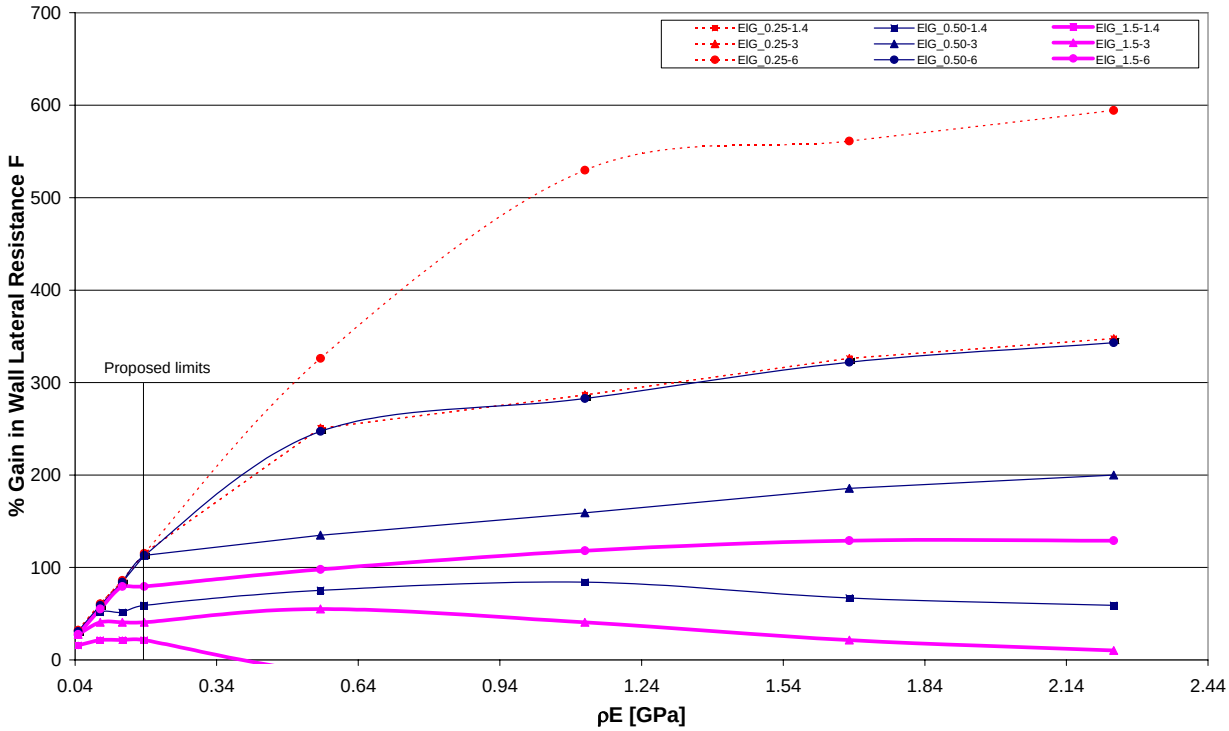

Figure 5.28: Effect of using different masonry with epoxy having different allowable shear stresses on gain in wall lateral resistance

5.5.2 Effects of ductility and shear modulus

In this section effect of epoxy ductility and shear modulus as well as masonry ductility on ζ, F_{FRP}, and F is investigated. For this investigation, 0.5 and 3.0 MPa are used as allowable shear stress for masonry and epoxy, respectively.

Effects of epoxy ductility and shear modulus

Since experimental evidences (Figure 5.9) show that the variations in epoxy ductility are too high; wide range of epoxy ductility has been examined. Values ranged from 2 to 20 has been assigned to epoxy ductility. In all cases, a value of 8 is assigned to masonry ductility (see discussion later). Figure 5.29 to 5.31 show the effect of epoxy ductility on ζ, F_{FRP}, and F, respectively. The figures show the following:

- For all epoxy ductility used in this comparison, the limit on masonry stiffness dominates the behavior for small values of ρE. As mentioned earlier, when masonry dominates the behavior ζ degradation rate is very slow. With increasing ρE, the limit on epoxy ductility starts to dominate URM-FRP behavior with a higher ζ degradation rate.
- With increasing epoxy ductility, ζ degradation rate decreases. However, after an approximate value of 1.12 GPa for ρE the effect of epoxy ductility vanish and all the curves start to be parallel to the second part of equation 5.4.
- As shown in the Figures 5.30 and 5.31, for small value of ρE (less than 0.14 GPa) there is no effect of epoxy ductility on either F or F_{FRP}. For ρE greater than 0.14 GPa, the highest epoxy ductility the highest F and F_{FRP}. The difference in F_{FRP} due to increasing epoxy ductility increase with increasing ρE. with increasing epoxy ductility from 2 to 6, F increased between 5 and 28% depends on ρE. By increasing epoxy ductility from 2 to 20, F increased between 34 and 64% depends on ρE.
- For a stiff epoxy (ductility=2), after $(\rho E)_{limit}$ of 1.7 GPa, FFRP reaches its upper limits i.e. any additional FRP has no effect. In addition, as explained earlier after $(\rho E)_{limit}$ there is a reduction in F.

Regarding the effect of epoxy shear rigidity (Figure 5.32), as expected the effect of increasing G modulus similar to decreasing ductility. So, the lower rigidity we have for epoxy the best ζ degradation rate. Conclusions similar to the previous four points can be drawn.

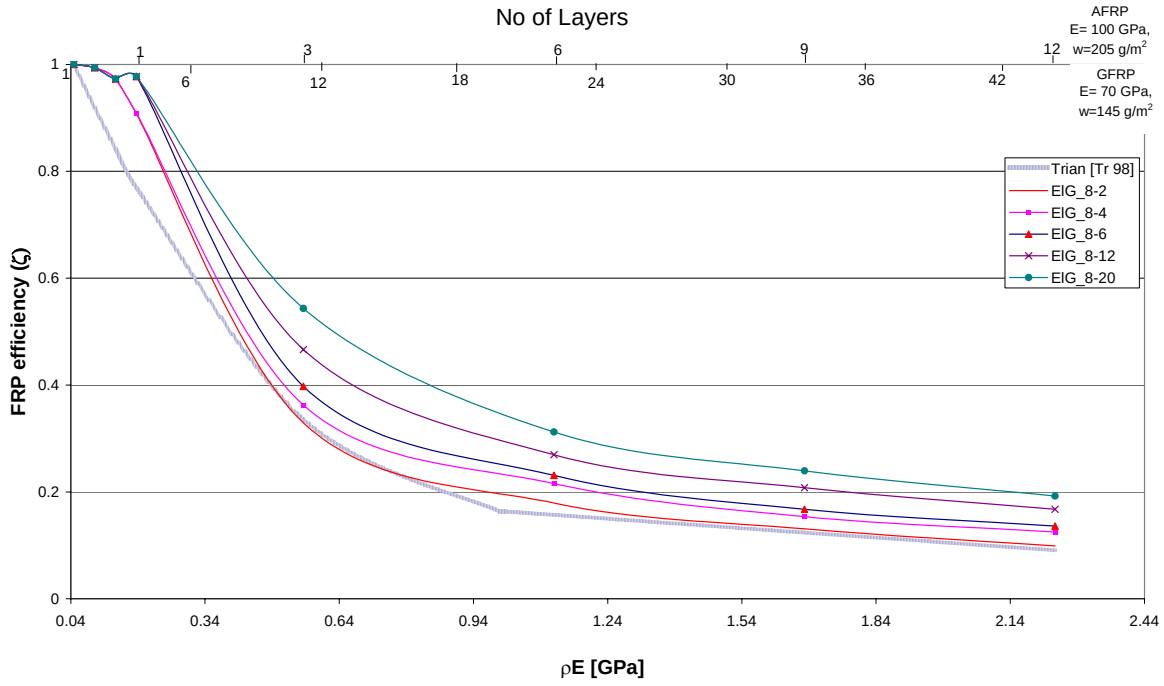

Figure 5.29: FRP efficiency (ζ) in terms of ρE for different epoxy ductility

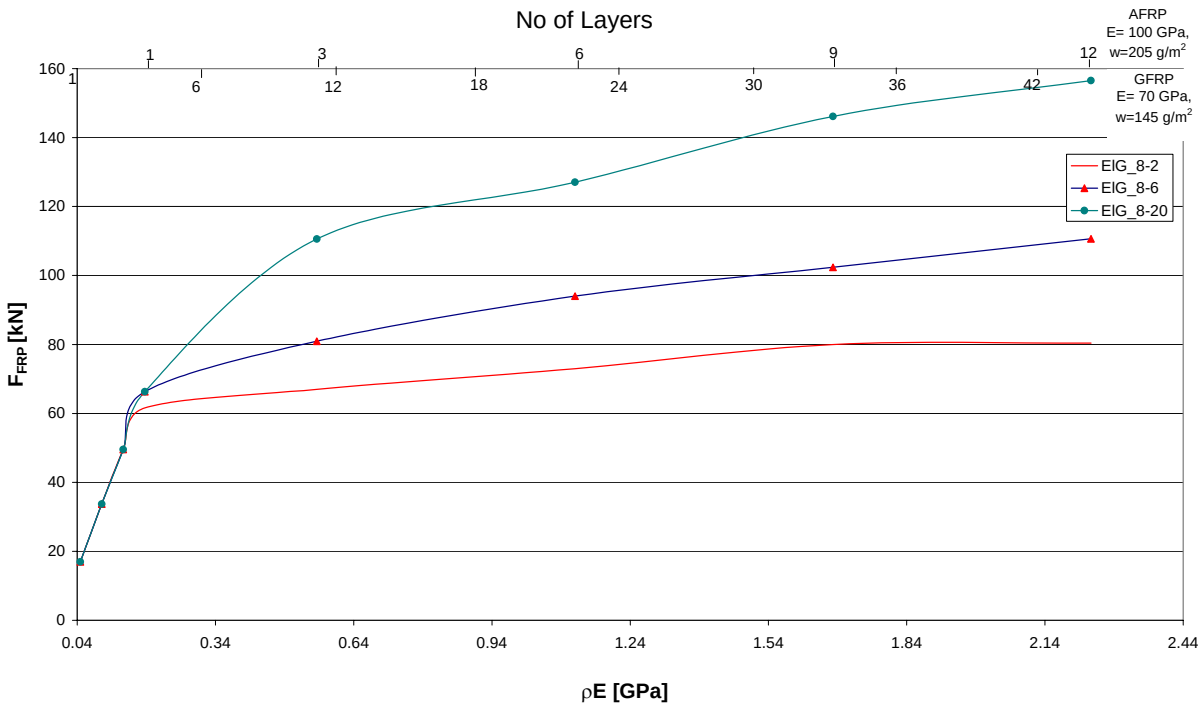

Figure 5.30: Contribution of FRP to lateral resistance in terms of ρE for different epoxy ductility

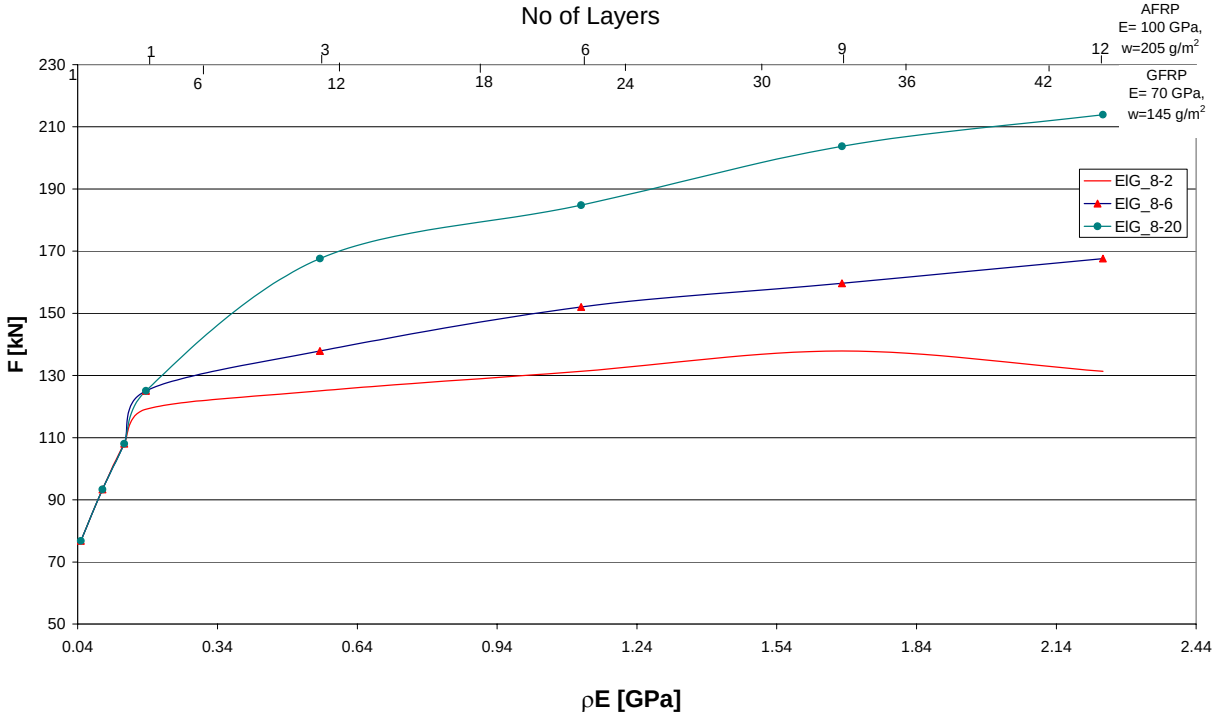

Figure 5.31: Lateral resistance of URM-FRP in terms of ρE for different epoxy ductility

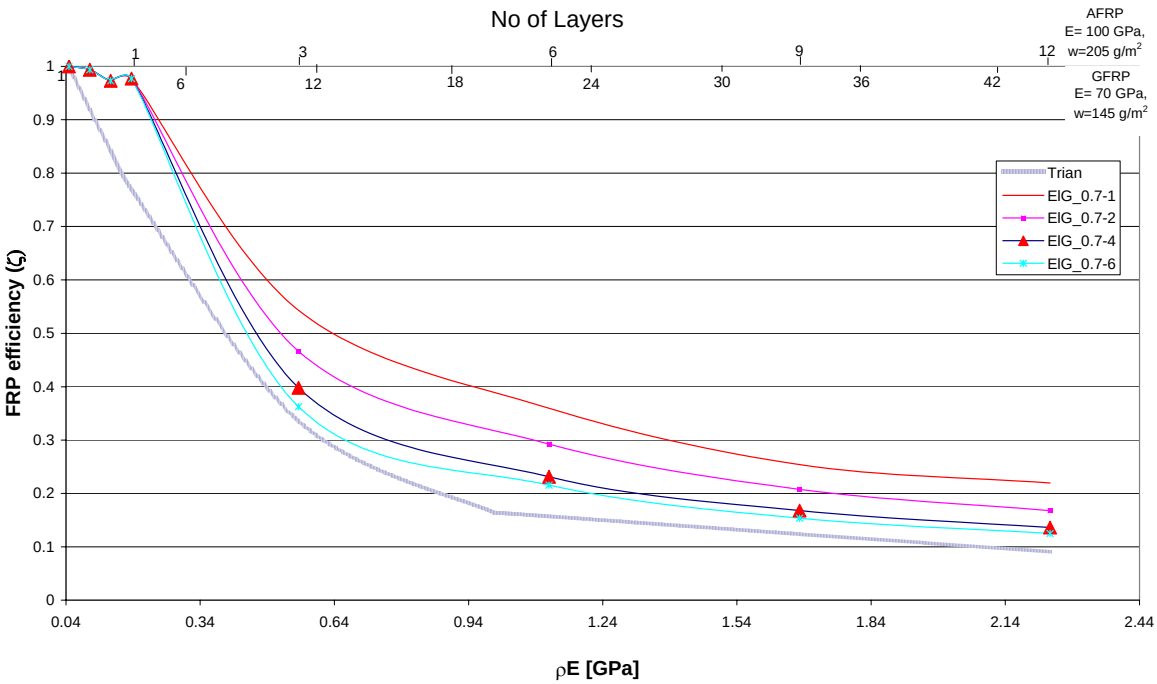

Figure 5.32: FRP efficiency (ζ) in terms of ρE for different epoxy rigidities

Masonry ductility

In this subsection effects of masonry ductility have been examined. Ductility that ranged from 2 to 20 for masonry has been examined. In all cases, a value of 7 is assigned to epoxy ductility (see discussion later). Again it should be noted that the upper value for masonry ductility examined here is just a value to investigate the full range of analytical model characteristics and do not necessarily represent realistic characteristics of particular URM wall. Regarding masonry ductility, as shown in Figures 5.33 to 5.35,

- For a stiff masonry panel (ductility = 2), approximately there was no reduction in ζ till ρE of 1 GPa. With increasing masonry ductility, ζ degradation rate increases.
- For a stiff masonry panel (ductility = 2) and at the beginning, there is efficiency value slightly greater than one. This unexpected increment in efficiency factor can be explained as flowing. At the beginning, the masonry ductility dominates the behavior while epoxy is still linear elastic. For a little higher amount of ρE, the limit on masonry stiffness dominates the URM-FRP behavior with mobilization of epoxy stiffness degradation this leads to higher stresses in the FRP, which appears in the beginning of Figure 5.33. Later and with increasing ρE, masonry dominates the behavior with high degradation in epoxy stiffness until ρE of approximately 1GPa. For values of ρE greater than 1 GPa, epoxy dominates URM-FRP behavior.
- Regardless of masonry ductility, for ρE greater than 1.12 GPa, all the curves are approximately parallel to the second part of equation 5.4 i.e. with the same degradation rate.
- Regarding the F_{FRP} and F, for ρE smaller than 1.12 GPa, with increasing masonry ductility both FRP contribution to lateral resistance and masonry lateral resistance increases. For higher values of ρE, there is no effect of masonry ductility since the limit on epoxy stiffness dominates the behavior.
- With increasing masonry ductility, $(\rho E)_{optimum}$ deceases with significant decrease in F_{FRP} and F

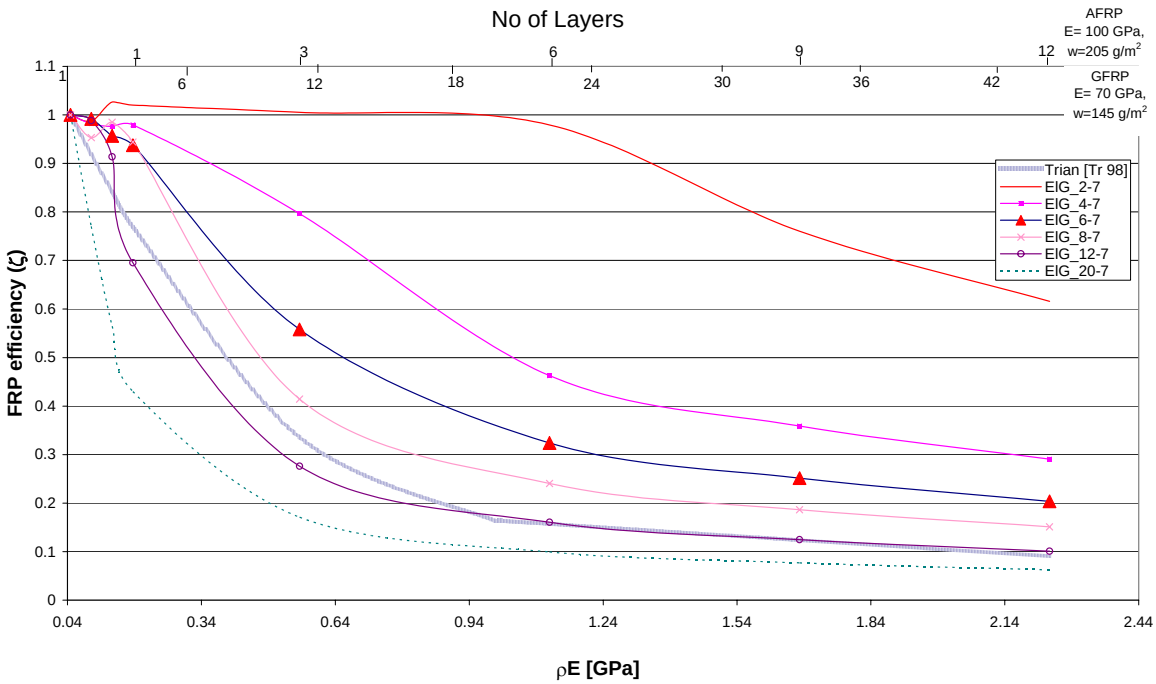

Figure 5.33: FRP efficiency (ζ) in terms of ρE for different masonry ductility

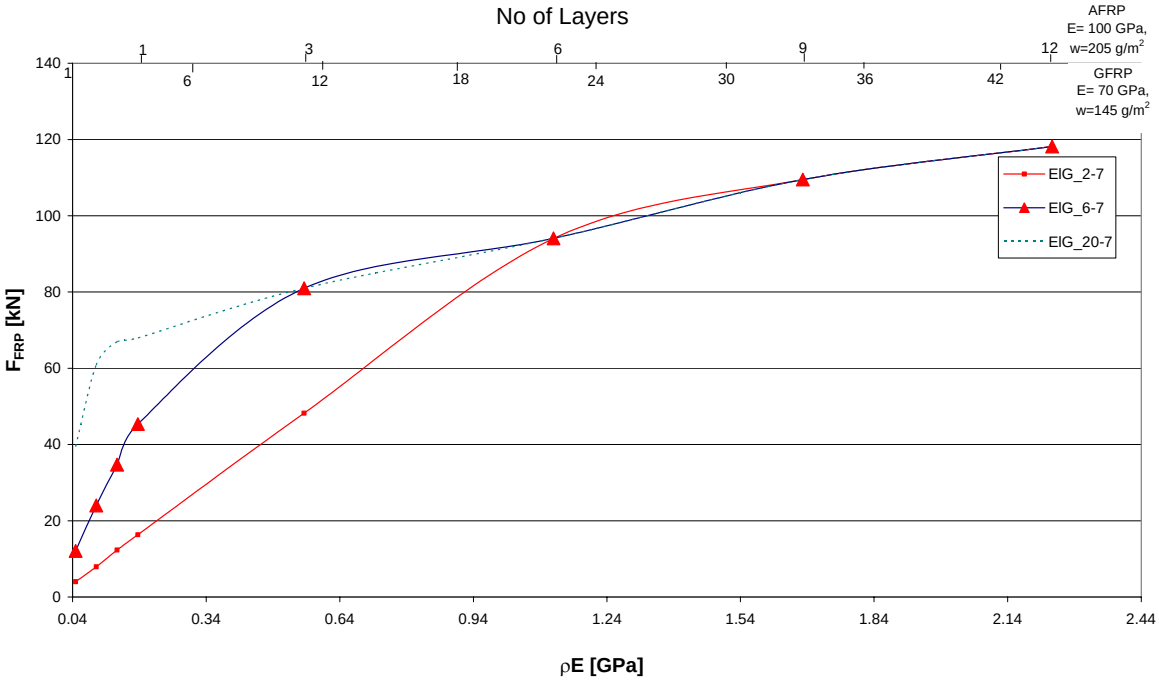

Figure 5.34: Contribution of FRP to lateral resistance in terms of ρE for different masonry ductility

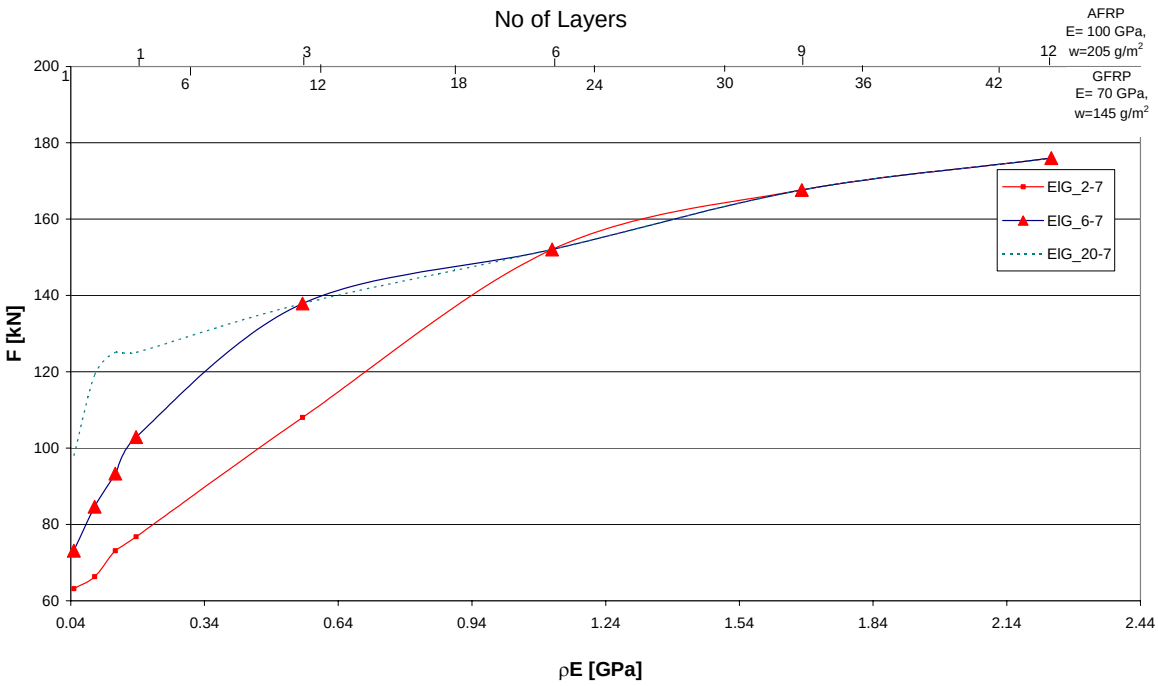

Figure 5.35: Lateral resistance of URM-FRP in terms of ρE for different masonry ductility

5.6 Convergence of Double Sine Series Solution

A drawback to the sine series solution (equation 5.33) is that convergence can be slow [KK 01]. Consequently, a high number of terms in equation 5.33 needs to be used in order to converge upon an accurate solution. In this section the effect of number of terms n and m on F and F_{FRP} is examined. A case with the following parameters has been studied: allowable shear stresses for masonry and epoxy are 0.48 and 3 MPa, respectively. The masonry and epoxy ductility is 8 and 7, respectively; see discussion in next section about these test parameters. Finally, a value of ρE of 0.19 GPa (one layer of AFRP of 0.14 mm thick) have been used in this comparison. Figure 5.36 shows the effect of number of terms taken in the double sine series solution (m and n) on F_{FRP} and F. The figure shows the following:

- It seems more appropriate to take a high number of terms when carrying out analysis using the proposed method. However, to have the line corresponding to n = 501 in Figure 5.36, the calculations take several hours (7 hours). This time reduces to several minutes for the line corresponding to n = 41.
- In general n has a significant effect on the results rather than m. in addition, for n greater than 41, the effect of m reduces
- All the comparisons given in the previous sections a value of 41 was used for m and n. The comparison between the case where m = n = 501 and the case where m = n = 41 (Figure 5.36), show that the error in later case is 70% in F_{FRP} and 27% in F. However, the comparisons in the previous sections was given to better understand the shear behavior rather than to have absolute values. In addition, for small values of ρE, effects of number of terms n and m are significantly reduced.
- In the comparison of the experimental data with the proposed model (next section), m = 501, n = 41 have been used. For the tested specimens, the comparison between the case where m = 501, n = 41 and the case where m = n = 101, show that the error in later case is between 0-18% in F_{FRP} and 0-7% in F. The higher the reinforcement ratio is the higher the error.

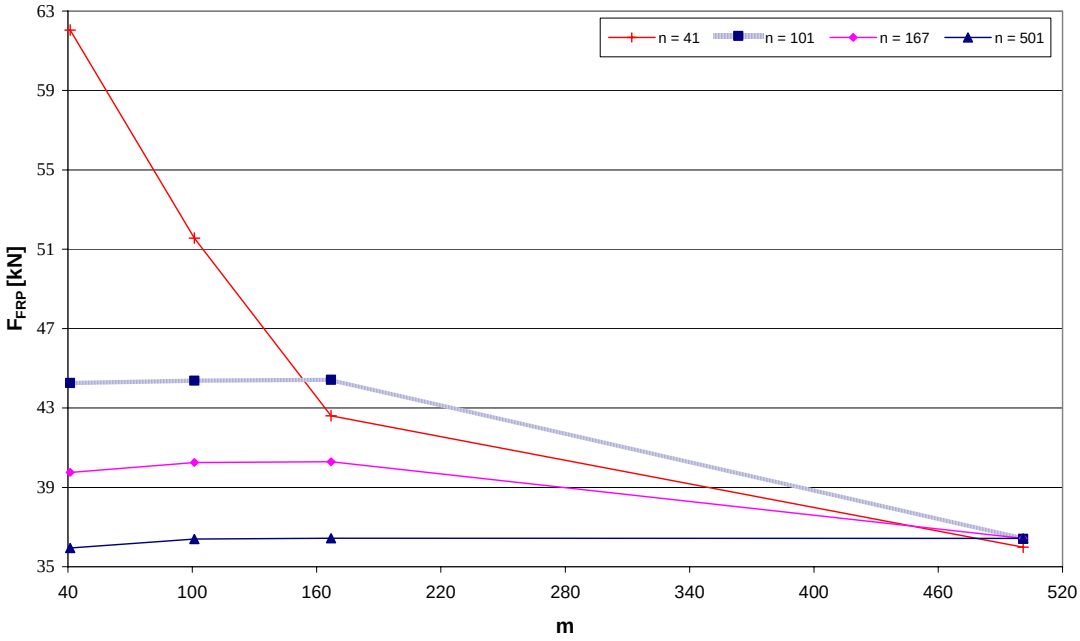

(a)

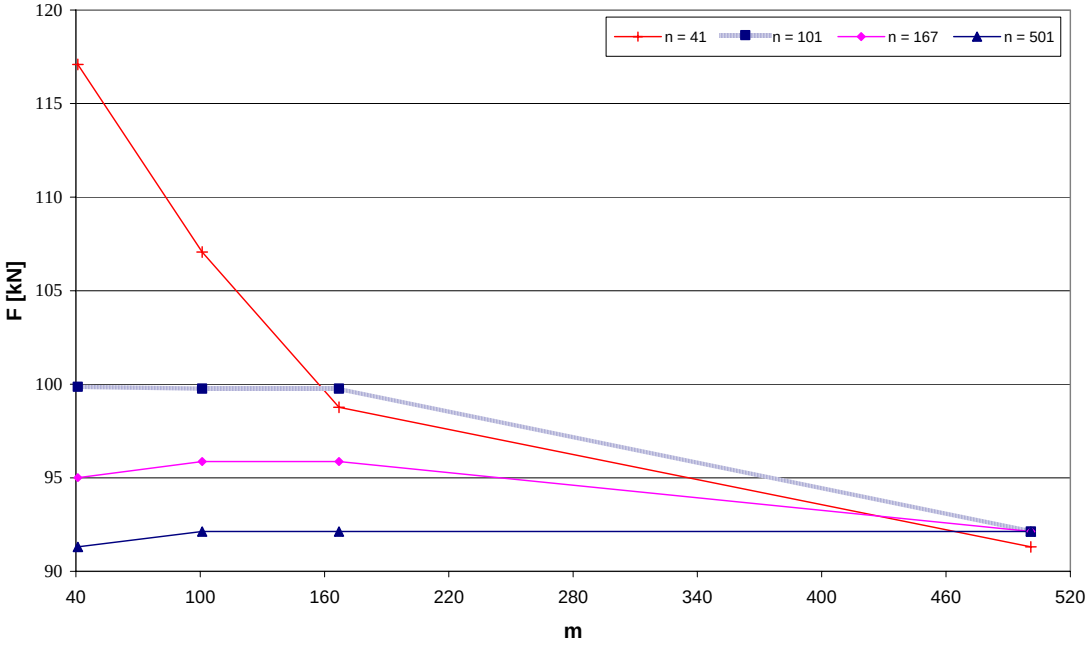

(b)

Figure 5.36: Effect of number of terms n and m in equation 5.33 on (a) F_{FRP} and (b) F

5.7 Calculations of FRP Contribution to Shear Resistance of URM-FRP

The proposed model has been used to calculate the shear resistance of the squat and midget specimens, which have been tested during the static cyclic and dynamic tests (Chapters 3 and 4). As discussed in previous sections material parameters plays essential role in this analytical model. The following parameters have been used in the verifications:

- Based on measured stiffness and calculated F (see discussion later), values of drift at first apparent yield $D_y = 0.7 \times 10^{-3}$ for squat and 0.55×10^{-3} for midget were assumed as yield drift.

- Since no reference specimen during the experimental work (static cyclic and dynamic) failed due to shear, it is decided to use an accepted ultimate drift. Magenes and Calvi [MC 97] carried out static cyclic and monotonic tests on URM walls with effective aspect ratio that ranged from 0.66 to 1.00 tested under normal forces ranged from 0.6 to 1.12 MPa. For these specimens, the drift at ultimate conditions was uniform with a mean value of 0.53% and a coefficient of variation of 10%. Of these specimens, the specimens which have effective aspect ratio of 0.67 have an ultimate drift of 0.59%. A value of 0.6% has been implemented in NLSFRP.
- Based on the properties of masonry and wall geometry it is possible to determine the initial stiffness for the tested specimens. Based on the measured initial stiffness, the EI (where E is the Young's modulus and I is the section moment of inertia) for the test specimens was back calculated. In addition, a value of approximately 4500 MPa was measured during the experimental program for E modulus. This measured value is approximately 750 times the masonry characteristic compressive strength. Based on a rectangular solid section, the section moment of inertia was calculated. The calculated EI based on measured stiffness was approximately 0.45 times the calculated EI based on material properties and geometry. Note that, this ratio is approximately the same between the sum of the web width in the brick used and the total brick width. However, in the program (NLSFRP) the value of EI which calculated from the measured initial stiffness was used. For epoxy and FRP, E values were given by the manufacture.
- One of the parameters in the program is elastic shear modulus of masonry, epoxy, and FRP. For a homogenous material G can be calculated as follows:

$$G = \frac{E}{2(1+\nu)} \tag{5.43}$$

where

ν = equivalent Poisson's ratio

For masonry panel, laboratory tests of URM shear walls [EA 89, AS 92] have found that the shear modulus of masonry does approach the value of 40% times the elastic modulus in compression; similar value is specified in EC 6 [EC6 99]. However, Tomazevic [To 95] shows that for several kinds of brick and mortar typical values of G ranged from 6 to 25% of E. Franklin et al. [FL 01], measured values of G = 28% of E. In addition, after cracking, the shear stiffness is known to reduce substantially as sliding along bed joints develops or as diagonal tension cracks open. For slender wall with aspect ratio of 1.5 (i.e. minimum shear deformations happened), the degradation was 12% of the elastic measured G [FL 01]. For epoxy and FRP used in this experimental program, there is a lack in the data regarding G. Finally, in NLSFRP the following values were assumed for G modulus:

$$G^m = 0.35\ E^m$$
$$G^f = 0.50\ E^f$$
$$G^e = 0.40\ E^e$$

- F for masonry was calculated based on a Mohr-Coulomb frictional model. The model is recommended by several researchers (e.g. [To 95]) and recent Codes (e.g. [EC6 99]). However, several researchers (e.g. [HD 94]) have found that at approximately compression stress of 2 MPa Mohr-Coulomb frictional model is not valid and more complicated models should be used (e.g. nonlinear relationship developed by Hendry [He 78] or Ali [Al 87]). Within the applied normal forces in the experimental program, Mohr-Coulomb frictional model can be used. Using this model, the ultimate shear stress can be calculated as follows:

$$\tau^m = c + \mu\sigma \tag{5.44}$$

where

c = initial shear strength under zero compressive stress (cohesion),

μ = friction coefficient, and

σ = average compression stress due to the vertical load

For the tested specimens, triplet tests show that $c = 0.2$ MPa and μ is estimated as 0.9 based on measured shear friction happened during testing specimens S2-REFE-ST and M2-WRAP-G-F-ST (after FRP rupture). Note that value of 0.1-0.3 MPa have been proposed by EC 6 [EC6 99] for c. Besides masonry panel, metal due to test set-

up at the RC head beam, and the head beam weight, the applied normal force produced an average compression stress of 0.37 MPa.

- The final parameter required for NLSFRP is the maximum allowable shear stress for epoxy. Several researchers (e.g. [CN 98], [AS 94]) assumed values between 3.5 and 4.0 MPa for epoxy allowable shear stress. In addition, they assumed that the maximum allowable shear stress is double the average epoxy shear stress. For URM, an average value of epoxy shear stresses of 1.5 MPa have been measured [CC 02]. In NLSFRP a value of 3.0 MPa is assumed as maximum allowable shear stress for epoxy with assumption that the average shear resistance of epoxy is 0.5 times the allowable shear stress.

5.7.1 Shear stress distribution on a URM-FRP

As an example for a URM-FRP, in this section specimen M2-WRAP-G-F-ST is examined in details. The specimen is analyzed using the parameters which are given in the previous section. Figures 5.37 to 5.42 show shear stress distributions on epoxy and FRP. The figures show the following:

- Stresses in FRP are approximately constant through the entire wall surface except near the boundary where stresses dropped gradually to zero
- Due to shear mechanism there is a stresses in the vertical FRP. These stresses are approximately equal to stresses in the horizontal direction. These stresses should be taken into considerations for any flexural design. These stresses are in the order of 10% of the FRP allowable tensile stresses; however, these stresses reduced with increasing ρE.
- Regarding shear stresses in epoxy layer, the forces transmitted from masonry to FRP through limited length of epoxy at edges. In addition, within this transmission length, the stress distribution is triangle this can justified the assumption used through this analysis of using allowable shear stress 0.5 times the maximum shear stress.

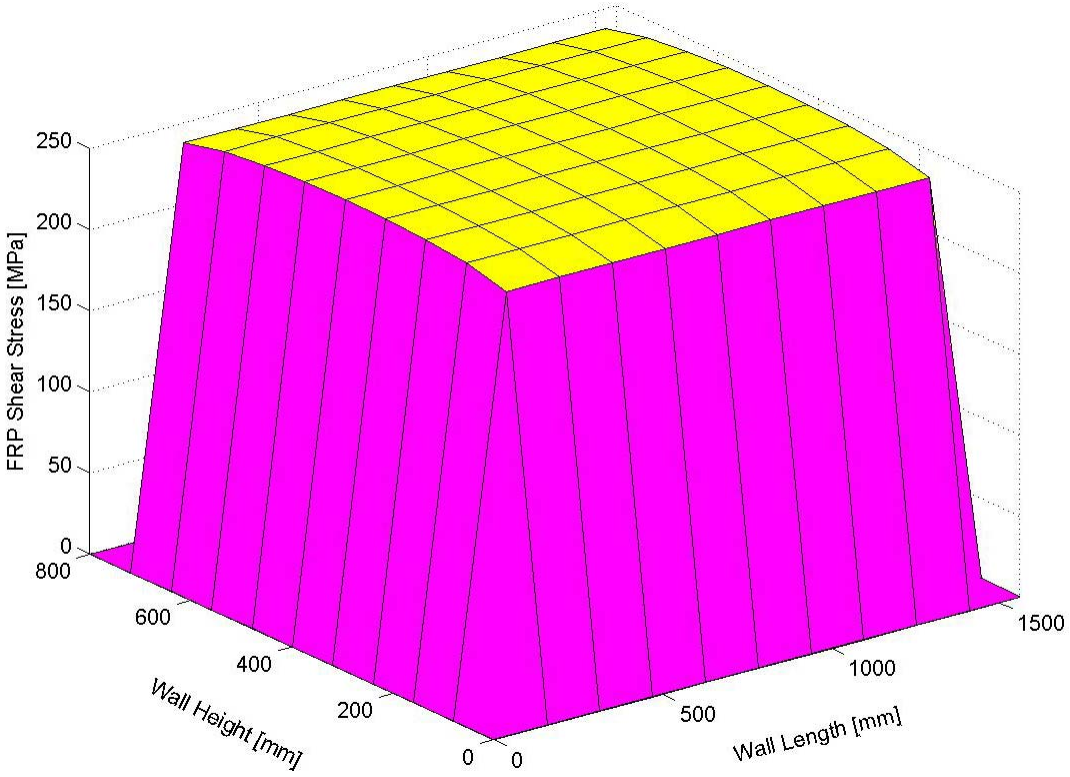

Figure 5.37: Shear stress in FRP through the entire wall surface

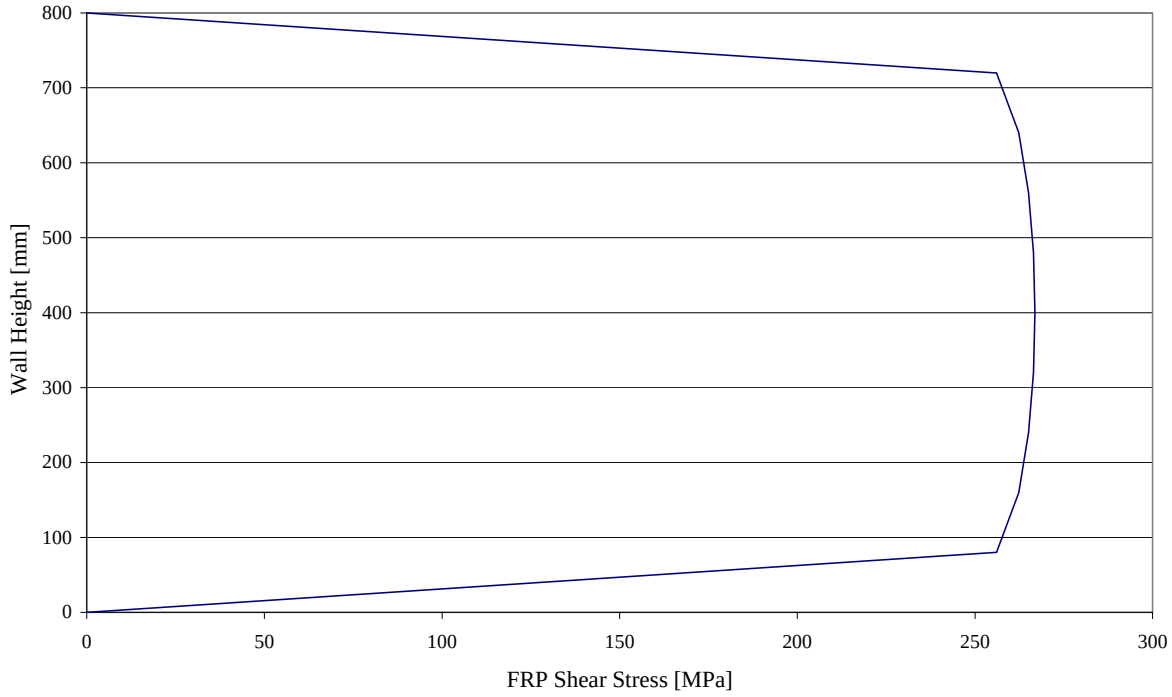

Figure 5.38: Distribution of stresses in FRP along section at x=L/2

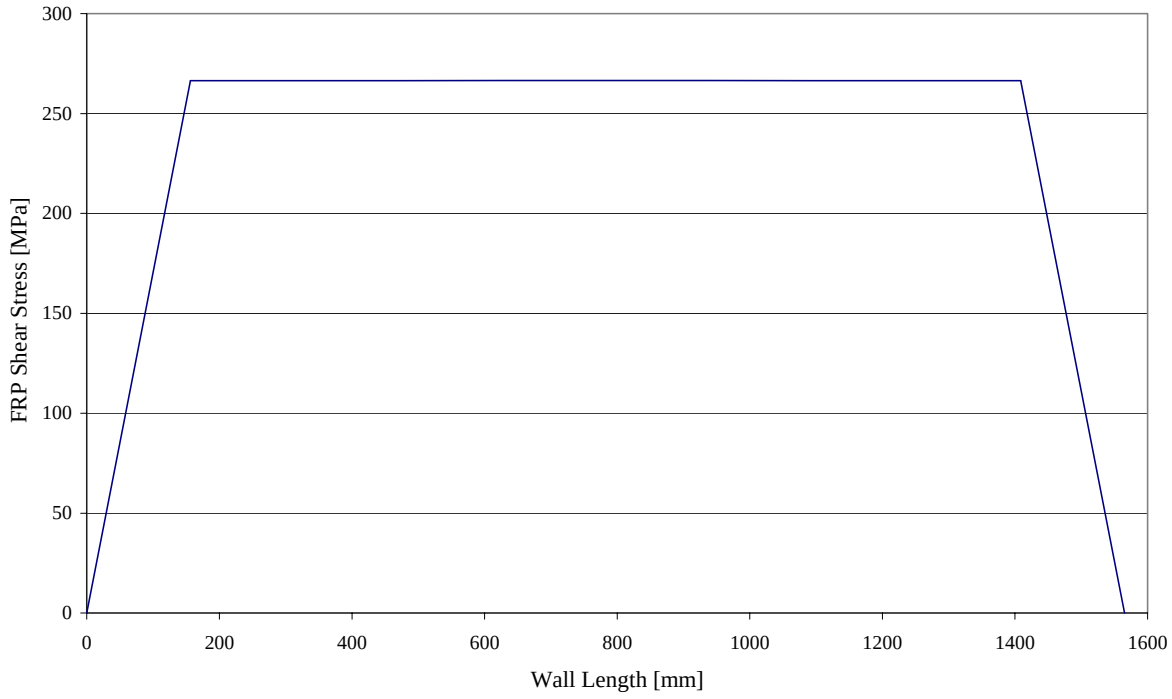

Figure 5.39: Distribution of shear stresses in FRP along section at y=h/2

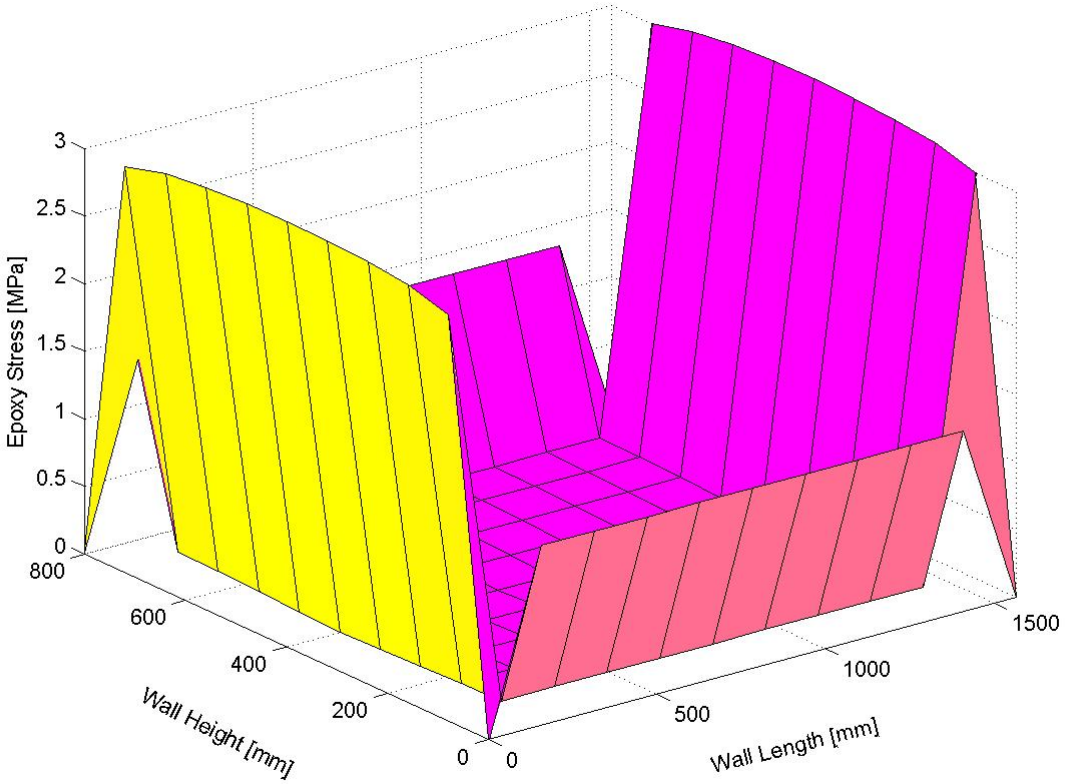

Figure 5.40: Resultant shear stresses in epoxy

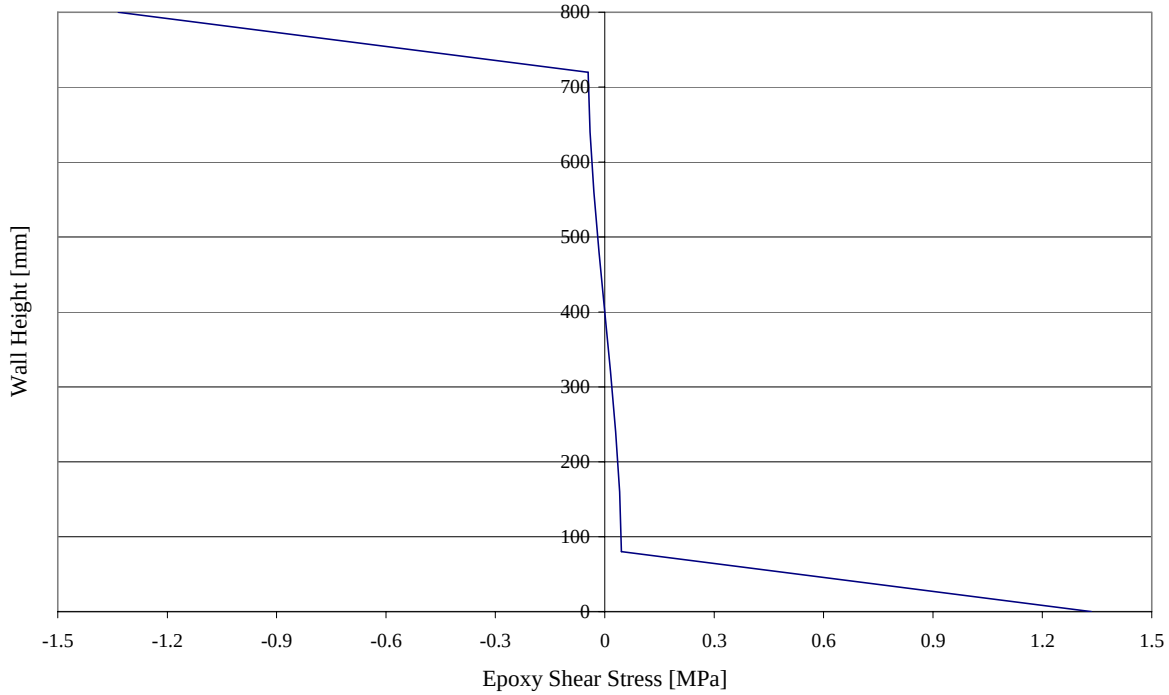

Figure 5.41: Distributions of resultant shear stresses in epoxy at x=L/2

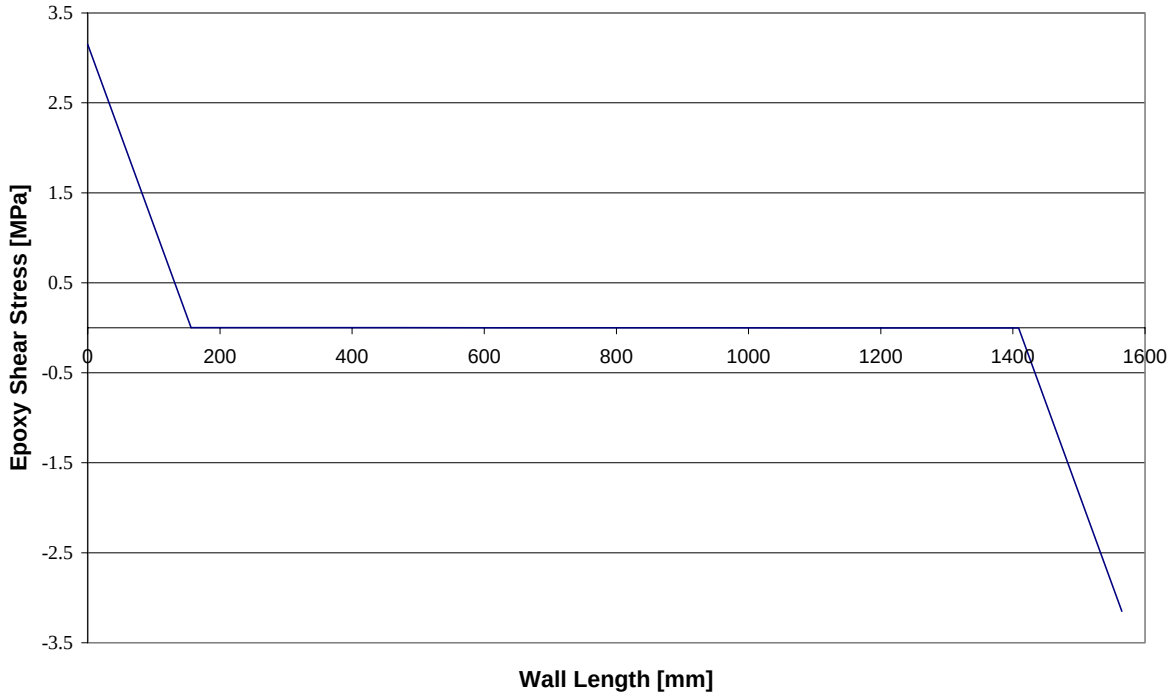

Figure 5.42: Distributions of resultant shear stresses in epoxy at y=h/2

5.8 Comparison of Analytical and Experimental Results

The shear contributions of FRP (F_{FRP}) as well as the total shear strength of the URM-FRP (F) are presented in Tables 5.1 to 5.4 as well as in Figures 5.43 and 5.44 . In Tables 5.1 and 5.3, each row containing estimation of F_{FRP} according to the different existing methods is followed by a row containing a quantity called $Diff_{FRP}$. This quantity is the ratio between F_{FRP} estimated according to the proposed model and F_{FRP} according to the existing model in the previous row i.e. it is defined as follows:

$$Diff_{FRP} = \frac{F_{FRP}\ \text{estimated according to the proposed model}}{F_{FRP}\ \text{estimated according to existing model}}\% \qquad (5.45)$$

Also in Tables 5.2 and 5.4, each row containing F is followed by a row containing $Diff_{Total}$. This quantity is the ratio between F estimated according to the model in the previous row to F according to the experimental values i.e. it is defined as follows:

$$Diff_{Total} = \frac{F\ \text{estimated according to the models}\left(\text{either proposed or existing}\right)}{F\ \text{experimental}}\% \qquad (5.46)$$

The comparison shows the following:

- Though the analytical model predicts an effective strain in the FRP close to Triantafillou [Tr 98], the absolute value between the two models is very fare. The proposed model predicts values that ranged from 18 to 34% of Triantafillou model with average of 25%. However, it should be keep in mind Triantafillou's model shortcomings (§ 5.1.1).
- For low reinforcement ratio, the proposed analytical model predicts F_{FRP} very close to AC125. With increasing reinforcement ratio (ρ), the AC125 estimates F_{FRP} higher than the proposed model. However, this is expected since AC125 used constant effective strain in the FRP regardless of ρ. In case of high reinforcement ratio, the debonding starts to dominate the behavior and the effective strain in the FRP reduced. In general the proposed model estimates approximately (42-122%) of F_{FRP} according to AC125 model with average of 81%.

- The proposed model estimates F_{FRP} lower than Triantafillou and Antonopoulos model approximately (60-92%) with average of 70%. This shows the importance of the improvements that Triantafillou and Antonopoulos introduced to Triantafillou original model.
- The proposed model predicts lateral resistance of the test specimens that ranged from 61 to 143% of the measured lateral resistance. It should be noticed that no specimen failed in pure shear during the experimental program. In addition, specimens S1-WRAP-G-F and S2-WRAP-A-F did not reach their ultimate lateral resistance. Finally, the low lateral resistance of specimen S2-WRAP-G-F-ST could be explained since their reference specimen had too heavy damage during the first part of the static cyclic (i.e. without reinforcement). The big difference between the estimated and measured lateral resistance of specimen M2-WRAP-A-F-ST can be attributed to the high ductility of this specimen. If we recall the force deformation curve of the reference specimen of this retrofitted specimen, the force deformation curve shows that the reference specimen had a ductility of 32 (see § 4.2). This high unexpected ductility is due to a diagonal crack which happened due to test set-up problems. During the calculation only ductility of 8 has been used for masonry. As shown in Figure 5.34, for ρE of 0.28 GPa (i.e. for specimen M2-WRAP-A-F-ST) by increasing masonry ductility from 6 to 20 F_{FRP} increases by approximately 30%. This gives an idea about the effect of increasing masonry ductility on the lateral resistance of the specimen. Another reason which influences the lateral resistance of all the specimens is the masonry shear resistance. Evidence show that the actual masonry shear resistance is at least 20% higher than the value used during the calculations (see discussion in next section).
- Triantafillou [Tr 98] model predicts approximately (173-338%) of measured lateral resistance.
- AC125 [IC 01] model predicts approximately (97-171%) of measured lateral resistance
- Triantafillou and Antonopoulos [TA 00] model predicts approximately (79-160%) of measured lateral resistance.

*Table 5.1: Comparisons between F_{FRP} estimated according to the proposed model and other models for the specimens tested in the **static cyclic** tests*

Parameters	S2-WRAP-G-F-ST	M2-WRAP-G-F-ST	M2-2WRAP-G-F-ST	M2-WRAP-A-F-ST
ρ [%]	0.072	0.072	0.144	0.280
E [GPa]	70	70	70	100
f_t [MPa]	2400	2400	2400	2880
ε [%]	3.0	3.0	3.0	2.8
ε_{eff} [-]	0.0109	0.0109	0.0099	0.0070
fj	280	280	280	400
F_{FRP} [kN] ElG	17	22	28	42
F_{FRP} [kN] [Tr 98]	64	64	118	229
$Diff_{FRP}$ [%]	27	34	24	18
F_{FRP} [kN] AC125 [IC 01]	18	18	36	99
$Diff_{FRP}$ [%]	94	122	78	42
F_{FRP} [kN] [TA 00]	24	24	45	70
$Diff_{FRP}$ [%]	71	92	62	60

*Table 5.2: Comparisons between F estimated according to the proposed model and other models as well as experimental results for **static cyclic** tests*

F_{total} Experimental	***51***	***70***	***95***	***160***
F_{total} ElG	73	78	84	97
$Diff_{Total}$ [%]	143	111	88	61
F_{total} [Tr 98]	121	173.9	120.8	285.6
$Diff_{Total}$ [%]	237	183	173	178
F_{total} AC125 [IC 01]	74	74	92	155
$Diff_{Total}$ [%]	145	106	97	97
F_{total} [TA 00]	80	80	101	126
$Diff_{Total}$ [%]	157	114	106	79

*Table 5.3: Comparisons between F_{FRP} estimated according to the proposed model and other models for the specimens tested in the **dynamic** tests*

Parameters	S1-WRAP-G-F	S2-WRAP-A-F
ρ [%]	0.072	0.189
E [GPa]	70	100
f_t [MPa]	2400	2880
ε [%]	3.0	2.8
ε_{eff} [-]	0.0109	0.0084
fj	280	400
F_{FRP} [kN] ElG	17	36
F_{FRP} [kN] [Tr 98]	64	186
$Diff_{FRP}$ [%]	27	19
F_{FRP} [kN] AC125 [IC 01]	18	67
$Diff_{FRP}$ [%]	94	54
F_{FRP} [kN] [TA 00]	24	59
$Diff_{FRP}$ [%]	71	61

*Table 5.4: Comparisons between F estimated according to the proposed model and other models as well as experimental results for **dynamic** tests*

F_{total} Experimental	***74***	***72***
F_{total} ElG	73	92
$Diff_{Total}$ [%]	99	128
F_{total} [Tr 98]	121	243
$Diff_{Total}$ [%]	164	338
F_{total} AC125 [IC 01]	74	123
$Diff_{Total}$ [%]	100	171
F_{total} [TA 00]	80	115
$Diff_{Total}$ [%]	108	160

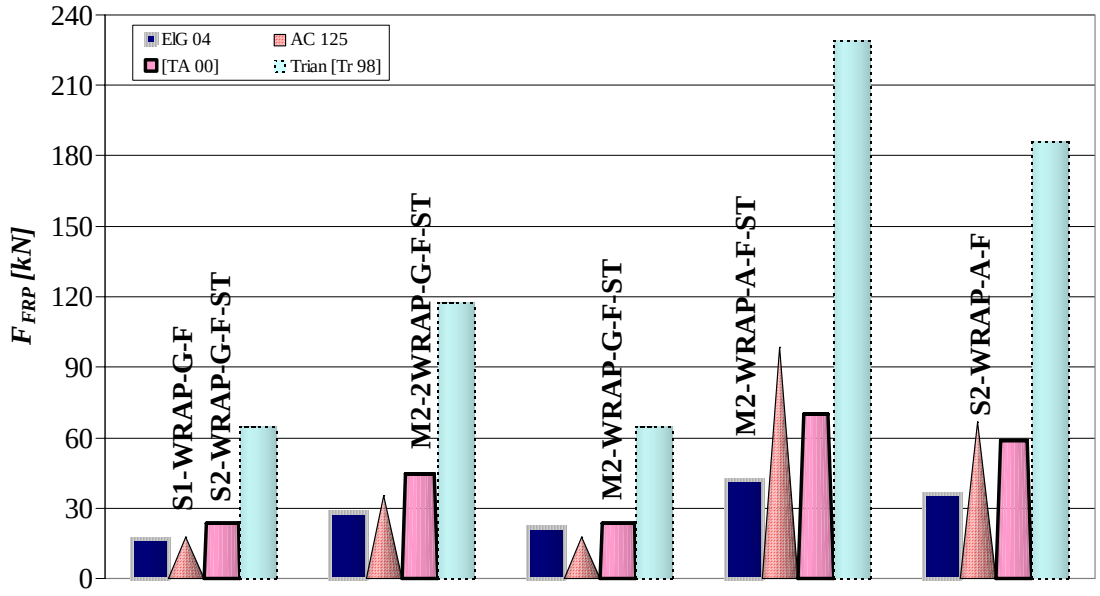

Figure 5.43: Comparison between different formulations to calculate the shear contribution of FRP (F_{FRP})

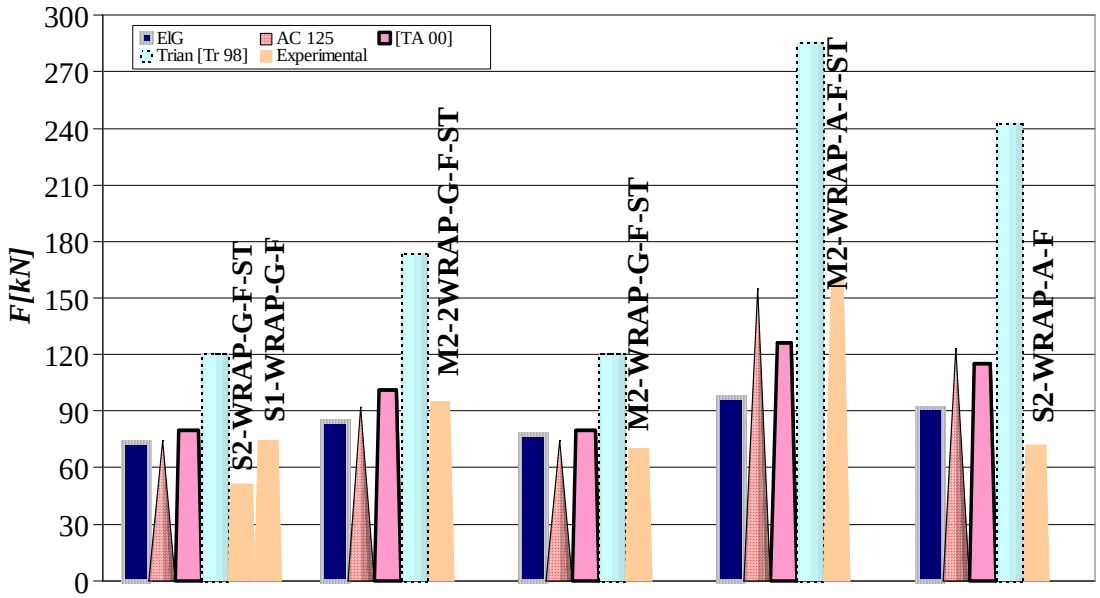

Figure 5.44: Comparison between experimental and calculated lateral resistance of URM-FRP (F)

5.9 Discussion about Shear Resistance of URM Walls

As mentioned in section 5.7, the masonry shear resistance was calculated using equation 5.43 with the parameters given in the same section. However, in order to have a better estimation of the shear resistance of the tested URM-FRP, a more accurate value of F_m should be used. The best way to have accurate value for F_m is to calculate it back from one of the tested specimens. For the tested specimens where vertical reinforcement only was used, if the dowel action of such vertical reinforcement is calculated and compared with the experimental lateral resistance, then it is easy to calculate back F_m. In this section the dowel action of the specimen which retrofitted using vertical reinforcement only is calculated.

5.9.1 Shear resistance of specimen S2-WIRE-F-S-ST

Several guidelines (e.g. FEMA 356 [FE 00]) for reinforced masonry neglect the effect of vertical reinforcement on shear resistance of masonry walls. However, according to Tomazevic [To 99], the lateral resistance of URM wall reinforced using vertical steel only can be calculated as following:

$$F = F_m + F_{hs} \tag{5.47}$$

$$F_{hs} = 0.806\, n\, d^2 \sqrt{f_m f_y} \tag{5.48}$$

where

n = number of vertical bars
d = bar diameter
f_m = masonry compressive strength
f_y = the yield strength of reinforcing steel

However, as the post-earthquake damage observations and experiments indicate, vertical steel alone is not capable of contributing to the shear resistance of masonry. Walls reinforced only with vertical reinforcement will fail in shear, despite their predicted flexural behavior (Figure 5.45).

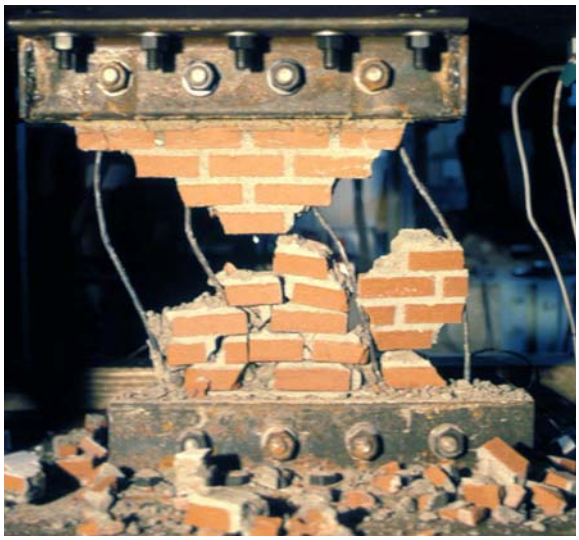

Figure 5.45: Shear failure of specimen retrofitted using vertical reinforcement only [Tomazevic 2003, personal communications]

Using equation 5.47 with n = 247, d^2 = 0.51 mm^2, f_m = 5.7 MPa, f_y = 3150 MPa results in F_{hs} of 13.6 kN. The experimental lateral resistance of specimen S2-WIRE-S-F-ST is approximately 83.9 kN. Using these values means that F_m is at least 70.3 kN or the allowable shear stress is at least 0.59 MPa. Keeping in mind that the specimen failed in flexural; then, the value used in the previous chapter to calculate the shear resistance of the specimens is at least 20% less than the actual value. Note that, Tomazevic [To 99] proposed this formula for grouted masonry walls in which the effect of dowel action should be more important than in such case where reinforcement glued to the surface. This possible increment in the shear lateral resistance of URM could be one of the reasons which explain why the retrofitted specimens reached the calculated shear capacity without shear failure.

5.10 Applications of the Proposed Model

The proposed model will make significant contributions to structural engineering community. The model has potential advantages which make it possible to apply in several ways such as:

- It can be used to prepare design charts which includes relations between ρE and (F_{FRP} and F) for different masonry types. Such charts, which do not exist, will be of great helpful for civil engineering designers.
- The relative values of the FRP efficiency (ζ) predicted by the model can replace the empirical functions proposed by Triantafillou [Tr 98]. Then, this efficiency factor could be combined with any absolute F_{FRP} calculated using either codes or design guidelines.

- The model is developed for the case of full coverage of entire surface of URM wall either single or double sides retrofitting. For partial coverage, it is believed that NLSFRP can be used with cautions. However, experimental verifications are required.
- For the case of inclined retrofitting, NLSFRP has it limitations for this problem. However, since the main assumption of NLSFRP is that masonry, epoxy, and FRP are isotropic materials, the NLSFRP results (F, F_{FRP}) should be divided by the sine of the angle of inclination (i.e. the angle between the diagonal and the horizontal axe).
- The values of ζ, F_{FRP}, F can be used to develop new retrofitting materials (i.e. epoxy and/or FRP) and improve the existing ones.

5.11 Summary and Findings

This chapter presents the first analytical model developed to predict the shear behavior of unreinforced masonry walls retrofitted using FRP. The proposed model idealized masonry, epoxy, and FRP in a URM-FRP as different layers with isotropic homogenous elastic materials. Then, using principles of theory of elasticity the govern differential equation of the system is formulated. A double Fourier sine series was used as closed form solution for the differential equations. The solution can be used to model the linear shear behavior of URM wall retrofitted using FRP. To take into consideration material nonlinearity, a step-by-step stiffness degradation of masonry as well as epoxy has been implemented in a program written in MATLAB [Ma 02]. The force deformation behavior of masonry layer as well as the epoxy layer has been idealized using bilinear curves (§ 5.3), the force deformation curve of FRP is idealized as linear elastic till failure. After every step of stiffness degradation, the equations were resolved. In general, either masonry or epoxy dominates the failure and in no case FRP reaches its ultimate load. The proposed model estimates lateral resistance of the tested specimens close to existing models and experimental results; however, more calibration of the model is still required.

Although the model is a fundamental analytical model, effects of different material properties were examined: allowable shear stresses for masonry and epoxy, epoxy ductility, epoxy shear modulus, and masonry ductility. Effects of these parameters on ζ, F, and F_{FRP} have been examined. The results show the following:

- The concept developed by Triantafillou [Tr 98] of using effective strain inversely proportional to the FRP axial rigidity seems more appropriate than using a constant strain value.
- The degradation rate given by Triantafillou [Tr 98] empirical equation (equation 5.4) is close to be an average of all the degradation rates given by different epoxy and masonry parameters. This is expected since Triantafillou developed his model based on curve fitting for different beams with different material parameters. However, the higher the allowable shear stress of epoxy, the lower the rate of degradation of ζ.
- When epoxy properties dominate URM-FRP shear behavior, the degradation rate of ζ includes three phases: high degradation rate until ρE of approximately 0.19 GPa, slow degradation rate for ρE greater than 1.12 GPa, between these two limits of ρE there is a transition phase with moderate degradation rate. In contrast, when masonry properties dominate URM-FRP shear behavior, the degradation rate of ζ is very slow.
- Triantafillou's original model estimated F_{FRP} higher than the proposed analytical model. The high difference between Triantafillou's model and the proposed model is expected since Triantafillou original model does not take into considerations the difference between two cases; wrapped retrofitting and unwrapped retrofitting. The stresses in the former case are generally higher than the later case. For all material properties examined here using the proposed model no FRP fracture happened.
- With few exceptions, until ρE of 0.19 GPa, AC125 estimated F_{FRP} close to the average of F_{FRP} estimated using different material properties. However, for ρE greater than 0.19 GPa the comparison between F_{FRP} estimated by AC125 [IC 01] and the proposed model seems difficult since the AC125 assumes a constant axial strain in the FRP. This concept of constant axial strain in FRP was possible in the past when the exiting FRP layers has a low amount of fiber (i.e. low axial rigidity); in the present where new fibers and products with higher Young's modulus and higher amount of fiber exist modern code should adapt the concepts of variable strain in FRP.
- Triantafillou and Antonopoulos [TA 00] model estimate approximately F_{FRP} close to the average F_{FRP} estimated by the analytical model with different material properties.

- By increasing epoxy allowable shear stress the FRP contribution to lateral resistance of URM-FRP increases. However, the increment in the F_{FRP} is approximately linear till a $(\rho E)_{optimum}$. Increasing ρE beyond $(\rho E)_{optimum}$ has less significant effect on F_{FRP}. This optimum value of ρE is not a constant value but depends on the material properties.
- There is interaction between masonry lateral resistance (F_m) and in-plane lateral resistance of URM-FRP (F). Using equation 5.1 (i.e. adding masonry lateral resistance to FRP contribution) is only correct until certain limits. Beyond these limits, this equation is no more valid. It is proposed that beyond a certain limits $(\rho E)_{limit}$ there is a reduction in the lateral resistance of URM-FRP. This reduction in lateral resistance is due to the following: beyond $(\rho E)_{limit}$ URM-FRP reaches the limit on epoxy stiffness degradation too early before masonry reaches its allowable shear stress.
- There is a threshold with respect to the axial rigidity of the FRP beyond which no increase in shear gain is expected. Such a threshold can be used as a criterion for a cost effective design. So and in order to have a cost effective safe URM-FRP, it is proposed to use a value of 0.19 GPa as limit on (ρE). This value satisfied $(\rho E)_{optimum}$ and $(\rho E)_{limit}$ in all the cases studied here.
- The parameters related to the properties of FRP are not the only parameters having a significant influence on the shear behavior of URM-FRP. The epoxy and masonry properties also have influence on the shear behavior of URM-FRP.
- Experimental data, in particular strains undergone by both the FRP and the epoxy, are essential for understanding the resistance mechanisms involved.
- The convergence of the sine series solution is very slow and a large amount of terms should be used. The higher the ρE the higher the divergence.
- For low reinforcement ratio, the proposed analytical model predicts F_{FRP} very close to AC125. In general the proposed model predicts approximately 83% of the values proposed by AC125.
- For the tested specimens, the proposed model predicts F_{FRP} approximately (60-92%) of Triantafillou and Antonopoulos model with average of 70%.
- For the tested specimens, the proposed model predicts F_{FRP} approximately (42-122%) of AC125 model with average of 81%.
- For the tested specimens, the proposed model predicts F_{FRP} approximately (18-34%) of Triantafillou model with average of 25%. However, it should be kept in mind Triantafillou's model shortcomings (§ 5.1.1).
- The proposed model predicts lateral resistance of the test specimens ranged from 61 to 143% of the measured lateral resistance. No specimen failed in shear during the experimental program.
- Triantafillou, Triantafillou and Antonopoulos, AC125 models predict lateral resistance approximately (173-338%), (79-160%), and (97-171%), respectively, of measured lateral resistance.

5.12 Conclusions

The proposed model represents the first analytical model which is originally developed for in-plane analysis of URM walls retrofitted using FRP (URM-FRP). The proposed model has the following advantages over existing models:

- It is the first analytical model originally developed for analysis of URM-FRP; it is based on theory of elasticity without empirical factors. This makes the model has a potential capability for future development and refinement. This is not the case for existing empirical models which suffer well known disadvantages of empirical equations (e.g. it is correct only within certain experimental conditions).
- For the first time in analysis of URM-FRP and using simple model, effects of epoxy ductility and masonry ductility have been studied. Such development of great interest for material producer.
- For the first time in analysis of URM-FRP, the interaction between masonry lateral resistance and FRP contribution to lateral resistance of URM-FRP has been reported, explained, and quantitatively determined. This phenomenon originally observed for RC beams retrofitted using FRP; however, no explanation or quantification exists for such phenomenon in case of RC beams.

- The model overcomes the main disadvantage of AC125 of using constant value for axial strain in FRP. The model estimates axial strain in FRP similar to the empirical function of Triantafillou [Tr 98]; in addition, it overcomes most of the shortcomings of Triantafillou's model (§ 5.1.1). However; more experimental calibration is required.

The results show that the axial strains in FRP are inversely proportional to FRP axial rigidity as correctly proposed by Triantafillou [Tr 98]. Since FRP can be considered as elastic linear material, the FRP contribution to lateral resistance FFRP can also considered inversely proportional to axial rigidity ρE. However, it is not possible to have a single function to represent the relation between ρE and F_{FRP}. The relation between the two quantities depends on several factors (e.g. allowable shear stresses in epoxy and masonry). Hence, any relation based only on empirical calibrations with experimental data without taking into considerations the effect of different material parameters will result in sort of "average" of F_{FRP} due to these different parameters. This average function, by its nature, overestimates F_{FRP} in some cases and in other cases underestimates F_{FRP}. However, after high values of ρE (approximately 1.12 GPa) it is possible to use a single function to describe the relation between ρE and FRP axial strain. Since for all material properties the degradation rate in axial strain was approximately the same and parallel to the second part of Triantafillou empirical equation.

The relation between axial forces in FRP (F_{FRP}) and FRP axial rigidity ρE should take into considerations allowable shear stresses in masonry, epoxy, and FRP as well as masonry and epoxy ductility. The results show the following:

- The higher the allowable shear stresses in epoxy are, the higher F and F_{FRP}; the increment in epoxy allowable shear stresses could be achieved by the development of new materials or by using mechanical anchorage system at the boundaries. As expected, the effect of such mechanical anchorage system is higher for high values of ρE.
- The lower the allowable shear stresses in masonry are, the lower F_{FRP} and the higher gain. Regarding ductility, the higher the epoxy ductility is the lower degradation rate in ζ. However, the effect of epoxy ductility on F_{FRP} and F for lower values of ρE is insignificance. For higher values of ρE there is a significant effect of epoxy ductility. This shows that for industrial companies in addition to developing FRP with higher density of FRP and higher Young's modulus, the development of ductile epoxy is an urgent need.
- Regarding masonry ductility, the results show that masonry ductility plays essential role in determining F and F_{FRP}. The model shows that there should be large masonry deformations and cracking to mobilize axial strains in FRP. However, for high values of ρE there is no effect of masonry ductility. This important conclusion means that for URM walls where cracking is not allowed, one should either use FRP with high axial rigidity to have effective retrofitting or not use FRP at all.

As mentioned, the proposed model quantifies the relation between F_m and F_{FRP}. The results show that adding F_m to F_{FRP} is only valid until certain limits after these limits any additional increment in FRP has no effect. In other words, there is a threshold with respect to the axial rigidity of the FRP beyond which no increase in shear gain is expected. Such a threshold can be used as a criterion for a cost effective design. Again such limits on ρE is not constant it depends on materials allowable stresses and ductility. However, a value of 0.19 GPa can be proposed as a limit on ρE which covers the practical values of material properties.

This research shows that much information is needed to refine characterizations of the material which used in URM-FRP system (i.e. masonry, epoxy, FRP). Yet, with the proposed model, which implicitly describes how URM-FRP behaves due to in-plane loading, much of the needed development is now placed in the proper perspective. For example, the unexpected high lateral resistance of the specimen where only vertical reinforcement is used (i.e. no horizontal reinforcements) suggest several questions about behavior of such retrofitted wall. One of possible explanations is that the vertical reinforcement reduced the crack opening of the retrofitted wall this led to a longer "uncracked" section allowed higher shear to transfer through this section. Another explanation is that, the calculated shear resistance of URM is much higher than the calculated values. Finally, there should be effect of dowel action and epoxy impregnation.

6 FLEXURAL BEHAVIOR

The shear behavior of URM walls retrofitted using FRP has been discussed in the previous chapter. In this chapter the flexural behavior of masonry walls retrofitted using FRP is addressed. The chapter starts with the calculation of the lateral resistance of the specimens, which failed in flexure; the calculations employed the linear elastic approach with the well-known assumptions of Navier-Bernoulli i.e. similar to the one usually done for design of a flexural section in RC elements. Then, the results are calibrated with the experimental results. Discussions about the dominante mode of failure for the tested specimens are presented. This section is followed by discussion about specimens' backbone curves and ductility in lights of definitions given in FEMA 356 [FE 00].

6.1 Flexural Design

A common method to calculate the flexural capacity of structural elements is the use of linear elastic approach. It is an easy method and intended to incorporate a realistic behavior of a structural element by assuming that it behaves linearly up to failure. In case of URM-FRP, this assumption is justified by the observed behavior of the tested specimens. The complete derivation of the mathematical equations is given in this section (equations 6.1 to 6.11); the derivation is based on the following assumptions:

- Plane section remains plane before and after deformations.
- Only rocking mode of failure is considered.
- Full composite action between composite material and the brick surface is assumed. Debonding of the composite material is avoided by choosing appropriate dimensions for composite and good anchorage system.
- Tensile strength in brick and adhesive is neglected; this means that all tensile stresses in the wall section are resisted by composite materials only.
- Masonry ultimate compressive strain is 0.0035, while the ultimate tensile strain in glass fiber is 0.03 for fabric glass, 0.04 for grid glass, and 0.028 for aramid woven.
- The effect of the thickness of the composite material has been ignored to simplify the design equations.
- Compressive force in the masonry is determined from Whitney's equivalent stress block

According to the notation in Figure 6.1, the following equations may be derived:

$$T - C = -N \tag{6.1}$$

$$T = 0.5(\rho_f lt)E_f \varepsilon \tag{6.2}$$

$$C = f_k ta \tag{6.3}$$

$$\rho_f = \frac{A_f}{Lt} = \frac{A_f}{A} \tag{6.4}$$

Where

T = tension force in the fiber,
C = compression force in the masonry,
f_f = fiber ultimate tensile strength,
f_k = ultimate masonry compressive strength,
ε = axial tensile strain in the fiber at the specimen edge computed based on linear variation of strains in the cross section,
E_f = fiber tensile modulus of elasticity,
A_f = fiber cross sectional area,
A = cross sectional area of the specimen,
L = wall length

x = compression zone length
l = cracking length

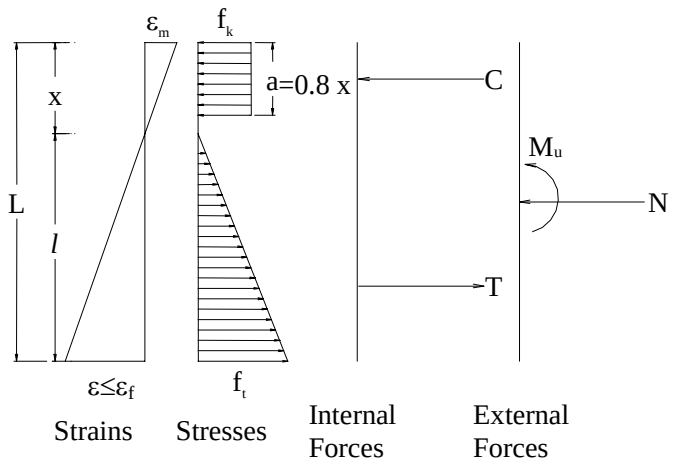

Figure 6.1: Strain, stresses, internal, and external forces in retrofitted masonry specimen

By substituting equations 6.2 to 6.4 into equation 6.1 and dividing by specimen cross sectional area and masonry ultimate compressive strength, this yield:

$$0.5\omega\left(\frac{l}{x}\right)\left(\frac{l}{L}\right) - 0.8\left(\frac{x}{L}\right) = \eta \tag{6.5}$$

$$\omega = \rho_f E_f \frac{\varepsilon_m}{f_k} \tag{6.6}$$

$$\eta = \frac{-N}{f_k A} \tag{6.7}$$

t = specimen thickness,
x = compression zone length,
ε_m = ultimate masonry strain,
M_u = ultimate moment of resistance.
ω = mechanical reinforcement ratio
η = normalized compressive strength

Solving equation 6.5 for x yields:

$$x = L\left(\frac{-(\eta+\omega)+\sqrt{\eta(\eta+2.0\omega)+1.6\omega}}{(1.6-\omega)}\right) \tag{6.8}$$

For low normal forces ($\eta \le 0.1$) and low mechanical ratio ($\omega \le 0.25$), the previous equation can be simplified [EL 03]; by neglecting $\omega\eta$ and ω^2 as well as ω in the denominator, this yields:

$$x = \frac{L}{1.6}\left(-\eta-\omega+\sqrt{1.6\omega}\right) \tag{6.9}$$

The difference between the simplified equation and the original equation is approximately less than 5%.
To avoid premature FRP fracture, the reinforced section should be over-reinforced or $\omega > \omega_{lim}$ [EL 03] where

$$\omega_{lim} = 2\left(\eta + 0.8\frac{\varepsilon_m}{\varepsilon_m+\varepsilon_f}\right)\left(1+\frac{\varepsilon_m}{\varepsilon_f}\right)\left(\frac{\varepsilon_m}{\varepsilon_f}\right) \tag{6.10}$$

The ultimate moment of resistance M_u is given by:

$$\frac{M_u}{f_k A} = 0.8x(0.5 - 0.4\frac{x}{L}) + 0.5\omega\frac{(L-x)^2}{x}(0.5 - \frac{L-x}{3L}) \quad (6.11)$$

This method is used to calculate the lateral resistances of the full surface retrofitted specimens (i.e. S1-WRAP-G-F and S2-WRAP-A-F, L1-WRAP-G-F, L2-GRID-G-F, S2-WRAP-G-F-ST, S2-WIRE-S-F-ST, M2-WRAP-G-F-ST, M2-2WRAP-G-F-ST, and M2-WRAP-A-F-ST). Note that, specimens S1-WRAP-G-F and S2-WRAP-A-F did not reach their ultimate resistance due to force limitations on the hydraulic jack of the earthquake simulator. The calculations were made based on FRP nominal material characteristics.

Tables 6.1 and 6.2 summarize the results for dynamic and static cyclic tests, respectively. As shown in the tables and excluding specimens S1-WRAP-G-F and S2-WRAP-A-F, the measured (experimental) lateral resistance ranged from 0.72 to 1.36 times the calculated lateral resistance. Note that, the main differences between these specimens are aspect ratio and reinforcement ratio. One should expect that, with reducing specimen aspect ratio the shear effect will increase. In addition, as shown in Chapter 5 with increasing reinforcement ratio the stresses in FRP reduce. Taking into considerations these two comments and care examination of the test results show that the ratio experimental/estimated lateral resistance is proportional to square of effective moment to shear ratio (i.e. aspect ratio) and mechanical reinforcement ratio (ω, see equation 6.6). Figure 6.2 shows the comparison between $\alpha^2\omega$ and the ratio experimental/estimated lateral resistance. Specimens which tested in the dynamic tests are separated from those tested during the static cyclic test. In addition, only two specimens failed in flexural during the dynamic tests while the other two did not reach their ultimate lateral resistance. For static cyclic, there are five specimens failed in flexural; of them, there was specimen which retrofitted using vertical reinforcement only and another one its results was affected by the sever damage in specimen before the test (see Chapter 3). For the rest of the five specimens (i.e. for three specimens) a regression analysis is carried out. Finally the figure shows the following notes:

- In case of static cyclic, linear elastic approach with stress block approximation overestimate the lateral resistance of the tested specimens. As mentioned this overestimations increased for specimens with low aspect ratio due to high shear effect. Also, increasing reinforcement mechanical ratio reduces axial stresses in FRP due to shear effect (see Chapter 5). The results suggested that the calculated lateral resistance using this method should be multiplied by a correlation factor of ($4.9\ \alpha^2\omega + 0.75 \leq 1$) to be a design value for lateral resistance, which should be divided by appropriate code reduction factors. It should be noted that this regression is carried out only on three specimens more experimental work is required before applying such factors.
- It seems that specimens that tested during the dynamic tests have lateral resistance greater than the estimated lateral resistance. In particular, the specimens which failed during the tests have lateral resistance approximately 1.3 times the estimated lateral resistance. For the other two specimens, though it is difficult to judge the behavior of S1-WRAP-G-F and S2-WRAP-A-F, it seems that specimen S1-WRAP-G-F (the first to left in the figure) was near rupture while specimen S2-WRAP-A-F was very far from rupture. Note that, during the test [EL 03] there were several delaminations in S1-WRAP-G-F at the test end while no such events happened in the second specimen. This higher resistance possible due in part to that masonry resistance increased during dynamic tests. In addition, there are uncertainties regarding FRP properties: during the dynamic tests the maximum axial strain measured in the grid GFRP was 2.5% also a value of 2.6% was measured during coupon tests, note that the ultimate strain in the grid is approximately 4%.

Table 6.1: Summary of flexural assessment of URM-FRP for dynamic tests

Parameters	S1-WRAP-G-F	S2-WRAP-A-F	L1-WRAP-G-F	L2-GRID-G-F
ρ [%]	0.072	0.189	0.072	0.068
ω [-]	0.029	0.140	0.029	0.036
η [-]	-0.060	-0.076	-0.1399	-0.098
X [mm]	246	422	354	311
M_u [kN.m]	76.55	105.4	93.3	71.24
F [kN]	80.7	113.5	45.3	34.9
$F_{(measured)}$ [kN]	74.1*	72.0*	57.3	47.5
$F_{(measured)}$/ F	0.91*	0.63*	1.26	1.36

* Earthquake simulator maximum force capacity

Table 6.2: Summary of flexural assessment of URM-FRP for static cyclic tests

Parameters	S2-WRAP-G-F-ST	S2-WIRE-S-F-ST	M2-WRAP-G-F-ST	M2-2WRAP-G-F-ST	M2-WRAP-A-F-ST
ρ [%]	0.072	0.083	0.072	0.140	0.280
ω [-]	0.0369	0.1266	0.0369	0.074	0.206
η [-]	-0.0753	-0.0753	-0.0753	0.0753	-0.075
X [mm]	282	407.5	282	346	473
M_u [kN.m]	67.48	101.36	64.48	84.77	118.76
F [kN]	71.3	109.0	88.7	112.6	159.9
$F_{(measured)}$ [kN]	50.8	83.9	69.7	95.2	160.4
$F_{(measured)}$/ F	0.72	0.77	0.79	0.84	1.00

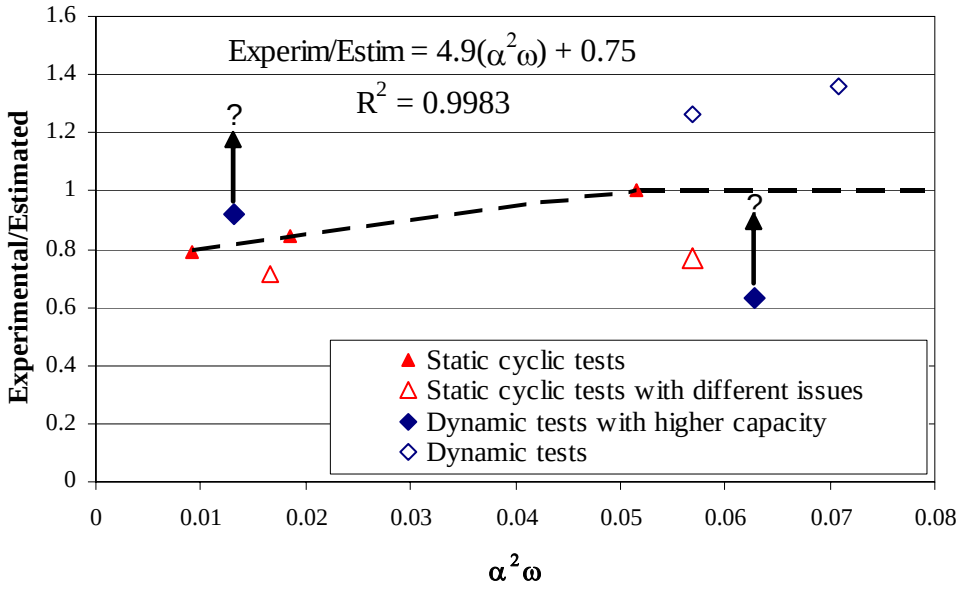

Figure 6.2: Experimental/estimated lateral resistance in terms of the square of effective aspect ratio times mechanical reinforcement ratio

6.2 Comparison between Shear and Flexural Capacity of Retrofitted URM-FRP

As presented in Chapter 5 the shear resistance of each specimen was calculated. In addition, the flexural resistance of the test specimens was calculated in this chapter. Comparisons between shear and flexural capacities as well as experimental lateral resistance are presented in Table 6.3. The table shows that for all the test specimens, except S2-WRAP-G-F-ST, the dominate mode of failure should be shear failure. However, in several cases the difference between the lateral resistances due to the two modes is within 10% making it difficult to accurately estimate which of the two modes will dominate the behavior. During the tests, as explained in Chapters 3 and 4, all the specimens failed due to flexural failure. As explained in the previous chapter, the resistance of URM itself under shear force is difficult to estimate correctly as well as the effect of the vertical reinforcement does not taken into considerations this led the proposed shear model to be conservative and in no case it overestimates the shear resistance of URM-FRP. Note that, the low shear resistance of specimen M2-WRAP-A-F-ST due in part to the high ductility of the masonry layer during testing this specimen (see Chapter 5). The underestimation of the model should be quantified with future development; however, overestimation of shear failure could results in a brittle mode of failure during an earthquake event.

Table 6.3: Estimated flexural, shear and experimental lateral resistance

Specimen	Shear resistance	Flexural resistance	Experimental
S1-WRAP-G-F	**73.4**	80.7	74.1
S2-WRAP-A-F	**99.7**	113.5	72.0
S2-WRAP-G-F-ST	73.4	**71.3**	50.8
S2-WIRE-S-F-ST	**69.9**	109.0	83.9
M2-WRAP-G-F-ST	**77.9**	88.7	69.7
M2-2WRAP-G-F-ST	**89.7**	112.6	95.2
M2-WRAP-A-F-ST	**103.7**	159.9	160.4

6.3 Performance Levels

In the previous section the flexural resistance of the tested specimens was evaluated. In this section the flexural behavior of the specimens is evaluated using the concept of performance levels, which proposed in FEMA 356 [FE 00].

6.3.1 Overview of performance levels according to FEMA 356

The leading document available today to guide civil engineers on the seismic retrofitting of existing buildings is FEMA 356 [FE 00]. FEMA 356 employs single shear spring to capture the response of individual piers in an URM wall. To calculate the story response of a wall, the displacements of each pier spring (within a story) are assumed to be equal and the resistances of these springs are added together. The response of the entire wall along the building height is then determined by combining the response of each story as springs in series [Mo 04].

FEMA allows the use of the previous model in conjunction with both linear static and nonlinear static (i.e. pushover) analysis. For linear static analysis, each spring's stiffness is taken as the elastic stiffness of the corresponding pier. For nonlinear static analysis, each spring is defined by a nonlinear force-displacement curve based on the governing failure mode. FEMA classified failure modes for any structural component into deformation-controlled modes and force-controlled modes. In the former case, the component could resist large inelastic deformations without a significant loss of its lateral resistance. The lateral resistance can be determined based on excepted masonry properties. In the later case, the ultimate failure can be abrupt with little or no subsequent deformations; in this case the lateral resistance of the specimen should be determined based on lower bound masonry properties. More details about expected and lower bound masonry properties are explained in Chapter 7 of the guidelines. Note that FEMA 356 does not permit the nonlinear static analysis procedure to be used if force-controlled failure modes govern the response of any pier within a certain wall.

FEMA 356 defines three general component behavior curves for general material performance in cyclic loading typical in earthquake developed from hysteretic backbone curves. The Type 1 curve is representative of typical ductile behavior and the Type 3 curve represents a brittle or nonductile failure behavior. Type 2 is a system between Type 1 and Type 3 that does not exhibit classic ductile behavior but does provide the ability to sustain loads after cracking. Figure 6.3 represents a general backbone curve for the three curve types where Q_y is the component expected "apparent" yield strength with corresponding "apparent" yield displacement or drift (g). Point 2 in the curves corresponds to component expected lateral resistance with corresponding displacement or drift (e). Finally, point 3 in the "shoulder" of Type 1 curve represents lateral resistance degradation. For nonstructural masonry walls, deterioration in the lateral resistance as high as 40% is accepted. In addition, primary components exhibiting backbone curves similar to Type 1 or 2 are classified as deformation-controlled if e is greater than or equal to twice g; otherwise, they shall be classified as force controlled.

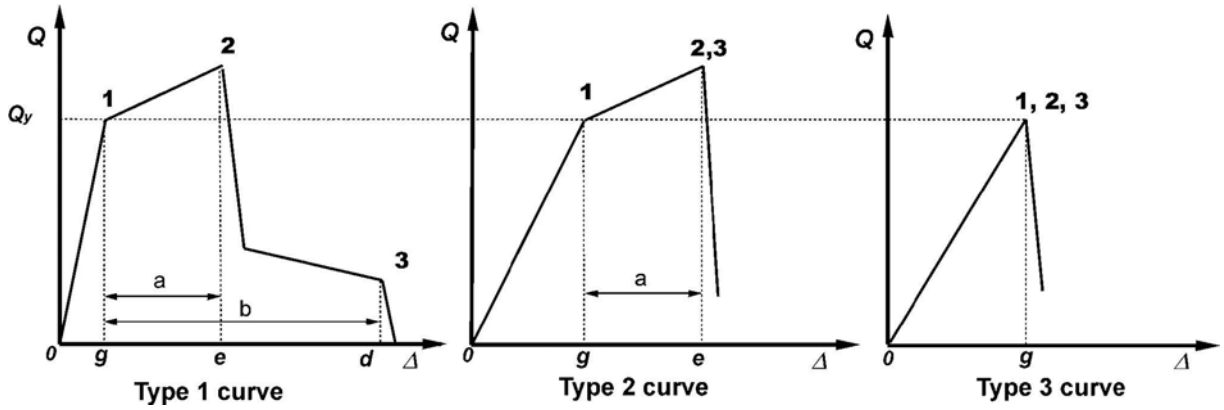

Figure 6.3: Component force vs. deformation curves [FE 00]

According to FEMA 356, the acceptance criterion for a structural component depends on mode of failure and analysis procedure. In general, the force capacity of force-controlled components should be less than or equal to the demand on this component. In case of deformation-controlled components, there are the following two cases:

- Linear analysis in which the force capacity of the component multiplied by a modifier factor m (greater than or equal to 1) should be less than or equal to the demand on this component. The factor m depends on component performance levels, which are based largely on the amount of damage that would be incurred.
- Nonlinear analysis in which the pier drifts shall not exceed certain values, given by FEMA 356, corresponding to different performance levels.

Three performance levels are defined and used as discrete points to guide a retrofitting design based on the expected performance of a building. Performance levels are based on the amount of damage to both structural and nonstructural elements. The damage to a building component is often considered to be a function of its lateral displacement or drift. Numerical coefficients relating drifts to damage were deduced from laboratory tests available at the time. The three defined levels are collapse prevention, life safety, and immediate occupation. Regarding retrofitted masonry, Franklin et al. [FL 01] defined these levels as following:

- Collapse prevention (CP): extensive cracks, dislodgement of units, noticeable offsets
- Life safety (LS): extensive cracks, no dislodgment of units, significant reserve capacity
- Immediate occupation (IO): minor crack

For an experimental program FEMA 356 (section 2.8.3) gives the following definition for these three performance levels:

- Collapse prevention (CP): the deformation at point 2 on the curves but not greater than 0.75 times the deformation at point 3
- Life safety (LS): 0.75 times the deformation at point 2 on the curves
- Immediate occupation (IO): the deformation at which permanent, visible damage occurred in the experiments but not greater than 0.67 times the deformation limits for LS

6.3.2 Performance levels for compression failure

As explain earlier FEMA 356 classified failure modes as force controlled or displacement controlled; regarding URM walls, rocking and sliding are classified as deformation-controlled modes of failure while toe crushing and diagonal tension are classified as force-controlled modes of failure. However, past experimental studies show that either rocking or flexural cracking always precedes toe crushing; hence, Moon [Mo 2004] combined the rocking and toe crushing failure modes into a single failure mode. This single failure mode is proposed to be treated as displacement-controlled mode of failure.

For URM walls retrofitted using FRP, URM-FRP, FEMA 356 does not explicitly address the behavior of such elements. Although, if FRP overlays are assumed to fall within the general category of external coatings, then FEMA 356 recommends that the retrofitted wall behaves as a composite section as long as adequate anchorage is provided. However, Franklin et al. [FL 01] show that using composite section for URM-FRP overestimated

many times the initial stiffness, and lateral resistance of URM-FRP. So, more research is required to formulate guidelines for URM-FRP.

For the tested specimens which failed due to masonry compressive crushing, the backbone, multi linear, and composite curves are presented in Figures 6.4 to 6.10. The curves are produced according to the procedure described in Chapters 2, 3, and 7 of the guidelines. The backbone curves indicate that the general component behavior of the retrofitted specimens remained at FEMA Type 2 performance curve. In addition, the ratio of e/g as defines in Figure 6.3 ranged from 2.4 to 6.9 i.e. in no case it was less than 2. This suggests that for URM-FRP which fails due to masonry compression failure under in-plane loading can be treated as displacement-controlled components.

In addition, the different performance levels of each specimen are presented on the composite curve of each specimen. In lights of the previous definitions for the different performance levels, for the test specimens the following definitions have been used to determine the different performance levels:

- Collapse prevention (CP): the deformation at point 2 for curve Type 2 or point 2' for curve Type 1, where point 2' is defined as the point at which there is a 25% decrease in specimen lateral resistance
- Life safety (LS): the deformation at point 2 for curve Type 2 or the deformation at which the crack propagate 50% of a specimen length or height
- Immediate occupation (IO): the deformation at which permanent, visible damage occurred in the experiments

Table 6.4 shows comparisons between drifts from the experimental program and FEMA 356 at the different performance levels. Comparisons between m-factors from the experimental program and FEMA 356 are also presented in the same table. As shown in the table, drifts estimated using FEMA 356 at the three performance levels are conservative. For example, for immediate occupation performance level, the drifts from the experimental program range from 1.4 to 4.1 times the drift given by FEMA. Regarding m-factor, FEMA is always overestimated this factor at IO performance level. Similar conclusion for URM wall retrofitted using FRP has been reported by Franklin et al. [FL 01]. However, some of these results influenced by the fact that there are specimens that were tested as URM specimens before retrofitted and retested again. This should not affect the reliability of the results since in real situations some cracking could appear in the masonry walls before retrofitting. Regarding m factor at LS and CP performance levels, FEMA estimates m factors between 0.95 to 0.38 times the experimental m factors. Again, similar conclusion for URM wall retrofitted using FRP has been reported by Franklin et al. [FL 01].

Based on these data and comparisons it is recommended to consider masonry compression failure in case of URM-FRP as a deformation-controlled mode of failure its resistance can be calculated as explained in the previous section. The limits given by FEMA 356 seems promising way to estimate both m factor and drift at different performance levels except m factor at IO level. However, these results should be treated carefully and more experimental work is required to verify this assumption since the tested specimens were tested under low normal force. This low normal force helps in creating "low level" rocking before masonry crushing. In addition, in such cases of dominant flexural mode the specimen deformations at its lateral resistance can be calculated as follows: assuming 0.0035 as ultimate strain in masonry and assume that curvature changes linearly along specimen height by integrating this simple curvature twice and use appropriate boundary conditions (no rotations or displacement at the base) the following expression is obtained:

$$\Delta = 95.24 h^2 x \qquad (6.12)$$

For slender walls (aspect ratio of 1.4) this expression estimated approximately 70% of the measured ultimate drift. This value consistent with what is observed during the experimental test that rocking responsible for approximately 83% of lateral displacement [EL 03]. However, as expected in some cases where shear deformation dominates this estimation are far from the measured lateral displacement. More work is required in this area to include shear deformations; however, this point is out of the scope of this research.

Table 6.4: Comparisons between different limits proposed by FEMA 356 and the experimental results

Specimen	Method	Acceptance Criteria			m-factors		
		Performance Level			Performance Level		
		IO [%]	LS [%]	CP [%]	IO	LS	CP
L1-WRAP-G-F	FEMA	0.10	0.42	0.56	2.10	4.20	5.60
	Experimental	0.16	0.67	0.90	0.75	3.14	4.22
L2-GRID-G-F	FEMA	0.10	0.42	0.56	2.10	4.20	5.60
	Experimental	0.14	0.44	1.01	0.75	2.36	5.41
S2-WRAP-G-F-ST	FEMA	0.10	0.20	0.27	1.00	2.00	2.67
	Experimental	0.21	0.25	0.41	2.25	2.68	4.39
S2-WIRE-S-F-ST	FEMA	0.10	0.20	0.27	1.00	2.00	2.67
	Experimental	0.41	1.21	2.79	0.86	2.19	2.79
M2-WRAP-G-F-ST	FEMA	0.10	0.15	0.20	1.00	1.50	2.00
	Experimental	0.21	0.42	0.73	0.75	1.50	2.61
M2-2WRAP-G-F-ST	FEMA	0.10	0.15	0.20	1.00	1.50	2.00
	Experimental	0.17	0.58	0.85	0.75	2.56	3.75
M2-WRAP-A-F-ST	FEMA	0.10	0.15	0.20	1.00	1.50	2.00
	Experimental	0.20	0.88	1.37	0.75	3.30	5.14

6.4 Conclusions

In this chapter the lateral resistance of the tested specimens were calculated using linear elastic approach, the test specimens were treated as RC beam columns. Then, the behaviors of the tested specimens were discussed in terms of the different performance levels given by FEMA 356. The presented analyses show the following:

- Using a procedure similar to the flexural design of RC beam-column and linear elastic approach seems appropriate for the flexural design of URM-FRP. However, to have a more accurate lateral resistance shear effects should be taken into consideration. A factor reflects the shear effect is suggested based on correlation with experimental data.
- Regarding the analysis procedure developed in FEMA 356 for retrofitting, the test results show that the composite curve of the test specimens is similar to curve Type 2 of FEMA 356 with ductility greater than two. This suggests that to treat URM-FRP, which fails due to toe compression failure as a displacement-controlled component rather than a force-controlled component.
- The different performance levels estimated by FEMA 356 for URM-FRP are conservative in terms of drifts; however, in terms of the m factor the immediate occupation level is unconservative and should be modified.

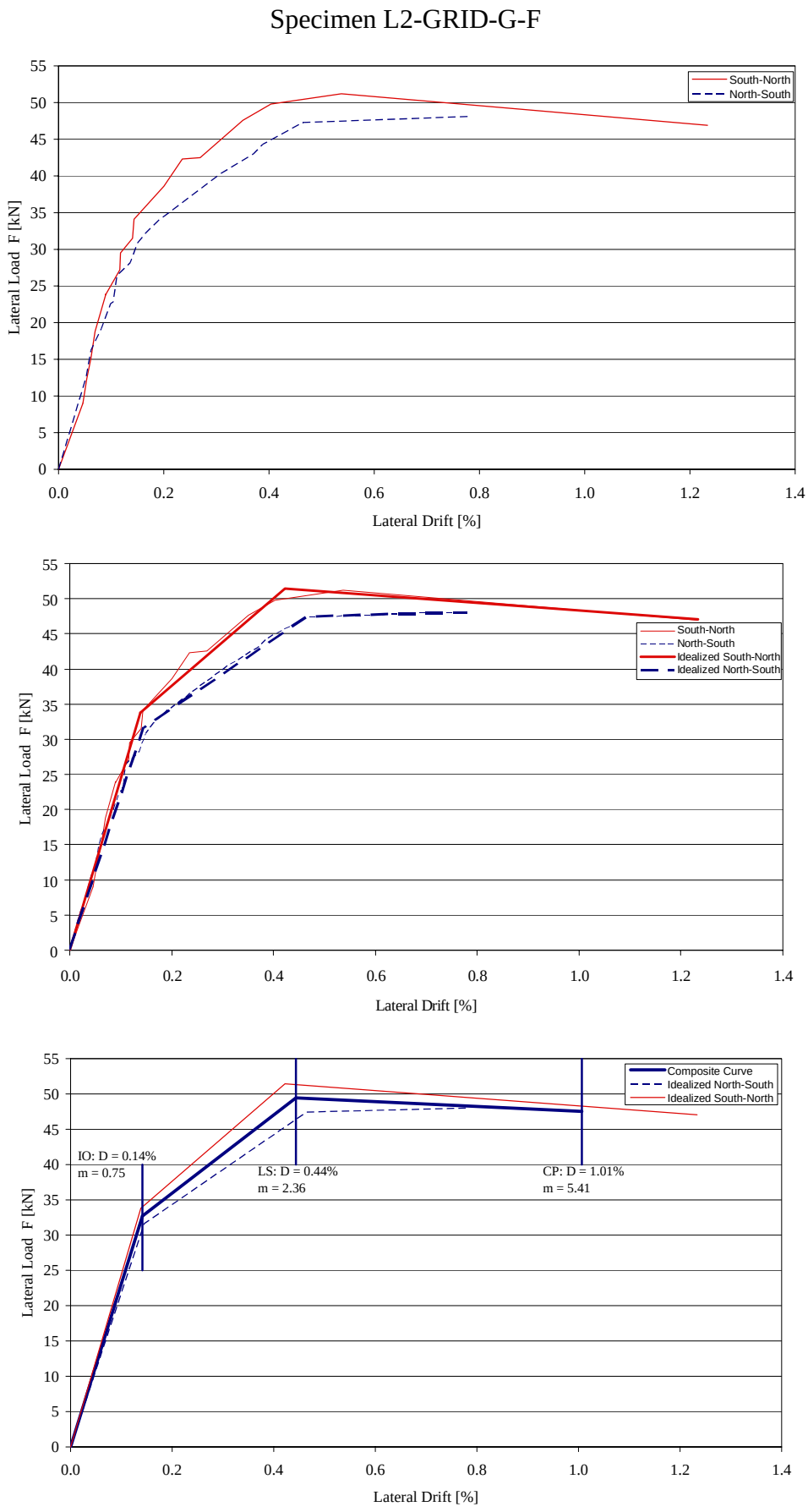

Figure 6.4: Different steps to have performance level acceptance criteria for specimen L2-GRID-G-F

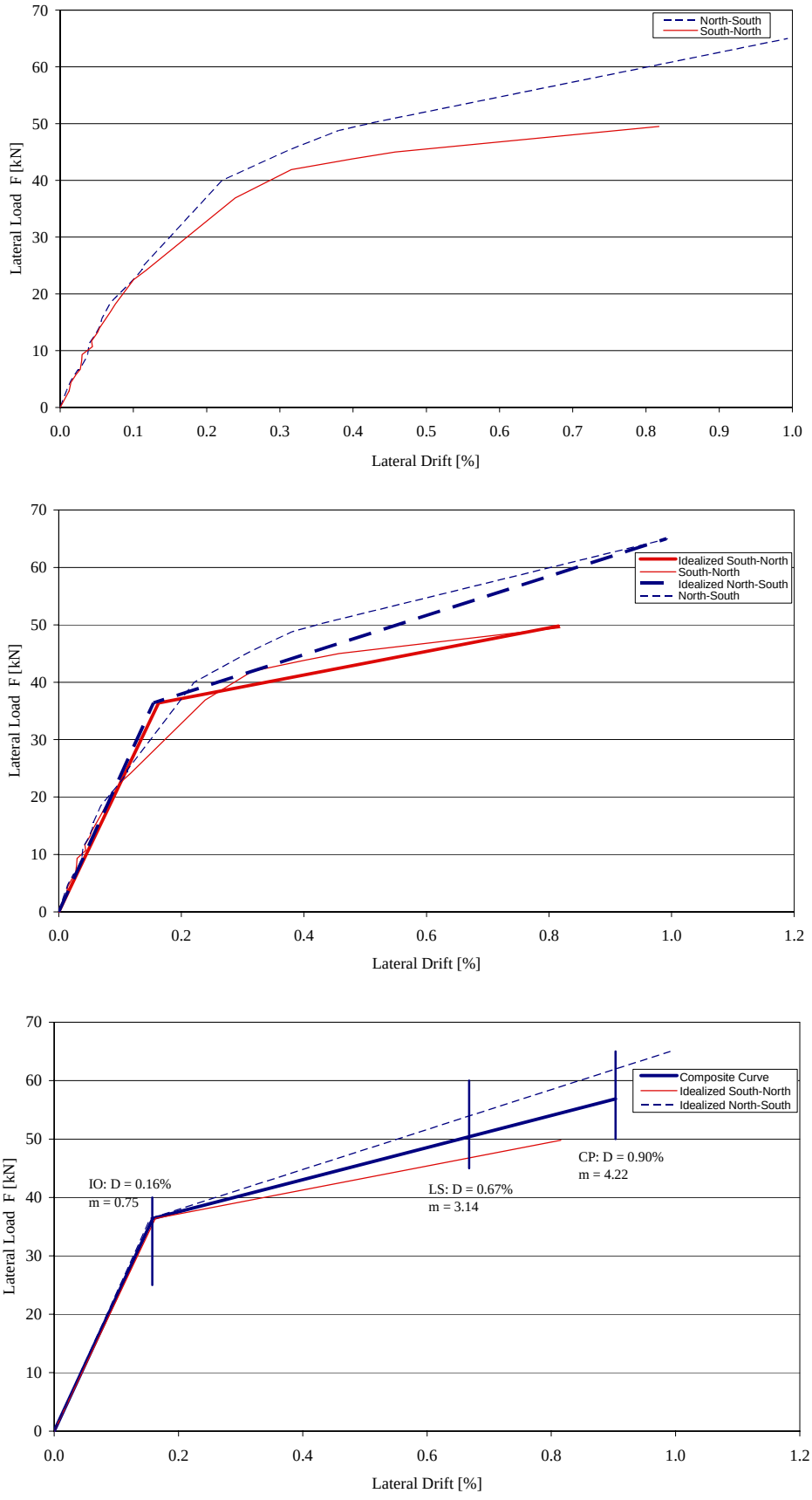

Figure 6.5: Different steps to have performance level acceptance criteria for specimen L1-WRAP-G-F

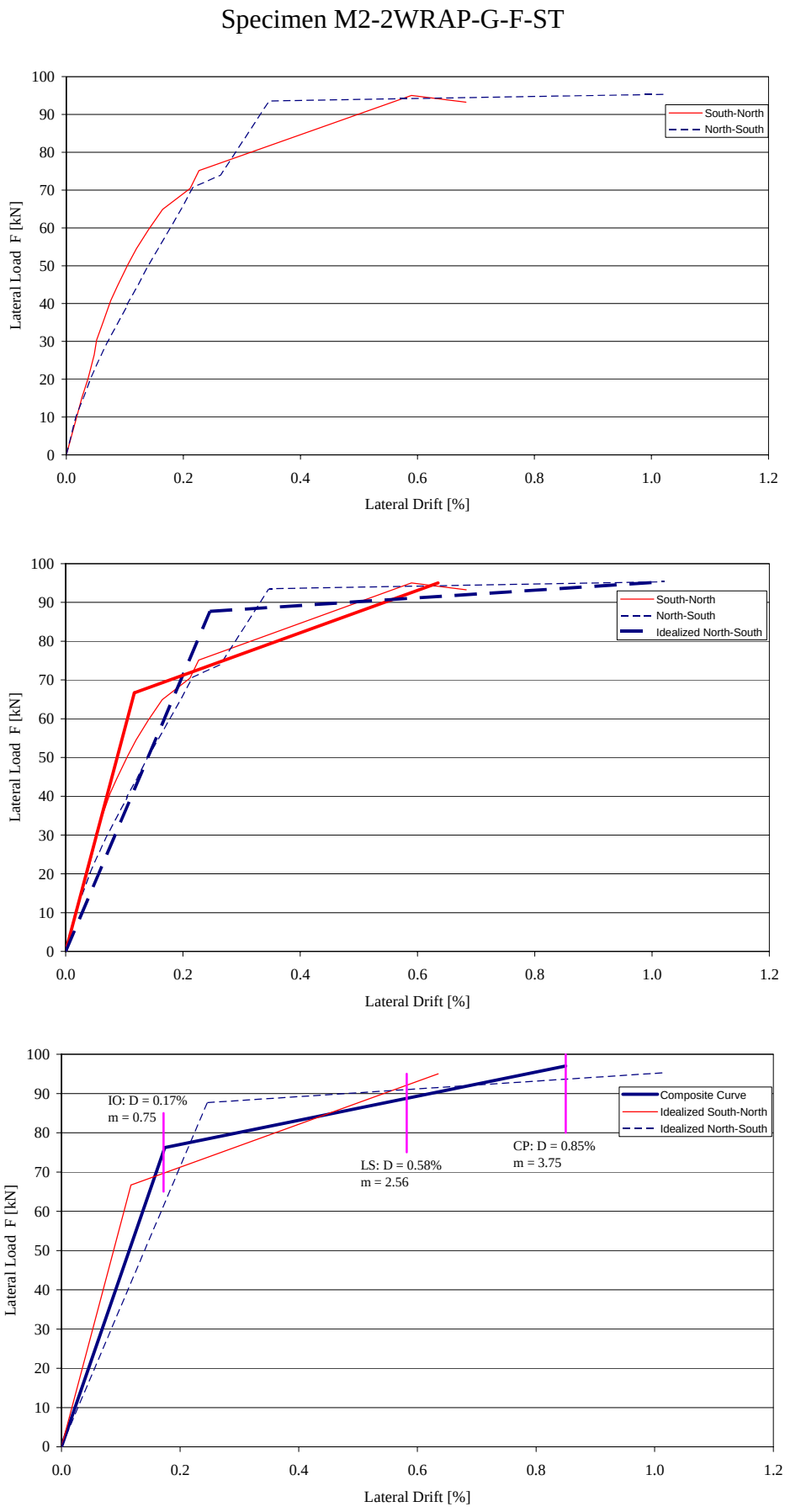

Figure 6.6: Different steps to have performance level acceptance criteria for specimen M2-2WRAP-G-F-ST

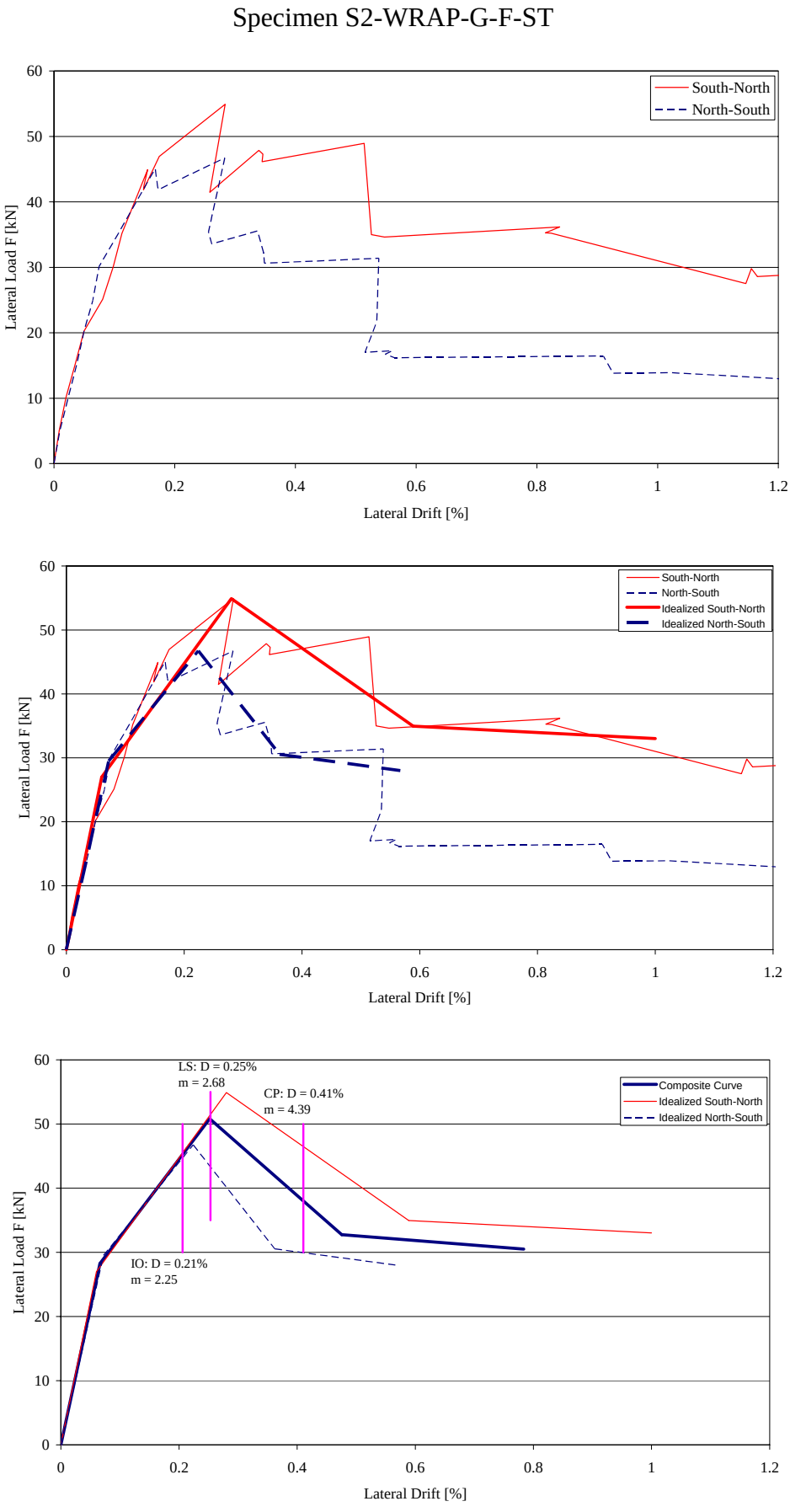

Figure 6.7: Different steps to have performance level acceptance criteria for specimen S2-WRAP-G-F-ST

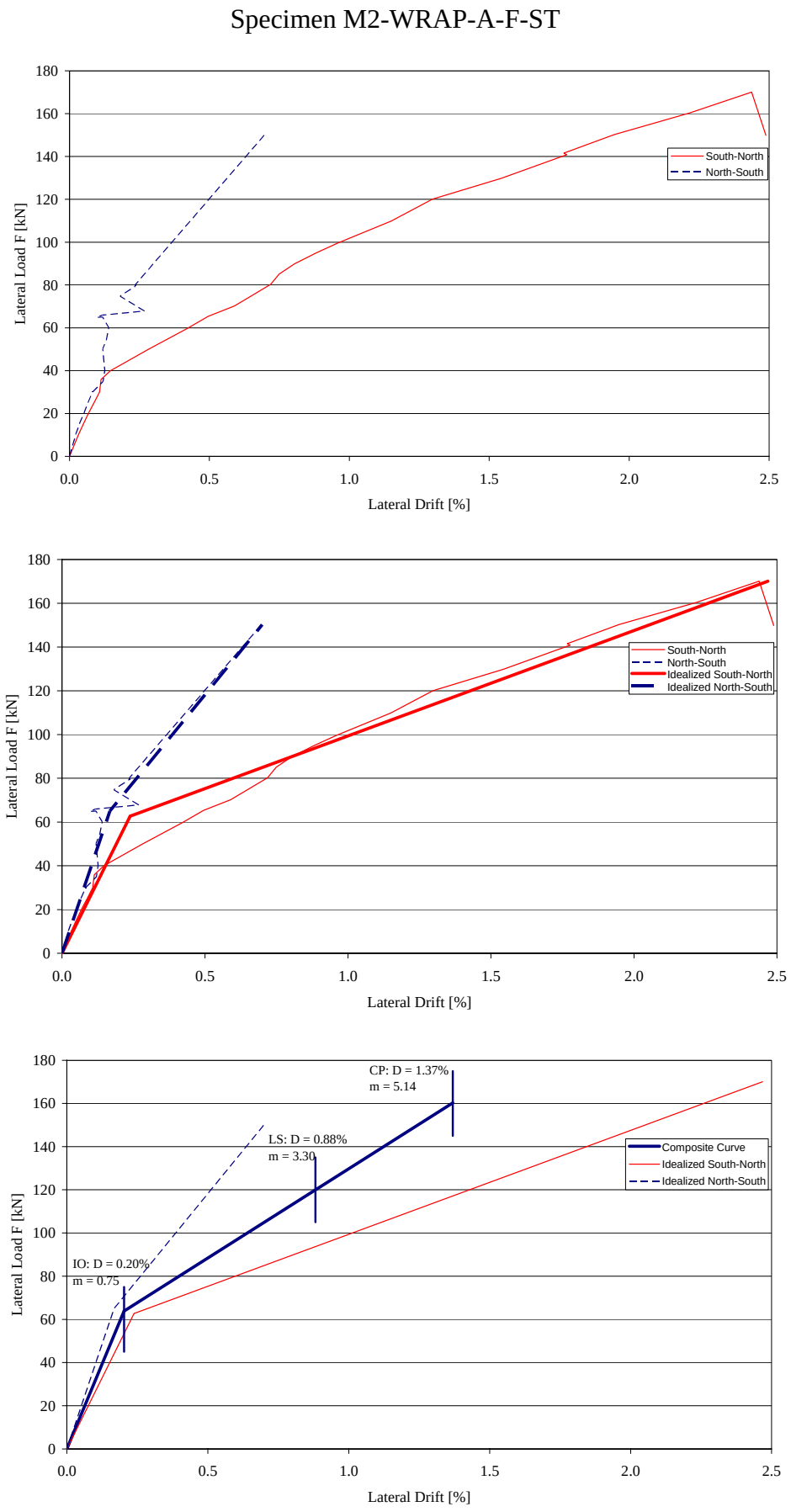

Figure 6.8: Different steps to have performance level acceptance criteria for specimen M2-WRAP-A-F-ST

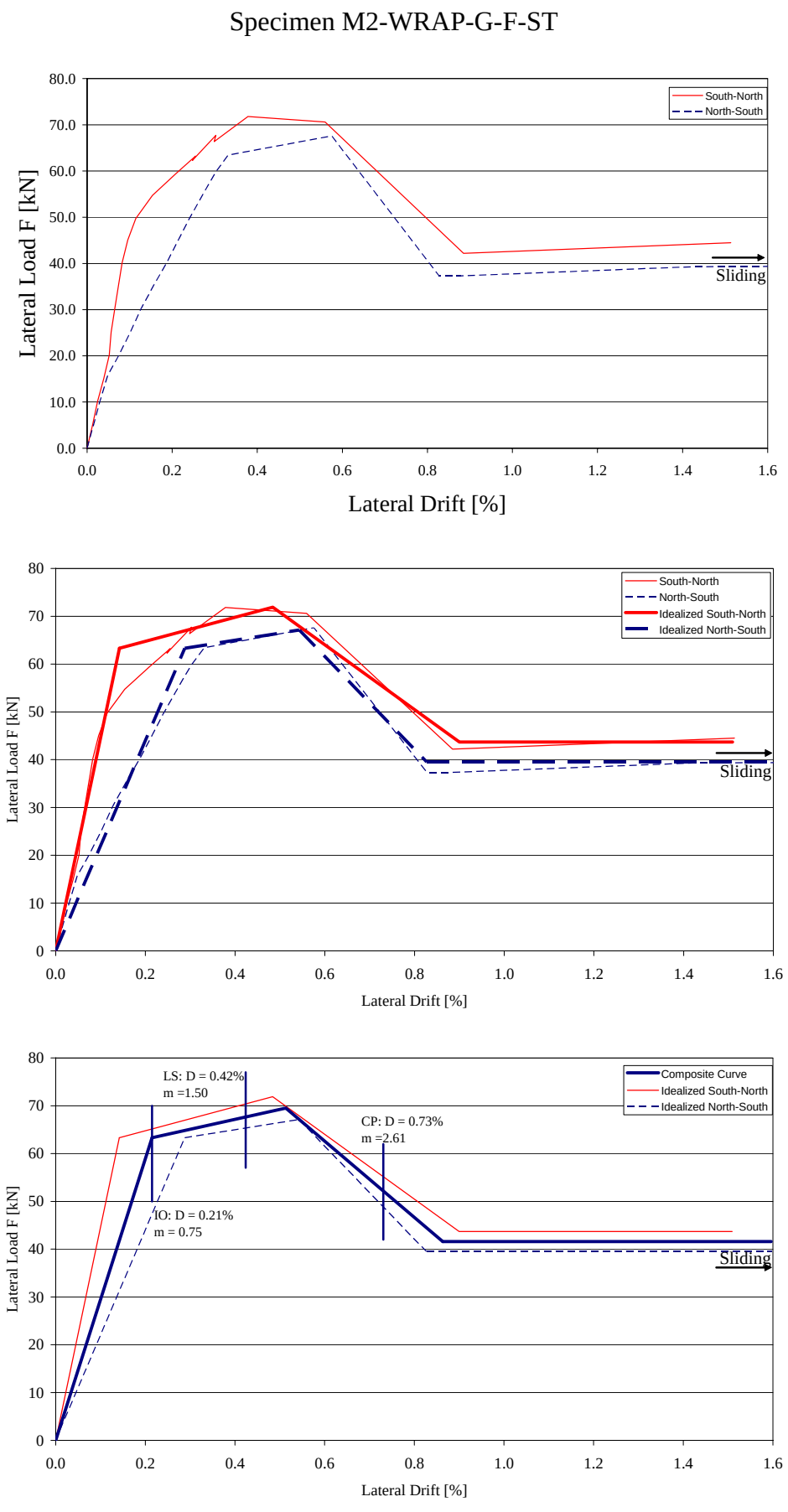

Figure 6.9: Different steps to have performance level acceptance criteria for specimen M2-WRAP-G-F-ST

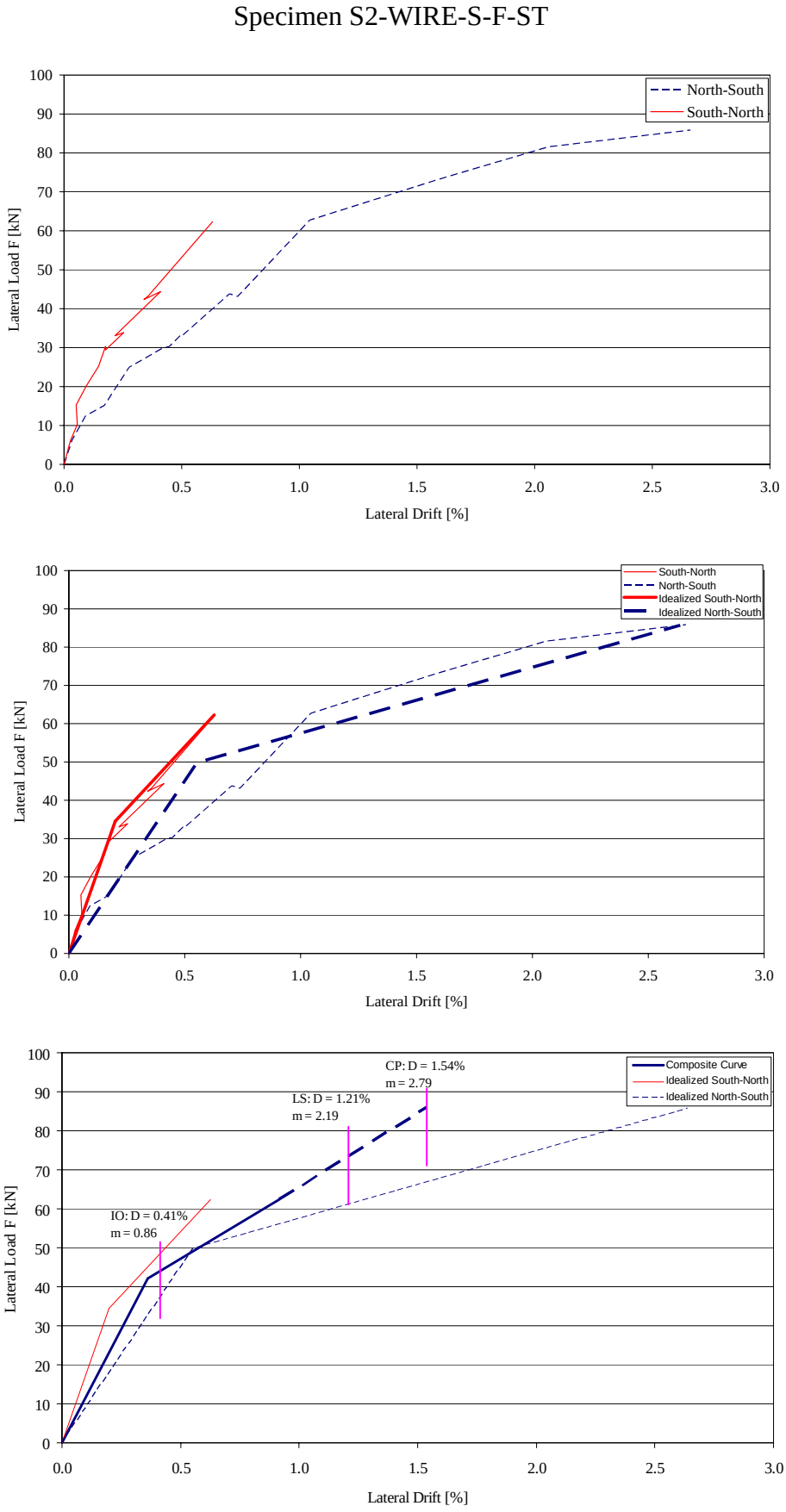

Figure 6.10: Different steps to have performance level acceptance criteria for specimen S2-WIRE-S-F-ST

7 SUMMARY AND CONCLUSIONS

Existing unreinforced masonry (URM) buildings, many of which have historical and cultural importance, constitute a significant portion of buildings stock around the world. Most of these buildings were built with little or no consideration for seismic design requirements. Recent earthquakes have shown that many such buildings are seismically vulnerable; therefore, improving existing methods and developing better methods for retrofitting existing seismically inadequate buildings is pressing. Numerous techniques are available to increase the strength and/or ductility of URM walls. However, there is a reliability issue with some of the commonly used techniques. Modern composite materials offer promising retrofitting possibilities for masonry buildings. This thesis focuses on in-plane behavior of unreinforced masonry walls retrofitted using fiber reinforced plastics (URM-FRP). Both the experimental and analytical aspects of this research are summarized in this chapter with an emphasis on findings and conclusions. This chapter ends with a brief description of the significance of this work as well as several areas where further research is recommended.

7.1 Findings of experimental work

The static cyclic and dynamic experimental testing of 20 masonry wall specimens before and after retrofitting, led to the following general findings.

7.1.1 Findings of dynamic tests

- The retrofitting materials increased the specimens' lateral resistance by a factor of 1.3 to 2.9 compared to the reference (URM) specimens. Expectedly, the ratio is higher for a lower normal force. At high normal force, the retrofitting contribution to the lateral resistance of URM-FRP wall is comparatively less.
- The enhancement in the ultimate drift for the slender retrofitted specimens was small, not exceeding 1.2 times the drift of the reference specimens. Furthermore, the ultimate drifts were independent of the reinforcement ratio and reinforcement type (grid or fabric); however, the ultimate drifts depend on the aspect ratio and the retrofitting configuration.
- Within the scope of testing, single-sided retrofitting appears to produce good behavior. No out-of-plane or uneven response of the specimens was observed. Small asymmetries in the transducers were recorded in the case of squat specimens. However, further dynamic investigations are required for squat specimens in the ultimate range.
- In some specimens there was debonding of the fibers/grids in the form of white spots. This debonding occurred at lateral load levels ranging from 50% to 80% of the ultimate load resistance. The lateral resistance at first delamination depends on the reinforcement ratio and specimen aspect ratio as well as the fiber characteristics.
- The fabric prevented falling of debris from the wall after failure; thus, preventing possible injuries to occupants in the vicinity of the wall in the event of a real earthquake.
- In general, the bi-directional surface type materials (fabrics and grids) applied on the entire surface of the wall (and correctly anchored) can help postpone the three classic failure modes of masonry walls: rocking ("flexural failure"), step cracking and sliding ("shear failures"). In other terms, retrofitting increases more robustness: even if the engineer is not sure of the expected failure mode before/after retrofit, the retrofit potentially adds to security. Additionally, in some situations, they will postpone in-plane collapse by "keeping the bricks together" under large seismic deformations.
- Carbon plates or fabric strips used in a diagonal pattern (X or XX) were less successful. This retrofitting configuration was used in the retrofitting of two specimens and in both cases "premature" failure developed (anchorage once and shear-flexure another). Even if improved retrofitting configuration and reinforcement ratio could have prevented the premature failure, test results indicate that these retrofits are less robust and less redundant.

7.1.2 Findings of static cyclic tests

- The retrofitting materials increased the specimens' lateral resistance by a factor of 1.7 to 5.9 compared to the reference (URM) specimens.
- The GFRP reduce the ultimate drift of the retrofitted specimen by a factor of 0.5. Furthermore, the ultimate drifts were independent of the reinforcement ratio.
- Unlike dynamic tests, no debonding of the fibers in the form of white spots was observed during the static cyclic tests.
- Using a post-tension force of 60 kN as retrofitting approximately doubled the lateral resistance of the reference specimen and was approximately equivalent to using a single layer of GFRP from both lateral resistance and drift point of view.
- Doubling the reinforcement ratio did not produce double the lateral resistance; the lateral resistance in the case of two layers of GFRP was approximately 1.4 times the lateral resistance in the case of a single layer of GFRP.
- Using steel hardwire increased the lateral resistance and drift, with respect to the reference specimen, by a factor of 2.3 and 1.5, respectively. In addition, despite the unidirectional hardwire oriented in the vertical direction only, no shear failure was observed either in the masonry itself or in the hardwire.
- All the retrofitting techniques succeeded in recovering the initial stiffness of the reference specimens.
- The initial stiffness for the reference and retrofitted specimens was approximately equal in the static cyclic and dynamic tests.

7.2 Conclusions of Experimental Work

- Within the scope of testing, single-sided retrofitting appears to produce good behavior. No out-of-plane or uneven response of the specimens was observed. Small asymmetries in the transducers were recorded in the case of squat specimens. However, further investigations are required for squat specimens in the ultimate range.
- The lateral resistance at first delamination depends on the reinforcement ratio and specimen aspect ratio as well as the fiber characteristics. However, unlike dynamic tests, no delamination of the fibers in the form of white spots has been observed during the static cyclic tests.
- The ultimate drifts were independent of the reinforcement ratio and reinforcement type; however, the ultimate drifts were dependent on the aspect ratio and the retrofitting configuration.
- All retrofitting techniques succeeded in recovering the initial stiffness of the reference specimens.

7.3 Findings of Analytical Model

The proposed model which is discussed in Chapter 5 idealizes masonry, epoxy, and FRP in a URM-FRP as different layers (Figure 7.1) with isotropic homogenous elastic materials. Then, using principles from the theory of elasticity the governing differential equation of the system is formulated. A double Fourier sine series was used as a solution for the differential equations. The solution can be used to model the linear shear behavior of URM wall retrofitted using FRP. To take into consideration material nonlinearity, a step-by-step stiffness degradation of masonry as well as epoxy has been implemented in a program written in MATLAB [Ma 02]. The force deformation behavior of the masonry layer as well as the epoxy layer has been idealized using bilinear curves (§ 5.3), the force deformation curve of FRP is idealized as linear elastic until failure. After every step of stiffness degradation, the equations were resolved. In general, the masonry or epoxy dominates the failure and in no case does FRP reach its ultimate load. In addition, the advantages of the homogenous material model are that it is easy to use and requires minimal input data and minimal computing power is required. However, for masonry, the influence of weak mortar joints was difficult to simulate for this kind of model. The model led to the following findings and conclusions.

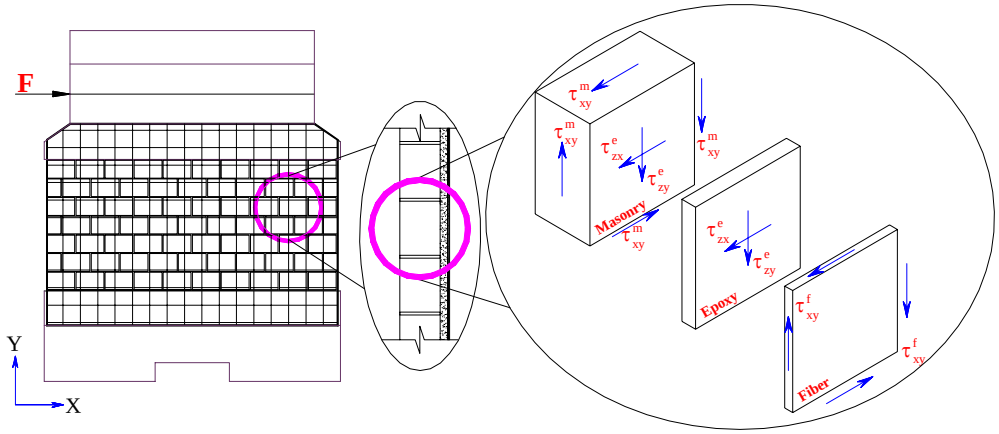

Figure 7.1: URM wall retrofitted using FRP (full surface, single side) and differential element of the same retrofitted wall showing masonry, epoxy, and fiber stresses

7.3.1 Findings

Although the presented model is a basic analytical model, effects of different material properties were examined: allowable shear stresses for masonry and epoxy, epoxy ductility, epoxy shear modulus, and masonry ductility. Effects of these parameters on FRP efficiency ζ, lateral resistance of URM-FRP walls F, and contribution of FRP to lateral resistance of URM-FRP walls F_{FRP} have been examined. The results show the following:

- The concept developed by Triantafillou [Tr 98] of using effective strain inversely proportional to the FRP axial rigidity is more appropriate than using a constant strain value. In addition, the degradation rate empirically developed by Triantafillou [Tr 98] is close to the average of the degradation rates given by different epoxy and masonry parameters. This is expected since Triantafillou developed his model based on curve fitting for different beams with different material parameters. However, the higher the allowable shear stress of epoxy, the lower the rate of degradation of ζ.
- When epoxy properties dominate URM-FRP shear behavior, the degradation rate of ζ includes three phases: high degradation rate until a ρE value of approximately 0.19 GPa, slow degradation rate for ρE greater than 1.12 GPa and between these two limits of ρE there is a transition phase with a moderate degradation rate. In contrast, when masonry properties dominate URM-FRP shear behavior, the degradation rate of ζ is very low.
- Triantafillou's original model estimated F_{FRP} higher than the proposed analytical model. The difference between Triantafillou's model and the proposed model is expected since Triantafillou original model implicitly assumes wrapped retrofitting whereas the proposed model distinguishes between wrapped and unwrapped retrofitting. The stresses in the wrapped case are generally higher than the unwrapped case. For all material properties examined here using the proposed model no FRP fracture occurred.
- With few exceptions, until ρE of 0.19 GPa, AC125 [IC 01] estimated F_{FRP} close to the average of F_{FRP} estimated using different material properties. However, for ρE greater than 0.19 GPa the comparison between F_{FRP} estimated by AC125 [IC 01] and the proposed model seems difficult since the AC125 assumes a constant axial strain in the FRP. This concept of constant axial strain in FRP was possible in the past when the existing FRP layers had a low amount of fiber (i.e. low axial rigidity). Presently, new fibers and products with higher Young's modulus and higher amount of fiber exist. Modern code should adapt to the concepts of variable strain in FRP.
- The Triantafillou and Antonopoulos [TA 00] model estimates F_{FRP} approximately close to the average F_{FRP} estimated by the analytical model, used here, using different material properties.
- By increasing the epoxy's allowable shear stress the FRP contribution to lateral resistance of URM-FRP increases. However, the increment in the F_{FRP} is approximately linear until $(\rho E)_{optimum}$. Increasing ρE beyond $(\rho E)_{optimum}$ has a less significant effect on F_{FRP}. This optimum value of ρE is not a constant value but depends on the material properties.
- There is interaction between masonry lateral resistance (F_m) and in-plane lateral resistance of URM-FRP (F). Adding masonry lateral resistance to the FRP contribution in order to have the lateral resistance of URM-FRP is only correct up to a certain limit. Beyond this limit the equation is not valid. In addition,

beyond a certain limits $(\rho E)_{limit}$ there is a reduction in the lateral resistance of URM-FRP. This reduction in lateral resistance is due to the following: beyond $(\rho E)_{limit}$ URM-FRP reaches the limit on epoxy stiffness degradation too early before masonry reaches its allowable shear stress.

- There is a threshold with respect to the shear rigidity of the FRP beyond which no increase in shear gain is expected. Such a threshold can be used as a criterion for a cost effective design. So and in order to have a cost effective safe URM-FRP, it is proposed to use a value of 0.19 GPa as limit on (ρE). This value satisfied $(\rho E)_{optimum}$ and $(\rho E)_{limit}$ in all the cases studied here.
- For the tested specimens, the proposed model predicts F_{FRP} approximately 25%, 70%, and 81% of those estimated by Triantafillou [Tr 98], Triantafillou and Antonopoulos, and AC125 models respectively.
- The proposed model predicts the lateral resistance of the test specimens to a precession of 61 to 143% of the measured lateral resistance. It should be noticed that no specimen failed in pure shear during the experimental tests.
- Using a procedure similar to the flexural design of RC beam-column and linear elastic approach seems appropriate for the flexural design of URM-FRP. However, to have a more accurate lateral resistance shear effects should be taken into consideration. A factor reflects the shear effect is suggested based on correlation with experimental data.
- Regarding the analysis procedure developed in FEMA 356 for retrofitting, the test results show that the composite curve of the test specimens is similar to curve Type 2 of FEMA 356 with ductility greater than two. This suggests that to treat URM-FRP, which fails due to toe compression failure as a displacement-controlled component rather than a force-controlled component.
- The different performance levels estimated by FEMA 356 for URM-FRP are conservative in terms of drifts; however, in terms of the m factor the immediate occupation level is unconservative and should be modified.

7.3.2 Conclusions

The results show that the axial strains in FRP are inversely proportional to FRP axial rigidity as already proposed by Triantafillou [Tr 98]. Since FRP can be considered as elastic linear material, the FRP contribution to lateral resistance FFRP can also be considered inversely proportional to axial rigidity ρE. However, it is not possible to have a single function to represent the relation between ρE and F_{FRP}. The relation between the two quantities depends on several factors (e.g. allowable shear stresses in masonry, epoxy, and FRP as well as masonry and epoxy ductility). Hence, any relation based only on empirical calibrations with experimental data without taking into considerations the effect of different material parameters will result in a sort of "average" value of F_{FRP} due to these different parameters. This average function, by its nature, overestimates F_{FRP} in some cases and in other cases underestimates F_{FRP}. However, using high values of ρE (approximately equal to or greater than 1.12 GPa) it is possible to use a single function to describe the relation between ρE and FRP axial strain. Since for all material properties the degradation rate in axial strain was approximately the same and parallel to the second part of Triantafillou empirical equation.

The relation between axial forces in FRP (F_{FRP}) and FRP axial rigidity ρE should be taken into consideration. The results show the following:

- The higher the allowable shear stresses in the epoxy are the higher F and $F_{FRP.}$ The increment in epoxy allowable shear stresses could be achieved by the development of new materials or by using mechanical anchorage system at the boundaries. As expected, the effect of such mechanical anchorage system is higher for high values of ρE.
- The lower the allowable shear stresses in masonry are the lower F_{FRP} and the higher gain. Regarding ductility, the higher the epoxy ductility is the lower degradation rate in ζ. However, the effect of epoxy ductility on F_{FRP} and F for lower values of ρE is insignificant. For higher values of ρE there is a significant effect of epoxy ductility. This shows that for industrial companies, in addition to developing FRP with higher density of FRP and higher Young's modulus, the development of ductile epoxy is an urgent need.
- Regarding masonry ductility, the results show that masonry ductility plays an essential role in determining F and F_{FRP}. The model shows that there should be large masonry deformations and cracking to mobilize axial strains in FRP. However, for high values of ρE there is no effect of masonry ductility.

This important conclusion means that for URM walls where cracking is not allowed it is recommended to use FRP with high axial rigidity to have effective retrofitting.

As mentioned, the proposed model quantifies the relation between F_m and F_{FRP}. The results show that adding F_m to F_{FRP} is only valid until certain limits and that beyond these limits any additional increment in FRP has no effect. In other words, there is a threshold with respect to the shear rigidity of the FRP beyond which no increase in shear gain is expected. Such a threshold can be used as a criterion for a cost effective design. Again, the limit on ρE is not constant but rather it depends on materials allowable stresses and ductility. However, a value of 0.19 GPa can be proposed as a limit on ρE which covers the practical values of material properties.

This research shows that much information is needed to refine characterizations of the materials which are used in URM-FRP system (i.e. masonry, epoxy, FRP). Yet, the proposed model implicitly describes how URM-FRP behaves due to in-plane loading so much of the needed development is now placed in the proper perspective. For example, the unexpected high lateral resistance of the specimen where only vertical reinforcement is used (i.e. no horizontal reinforcements) suggests several questions about the behavior of such a retrofitted wall. One of possible explanations is that the vertical reinforcement reduced the crack opening of the retrofitted wall and that this led to a longer "uncracked" section and allowed higher shear to transfer through this section. Another explanation is that, the calculated shear resistance of URM is much higher than the calculated values. Finally, there should be an effect of dowel action and epoxy impregnation. However, the proposed model does not take into considerations such effects.

Regarding flexural analysis, using a linear elastic approach with the well-known assumptions of Navier-Bernoulli and Whitney's equivalent stress block leads to unconservative design. Correlation analysis of the test data show that the ratio between the experimental lateral resistance to the estimated flexural lateral resistance is proportional to the reinforcement mechanical ratio times the square of the effective moment/shear ratio up to a certain limit. Within the test limits, a correlation factor is proposed.

7.4 Significance

The seismic upgrading of URM buildings built in seismic zones prior to the introduction of modern seismic codes and design practice is recognized as an important task of structural engineering. The use of epoxy-bonded FRP is emerging as an efficient and cost effective technique for retrofitting of existing structural elements. Several reliable methods exist for the out-of-plane design of URM-FRP. However, this is not the case for in-plane design of URM-FRP where a satisfactory analysis method has not been achieved so far. The absence of a physical design model for upgrading reflects the lack of knowledge in this field and form the basis for an important research effort in this area. The behavior of URM-FRP in shear is complex and involves numerous interacting parameters. This research attempts to provide a comprehensive assessment of these parameters resulting from the findings of a parametric study using a new analytical model. In addition, it pin-points the aspects that have not been studied sufficiently, and it suggest where further research is required. The research outlined in this thesis offers major advantages over some existing empirical models and it provides a better understanding of the in-plane response of the URM-FRP and will be useful tool for checking and retrofitting of existing URM buildings to withstand seismic loading. The proposed model will make significant contributions to the structural engineering community for five reasons, which are summarized as follows:

- The analytical model presented in Chapter 5 represents the first simplified analytical model and could be extended to create a design tool that considers epoxy properties (shear modulus, ductility), masonry properties (allowable shear stress, ductility) as well as FRP properties. This represents a strong improvement over the current empirical models, which are based almost solely on tests of RC elements. Such improvement will be useful not only for structural engineers but also for material producers.
- The identification of the interaction between masonry lateral resistance and the FRP contribution to lateral resistance of URM-FRP greatly improves the understanding of URM-FRP structural response. In addition, these findings enable the use of FRP more effectively to retrofit URM walls.
- Although the model is simple, it overcomes the main disadvantage of AC125 [IC 01] that uses a constant value for axial strain in FRP. The model estimates axial strain in FRP similar to the empirical function of Triantafillou [Tr 98]. In addition, it overcomes most of the shortcomings of Triantafillou's model (§ 5.1.1). However, more experimental calibration is required.
- This study represents the first time that a single leaf hollow clay URM wall retrofitted using different FRP materials, configurations, and aspect ratios has been assessed using dynamic testing. The results

presented here and in ElGawady et al. [EL 03] provide insight into how these techniques contribute to the lateral response, which is required to permit their safe and effective application for seismic retrofitting of URM walls.

- The detailed documentation of the experimental work presented here and in ElGawady et al. [EL 03] provides a means to validate any future analytical models and current code provisions, thus increasing the accuracy of analysis tools available to practicing engineers.

Aside from its scientific significance, the thesis has an economic significance. Because of the large exposure linked to seismic hazard and the very high cost of reducing the risk linked to existing vulnerable URM buildings (US$ 4 billions required for upgrading in California alone), it is critical to optimize the upgrading strategies. The models developed and improved in this research will provide improved capabilities for engineers to assess the upgrading strategies. In addition, the experimental data (e.g. stiffness degradation, ultimate drift) provide essential information for seismic engineers, which could be integrated in URM building evaluation.

7.5 Future Work

The investigation of the effect of retrofitting of URM using FRP is far from complete. It is believed, however, this research provides a milestone in the efforts to utilize FRP in retrofitting of URM walls. As mentioned, the model is the first analytical model, which is developed for in-plane lateral resistance of URM-FRP. The model has several short comings and limitations; however, future development seems possible and necessary to simulate more realistically the shear behavior of URM-FRP. In addition, this study revealed numerous gaps that need to be addressed. The following points are the most important:

- There is a strong need to have accurate values for shear modulus of masonry. While several codes have adapted value of approximately 0.4 of Young's modulus, Tomazevic [To 99] measured values as low as 6%. This value strongly influences the contribution of FRP to shear resistance of URM-FRP.
- Developing failure criterion for epoxy under shear and normal stresses. Such development will be of useful to introduce into the proposed 2-D model. Otherwise, a complicated 3-D should be developed to take into considerations the effect of normal stresses.
- In the proposed model, further examination of the boundary conditions at the base and top is required
- An accepted ultimate drift should be developed for URM walls failing in shear. This is very important to determine the shear resistance of URM-FRP.
- A more accurate method of determining the diagonal strength of URM walls is required. Such a model should include a method to separate diagonal tension failures that occur through brick units with those that occur in a stair-stepped pattern to allow for the differences in displacement capacity to be considered.
- Conducting further analytical work on the effect of material models.
- Conducting experimental tests using higher normal forces than used in this research. High normal forces could affect the backbone curves (see Chapter 6).
- More realistic values should be measured for epoxy and masonry ductility.
- Static cyclic and dynamic forces can replace the static lateral forces in the proposed model.
- Calibration with specimens failing in combinations of shear and moment is required to take into considerations flexural effects.
- Considering masonry as an orthotropic material rather than an isotropic material; following this step, the orthotropic properties of masonry could be used to carry out analysis for inclined retrofitting.
- Provide design guidelines for the FRP-masonry in order to optimize the selection of the composite materials to retrofit URM walls.
- Experimental work should carry out on specimens retrofitted using vertical reinforcement only to quantify the effect of vertical reinforcement on shear resistance.
- Investigating the use of different composite fabrics to retrofit full-scale URM walls, including varying the fiber orientation within FRP types (i.e. use ±45º rather than 0/90º). It is expected that the behavior will be more ductile since the stress strain curve of ±45º in direct tension can be idealized as a bilinear curve.

- Experimentally studying the effectiveness of retrofitting URM walls containing different opening configurations such as for windows and doors with FRP.

APPENDIX A

A REVIEW OF CONVENTIONAL SEISMIC RETROFITTING TECHNIQUES FOR URM

Matthys and Noland [MN 89] estimated that more than 70% of the buildings inventory worldwide is masonry buildings. Moderate to strong earthquakes can devastate complete cities and villages resulting in massive death toll and cause extensive losses. Most of these losses are caused by failure of unreinforced masonry (URM) buildings. Since demolition and replacement of these masonry structures is generally not feasible due to several factors this rises the question whether such buildings should be retrofitted. Nuti and Vanzi [NV 03] proposed a simple procedure to make a decision whether it is economically pertinent to retrofit a structure or not.

Although a variety of technical solutions have been implemented for seismic retrofitting, there exists little information or technical guidelines with which an engineer can judge the relative merits of these methods. Furthermore, no reliable analytical techniques are available to evaluate the seismic resistance of retrofitted masonry structures. This appendix reviews common conventional techniques used in retrofitting of existing URM buildings.

A.1 Retrofitting Methods

A.1.1 Surface treatment

Surface treatment is a common method, which has largely developed through experience. Surface treatment incorporates different techniques such as ferrocement, reinforced plaster, and shotcrete. By nature this treatment covers the masonry exterior and affects the architectural or historical appearance of the structure.

Ferrocement

Ferrocement consists of closely spaced multiple layers of hardware mesh of fine rods (Figure A.1(a)) with reinforcement ratio of 3-8% completely embedded in a high strength (15-30 MPa) cement mortar layer (10- 50 mm thickness). The mortar is troweled on through the mesh with covering thickness of 1-5 mm. The mechanical properties of ferrocement depend on mesh properties. However, typical mortar mix consists of 1 part cement: 1.5-3 parts sand with approximately 0.4 w/c ratio (the ferrocement network, Montes and Fernandez 2001). The behavior of the mortar can be improved by adding 0.5-1% of a low-cost fiber such as polypropylene.

(a)

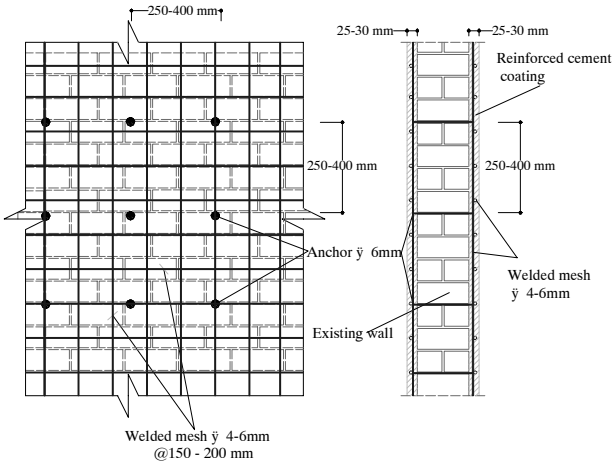

(b)

(c)

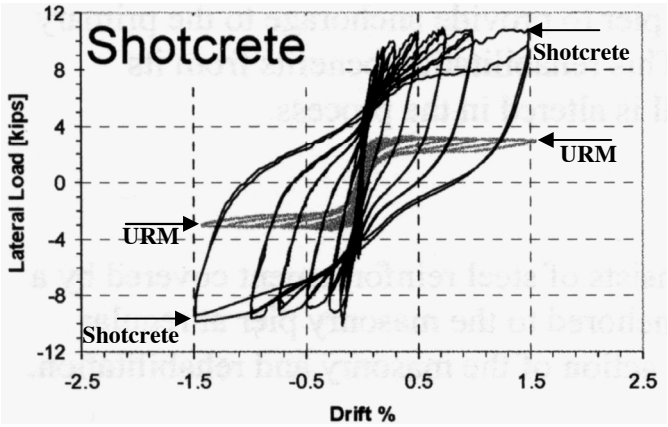

(d)

Figure A.1: Surface treatment:(a) hardware samples used in ferrocement (TWP Inc.), (b) reinforced plaster typical dimensions, (c) application of shotcrete for test specimen [EH 04], and (d) hysteretic curves for a specimen before and after retrofit using shotcrete [AL 01]

In order to reduce the mortar cost, it is possible to replace 20% of cement by fly ash or rice-husk; this replacement increases durability and decreases overall porosity as well as makes the mortar more plastic with a limited effect on overall strength [the ferrocement network].

Ferrocement is ideal for low cost housing since it is cheap and can be done with unskilled workers. It improves both in-plane and out-of-plane behavior. The mesh helps to confine the masonry units after cracking and thus improves in-plane inelastic deformation capacity. In a static cyclic test [AL 01], this retrofitting technique increased the in-plane lateral resistance by a factor of 1.5. Regarding out-of-plane behavior, ferrocement improves wall out-of-plane stability and arching action since it increases the wall height-to-thickness ratio.

Reinforced plaster

A thin layer of cement plaster applied over high strength steel reinforcement can be used for retrofitting [ST 80]. The steel can be arranged as diagonal bars or as a vertical and horizontal mesh. A reinforced plaster can be applied as shown in Figure A.1(b).

In diagonal tension test and static cyclic tests, the technique was able to improve the in-plane resistance by a factor of 1.25-3 [JK 80, ST 80]. The improvement in strength depends on the strengthening layer thickness, the cement mortar strength, the reinforcement quantity and the means of its bonding with the retrofitted wall, and the degree of masonry damage.

Shotcrete

Shotcrete overlays are sprayed onto the surface of a masonry wall over a mesh of reinforcing bars (Figure A.1(c)). Shotcrete is more convenient and less costly than cast-in-situ jackets. The thickness of the shotcrete can be adapted to the seismic demand. In general, the overlay thickness is at least 60 mm [AL 01, To 99, KF 92, Ka 84, HY 84]. The shotcrete overlay is typically reinforced with a welded wire fabric at about the minimum steel ratio for crack control [KF 92].

In order to transfer the shear stress across shotcrete-masonry interface, shear dowels (6-13 mm diameter @ 25-120 mm) are fixed using epoxy or cement grout into holes drilled into the masonry wall [AL 01, To 99, KF 92, Ka 84]. Other engineers believe that a bonding agent like epoxy is required to be painted or sprayed on the brick so that adequate brick-shotcrete bond is developed [Ka 84]. However, there is no consensus on brick-to-shotcrete bonding and the need for dowels. Diagonal tension tests of single and double wythe URM panels [Ka 84] retrofitted with shotcrete showed that, dowels did not improve the composite panels response or the brick-shotcrete bonding; header bricks satisfactory joined the wythe of existing masonry panels. In addition, Tomazevic [To 99] and Kahn [Ka 84] recommended wetting the masonry surface prior to applying shotcrete. Kahn [Ka 84] shows that such brick surface treatment does not affect significantly the cracking or ultimate load, it affects to limited extend the inelastic deformations.

Retrofitting using shotcrete significantly increases the ultimate load of the retrofitted walls. Using a one-sided 90 mm thick shotcrete overlay and in diagonal tension test, Kahn [Ka 84] increased the ultimate load of URM panels by a factor of 6-25. Abrams and Lynch [AL 01], in a static cyclic test, increased the ultimate load of the retrofitted specimen by a factor of 3. This retrofitting technique dissipates high-energy due to successive elongation and yield of reinforcement in tension (Figure A.1(d)). Although in diagonal tension test (Kahn 1984) the improvement in the cracking load was very high, in static cyclic test [AL 01] the increment in the cracking load was insignificant.

Typically, the shotcrete overlay is assumed to resist all the lateral force applied to a retrofitted wall with the brick masonry being neglected all together [AL 01, HY 84]. This is reasonable assumption for strength design since the flexural and shear strength of the reinforced shotcrete overlay can be many times more than that of the URM wall. This assumption may result in some cracking of the masonry as the reinforcement in the shotcrete strains past yield. This may violate a performance objective for immediate occupancy or continued operation.

A.1.2 Grout and epoxy injection

Grout injection is a popular strengthening technique, as it does not alter the aesthetic and architectural features of the existing buildings. The main purpose of injections is to restore the original integrity of the retrofitted wall and to fill the voids and cracks, which are present in the masonry due to physical and chemical deterioration and/or mechanical actions. For multi wythes masonry walls, injecting grout into empty collar joint enhances composite action between adjacent wythe. The success of a retrofit by injection depends on the injectability of the mix used, and on the injection technique adopted. The injectability of the mix influences by mixís mechanical properties and its physical chemical compatibility with the masonry to be retrofitted.
For injection, epoxy resin is used for relatively small cracks (less than 2 mm wide); while, cement-based grout is considered more appropriate for filling of larger cracks, voids, and empty collar joints in multi-wythe masonry walls [CM 94, SA 94]. However, Schuller et al. [SA 94] used a cement-based grout (100% type III Portland cement ASTM C150 with expansive admixture and w/c ratio of 0.75) to inject 0.08 mm wide cracks.

The retrofit of walls by cement grouting can be carried out as follows [HE 99, CM 94, SA 94]:

- Placement of injection ports and sealing of the cracked areas in the basic wall as well as around injection ports.
- Washing of cracks and holes with water. Inject of water (soak of the bricks), from the bottom to the top of the wall, to check which tubes are active.
- Injection of grout (Figure A.2(a)), with injection pressure of less than 0.1 MPa, through each port in succession. Begin injection at the lower-most port. After filling all large voids, a second grout mix (cement-based or epoxy) is used for fine cracks.

This retrofitting technique improves the overall behavior of the retrofitted URM; non-destructive testing (sonic tomography) of a bridge pier shows how the injection transformed relatively poor quality limestone masonry into relatively good in situ quality [PK 02]. The technique is effective at restoring the initial stiffness and strength of masonry. Cement-based grout injection is capable of restore up to about 0.8 of the unretrofitted masonry compressive strength [SA 84], 0.8-1.1 of the unretrofitted wall in-plane stiffness and 0.8-1.4 of the wall unretrofitted in-plane lateral resistance [ST 80, MS 96, CM 94]. In addition, cement-based grout injection can increase the interface shear bond of multi-wythe stonewalls by a factor of 25-40 [HE 99]. Walls retrofitted with epoxy injection tend to be stiffer than the unretrofitted, but the increase in stiffness (10- 20%) is much less dramatic than the increase in strength. The increment in lateral resistance ranged from 2-4 times the unretrofitted resistance. The use of epoxy resins can be advisable when a through study of the structural consequences of such an increment in strength in selected portions of the building shows that there is no danger of potential damage to other portions.

A.1.3 External reinforcement

A steel plates or tubes can be used as external reinforcement for existing URM buildings. Steel system is attached directly to the existing diaphragm and wall (Figure A.2(b)); however, Rai and Goel [RG 96] show that horizontal element can be connected to two vertical members (via pin connections), which are placed next to the existing wall (i.e. creating in-fill panel) can be used (A.2(c)).
The relative rigidities of the unretrofitted structure and the new steel bracing are an important factor that should be taken into consideration. In an earthquake, cracking in the original masonry structure is expected and after sufficient cracking has occurred, the new steel system will have comparable stiffness and be effective (Hamid et al. 1996, Rai and Goel 1996).

The vertical and diagonal bracing improves the lateral in-plane resistance of the retrofitted wall by a factor of 4.5 [Ta 00]. The increment in the lateral resistance was limited by crushing of the masonry at ends (toes) followed by vertical strips global buckling. In the case of creating infill panel, the rocking motion of the pier is associated with a vertical movement of its corner butting against the support masonries and the steel verticals resist the motion by restringing this vertical movement. This mechanism put both vertical members under tension forces (Figure A.2(c)). The system increased the in-plane lateral resistance of the retrofitted wall by a factor of 10. In addition, the external steel system provides an effective energy dissipation mechanism [Ta 00, RG 96].

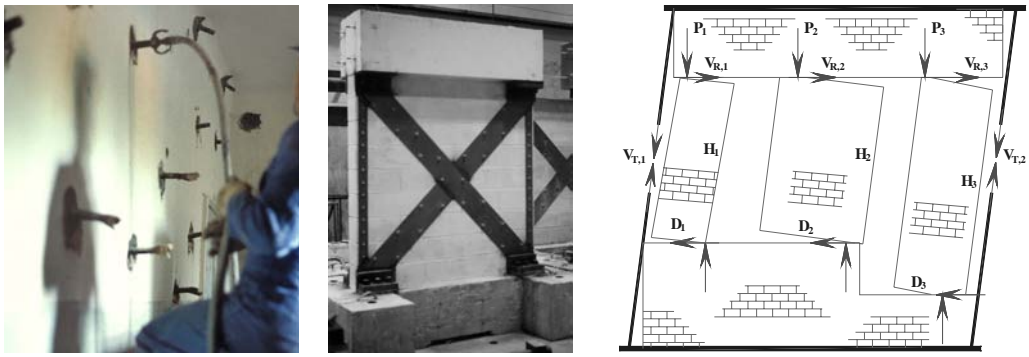

(a) (b) (c)

Figure A.2: (a) Grout injection (Tomazevic, personal communication), and external reinforcement (b) Using vertical and diagonal bracing [Ta 00], (c) Creating in-fill panel (reproduced after [RG 96])

A.1.4 Confining URM using RC tie columns

Confined masonry with RC ì weak frameî represents one of the most widely used masonry construction system in Asia and Latin America. In Europe, Eurocode 8 (EC 8) recommends the usage of such confined system for masonry constructions. In China, they used such confinement in new masonry buildings as well as it is used as retrofitting for existing URM buildings. However, it is not easy to construct such confinement in existing masonry buildings. The basic feature of confined masonry structures is the vertical RC or reinforced masonry tie columns, which confine the walls at all corners and wall intersections as well as the vertical borders of doors and windows openings. In order to be effective, tie columns should connect with a tie beam along the walls at floors levels. An elastic finite element analysis [KF 92] shows that tie columns alone i.e. without tie beams do not have a significant positive effect on walls behavior

The confinement prevents disintegration and improves ductility and energy dissipation of URM buildings, but has limited effect on the ultimate load resistance [CG 97, Zhang et al. 1997, ZQ 84]. For new constructions, according to EC 8, no contribution of vertical confinement to lateral resistance should be taken into account in the design [TK 97]. However, the real confinement effect mainly depends on the relative rigidity between the masonry wall and the surrounding frame and to less extend on material characteristics. Before cracking, the confinement effect can be neglected [TK 97, CG 97, KF 92]. However, for very squat URM walls (geometrical aspect ratio of 0.33 and double fixed boundary conditions) the confinement increased the cracking load by a factor of 1.27. At ultimate load, the confinement increased the lateral resistance by a factor of 1.2 [ZQ 84, Zhang et al. 1997, CG 97]. However, for walls with higher aspect ratio, the confinement increased the lateral resistance by a factor of 1.5 [TK 97]. In addition, the confinement improved the lateral deformations and energy dissipation by more than 50% [TK 97, ZQ 84].

The amount of reinforcement and concrete dimensions for this system is determined on the basis of experience, and depends on the height and size of the building. The Technology Code for Confined Brick Masonry (DB32/113-95) recommended spacing of 1.5-2.5 m between columns as well as minimum dimensions and reinforcement for a column as shown in Figure A.3. In addition, it is recommended to use 120-180 mm depth ring beam with width equal to wall thickness and 4 bars 8-14 mm diameter.

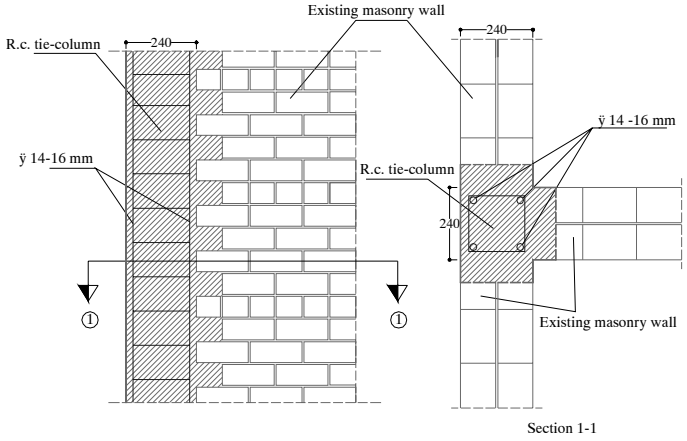

(a)

Figure A.3: Placement of new tie-columns in a brick-masonry wall

A.1.5 Post-tensioning

Post-tensioning involves a compressive force applied to masonry wall; this force counteracts the tensile stresses resulting from lateral loads. There has been little application of this technique; post-tensioning is mainly used to retrofit structures characterized as monuments. This is due in part to lack of knowledge about the behavior of post-tensioning masonry [FM 00, LS 99, IL 98, KF 92]. In addition, the codification of post-tensioning masonry has only begun recently (e.g. MSJC 1999). Much research has been conducted in the last decade on post-tensioning masonry worldwide (e.g. [LS 03, RK 03, SB 03, LD 02]. Post-tensioning tendons are usually in the form of alloy steel thread bars [SB 03, FM 00, KF 92], although mono-strand tendons are not uncommon [MM 96, AN 87]. Bars typically show higher relaxation losses (2-3 times strand losses) and much lower strength/weight ratio (VSL 1990); in addition, a major drawback for using of steel bars is corrosion. However, fiber reinforced plastic presents a promising solution for this problem [LS 03, Figure A.4).

Tendons are placed inside steel tube (duct) either within holes drilled along the mid-plane of the wall or along groves symmetrically cut on both surfaces of the wall. Holes are cement grouted and external grooves are filled with shotcrete [RK 03, AN 87]. In this case, the tendons are fully restrained (i.e. it is not free to move in the holes). This is true even if the tendon is un-bonded i.e. no grout is injected between the duct and the tendons [MM 96]. However, the holes can be left un-grouted (unguided unrestrained). This simplifies the strengthening procedure and allows future surveillance, re-tensioning, or even removal of the post-tensioning bars [SB 03, KF 92]. It is important for un-bonded bars to continue the protection of the bar inside the foundation to avoid differential oxidation [FM 00]. MSJC [MS 99] provisions for masonry new constructions accept both restrained and unrestrained post-tensioning systems [SB 03].

Anchorage of post-tensioning in masonry is more complicated than in RC as masonry has a relatively low compressive strength. The self-activating dead end can be encasing to continuous and heavy RC foundation beams, constructed on either side of the wall bottom and connected well with it. At the top, post-tensioning is anchored in the existing RC elements (Figure A.4(c)) or in a new precast RC special beam or specially stiffened steel plates. Anchorage devices and plates are usually placed in a recess of the surface, and covered later on with shotcrete or cement mortar. The requirement for bottom anchorage penalizes considerably this retrofitting technique.

Vertical post-tensioning resulting in substantial improvement in wall ultimate behavior for both in-plane and out-of-plane; in addition, it improves both cracking load and distribution. Rosenboom and Kowalsky [RK 03] show that for cavity walls, the post-tension grouted specimen has lateral resistance much higher (40%) than the un-grouted one. For grouted specimens, although to bond or not the bars have insignificant effect on lateral resistance; the specimen who has un-bonded bars has higher lateral drift (70%) over the bonded specimen. The un-bonded grouted specimen has a drift up to 6.5%. However, un-bonded post-tension tendons may show low energy dissipation due to the lack of yielding of reinforcement (VSL 1990).

The effect of horizontal post-tensioning needs extensive experimental examination. Although some basic calculations of principle stresses show that the horizontal post-tensioning improves the resistance, Page and Huizer [PH 94] experimental test did not proof these calculations. In a linear finite element model, Karantoni and

Faradis [KF 92] show that horizontal post-tensioning of spandrels did not significantly improve the building behavior. In addition, they show that if horizontal and vertical post-tensioning is combined together the resulting positive effect is higher than the sum of the individual effects of the two directions post-tensioning.

For bonded grouted post-tensioning the ultimate tendon force may be determined assuming rigid bond and plane sections similar to design of RC post-tensioning. Thus, the tendon will reach their yield force. For un-bonded post-tensioning the tendon force will increase from service up to ultimate load depending on the deformations. This increment in the tendon force may be estimated by applying rigid mechanisms. For short time behavior and under the same post-tensioning force, strand configuration and amount has insignificant effect on wall behavior [AN 87].

A.1.6 Center core technique

The center core system consists of a reinforced, grouted core placed in the center of an existing URM wall. A continuous vertical hole is drilled from the top of the wall into its basement wall. The core achieved by this oil-well drilling technique may be 50-125 mm in diameter, depending on the thickness of the URM wall and the retrofitting required. With existing technology, this core can be drilled precisely through the entire height of two or three-story masonry wall. The drilling is a dry process with the debris removal handled by a vacuum and filter system that keeps the dust to a minimum. After placing the reinforcement in the center of the hole, a filler material is pumped from the top of the wall to the bottom such that the core is filled from the bottom under pressure controlled by the height of the grout.

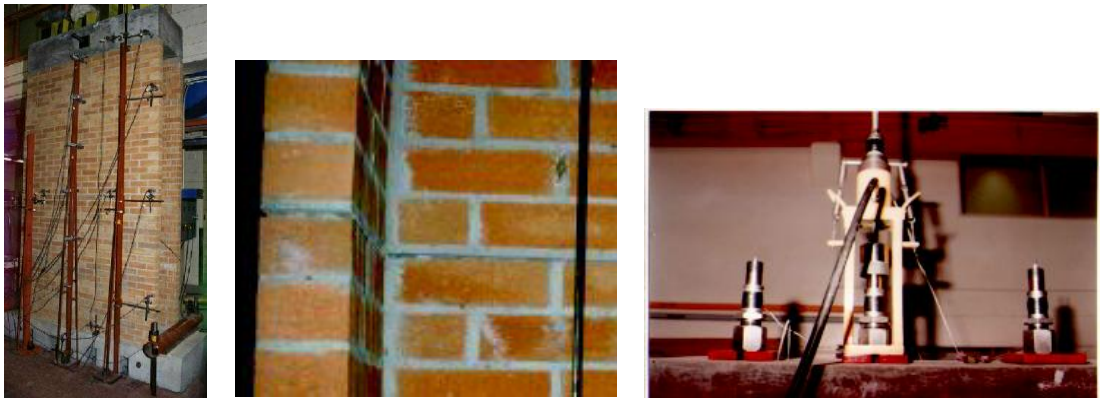

(a) (b) (b)

Figure A.4: (a) post-tensioning using FRP, (b) flexural crack in post-tension wall, (c) post-tensioning jacking frame [ISIS]

The placement of the grout under pressure provided by the height of the core provides a beneficial migration of the grout into all voids adjacent to the core shaft. The strong bonding of the grout to the inner and outer wythes of brick provides a "homogeneous" structural element much larger than the core itself [PC 86]. This reinforced "homogeneous" vertical beam provides strength to the wall with a capacity to resist both in-plane and out-of-plane loading. Wall anchors for lateral ties to the roof and floors are placed at the core location to make a positive connection to the wall.

The filler material itself consists of a binder material (e.g. epoxy, cement, and polyester) and a filler material (e.g. sand). Shear tests [PC 86] show that specimens made with cement grout were generally 30% weaker than specimens made with sand/epoxy or sand/polyester grouts. However, based on material price, it is recommended to use polyester and to keep the sand/polyester volume ratio between 1:1 and 2:1. For cement-based grout, the volume proportions of the components play an essential role in the shear resistance. However, of different grout types, the best type had components of 1:0.125:1 cement: lime: sand proportions by volume.

This technique is successfully used to double the resistance of URM wall in a static cyclic test [AL 01]. Although the high lateral displacement achieved (Figure A.5) during the test, the energy dissipated was limited. The tensile yield of the bar did not occur due to the bar anchorage problem. However, the system has several advantages: it will not alter the appearance of wall surface as well as the function of the building will not be impaired since the drilling and reinforcing operation can be done externally from the roof. The main disadvantage is this technique tends to create zones with widely varying stiffness and strength properties.

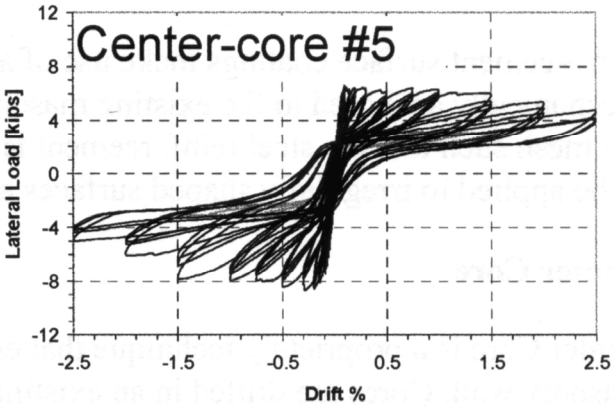

Figure A.5: hysteretic curve for a URM specimen after retrofitting using center core [AL 01]

A.2 Summary

Based on the literature survey, Table A.1summarizes the efficiency, advantage, and disadvantage of each technique. Where available, figures from static cyclic or dynamic tests are given to indicate the improvement in the retrofitted walls.

Table A.1: Survey summary

Tech.	Efficiency		Advantage	Disadvantage
	In-plane	Out-of-plane		
Ferrocem-ent	$F_r \rightarrow 1.5\ F_{ur}$ $D_r \rightarrow 1.7\ D_{ur}$	Improves stability	Low cost Low technology Limited added mass	Space reduction Arch. Impact Requires arch. finishing Limited efficiency Limited E.D.
Reinforc-ed Plaster	$F_r \rightarrow$2-3 F_{ur} Improves D_r	Improves stability	Low technology Limited added mass	Space reduction Arch. Impact Required arch. finishing
Shotcrete	$F_r \rightarrow 3\ F_{ur}$ $D_r \rightarrow D_{ur}$	Improves stability	High increment in F_{ur} Very significant improvement in E.D.	Space reduction Heavy mass Violation of perform. level Disturbance occupancy Arch. Impact Required arch. finishing
Injection	Restores initial stiffness $F_r \rightarrow$0.8-1.4 F_{ur}	Can restores initial stiffness	No added mass No effect on building function No space reduction No arch. Impact	Epoxy create zones with varying stiffness and strength High cost of epoxy No significant increment in F_r using cement-based grout
External Reinforc-ement	$F_r \rightarrow$4.5-10 F_{ur} $E.D_r$.>1.5 $E.D_{ur}$.	N.A.	High increment in F_{ur} Prevent disintegration Improves ductility and E.D.	Corrosion Heavy mass Violation of performance level Requires arch. Finishing Disturbance occupancy
Confinem-ent	$F_r \rightarrow$1.2-1.5 F_{ur} $D_r \rightarrow D_{ur}$	Prevent disintegration	Prevent disintegration Improve ductility and E.D.	Not easy to introduce Limited effect on F_{ur} Required arch. finishing Disturbance occupancy
Post-tension	Improves F_{ur}	Improves F_{ur}	No added mass No effect on building function	High losses Anchorage system Corrosion potential

Center Core	$F_r \rightarrow 2\ F_{ur}$ $D_r \rightarrow 1.3\text{-}1.7\ D_{ur}$	Improves F_{ur}	No space reduction No arch. Impact No effect on building function	Creation of zones with varying stiffness and strength.

F_r, F_{ur}: lateral resistance for retrofitted and unretrofitted specimens respectively, D_r, D_{ur}: lateral displacement for retrofitted and unretrofitted specimens respectively, E.D.: energy dissipation

REFERENCES

[Ab 92] Abrams, D. (1992). "Strength and behavior of unreinforced masonry elements." *10th World Conference on Earthquake Engineering*, Madrid, Spain, 3475-3480.

[AE 01] Albert, M., Elwi, A., and Cheng, J. (2001). "Strengthening of unreinforced masonry walls using FRPs." *Journal of Composites for Construction*, ASCE, 5(2), 76-84.

[AH 99] Al-Chaar, G., and Hasan, H. (1999). " Masonry bearing and shear walls retrofitted with overlay composite material." U.S. Army, Corps of Engineers, Champaign, *Technical Report 98/86*.

[AHH 90] Abboud, B., Hamid, A., and Harris, H. (1990) "Small-Scale Modeling of Concrete Block Masonry Structures." *ACI Structural Journal*, 87(2), 145-155.

[AL 01] Abrams, D., and Lynch, J. (2001). "Flexural behavior of retrofitted masonry piers." *KEERC-MAE Joint Seminar on Risk Mitigation for Regions of Moderate Seismicity*, Illinois, USA.

[Al 87] Ali, S. (1987). "Concentrated loads on solid masonry." PhD. dissertation, Newcastle University, Australia.

[AMM 94] Anthoine, A., Magonette G., and Magenes G. (1994). "Shear-compression testing and analysis of brick masonry walls." *10th European Conference on Earthquake Engineering*, Vienna, Austria, 1657-1662.

[AN 87] Al-Manaseer, A., Neis, V., (1987). "Load tests on post-tensioned masonry wall panels," ACI Struc. Journal, 84 (6), 467-472.

[An 95] Anthoine A. (1995). "Derivation of the in-plane elastic characteristics of masonry through homogenization theory." International Journal of Solids and Structures, 32 (2), 137-163.

[Ar 88] Arya, A. S. (1988). "Repair and strengthening of damaged stone houses after Dhamar earthquake of Dec. 1982." *9th World Conference on Earthquake Engineering*, Tokyo-Kyoto, Japan, 1141-1146.

[AS 92] Abrams, D., and Shah, N. (1992). "Cyclic load testing of unreinforced masonry walls." *Report No. 92-26-10*, Advanced Construction Technology Center, Newmark Civil Engineering Laboratory, Department of Civil Engineering, University of Illinois at Urbana-Champaign, USA.

[AS 94] Al-Sulaimani, G., Sharif, A., Basunbul, I., Baluch, M., Ghaleb, N. (1994) " Shear repair for reinforced concrete by fiber glass plate bonding,"ACI Structural Journal, 91(3), 458-464

[BA 02] Berman, J., Al-Chaar, G., Dutta, P. (2002). « Biaxial loading and failure behavior of brick triplets with fiber-reinfoced polymer composite upgrades, » US army corps of engineers, report No. ERDC TR-02-7

[BB 02] Brennet G., Badoux M. (2002). "Seismic inventory of the city of Aigle (Switzerland)." *12th European Conference on Earthquake Engineering*, London, England, Paper No. 621

[BBB 02] Bakis, C., Bank, L., Brown, L., Cosenza, E., Davalos, M., Lesko, J., Machida, A., Rizkalla, S., and Triantafillou, T. (2002). "Fiber-reinforced polymer composites for

construction- State-of-the-art review." *Journal of Composites for Construction*, ASCE, 6(2), 73-87.

[BC 04] Bousselham, A., Chaallal, O., (2004). "Shear strengthening RC beams with FRP: assessment of influencing parameters and required research," ACI Structural Journal 101(2), 219-227.

[BEL 02] Badoux, M., Elgwady, M., and Lestuzzi, P. (2002). "Earthquake simulator tests on unreinforced masonry walls before and after upgrading with composites." *12th European Conference on Earthquake Engineering*, London, England, Paper No. 862.

[BH 97] Benli, G., Houqin, Z., (1997). "An introduction to the technology code for construction of confined brick masonry," 11th IB2MaC, Shanghai, China, 1000-1006.

[BM 01] Bonacci F. J.; Maalej, M (2001), "Behavioral Trends of RC Beams Strengthened with Externally Bonded FRP" *Journal of Composites for Construction*, ASCE, 5(2), 102-113.

[BM 92] Button, M., Mayes, R. (1992). "Out of Plane Seismic Response of Reinforced Masonry Walls." *Journal of Structural Engineering*, ASCE, 118(9), 2495-2513.

[BMT 80] Bernardini, A., Modena, C., Turnsek, V., and Vescovi, U. (1980). "A comparison of three Laboratory test methods used to determine the shear resistance of masonry walls." *7th World Conference on Earthquake Engineering*, Istanbul, Turkey, 181-184.

[Bo 01] Borgogno, W. (2001). "Earthquake retrofit of a low rise building –composite fiber plates for strengthening of masonry walls and their anchorage." *20th EAEE Regional Earthquake Engineering*, Sion, Switzerland, 121-122.

[Br 95] Bruneau, M. (1995). "Damage to masonry buildings from the 1995 Hanshin-Awaji (Kobe, Japan) earthquake – preliminary report." 7th Canadian Masonry Symposium, 1, 84-98.

[Br 94a] Bruneau, M. (1994). "State-f-the-art report on seismic performance of unreinforced masonry buildings." *Journal of Structural Engineering*, ASCE, 120(1), 230-251.

[Br 94b] Bruneau, M. (1994). "Seismic evaluation of unreinforced masonry buildings - State-f-the-art report." *Canadian Journal of Civil Engineering*, 21, 512-539.

[BWB 99] Bachmann H., Wenk T., Baumann M., Lestuzzi P. (1999). "Der neue ETH-Erdbebensimulator." *Schweizer Ingenieur und Architekt*, SI+A, 4/99, Zürich.

[Ch 95] Chopra, A. K. (1995). *Dynamics of structures*. Prentice Hall, Englewood Cliffs, New Jersey.

[CC 02] Campione, G., Cucchiara, L., La Mendola, L., Zingone, G. (2002). "Interfacial phenomena in masonry members reinforced with FRP," *12th European Conference on Earthquake Engineering*, London, England, Paper No. 609.

[Co 02] Costa, A. (2002). "Determination of mechanical properties of traditional masonry walls in dwellings of Faial Island, Azores." *Earthquake Engineering and Structural Dynamics*, 31, 1361-1382.

[CM 94] Calvi, G., Magenes, G., (1994). "Experimental results on unreinforced masonry shear walls damaged and repaired," 10th IB2MaC, Calgary, Canada, 509-518.

[CN 98] Chaallal, O., Nollet, M., Perraton, D. (1998). "Strengthening of reinforced concrete beams with externally bonded fiber-reinforced-plastic plates: design guidelines for shear and flexure," *Canadian Journal of Civil Engineering*, 25, 692-704.

[CS 02] Chaallal, O., Shahawy, M., Hassan, M. (2002). "Performance of reinforced concrete T-girders strengthened in shear with GFRP fabrics," *ACI structural Journal*, 99(3), 335-343.

[EA 89] Epperson, G., and Abrams, D. (1989). "Nondestructive evaluation of masonry buildings."ACTC No. 89-26-03, USA.

[EC6 99] "Design of masonry structures," (1999). *Eurocode 6*, Comite Euro-International du Béton, Lausanne, Switzerland.

[EC8 95] "Design provisions for earthquake resistance of structures," (1995). *Eurocode 8*, Part 1-1: General rules and rules for buildings- seismic actions and general requirements for structures. Comite Euro-International du Béton, Lausanne, Switzerland.

[ED 02] El-Dakhakhani, W. W. (2002). "Experimental and analytical seismic evaluation of concrete masonry-infilled steel frames retrofitted using GFRP laminates." PhD dissertation, college of Engineering, Drexel University, USA.

[Elg 99] Elgwady, M. A. (1999). "Strengthening of short corbels using CFRP." MSc. thesis, Department of Civil Engineering, Cairo University, Giza, Egypt.

[EL 03] ElGawady, M., Lestuzzi, P., Badoux, M. (2003). "Dynamic tests on URM walls before and after upgrading with composites." *Experimental Report*, EPFL-ENAC-IS-IMAC, Applied Computing and Mechanics Laboratory.

[EL 04] ElGawady, M., Lestuzzi, P., Badoux, M. (2004) (In preparation). "Static cyclic tests on URM walls before and after upgrading with composites." *Experimental Report*, EPFL-ENAC-IS-IMAC, Applied Computing and Mechanics Laboratory.

[ELB 02] Elgwady, M. A., Lestuzzi, P., and Badoux, M. (2002). "Dynamic in-plane behavior of URM wall upgraded with composites." *3rd International Conference for Composite in Infrastructure*, San Francisco, USA, Paper No. 009.

[ES 97] Ehsani, M. R., and Saadatmanesh, H. (1997). "Fiber composites: an economical alternative for retrofitting earthquake-damaged precast-concrete walls." *Earthquake Spectra*, (13)2, 225-241.

[ES 97] Ehsani, M. R., Saadatmanesh, H., Al-Saidy, A. (1997). "Shear behavior of URM retrofitted with FRP overlays." *Journal of Composites for Construction*, ASCE, 1(1), 17-25.

[ES 99] Ehsani, M. R., Saadatmanesh, H., Velazquez-Dimas, J. I. (1999). "Behavior of retrofitted URM walls under simulated earthquake loading." *Journal of Composites for Construction*, ASCE, 3(3), 134-142.

[ES 91] Ehsani, M., Saadatmanesh, H., Abdelghany, I., and Elkafarwy,w., "Flexural Behavior of Masonry Walls Strengthened with Composite Fabrics," SP-138, ACI, Detroit MI, 1991.

[FE 00] Applied Technology Council (ATC) (2000). "Prestandard and commentary for the seismic rehabilitation of buildings", Publication No. 356, Federal Emergency Management Agency, Washington, D.C. (FEMA-356).

[fi 03] fib Bulletin No. 24 (2003). "Seismic assessment and retrofit of reinforced concrete buildings,"

[FL 01] Franklin, S., Lynch, J, Abrams, D. (2001). "Performance of rehabilitated URM shear walls: flexural behavior of piers," Department of civil engineering, University of Illinois at Urbana-Champaign, CD Release 03-03.

[FM 00] Foti, D., and Monaco, P., 2000, Post-tensioned masonry: state of the art, Prog. Struc. Eng. Mat., 2, 311-318.

[GD 98] Gilstrap, J., and Dolan, C.(1998). "Out-of-plane bending of FRP-reinforced masonry walls," *Comp. Science and Tech.*, 58, 1277-1284.

[GGS 89] Ganz, H., Guggisberg, R., Schwartz, J., and Thürlimann, B. (1989). " Contribution to the design of masonry walls," *Internal Report*, Institute of Structural Engineering, Department of Civil, Environmental and Geomatics Engineering, Swiss Federal Institute of Technology, Zurich, ETH No. 168.

[GKM 87] Geymonate, G., Krasucki, F., and Marigo, J (1987). "Sur la commutativité des passages à la limite en théorie asymptotique des pouters composites." C. R. Acadmic Science, Paris, 305 (2), 225-228.

[GL 94] Gambarotta, L., and Lagomarsino, S. (1994). "Modeling unreinforced brick masonry wall," U.S.-Italy workshop on Guidelines for Seismic Evaluation and Rehabilitation of Unreinforced Masonry Buildings, Pavia, *Technical Report NCEER-94-0021*, National Center for Earthquake Engineering, Buffalo.

[HD 01] Hamilton III, H. R., and Dolan, C. W. (2001). "Flexural capacity of glass FRP strengthened concrete masonry walls." *Journal of Composites for Construction*, ASCE, 5(3), 170-178.

[HE 99] Hamid, A., El-Sayed, T., Salama, A., (1999). "Seismic retrofit of historic multiwythe stone masonry walls," 8th NAMC, Austin, Texas, USA.

[HH 99] Hamilton III, H. R., Holberg, A., Caspersen, J. and Dolan, C. W. "Strengthening concrete masonry with fiber reinforced polymers," SP-138, ACI, 1999, Detroit MI. 1103-1115.

[HH 02] Holberg, A. M., and Hamilton, H. R., (2002). "Strengthening URM with GFRP composites and ductile connections." *Earthquake Spectra*, (18) 1, 63-84.

[HM 94] Hamid, A., Mahmoud, A., Abo El Maged, S., (1994). "Strengthening and repair of unreinforced masonry structures: state-of-the-art," 10th IB2MaC, Calgary, Canada, 485-497.

[HM 03] Hamoush, S., McGinley, W., Woodson, S. and Mlakar, P., (2003). "Influence of the FRP reinforcement ratio on the out-of-plane shear strength of externally reinforced masonry wall systems," 9th NAMC, Clemson, South Carolina, USA, 180-191.

[HMA 03] Haroun, M., Mosallam, A., and Allam, K. (2003). "In-plane shear behavior of masonry walls strengthened by FRP laminates", the 2nd international workshop on structural composites for infrastructure applications, Cairo, Egypt, 17-18 December.

[HM 02] Hamoush, S., McGinley, W., Mlakar, P., and Muhamed, T., "Out-of-plane behavior of surface-reinforced masonry walls," Cons. and Buil. Mat. , 16, 2002, pp 341-351.

[HM 01] Hamoush, A. S., McGinley, W. M., Mlakar, P., Scott, D., and Murray, K. (2001). "Out-of-plane strengthening of masonry walls with reinforced composites." *Journal of Composites for Construction*, ASCE, 5(3), 139-145.

[HSD 97] Hendry, A. W., Sinha, B. P., and Davies, S. R. (1997). *Design of Masonry Structures*. E & FN Spon.

[HSH 02] Hall, J. D., Schuman, P. M., and Hamilton III, H. R. (2002). "Ductile anchorage for connecting FRP strengthening of under-reinforced masonry buildings." *Journal of Composites for Construction*, ASCE, 6(1), 3-10.

[HY 84] Hutchison, D., Yong, P., McKenzie, G., 1984, Laboratory testing of a variety of strengthening solutions for brick masonry wall panels, 8th WCEE, San Francisco, USA, 575-582.

[IC 01] ICBO Evaluation Service, Inc. (2001). "Acceptance criteria for concrete and reinforced and unreinforced masonry strengthened using fiber-reinforced polymers (FRP), composite systems" AC125.

[JCI 98] Japan Concrete Institute (1998). "Technical report on continues fiber reinforced concrete," Tokyo.

[JK 80] Jabarov, M., Kozharinov, S., Lunyov, A., (1980). "Strengthening of damaged masonry by reinforced mortar layers," 7th WCEE, Istanbul, vol. 6, 73-80

[Ka 84] Kahn, L., (1984). "Shotcrete retrofit for unreinforced brick masonry," 8th WCEE, USA, 583-590.

[KAN 99] Khalifa, A., Alkhrdaji, T., Nanni, A., and Lansburg, S. (1999). "Anchorage of surface mounted FRP reinforcement." *Concrete International: Design and Construction*, 21(10), 49-54.

[Ke 96] Kehoe, B. E. (1996). "Performance of retrofitted unreinforced masonry buildings." *11th World Conference on Earthquake Engineering*, Acapulco, Mexico, Paper No. 1417.

[KEC 03] Kuzik, M. D., Elwi, A. E., and Cheng, J. J. R. (2003). "Cyclic flexural tests of masonry walls reinforced with glass fiber reinforced polymer sheets." *Journal of Composites for Construction*, ASCE, 7(1), 20-30.

[KF 92] Karantoni, F., Fardis, M., (1992). "Effectiveness of seismic strengthening techniques for masonry buildings," ASCE, 118(7), 1884-1902.

[KF 92a] Karantoni, F., and Fardis, M. N. (1992). "Effectiveness of seismic strengthening techniques for masonry buildings." *Journal of Structural Engineering*, ASCE, 118(7), 1884-1902.

[KF 92b] Karantoni, F., and Fardis, M. N. (1992). "Computed versus observed seismic response and damage of masonry buildings." *Journal of Structural Engineering*, ASCE, 118(7), 1802-1821.

[KG 98] Khalifa, A., Gold, W., Nanni, A., and Abdel Aziz, I. (1998). "Contribution of externally bonded FRP to shear capacity of RC flexural members." *Journal of Composites for Construction*, ASCE, 2(4), 195-202.

[KK 01] Kim, H., Kedward, K. (2001). "Stress analysis of in-plane shear loaded adhesively bonded composite joints and assemblies," Office of aviation research, Washington, D.C. Report No. DOT/FAA/AR-017

[KMÖ 88] König, G., Mann, W., and Ötes, A. (1988). "Experimental investigation on the behavior of unreinforced masonry walls under seismically induced loads and lessons derived." *9th World Conference on Earthquake Engineering*, Tokyo-Kyoto, Japan, 1117-1122.

[Ko 98] Kolsch, H. (1998). "Carbon fiber cement matrix (CFCM) overlay system for masonry strengthening." *Journal of Composites for Construction*, ASCE, 2(2), 105-109.

[KPD 02] Kappos, J. A., Penelis, G. G., and Drakopoulos, G. C. (2002). "Evaluation of simplified models for lateral load analysis of unreinforced masonry buildings." *Journal of Structural Engineering*, ASCE, 128(7), 890-897.

[GT 03] Galati, N., Tumialan, G., Nanni, A, (2003). "Arching effect in masonry walls reinforced with fiber reinforced polymer (FRP) materials," Center for Infrastructure and Engineering Studies, University of Missouri-Rolla, 209.

[La 02] Lang, K. (2002). "Seismic vulnerability of existing buildings." PhD dissertation, Institute of Structural Engineering, Department of Civil, Environmental and Geomatics Engineering, Swiss Federal Institute of Technology, Zurich, Switzerland.

[LBB 99] Lee, J. Y., Boothby, E. T., Bakis, E. C., and Nanni, A. (1999) "Slip modulus of FRP sheets bonded to concrete." *Journal of Composites for Construction*, ASCE, 3(4), 161-167.

[LD 02] Laursen, P., Davidson, B., Ingham, J., (2002). "Seismic analysis of prestressed concrete masonry shear walls," 12th ECEE, London, England, Paper reference 247.

[Le 00] Lestuzzi, P. (2000). "Dynamisches plastisches verhalten von stahlbetontragwänden unter erdbebeneinwirkung." PhD dissertation, Institute of Structural Engineering, Department of Civil, Environmental and Geomatics Engineering, Swiss Federal Institute of Technology, Zurich, Switzerland.

[LK 97] Liu, L., Kajiwara, K., Yoshimura, K., Kikuchi, K., Sanchez, T., 1997, Effect of applied lateral forces and wall reinforcement on seismic behaviour of confined concrete masonry walls, 11th IB2MaC, Shanghai, China, 585-594.

[Lo 96] Lourenço, P. (1996). "Computational strategies for masonry structures." PhD dissertation, Department of Civil Engineering, Delft University of Technology, Delft, The Netherlands.

[LG 03] Lissel, S and Gayevoy, A., (2003). "The use of FRPs in masonry: a sate of the art review," *ICPCM*, Cairo, Egypt.

[LS 94] Lotfi, R., and Shing, B. (1994). "Interface model applied to fracture of masonry structures." *Journal of Structural Engineering*, ASCE, 120(1), 63-80.

[LS 03] Lissel, S., Shrive, N., (2003). "Construction of diaphragm walls post-tensioned with carbon fiber reinforced polymer tendons," 9th NAMC, Clemson, South Carolina, USA, 192-203.

[LWB 99] Lestuzzi, P., Wenk, T., and Bachmann, H. (1999). "Dynamic tests of RC structural walls on the ETH earthquake simulator." *Report No. 240*, Institute of Structural Engineering, Department of Civil, Environmental and Geomatics Engineering, Swiss Federal Institute of Technology, Zurich, Switzerland.

[CGM 90] Clouth, W. R., Gülkan, P., Mayes, L. R., and Manos, C. G. (1990) "Seismic Testing of Single-Story Masonry Houses: Part 2." *Journal of Structural Engineering*, ASCE, 116(1), 1884-1902.

[CG 97] Chuxian, S., Guiqiu, L., Wenchao, W., (1997). "The design of brick masonry structure with concrete column," 11th IB2MaC, Shanghai, China, 626-633.

[Ma 02] MATLAB Version 6.5.1 (2002). The language of technical computing, the Mathworks Inc.

[MC 97] Magenes G., and Calvi G. M. (1997). "In-plane seismic response of brick masonry walls." *Earthquake Engineering and Structural Dynamics*, 26, 1091-1112.

[MC 94] Magenes G., and Calvi G. M. (1994). "Shaking table tests on brick masonry walls." *10th European Conference on Earthquake Engineering*, Vienna, Austria , 2419-2424.

[MC 92] Magenes G., and Calvi G. M. (1992). "Cyclic behavior of brick masonry walls." *10th World Conference on Earthquake Engineering*, Madrid, Spain, 3517-3522.

[Me 04] Meyer, U. (2004). "In plane shear strength of vertically perforated clay unit masonry a survey of recent test results," 13th IB^{2}Mac, Amsterdam, Holland.

[MH 03] Mosallam, A., Haroun, M. (2003). "Seismic strengthening of unreinforced thick masonry walls using polymer composites," Structural Faults + Repair, UK.

[MF 01] Montes, P., Fernandez, A., (2001). "Behaviour of a hemispherical dome subjected to wind loading," J. of Wind Eng. and Indus. Aerodynamics, 89, 911-924

[MM 96] Mojsilovic, N, Marti, P., (1996). "Load tests on post-tensioned masonry walls," IBK Nr. 0011, Swiss Federal Institute of Technology, Zurich, Switzerland.

[Mo 04] Moon, F. (2004). "Seismic strengthening of low-rise unreinforced structures with flexible diaphragms" PhD dissertation, Georgia Institute of Technology, USA.

[Mos 96] Mostafa, H. (1996). "Behavior of hollow concrete masonry walls under the effect of vertical and in-plane static horizontal load." PhD dissertation, Department of Civil Engineering, Cairo University, Egypt.

[MN 99] Miller, B., and Nanni, A. (1999). "Bond between CFRP sheets and concrete." 5th ASCE Materials Congress, Cincinnati, Ohio, USA, 240-247.

[MN 89] Matthys, H., Noland, L., (1989). "Proceedings of an international seminar on evaluation, strengthening and retrofitting masonry buildings," TMS, Colorado, USA.

[MS 99] MSJC, (1999). "Building code requirements for masonry structures," Masonry Stand. J. Committee

[MST 99] Marshall, Jr., Sweeney, S. C., and Trovillion, J. C. (1999). "Seismic rehabilitation of unreinforced masonry walls." *ACI Special Publications 188-26*, 287-295.

[Mu 87] Musgrove, J. (1987). *A history of architecture*, Butterworths, London, England.

[MW 96] Matsumura, A., Watanabe, M., Nobusawa, H.,(1996). "Damage to masonry buildings caused by the 1995 Hyogoken-Nanbu earthquake," 7th NAMC, 930-940.

[MYL 02] Moon, F. L., Yi, T., Leon, R. T., and Kahn, L. F. (2002). "Seismic strengthening of unreinforced masonry structures with FRP overlays and post-tensioning." *12th European Conference on Earthquake Engineering*, London, England, Paper No. 613.

[NK 01] Nakaba, K., Kanakubo, T., Furuta, T., and Yoshizawa, H. (2001). "Bond behavior between fiber-reinforced polymer laminates and concrete." *ACI Structural Journal*, 98(3), 359-367.

[NT 03] Nanni, A., and Tumialan, J., (2003). "Fiber reinforced composites for the strengthening of masonry structures," Struc. Eng. Int., 4, 271-278.

[NV 03] Nuti, C., Vanzi, I., (2003). "To retrofit or not to retrofit," J. Eng. Struc., 25, 701-711

[OYB 88] Ottazzi, G., Yep, J., Blodet, M., Villa-Garacia, G., and Ginocchio, J. F. (1988). "Shaking table tests of improved adobe masonry houses." *9th World Conference on Earthquake Engineering*, Tokyo-Kyoto, Japan, 1123-1128.

[Pa 91] Page, A. W. (1991). "The Newcastle earthquake - behavior of masonry structures." Masonry International, 5(1), 11-18.

[Pa 78] Page, A. W. (1978). "Finite element model for masonry." *Journal of Structural Engineering*, ASCE, 104(8), 1285-1367.

[PC 86] Plecnik, J., Cousins, T., O'conner, E., (1986). "Strengthening of unreinforced masonry buildings," J. of Struc. Eng., ASCE, 112, 1070-1087.

[PCO 86] Plecnik, J., Cousins, T., and O'conner, E. (1986). "Strengthening of unreinforced masonry buildings." *Journal of Structural Engineering*, ASCE, 112(5), 1070-1087.

[PK 02] Perret, S., Khayat, K., Gagnon, E., Rhazi, J., (2002). "Repair of 130-year old masonry bridge using high performance cement grout," J. Bridge Eng., ASCE, 7, 31-38

[PP 92] Paulay, T., and Priestley, M. J. N. (1999) *Seismic design of reinforced concrete and masonry building.* John Wily & Sons, New York, USA.

[Re 97] Reddy, J. (1997). *Mechanics of laminated composite plates theory and analysis.* CRC Press, New York, USA.

[RG 96] Rai, D., Goel, S., (1996). "Seismic strengthening of unreinforced masonry piers with steel elements," Earth. Spec., 12, 845-862.

[RK 03] Rosenboom, O., Kowalsky, M., (2003). "Investigation of alternative details for seismic design of post-tensioned clay masonry walls," 9th NAMC, South Carolina, USA, 475-485.

[RM 95] Reinhorn, A. M., Maden, A. (1995). "Evaluation of TYFO-W fiber wrap system for in plane strengthening of masonry walls" *Report No. 95-0002*, Department of Civil Engineering, State University of New York at Buffalo, USA.

[Ro 89] Roberts, M. T. (1989). "Approximate analysis of shear and normal stress concentrations in the adhesive layer of plated RC beams." The Structural Engineering, 67(12), 229-233.

[RS 86] Reinhorn, A. M., and Sherwood, P. P. (1986). "Ferrocement in a large shaking table." *Journal of Structural Engineering*, ASCE, 112(2), 401-416.

[SA 94] Schuller, M., Atkinson, R., Borgsmiller, J., (1994). "Injection grouting for repair and retrofit of unreinforced masonry," 10th IB2MaC, Calgary, Canada, 549-558B.

[SB 03] Schultz, A., Bean, J., Stolarski, H., 2003, Resistance of slender post-tensioned masonry walls with unbonded tendons to transversal loading, 9th NAMC, South Carolina, USA, 463-473

[Sc 94] Schwegler, G. (1994). "Masonry construction strengthened with fiber composites in seismically endangered zones." *10th European Conference on Earthquake Engineering*, Vienna, Austria, 2299-2303.

[SIA 89] "Actions on structures," *Standard* (1989). Swiss Society of Engineers and Architects.

[SIM 76] Gasparini D. A., and Vanmarcke, E. H. (1976). "Simulated earthquake motions compatible with prescribed response spectra (SIMQKE procedure)." *MIT Civil Engineering Research Report R76-4*. Massachusetts Institute of Technology, Cambridge, Mass.

[SK 96] Schwegler, G., and Kelterborn, P. (1996). "Earthquake resistance of masonry structures strengthened with fiber composites." *11th World Conference on Earthquake Engineering*, Acapulco, Mexico, Paper No. 1460.

[So 02] Sofronie R. A. (2002). "Repair and retrofitting masonry buildings." *12th European Conference on Earthquake Engineering*, London, England, Paper No. 183.

[ST 80] Sheppard, P., Tercelj, S., (1980). "The effect of repair and strengthening methods for masonry walls," 7th WCEE, Istanbul, vol. 6, 255-262.

[SYP 01] Sutcliffe, D., Yu, S., and Page, A. (2001). "Lower bound limit analysis of unreinforced masonry shear walls." *Computers and Structures,* 79 (2001), 1295-1312.

[Ta 00] Taghdi, M. (2000). "Seismic retrofit of low-rise masonry and concrete walls by steel strips." PhD dissertation, Department of Civil Engineering, University of Ottawa, Ottawa, Canada.

[TA 00] Triantafillou, T., Antonopoulos, C. (2000) "Design of concrete flexural members strengthened in shear with FRP," *Journal of Composites for Construction,* ASCE, 4(4), 198-205

[TM 02] Tumialan, J., Morbin, A., Micelli, F., and Nanni, A., (2002). "Flexural strengthening of URM walls with FRP laminates," 3rd ICCI'02, Ca, USA.

[To 99] Tomazevic, M. (1999). *Earthquake-resistant design of masonry buildings.* Imperial College Press, London, England.

[Tr 98] Triantafillou, T. (1998). "Strengthening of masonry structures using epoxy-bonded FRP laminates." *Journal of Composites for Construction,* ASCE, 2(2), 96-104.

[TS 81] Turnsek, V., and Sheppard, P. (1981). "The shear and flexural resistance of masonry walls." International Research Conference on Earthquake Engineering, Skopje, PP. 517-573.

[Tu 01] Tumialan, J., (2001). "Strengthening of masonry structures with FRP composites," PhD diss., Dept. of Civil Eng., Univ. of Missouri-Rolla, Rolla, Missouri.

[UC 90] "Seismic strengthening provisions for unreinforced masonry bearing wall buildings," (1990). Appendix Chapter 1, Uniform Code for Building Conservation.

[Uj 92] Uji, K. (1992). "Improving the shear capacity of existing reinforced concrete members by applying carbon fiber sheets," Trans. Japan Concrete Institute, Tokyo, 14, 253-266

[Ve 98] Velazquez-Dimas, J. I. (1998). "Out-of-plane cyclic behavior of URM walls retrofitted with fiber composites," *PhD diss.*, Univ. of Arizona.

[VE 00a] Velazquez-Dimas, J. I., and Ehsani, M. R. (2000). "Out-of-plane behavior of brick masonry walls strengthened with fiber composites." *ACI Structural Journal,* 97(3), 377-387.

[VE 00b] Velazquez-Dimas, J. I., and Ehsani, M. R. (2000). "Modeling out-of-plane behavior of URM walls retrofitted with fiber composites." *Journal of Composites for Construction,* ASCE, 4(4), 172-181.

[VE 02] Velazquez-Dimas, J. I., Ehsani, M. R., Castorena Gonzalez, J. H., and Reyes Salazar, A., (2002). "Modeling the out-of-plane bending behavior of retrofitted URM walls," *3rd ICCI'02*, Ca, USA.

[VG 02] Vandergrift, J., Gergely, J., and Young, D., (2002). "CFRP retrofit of masonry walls," 3rd ICCI'02, San Francisco, Ca, USA, Paper No. 047.

[VSL 90] VSL, (1990). "Post-tensioned masonry structures," VSL Report Series # 2, VSL Int. ltd., Switzerland.

[WS 94] Weeks, J., Seible, F., Hegemier, G., Priestly, N. (1994). "The U. S. – TCCMAR Full-Scale Five-Story Masonry Research Building Test." University of California, San Diego.

[YH 97] Yasuhisa, Sonobe et al. "Design guidelines of FRP reinforced concrete building structures," *Journal of Composites for Construction,* ASCE, 1(3), 90-115.

[Zh 95] Zhuge, Y. (1995). “Nonlinear dynamic response of unreinforced masonry under in-plane lateral loads.” PhD. dissertation, School of Civil Engineering, Queensland University of Technology, Australia.

[YZ 97] Yu, Z., Zhengyun, W., and Weiping, Z., (1997). “Experimental research on aseismic strengthening of block masonry buildings using thin structural columns,” 11th IB2MaC, China, 626-633.

[ZQ 84] Zezhen, N., Qi, D., Jianyou, C., Runtao, Y., (1984). “A study of aseismic strengthening for multi-story brick building by additional R/C columns,” 8th WCEE, USA, 591-598.

[ZSS 02] Zilch, K., Schermer, D., and Scheufler, W. (2002). “Simulated earthquake behavior of unreinforced masonry walls.” Proceedings of the Fifth European Conference on Structural Dynamics - EURODYN 2002, September TU München., Munich, Germany.

[ZX 03] Zhao, T., Xie, J., Li, H., (2003). “Strengthening of cracked concrete block masonry walls using continues carbon fiber sheet,” 9th NAMC, Clemson, South Carolina, USA, 156-167.

TWB Inc. http://www.twpinc.com

The ferrocement network http://WWW.Ferrocement.net

ISIS, intelligent sensing for innovative structures http://www.isiscanada.com

ELGAWADY MOHAMED

Ch de Bois Gentil 144 ++41 (0) 21 693 24 98
1018 Lausanne, Switzerland ++41 (0) 76 421 75 44

CAREER SUMMARY

Has successfully held the following responsibilities in Switzerland and Egypt:

- Theoretical and experimental research (monotonic, static cyclic, and dynamic tests)
- Academic teaching
- Engineering design and consultancy (bridges, residential, and commercial buildings)
- Project management

Education

1992-1997	:	Bachelor of civil engineering, Cairo University, Egypt "V. Good with Honor Degree"
1998-2000	:	Master of structural engineering, Cairo University, Egypt Thesis title "*Strengthening of Short Cantilevers Using Carbon Fiber Reinforced Plastic*"
2000- 2004	:	Ph.D. Swiss Federal Institute of Technology at Lausanne (EPFL) Thesis title "*Seismic In-Plane Behavior of URM Walls Upgraded with Composites"*

Work History

2000-now : Researcher at EPFL-ENAC-IMAC

Tasks: Carried out dynamic and static cyclic tests on URM walls before and after upgrading (using composites, shotcrete, and post-tensioning). Evaluate existent buildings using simple linear elastic methods. Carried out dynamic linear analysis for perforated URM walls using ANSYS. Contributed to static and dynamic loading test and survey measurements for a long span bridge. Helped in supervising a graduation project "equivalent to master work".

1997-2000 : Teaching Assistant at High Institute for Engineering and Management, Cairo, Egypt

Tasks: Taught and solved problems for students in classes of about 30 students in the following subjects: design of reinforced concrete structures, design of steel structures, soil mechanics and foundation design, principles of mechanics, material properties and strength, and structure analysis

1997-2000 "part time" : Bridge Designer Engineer at Arab Consulting Engineers (ACE Moharram – Bakhoum) (the leading consulting office in Egypt and one of the leading consulting offices in the Middle East and Africa)

Tasks: Contributed to the design of several one span composite bridges, the beltway around Cairo including box girder systems. Contributed to the design and management of several units "mixers, belt conveyors, and administrative buildings" in MISR BENI SUEF Cement Factory. Contributed to several loading tests of bridges in Cairo.

1997-1999 "part time" : Designer Engineer at Prof. Ahmed Sabry consulting office

Tasks: Designed several multi-stories (between 5-13 stories) residential and commercial buildings

1997-2000 : Private work

Tasks: Designed several villas around Cairo and Port-Said "north of Egypt"

Awards and Scholarships

- Fellowship from DAAD (German Academic Exchange Service) to give a lecture and attend a short course on "Retrofitting of Masonry Structures and Earthquake Resistant Design" at Dresden University of Technology from 7/12/2003 till 18/12/2003.
- PhD. scholarship from IMAC department, EPFL 2002 till now
- Scholarship form Swiss government (FCS) from 15/7/2000 till 30/3/2002
- Egyptian government Award of Excellence in Undergraduate Studies in the faculty of engineering from 1/10/1992 till 1/7/1993 then from 1/10/1994 till 1/7/1997

Publications

Journals

- **ElGawady**, M. A.; Lestuzzi, P.; Badoux, M. "In-plane seismic response of URM walls upgraded with FRP", sent to ASCE journal.
- **ElGawady, M. A.;** Lestuzzi, P.; Badoux, M. "Performance of URM walls under seismic loading", sent to TMS journal.
- **ElGawady**, M. A.; Lestuzzi, P.; Badoux, M. "Experimental investigation of seismic retrofitting of unreinforced masonry walls using FRP", sent to Composites Part B journal.
- **ElGawady**, M. A.; Lestuzzi, P.; Badoux, M. "Static cyclic behavior of URM walls retrofitted with FRP", sent to Engineering Structures journal.
- **ElGawady**, M. A.; Lestuzzi, P.; Badoux, M. "Analytical shear model for URM walls upgraded with FRP", (in preparation).

Conferences

- **ElGawady** M., Lestuzzi P., Badoux M., J. Hegner. "Retrofitting of URM Walls Using Post-tensioning and GFRP" 2nd Mechanics of Masonry Structures with FRP-materials: Modeling, Design, Control, Venice, Italy; December 6-8, 2004.
- **ElGawady** M. A., Lestuzzi P., Badoux M. "A Review of Retrofitting of URM Walls Using Composites" 4th International Conference on Advanced Composite Materials in Bridges and Structures, Calgary, Alberta, Canada; July 20 – 23, 2004.
- **ElGawady**, M. A., Lestuzzi, P.; Badoux, M." A review of conventional seismic retrofitting techniques for URM", 13th Brick/Block Masonry Conference, Amsterdam, Holland; July 4-7, 2004.
- **ElGawady**, M. A.; Lestuzzi, P.; Badoux, M. "Static cyclic tests on URM walls before and after retrofitting with composites", 13th Brick/Block Masonry Conference, Amsterdam, Holland; July 4-7, 2004.
- **ElGawady**, M. A.; Lestuzzi, P.; Badoux, M. "Dynamic versus static cyclic tests of masonry walls before and after retrofitting with GFRP", 13th World Conference on Earthquake Engineering, Vancouver, Canada; August 1 - 6, 2004.
- **ElGawady**, M. A.; Lestuzzi, P.; Badoux, M. "Rehabilitation of unreinforced brick masonry walls using composites", Retrofitting of Masonry Structures and Earthquake Resistant Design, Short Course, Dresden, Germany; December 7-18, 2003 (invited).
- **ElGawady**, M. A.; Lestuzzi, P.; Badoux, M. "In-plane lateral behavior of URM walls upgraded with composites", Response of Structures to Extreme Loadings XL2003, Toronto, Canada; August 3-6, 2003.
- **ElGawady**, M. A.; Lestuzzi, P.; Badoux, M. "Dynamic in-plane tests on URM", Response of Structures to Extreme Loadings XL2003, Toronto, Canada; August 3-6, 2003.
- **ElGawady,** M. A.; Lestuzzi, P.; Badoux, M. "Dynamic tests of URM wall before and after upgrading with composites", Experimental Report, EPFL-ENAC-IS-IMAC, Applied

EPFL-ENAC-IMAC
1015 Ecublens-Lausanne
Tel. ++41 (0) 76 421 75 44
e-mail : mohamed.elgwady@epfl.ch
Fax : ++41 (0) 21 693 4748

Computing and Mechanics Laboratory. Publication Nr. 1. Lausanne, Switzerland; May 2003.

- Badoux, M.; **ElGwady**, M. A.; Lestuzzi, P. “Earthquake simulator tests on unreinforced masonry walls before and after upgrading with composites”, The 12th European Conference on Earthquake Engineering, London, UK; Paper reference 862; September 9-13, 2002.
- **ElGwady**, M. A.; RABIE, M.; Talat M.” Strengthening of corbels using CFRP an experimental program”, 3rd International Conference for Composite in Infrastructure ICCI’02, San Francisco, USA, Paper No. 013; 2002.
- **ElGwady**, M. A.; Lestuzzi, P.; Badoux, M. “Dynamic in-plane behavior of URM walls upgraded with composites”, 3rd International Conference for Composite in Infrastructure ICCI’02, San Francisco, USA, Paper No. 009; 2002.
- **ElGwady**, M. A.; Lestuzzi, P.; Badoux, M. “Seismic upgrading of URM walls using composite fiber laminates”, 20th EAEE Seminar; Sion, Switzerland; September 1-7, 2001.
- **ElGwady,** M. A. "Strengthening of short cantilevers using carbon fiber reinforced plastic", Master thesis, Civil Engineering Department, Faculty of Engineering, Cairo University, Egypt; October 2000.

Miscellaneous

Personal data	:	Born 1975, Egyptian citizen, married, two children
Language	:	Arabic mother tongue English very good French good German Basics
Professional organizations	:	ASCE, TMS, Egyptian Syndicate of Engineers
Computer programs	:	SAP, ANSYS, AutoCAD, BASIC, FORTRAN

EPFL-ENAC-IMAC
1015 Ecublens-Lausanne

Tel. ++41 (0) 76 421 75 44
e-mail : mohamed.elgwady@epfl.ch
Fax : ++41 (0) 21 693 4748